DESIGN AND IMPLEMENTATION OF BASIC TERNARY LOGIC GATES USINGCMOS CIRCUIT

P.R. Deshmukh[1], A. Badwaik [2], M.Bonde[3], S. Dalne[4] and R. Hiwanj[5]
Dept. of Electronics and Telecommunication Engineering,Government College of Engineering, Nagpur
[1]pr_deshmukh@yahoo.com, [2]sakshi28dalne@gmail.com, [3]meghabonde78@gmail.com,
[4]akankshasbadwaik@gmail.com, [5] renuka15hiwanj@gmail.com

ABSTRACT

In a conventional binary (Two valued) logic system, there is a constraint for a system to decide an output in two ways. Although efficient and powerful, binary logic is not the most efficient & powerful switching logic. The MVL technique is used to overcome the difficulties in the analysis of problems in binary digital systems, such as the design of fault simulators. The multi-value logic system specifically the ternary logic system can be a good alternative in the processing of digit signal, As it provides an alternate solution to the system giving the decision in 'third' state thus giving a complete solution to the problems. This paper presents the design, implementation, and analysis ofbasic Ternary logic gates and combinational circuits that have been validated using Multisim Software.

Keywords: *Multivalued logic, Ternary logic, STI, NTI, PTI, TAND, TNAND, TOR, TNOR*

1. Introduction

The intrinsic switching behavior of many electronic devices makes them appropriate for implementing binary digital integrated circuits. Binary logic circuits are the most prevalent computing technology today. Therefore, need a large number of logic gates and transistors to reachthe required data size. Besides, even more, interconnected wirings between the system components are required in binary logic circuits. In binary logic, only two logic levels (0, 1) can be transmitted over a given set of lines. So from this the main disadvantages of the binary integrated circuits, which are the interconnection of the input output lines and pin-out problems, cause limitations on the number of connections inside and outside of the circuit [4]. Due to an increasing density of chips, the number of inter-chip connections between input and output is greatly increased as more and more functions are put on the same chip because of this the size and performance of the chip are mostly dominated by wiring rather than devices. [1]

One of the most promising approaches to solve the interconnection problems is the use of multiple-valued logic (MVL) inside the VLSI chip. Due to the reduced complexity of interconnections of input and makes the chip area and the delay much smaller. MVL reduces the number of signals involved in the communication increasing their information content. The multi - valued logic system memories are implemented commercially. By considering the cost and radix relation theoretically, the ternary logic circuits are more economical than binary logic circuits.

A two-valued logic can be extended to n-valued logic, that is, for example, in a three-valued logic radix is three, which is termed as ternary logic. In a binary system, one bit is equivalent to $\log_2 2 = 1$, which is a single bit of binary contains one bit of information, however, in the Ternary systemone trit that is the single unit of ternary contains $\log_2 3 = 1.53$ bits of information. Alexander [1964] showed that the natural base ($e \approx 2.71828$) is the most efficient radix for the implementation of switching circuits. It seems that the most efficient radix for the implementation of a digital system is 3 than 2. [2]. For representing decimal number 16 in binary, 5 bits are required (10000) whereas representing the same number in ternary requires 3 bits (121). There are two types of ternary logic

state based on their voltage mode of operations that are Balanced Ternary (-1, 0, 1) and Unbalanced Ternary (0, 1, 2). This paper provides an implementation of the basic ternary logic gates in Unbalanced Ternary. [5]

2. Design of Ternary Inverter

The Ternary Inverters are further classified based on the output obtained for corresponding input levels. Ternary Inverters are classified into three types of Inverters: 1) Standard Ternary Inverter (STI), 2) Positive Ternary Inverter (PTI), and 3) Negative ternary Inverter (NTI). The input and output of STI inverter take three possible voltage levels which describe the three logic levels (0, 1, and 2). On the other hand, PTI and NTI outputs take only two voltage levels, either high or low. In case of NTI, the input middle voltage level goes to the low output voltage. However, for PTI, the input middle level voltage goes to high output voltage.

STI INVERTER

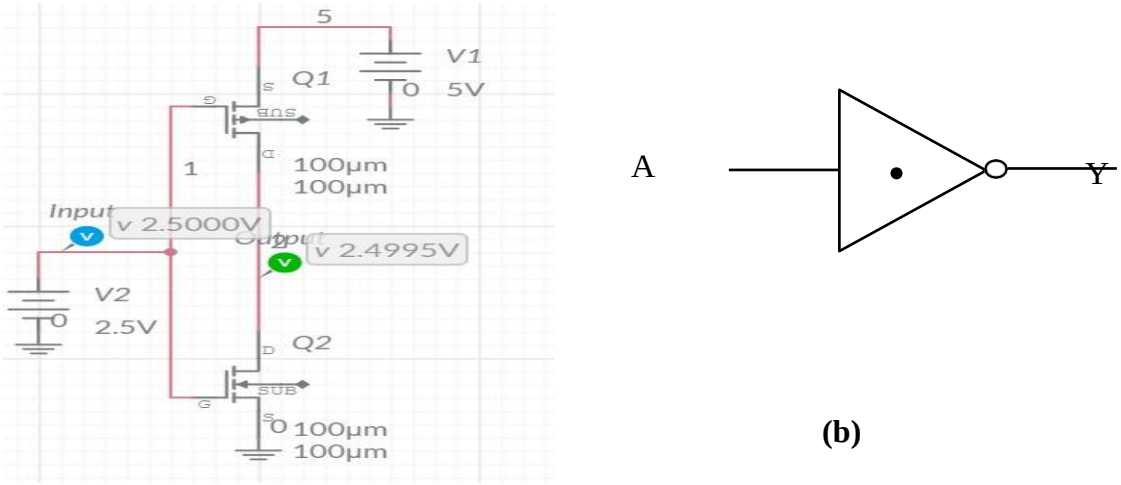

Fig. -1: (a) Schematic of STI (b) Symbol of STI

The Simple Ternary Inverter (STI) consists of two MOS (Metal-Oxide-Semiconductor) transistors that are NMOS (N-Channel MOS) and PMOS (P-Channel MOS). In which input voltage is applied as a gate to source voltage (Vgs) by connecting the gate terminals of the PMOS and NMOS. The output voltage of STI at threshold voltages of PMOS and NMOS 0V is obtained as a drain to source voltage (Vds) by connecting the drain terminals of the PMOS and NMOS. As the source terminal of the PMOS is connected to a battery voltage of 5 (logic 2) whereas the source terminal of the NMOS is kept ground (logic 0).

The working of STI is, if the input voltage is 0volts (logic 0), then NMOS becomes off and PMOS becomes on, as a result, NMOS becomes open-circuited (open switch) and PMOS becomes short-circuited (close switch) and there will be no flow of current in a circuit so the output becomes 5 volts (logic 2). On contrary, if the input voltage is 5 volts (logic 2), then NMOS becomes turned on that is short-circuited (close switch) and PMOS is turned off that is open- circuited (open switch), which impacts as there will be no flow of current in the circuit so the output becomes 0 volts (logic 0). And if the input voltage is 2.5 volts (logic 1), which is equal to the VDD/2 voltage level, both PMOS and NMOS become turned on and the circuit is completed, and consequently current could flow in both the PMOS and NMOS. [5] The circuit is supplied with different VDD voltage values that are 0V, 2.5V, and 5V is required to detect three different logic levels which are 0, 1, and 2 for the input signal. [2]

Input LogicLevel (A)	Output LogicLevel (Y)
0	2
1	1
2	0

Table-1: Truth Table of STI

PTI INVERTER

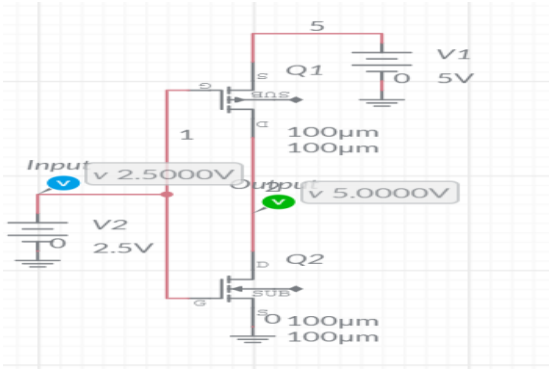

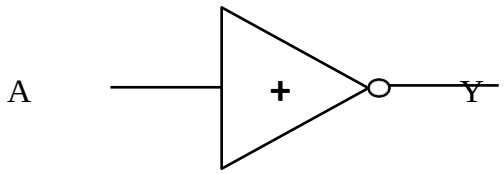

(a) **(b)**

Fig. -2: (a) Schematic of PTI (b) Symbol of PTI

The Positive Ternary Inverter (PTI) is similar in structure as the Simple Ternary Inverter consists of two MOS (Metal-Oxide-Semiconductor) transistors that are NMOS (N-Channel MOS) and PMOS (P-Channel MOS). Here the only change is in threshold voltages of PMOS and NMOS. The threshold voltages of PMOS is -2 volt and NMOS is 3 volt. The output of the PTI gives HIGH logic level (logic 2) for two LOW logic level (logic 0 &1) inputs. The schematic of a Positive Ternary Inverter is shown in Figure 4.1.2(a). In the case of PTI, when the input reaches 0 volts (logic 0) then the output is 5 volts (logic2) because at that time PMOS is turned on that is short-circuited (close switch) and NMOS is turned off that is open-circuited (open switch) since the total voltage drop appears at the output terminal is same as like battery voltage (source voltage of PMOS) 5 volts. When input voltage appears as 5 volts (logic 2) then the output is0 volts (logic 0) because at that time PMOS is turned off that is open- circuited (open switch) and NMOS is turned on that is short-circuited (close switch) since the total voltage drop appears at the output terminal is same as the ground voltage (source voltage of NMOS) 0 volts. When the input voltage is 2.5 volts (logic 1) then PMOS is on and NMOS is off and current will flow only through PMOS and the output voltage is 5 volts (logic 2) due to the threshold voltage (Vth) of NMOS is greater than the input voltage (Vgs). Here the NMOS will be in off condition until and unless the input voltage (Vgs) is less than the threshold voltage (Vth) of NMOS due to this at the intermediate level PTI gives HIGH output value of 5 volts (logic 2). [5][2] The Positive Ternary Inverter is similar with the Standard Ternary Inverter the only difference in the output at the intermediate state that is at input voltage of 2.5volts where the output voltage is 5volts that is high output that's why this ternary inverter is called as Positive Ternary Inverter.

Input Logic Level (A)	Output Logic Level (Y)
0	2
1	2
2	0

Table-2: Truth Table of PTI

NTI INVERTER

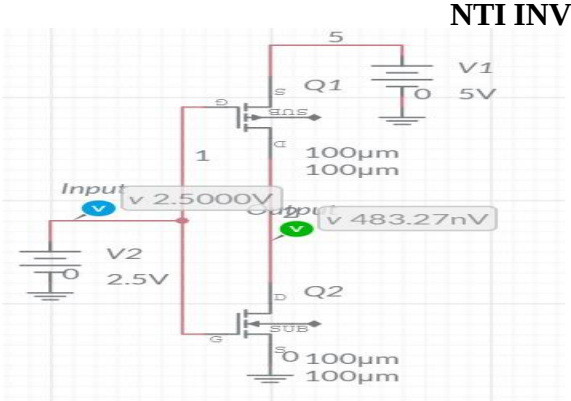

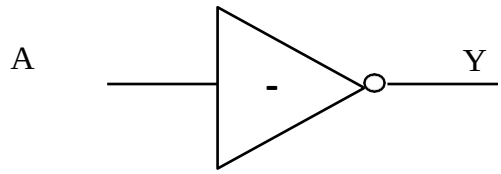

(a) **(b)**

Fig. -3: (a) Schematic of NTI (b) Symbol of NTI

The Negative Ternary Inverter (NTI) is similar in structure as the Simple Ternary Inverter consists of two MOS (Metal-Oxide-Semiconductor) transistors that are NMOS (N-Channel MOS) and PMOS (P-Channel MOS). Here the only change is in threshold voltages of PMOS and NMOS. The threshold voltages of PMOS is -2.5 volt and NMOS is 2 volt. The output of the NTI gives LOW level (logic 0) for two HIGH logic level (logic 1 &2) inputs.

The schematic of a Negative Ternary Inverter is shown in Figure 4.1.3(a) In the case of NTI, when the input reaches 0 volts (logic 0) then the output is 5 volts (logic2) because at that time PMOS is turned on that is short-circuited (close switch) and NMOS is turned off that is open-circuited (open switch) since the total voltage drop appears at the output terminal is same as like battery voltage (source voltage of PMOS) 5 volts. When input voltage appears as 5 volts (logic 2) then the output is 0 volts (logic 0) because at that time PMOS is turned off that is open- circuited (open switch) and NMOS is turned on that is short-circuited (close switch) since the total voltage drop appears at the output terminal is same as the ground voltage (source voltage of NMOS) 0 volts. When the input voltage is 2.5 volts (logic 1) then PMOS is off and NMOS is on and current will flow only through NMOS and the output voltage is 0 volts (logic 0) due to the threshold voltage (Vth) of NMOS is less than the input voltage (Vgs). Here the NMOS will be in off condition until and unless the input voltage (Vgs) is less than the threshold voltage (Vth) of NMOS due to this at the intermediate level NTI gives LOW output value 0 volt (logic 0). [5][2] The Negative Ternary Inverter is similar with the Standard Ternary Inverter the only difference in the output at the intermediate state that is at input voltage of 2.5volts where the output voltage is 0volts that is high output that's why this ternary inverter is called as Negative Ternary Inverter.

Input Logic Level (A)	Output Logic Level (Y)
0	2
1	0
2	0

Table-3: Truth Table of NTI

3. Design Of Ternary Gates

Using ternary inverters, the ternary logic gates are implemented. Like Binary NAND and NOR gates, ternary NAND and NOR gates can also be implemented. Here are some simple ternary NAND, T- NOR, T-AND, and T-OR gates that are designed and implemented. The implementation of ternary logic gates like T-NAND, T-NOR, T-AND, and T-OR are shown below. Depending upon the inverters used, T-AND and T-OR can be design using Standard, Positive and Negative T-AND and T-OR gates which will realize the function that are used in its applications.

T-NAND & T-AND GATES

The configuration of the T-NAND circuit is that the two PMOS circuits are connected in paralleland the two NMOS circuits are connected in series and both the combinations are connected inseries. The T-AND circuit is configured by connecting the Standard Ternary Inverter (STI) at the output of the T-NAND circuit.

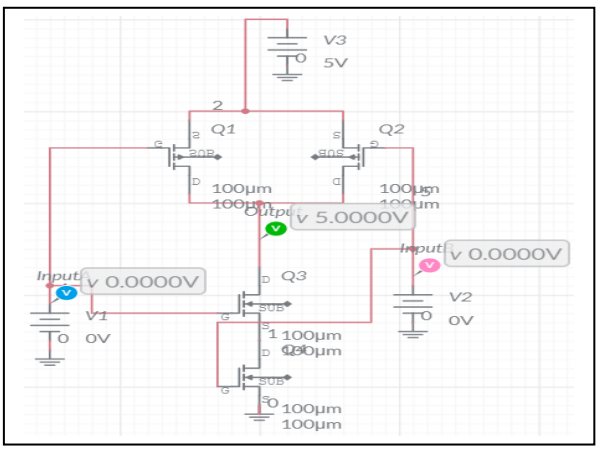

Fig. -4: (a) Schematic of T-NAND

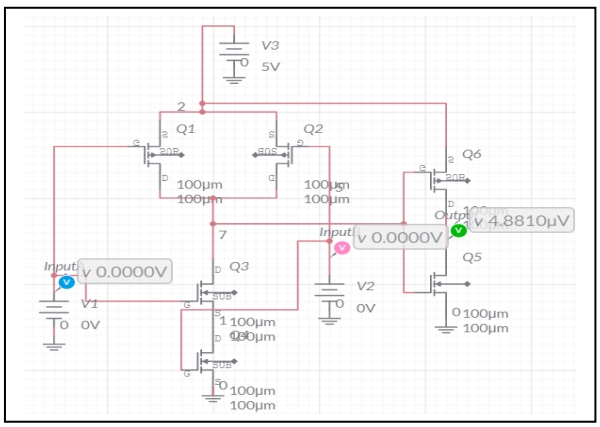

Fig. -5: (a) Schematic of T-AND

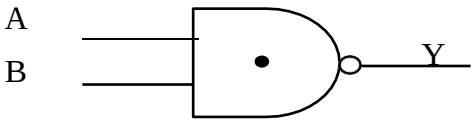

Fig. -4: (b) Symbol of T-NAND

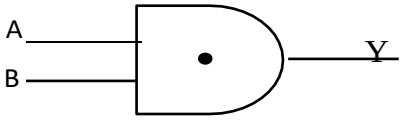

Fig. -5: (b) Symbol of T-AND

$Y_{NAND} = \min \{A, B\} Y_{AND} = \min \{A, B\}$

For the T-NAND, it contains two steps of logic operations: Firstly it minimizes the two inputs of A and B and then outputs the result after a NOT transformation. If the minimum input is "0", the output is "2". If the minimum input is "1", the output is "1". If the two inputs are all "2", the output is "0". The output of T-AND is the complement of T-NAND. [7]

Input Logic Level		Output Logic Level (Y)	
A	**B**	**T-NAND**	**T-AND**
0	0	2	0
0	1	2	0
0	2	2	0
1	0	2	0
1	1	1	1
1	2	1	1
2	0	2	0
2	1	1	1
2	2	0	2

Table-4: Truth Table of T-NAND and T-AND

T-NOR & T-OR GATES

The configuration of the T-NOR circuit is that the two PMOS circuits are connected in series and the two NMOS circuits are connected in parallel and both the combinations are connected in series. The T-OR circuit is configured by connecting the Standard Ternary Inverter (STI) at the output of the T-NOR circuit.

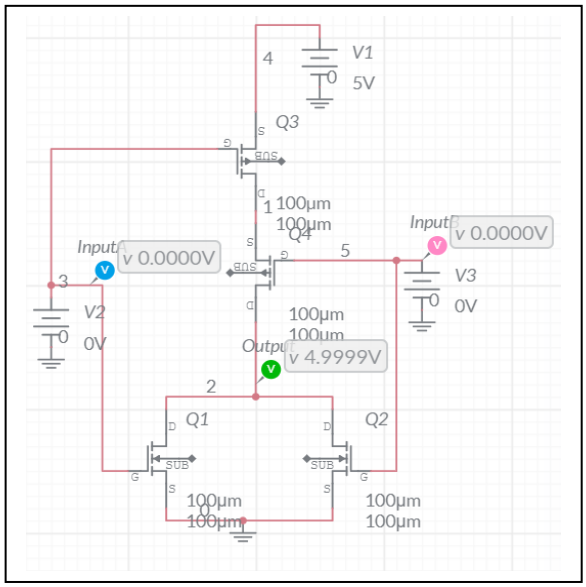

Fig. -6: (a) Schematic of T-NOR

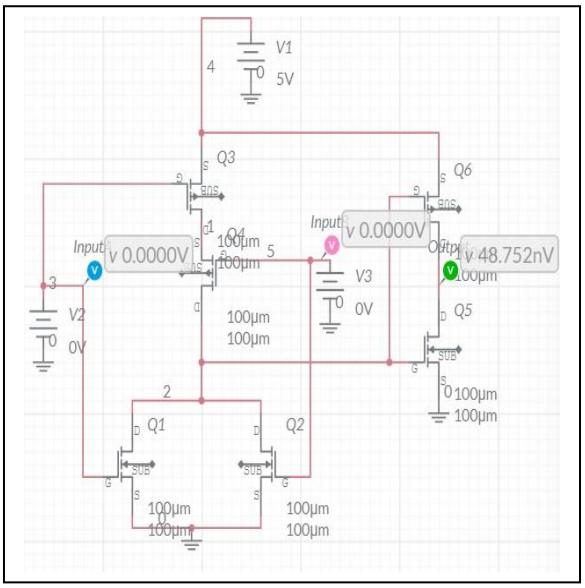

Fig. -7: (a) Schematic of T-OR

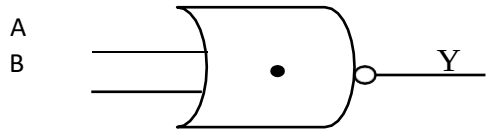

Fig. -6: (b) Symbol of T-NOR

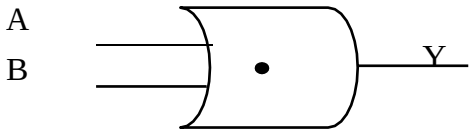

Fig. -7: (b) Symbol of T-OR

$Y_{NOR} = \max \{A, B\} Y_{OR} = \max \{A, B\}$

For the T-NOR, also contains two-step of logic operations: It maximizes the two inputs of A and B and then outputs the result after a NOT transformation. If the maximum input is "2", the output is "0". If the maximum input is "1", the output is "1". If the two inputs are both "0", the output is "2". [7]

Input Logic Level		Output Logic Level (Y)	
A	**B**	**T-NOR**	**T-OR**
0	0	2	0
0	1	1	1
0	2	0	2
1	0	1	1
1	1	1	1
1	2	0	2
2	0	0	2
2	1	0	2
2	2	0	2

Table-5: Truth Table of T-NOR and T-OR

4. SIMULATION AND RESULT

The designs and working of the basic ternary logic gates are explained in previous chapter. This chapter is about the simulations and result of the basic ternary logic gates and they are explain belowin brief as follows:

Standard Ternary Inverter (STI)

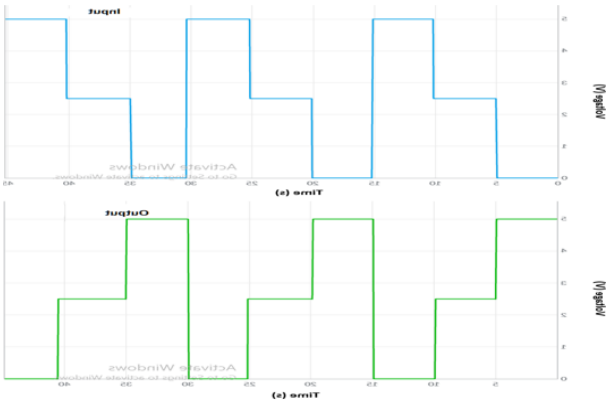

Input Voltage (V)	Output Voltage (V)	Threshold Voltage (V)
0	5	PMOS = 0 NMOS = 0
2.5	2.5	
5	0	

Fig. -8: Output Waveform and Observation Table of STI

The waveform and observation table of STI is mentioned above. We verified the observation table of STI with the standard observation table with the threshold values of PMOS and NMOS as 0 Volt. We observed in the waveform that when we apply the 0 volt then we get output as 5 volts and at 5 volts we get the output voltage as 0 volt and for the intermediate level i.e. 2.5 volts we get the output voltage same as the input voltage 2.5 volts.

Positive Ternary Inverter (PTI)

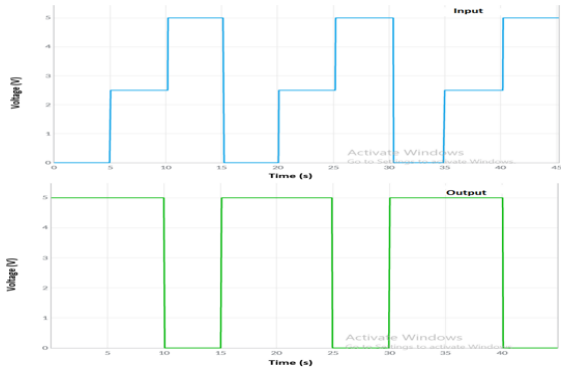

Input Voltage (V)	Output Voltage (V)	Threshold Voltage (V)
0	5	PMOS = -2 NMOS = 3
2.5	5	
5	0	

Fig.-9: Output Waveform and Observation Table of PTI

The waveform and observation table of PTI is mentioned above. We verified the observation table of PTI with the standard observation table with the threshold values of PMOS as -2 Volts and NMOS as 3 Volts. We observed in the waveform that when we apply the 0 volt then we get output as 5 volts and at 5 volts we get the output voltage as 0 volt and for the intermediate level i.e. 2.5 volts we get the output voltage as 5 volts. As we get the high voltage at the intermediate level therefore this ternary inverter known as Positive Ternary Inverter.

Negative Ternary Inverter (NTI)

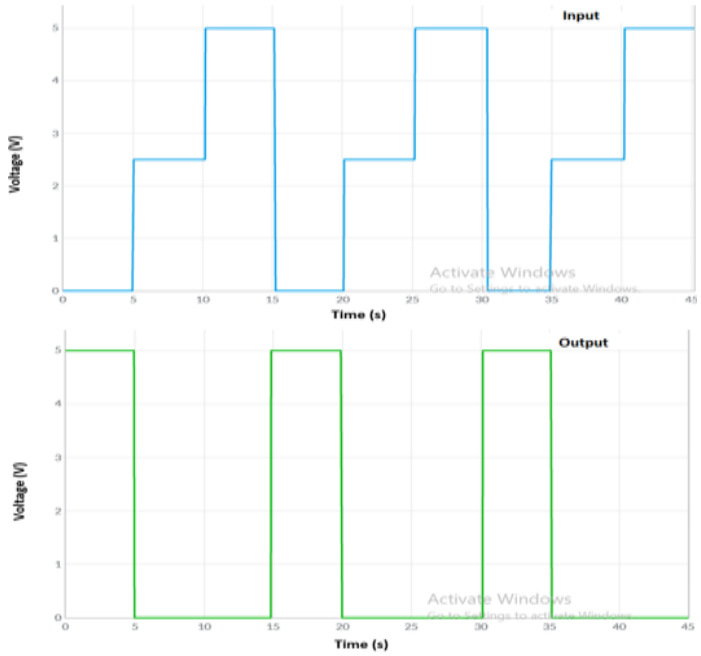

Input Voltage (V)	Output Voltage (V)	Threshold Voltage (V)
0	5	PMOS = -2.5 NMOS = 2
2.5	0	
5	0	

Fig. -10: Output Waveform and Observation Table of NTI

The waveform and observation table of NTI is mentioned above. We verified the observation table of NTI with the standard observation table with the threshold values of PMOS as -2.5 Volts and NMOS as 2 Volts. We observed in the waveform that when we apply the 0 volt then we get output as 5 volts and at 5 volts we get the output voltage as 0 volt and for the intermediate level i.e. 2.5 volts we get the output voltage as 0 volts. As we get the low voltage at the intermediate level therefore this ternary inverter known as Negative Ternary Inverter.

Ternary NAND (T-NAND)

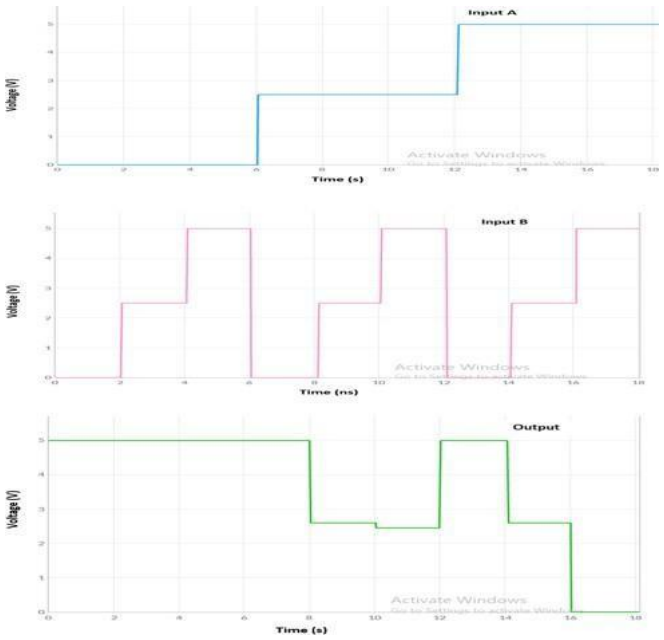

Input Voltage (V)		Output Voltage (V)	Threshold Voltage (V)
A	**B**	**T-NAND**	
0	0	5	
0	2.5	5	PMOS = -2.5
0	5	5	NMOS = 4.5
2.5	0	5	
2.5	2.5	2.5	
2.5	5	2.5	
5	0	5	
5	2.5	2.5	
5	5	0	

Fig. -11: Output Waveform and Observation Table of T-NAND

The waveform and observation table of T-NAND is mentioned above. We verified the observation table of T-NAND with the standard observation table with the threshold values of PMOS as -2.5 Volts and NMOS as 4.5 Volts. When we applied both the inputs as 0 volts we get the output as 5 volts. Similarly, when we applied both the inputs as 5 volts we get 0 volts and at intermediate level when we applied both the inputs as 2.5 volts we get output as 2.5 volts.

Ternary AND (T-AND)

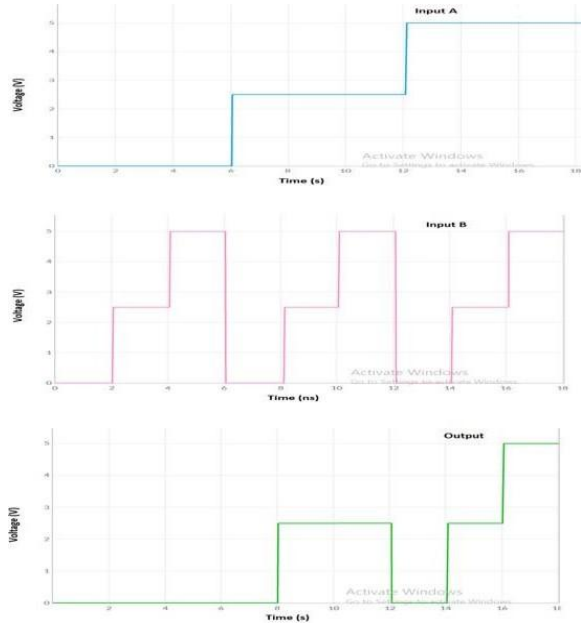

Input Voltage (V)		Output Voltage (V)	Threshold Voltage (V)
A	**B**	**T-AND**	
0	0	0	
0	2.5	0	PMOS = -2.5
0	5	0	NMOS = 4.5
2.5	0	0	
2.5	2.5	2.5	
2.5	5	2.5	
5	0	0	
5	2.5	2.5	
5	5	5	

Fig. -12: Output Waveform and Observation Table of T-AND

The waveform and observation table of T-AND is mentioned above. We verified the observation table of T-AND with the standard observation table with the threshold values of PMOS as -2.5 Volts and NMOS as 4.5 Volts. As we know that Ternary AND is the complement of the Ternary NAND inverter therefore When we applied both the inputs as 0 volts we get the output as 0 volts. Similarly, when we applied both the inputs as 5 volts we get 5 volts and at intermediate level when we applied both the inputs as 2.5 volts we get output as 2.5 volts.

Ternary NOR (T-NOR)

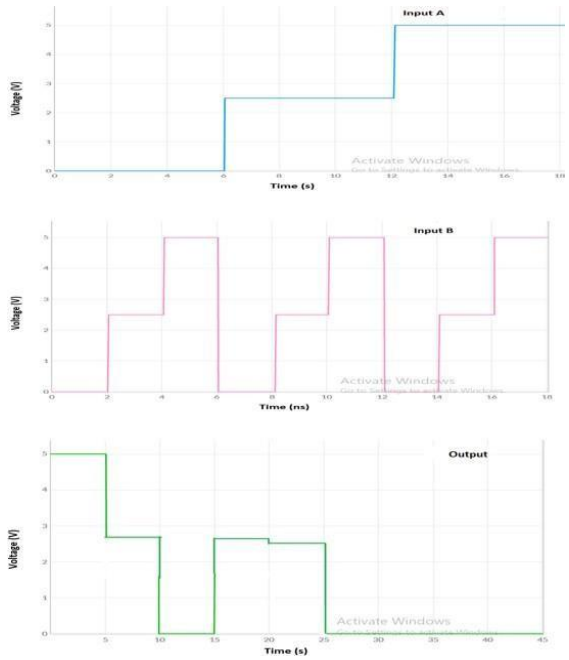

Input Voltage (V)		Output Voltage (V)	Threshold Voltage (V)
A	**B**	**T-NOR**	
0	0	5	
0	2.5	2.5	
0	5	0	PMOS = -4
2.5	0	2.5	NMOS = 2.5
2.5	2.5	2.5	
2.5	5	0	
5	0	0	
5	2.5	0	
5	5	0	

Fig. -13: Output Waveform and Observation Table of T-NOR

The waveform and observation table of T-NOR is mentioned above. We verified the observation table of T-NOR with the standard observation table with the threshold values of PMOS as -4 Volts and NMOS as 2.5 Volts. When we applied both the inputs as 0 volts we get the output as 5 volts. Similarly, when we applied both the inputs as 5 volts we get 0 volts and at intermediate level when we applied both the inputs as 2.5 volts we get output as 2.5 volts.

Ternary OR (T-OR)

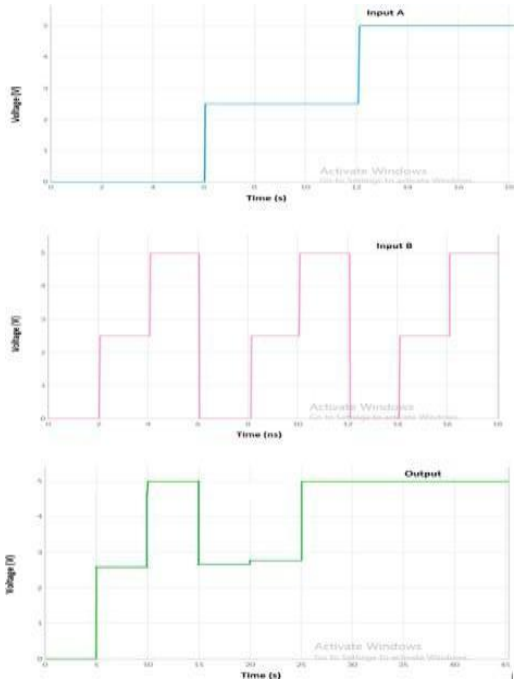

Input Voltage (V)		Output Voltage (V)	Threshold Voltage (V)
A	B	T-OR	
0	0	0	
0	2.5	2.5	
0	5	5	
2.5	0	2.5	PMOS = -4
2.5	2.5	2.5	NMOS = 2.5
2.5	5	5	
5	0	5	
5	2.5	5	
5	5	5	

Fig. -14: Output Waveform and Observation Table of T-OR

The waveform and observation table of T-OR is mentioned above. We verified the observation table of T-OR with the standard observation table with the threshold values of PMOS as -4 Volts and NMOS as 2.5 Volts. As we know that Ternary OR is the complement of the Ternary NOR inverter therefore When we applied both the inputs as 0 volts we get the output as 0 volts. Similarly, when we applied both the inputs as 5 volts we get 5 volts and at intermediate level when we applied both the inputs as 2.5 volts we get output as 2.5 volts.

Power Consumption Waveform of Binary Inverter

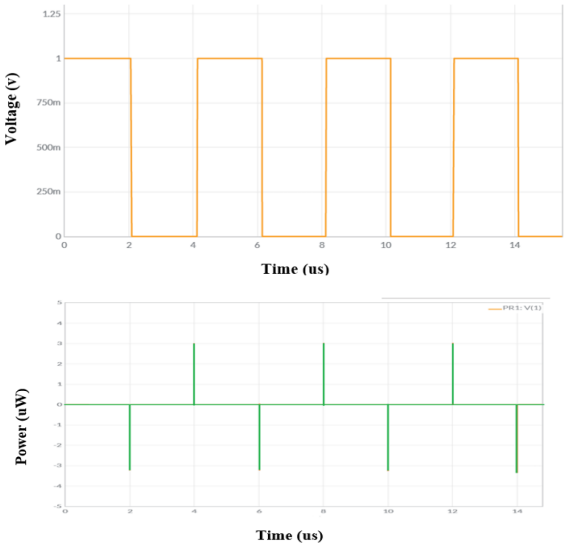

Logic Levels	Power Consumption (uW)
0-1	3.4
1-0	4

Fig. -15: Power Consumption Waveform of Binary Inverter

The power consumption waveform of Binary Inverter is shown above. The numeric values of power consumption in micro Watt (uW) are shown in the table. In which the power consumption of Binary Inverter for logic levels low to high we observed the power consumption is about 3.4uW and for logic levels high to low the power consumption is observed as 4uW.

Power Consumption Waveform of Ternary Inverter

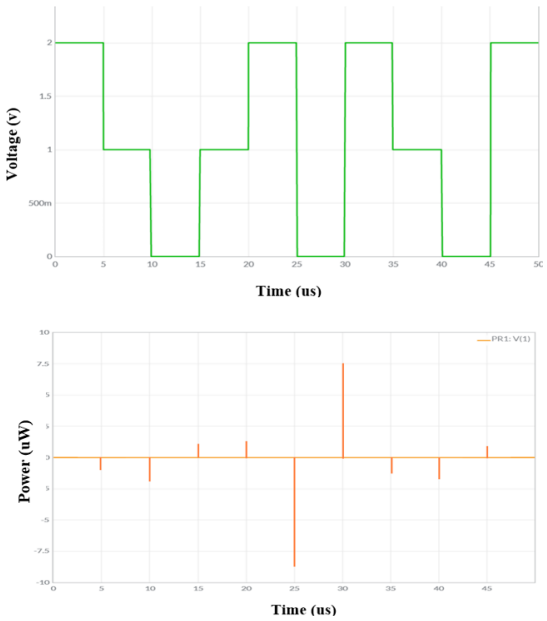

Logic Levels	Power Consumption (uW)
0-1	1
1-2	1.2
2-1	1
1-0	2
0-2	7.5
2-0	8.7

Fig. -16: Power Consumption Waveform of Ternary Inverter

By analyzing the numerical values for the maximum power consumption, listed in Table one can easily observe that the power consumption is noticeably smaller for edges between intermediate levels than for extreme levels (0 to 2, 2 to 0). The values for intermediate level edges are similar, so they cannot be used to identify the transition type (positive/negative). The power consumption for edges between extreme values is about five times bigger than the one for intermediate levels and the edge of the output voltage can be identified.

Compared to the values obtained for the extreme level's edges of the ternary inverter, the power consumption for the binary inverter is about 50% smaller, but still bigger than the values for the edges between intermediate levels. The edges of the output signal can easily be deduced by analyzing the power consumption, which makes the binary inverter vulnerable to power analysis attacks.

5. Conclusion

In the nutshell, all the listed project objective which to design the standard cell of CMOS Ternary inverter, Ternary NAND and Ternary NOR was successful and all the desired output produced is stated and tabulated. All the simulation process is designed using the EDA tools which is online Multisim Software. From the implementation of basic ternary logic gates, we can conclude that in ternary more bits of information can process than binary. The implementation of basic ternary logic gates can be achieved by changing the threshold voltages in Standard Ternary Inverter. As there is more power dissipates in the registers, we proposed the ternary designs without using registers. A comparison on the power consumption analysis between Binary and Ternary design has been made, it shows that the Ternary standard cell consumes more power to produce the output than in Binary. Hence, Ternary can load more data at one time than the Binary which signed that there is a

trade-off between power and the complexity of interconnections.

6. Future scope

Based on this project study, it is recommended that using a Ternary schematic design cell which is Ternary inverter, NAND and NOR will reduce the interconnections and complexity of the circuit. However, as the elements in the MVL are increased, the process of fabricating the circuit also increase as the increase in the complexity. Next, it is recommended that Ternary standard cell shouldbe used in developing technology such as Switch Box and other FPGA applications. As the technology keep in advancing, continuous and dedicated study on other application of Ternary can play major role and difference in the future technology.

References

1. Savitri Vanjol, Pradnya Pawar, "Design of Low Power CMOS Ternary Logic Gates".
2. A.P.Dhande, V. T. Ingole (2005) "Two Digit Parallel Analog to Ternary Converter".
3. Makani Nailesh Kishor, and Satish S. Narkhede (2016) "A Novel Finfet Based Approach For The Realization Of Ternary Gates".
4. E. Dubrova, "Multiple-valued logic in VLSI: challenges and E. Dubrova, "Multiple-valued logic in VLSI: challenges and 340- 350.
5. G. Thrishala, K.Ragini (2020) "Design and Implementation of Ternary Logic Circuits for VLSIApplications".
6. Emilia SIPOS, Robert GROZA, Laura N. Ivanciu (2017), "Power Consumption And Noise Margin Comparison Between Simple Ternary Inverter And Binary Inverter".
7. Mingqiang Huang, Xingli Wang, Guangchao Zhao, Philippe Coquet, and Bengkang Tay, (2019) "Design and Implementation of Ternary Logic Integrated Circuits by Using Novel Two-Dimensional Materials".

IMPLEMENTATION OF MPPT ALGORITHM FOR GRID INTERFACE PV SYSTEM USING TWELVE PULSE CONVERTER

H.R. Patil[*1], P.A. Kale[2] and P.V.Kapoor[3]
Shri Ramdeobaba College of Engineering and Management, Nagpur
[1]patilhr@rknec.edu, [2]kalepa@rknec.edu,[3]kapoorpv@rknec.edu

ABSTRACT

In the era of "Green energy – Clean energy" solar photovoltaic system comes out to be the foremost prominent alternative within electricity sector. The performance of the solar photovoltaic array gets easily altered by variation in irradiance and temperature attributable to its non-linear I-V characteristics resulting shift in its maximum power point. To extend or to maximize the output power of the solar photovoltaic (PV) system, Maximum Power Point Tracking (MPPT) techniques are accustomed operate the PV system at its maximum power point. During this paper, a grid-tied PV system through a three-phase twelve pulse line commuted converter (LCC) is proposed with an efficient maximum point tracking controller which is modeled using Perturb and Observe method. The paper presents the design and simulation of the proposed grid feeding PV system. Developed MPPT controller tracks the MPP by sensing the current and voltage of PV system which accordingly computes, generates, and maintains firing angle alpha of the LCC for Maximum point operation.

Keywords: *Line commuted converter, Maximum power point tracking, Photovoltaic Array, Voltage source inverter.*

1. Introduction

The growth in industrialization, population, and urbanization is continuously increasing the energy demand. The dearth of fossil fuels and climate-related changes leads to energy crises in the coming decades. Solar energy is nothing, but renewable energy becomes very popular and its energy imports have increased consistently by 25%-30% every year, over the past two decades. Therefore, renewable-based power generation system and their grid interconnection throughout the world came into the picture(RamanujaPanigrahi, Santanu K. Mishra, 2020). Solar energy with its wide availability and negligible operational and maintenance cost has become the most promising substitute. Solar PV systems deliver DC power which has to be converted to AC employing a power electronic interface. Voltage source inverter topologies with pulse width modulation technique to improve quality of injected power are most popular for such interfacing PV system with AC grid (J. M. Kumbhare, M. M. Renge, 2014).

With such topologies Grid synchronization becomes a difficult task for interfacing converters with the grid as in synchronization, information about the phase angle of grid voltage is necessary to transfer the power from converters. Phase-Locked Loop, Fourier analysis techniques are used to maintain the synchronism (Yasir Sheikh, SudarshanKhond, Dr. M. M. Renge, 2019). Conventional HVDC link interfaces dc grid with ac grid with natural commutation. These line commuted converters do not need a dedicated synchronizing circuit like a VSI converter when connected to ac grid. These line commuted converter LCC also provides the inherent anti-islanding feature along with improved harmonic mitigation as it eliminates harmonics up to 11^{th} order resulting in enhanced power quality.

As the output power output delivery of the photovoltaic system is associated with the temperature and irradiance the abrupt change in condition directly affects the power delivered affecting the overall efficiency of the system. MPPT controllers are used to controlling power output and to ensure that maximum power is extracted irrespective of variation in irradiance and temperature (Abhishek Kumar Gupta, Ravi Saxena, 2016). Different algorithms have been developed for MPPT tracking such as the P&O method, incremental conductance method, fuzzy logic controller, and genetic algorithm. Perturbation and observe and incremental conductance are the most widely used MPPT algorithms as they are most efficient and hands-free to implement.

2. System Description and Working Principle

A schematic diagram for a Grid-connected PV system employing a three-phase twelve pulse

LCC is shown in Fig.1. The elementary scheme utilizes a power electronic interface (LCC) for interfacing PV array with AC grid. Series and parallel combination of PV module is accordingly computed for desired power output. The MPPT control computes alpha at MPP. The firing angle control generates this firing angle alpha to work twelve pulse LCC at inversion mode ensuring maximum point operation of the PV system.

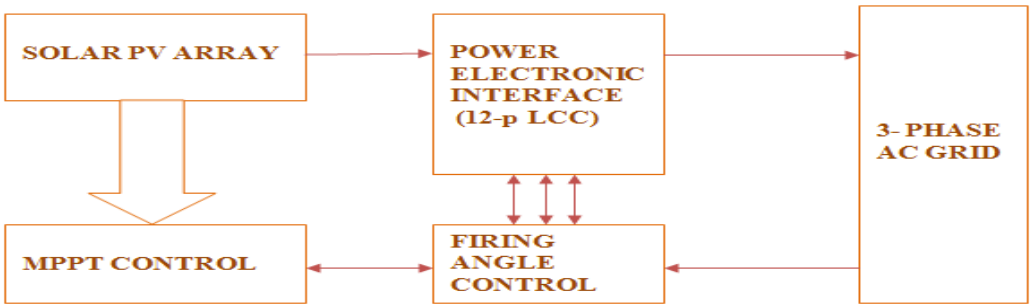

Figure 1. Schematic block diagram

2.1. Line Commutated Converter

A twelve-pulse converter is obtained by suitably connecting two Six-pulse converters. The fifth and seventh harmonics in input current are eliminated in twelve pulse converters. Also, the layout of smoothing inductance is reduced due increase in pulse number which minimizes the ripple in output. The development of distortion factor results in improvement of power factor. A rectification mode for firing angle ($\alpha<90°$) is the mode of operation of a line commuted twelve pulse converters. The transformers utilized in the twelve pulse converter are going to be normally connected with primary Y-Y and secondary is Y-Δ winding(O.Wasynczuk,1989).

The most purpose of this is often to supply a 30° phase shift, which may be ready to provide twelvepulses output also on provide isolation between the two six pulse bridge rectifier circuits. Since two valves conduct at an equivalent time in each bridge, there'll be 4 valves conducting at a time during a 12-pulse bridge converter. When firing angle ($\alpha>90°$), the converter operates in inversion mode. The converter operation in inversion mode can only be maintained if the DC load is replaced by a DC source.

This DC source must get replaced such positive polarity is connected to the common anodes and negative polarity to the common cathodes with the goal that it defeats negative voltage and forces the present to steer an identical way contrary to the actuated EMF within the converter transformer. This recommends power is being provided from the DC to the AC system. The converter is functioning as an inverter. Within the proposed scheme, it's working as an inverter with a firing angle $\alpha=155°$, delivering the DC power of the PV array to the AC grid.

2.2. Solar Photovoltaic Array

A solar cellisa tool that converts light energy into electrical form. The photovoltaic cells are connected in serial and parallel combinations depending upon the need of the load. Parallel cells end within the addition of currents while keeping the voltage constant whereas the series combination adds the voltage magnitudes. The PV array is interfaced with an AC grid line with a line voltage of 440 V. SOLO TECH 1STH-230P solar array is employed.

A string of four PV panels is connected serial to urge dc-link voltage and to provide the specified current one string is connected in parallel. The specification of solar array as follows, V_{OC} =37.1 V, I_{SC} = 8.18A, V_{MPP} =29.9v, I_{MPP} =7.65A, N_{CELL}=60/Module.

2.3. Maximum Power Point Tracking (MPPT)

The Perturb-and-observe algorithm for max point tracking is that the only technique among all the MPPT techniques in pieces of literature. It's supported the straightforward mathematical condition, i.e. $\Delta P/\Delta V = 0$, where P and V are power and voltage at the output of the PV module respectively (S. Lenin Prakashl, M. Arutchey,S. Stephy Sharon, 2015). PV array voltage (V_{PV}) is obtained by this method to manage the facility flow between the ac grid

and thus the PV system also it's possible to understand the utmost point tracking (MPPT) of the PV array by changing the firing angle of LCC for various solar irradiance. The developed method observes the power of the PV array by changing the supplied voltage. If there is a rise in power due to increasing voltage then further firing angle α is incremented otherwise start decrementing the firing angle (α). this is often continued till maximum point is detected.

3.Simulation Results and Validation

Simulation architecture of proposed grid-connected PV system is shown in Fig. 3. To verify the validity of the proposed technique, Simulation is administered in MATLAB/Simulink. A three-phase twelve pulse line commuted converter is implemented for interfacing solar PV array with AC grid. The specification of the solar PV array is chosen to transfer 1 kW power to the AC grid. The simulation is run under constant also as varying irradiance to research the effectiveness of the proposed scheme.

In the proposed scheme, LCC is operated as an inverter. Firing angle control sense the voltage ii incoming and outgoing phase of conducting sequence to effectively detect the firing instant to urge gate pulse for the corresponding thyristor at a daily interval of 30°. Maximum point Tracking (MPPT) algorithm is implemented which is modelled using the Perturb and Observe method which tracks the utmost point (MPP) continuously and accordingly controls firing angle alpha during the operation to maximize the power delivery by the PV system.

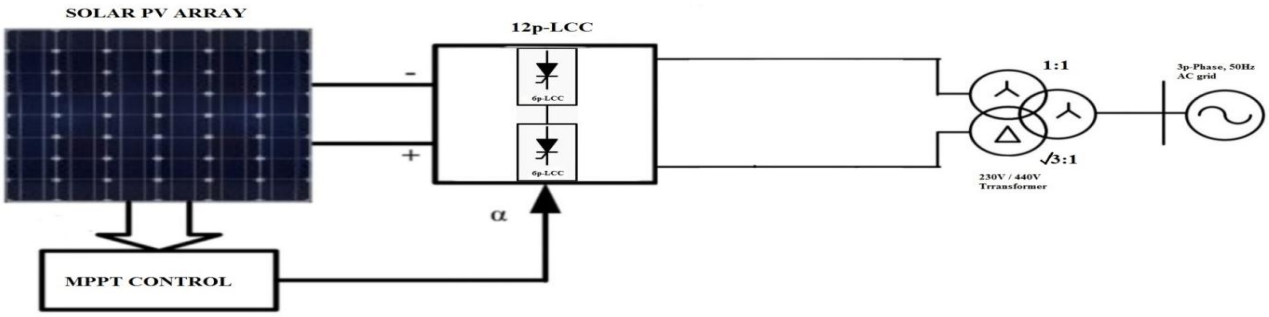

Figure 2. Configuration of simulated architecture

Simulation is performed by varying the firing angle (α) within the range 120° to 180°. Fig. 4 shows the PV array voltage (V_{PV}), the facility delivered by it (P), and therefore the firing angle (α) without the controller. Results show us that variation within the firing angle (α) also results in variation in MPP. The MPP is detected at firing angle α=155°.

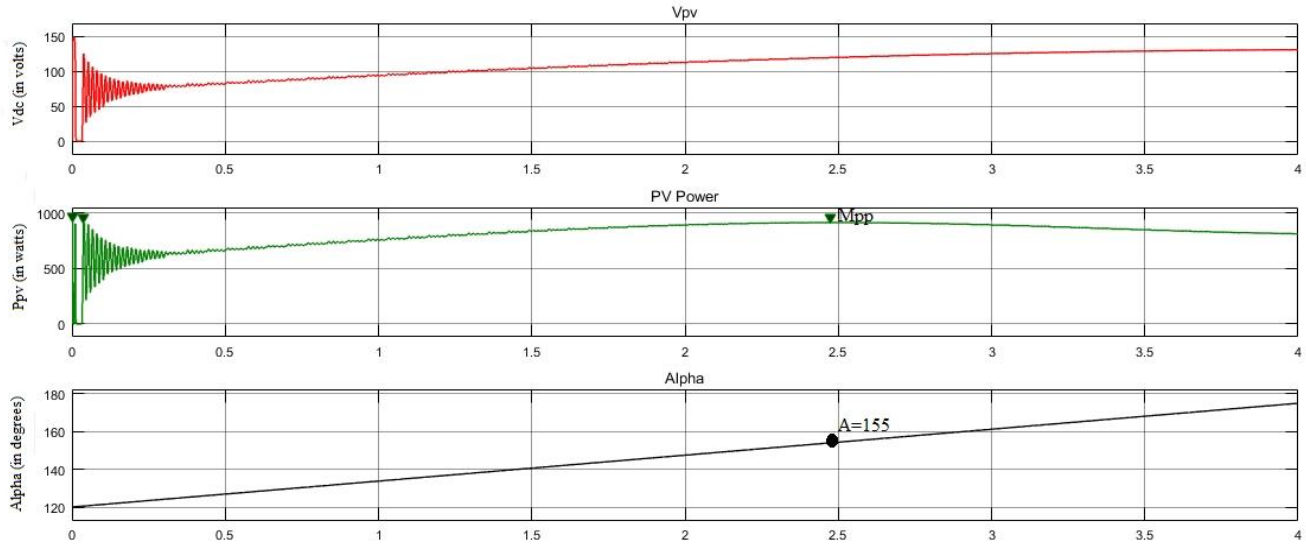

Figure 3. PV voltage (V_{PV}), PV array power (P_{PV}), and Firing angle Alpha (α) without MPPT controller for constant irradiance (1000W/m²)

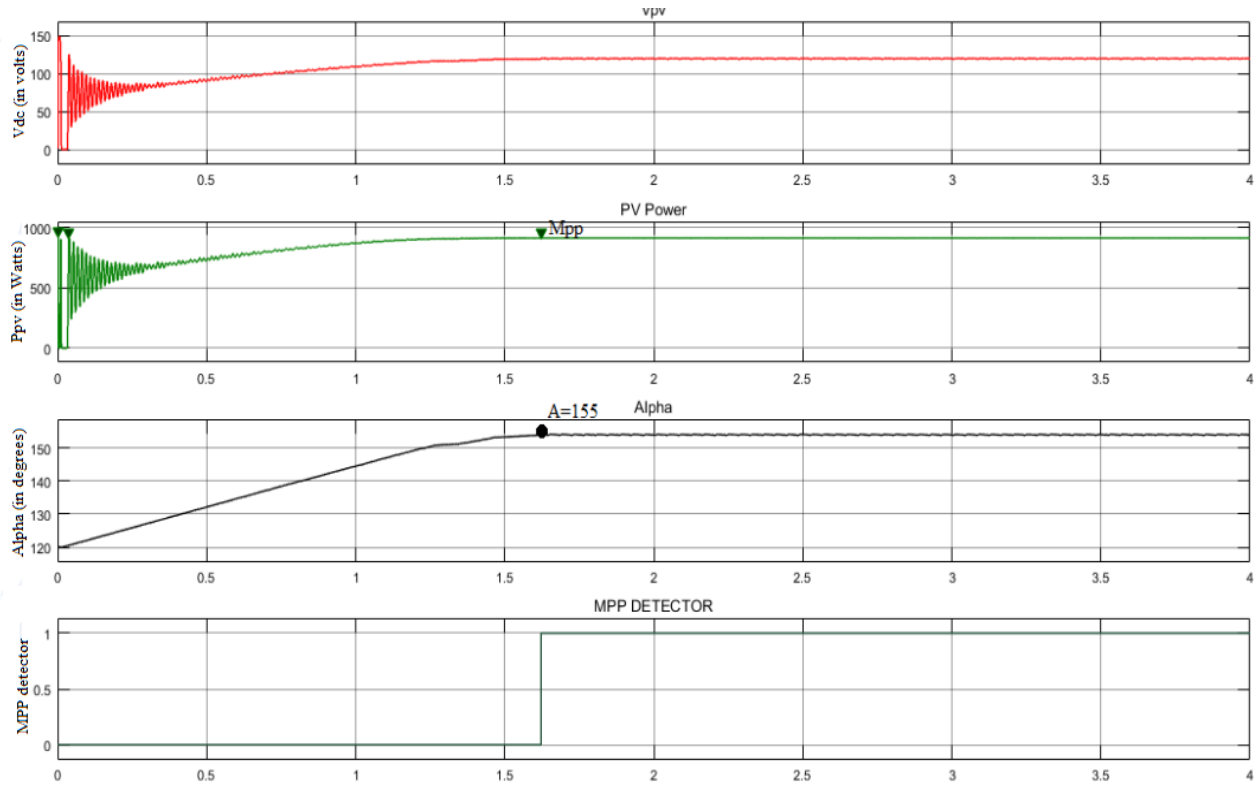

Figure 4.PV voltage (V_{PV}), PV array power (P_{PV})and Firing angle Alpha (α) withMPPT controller for constant irradiance (1000W/m²)

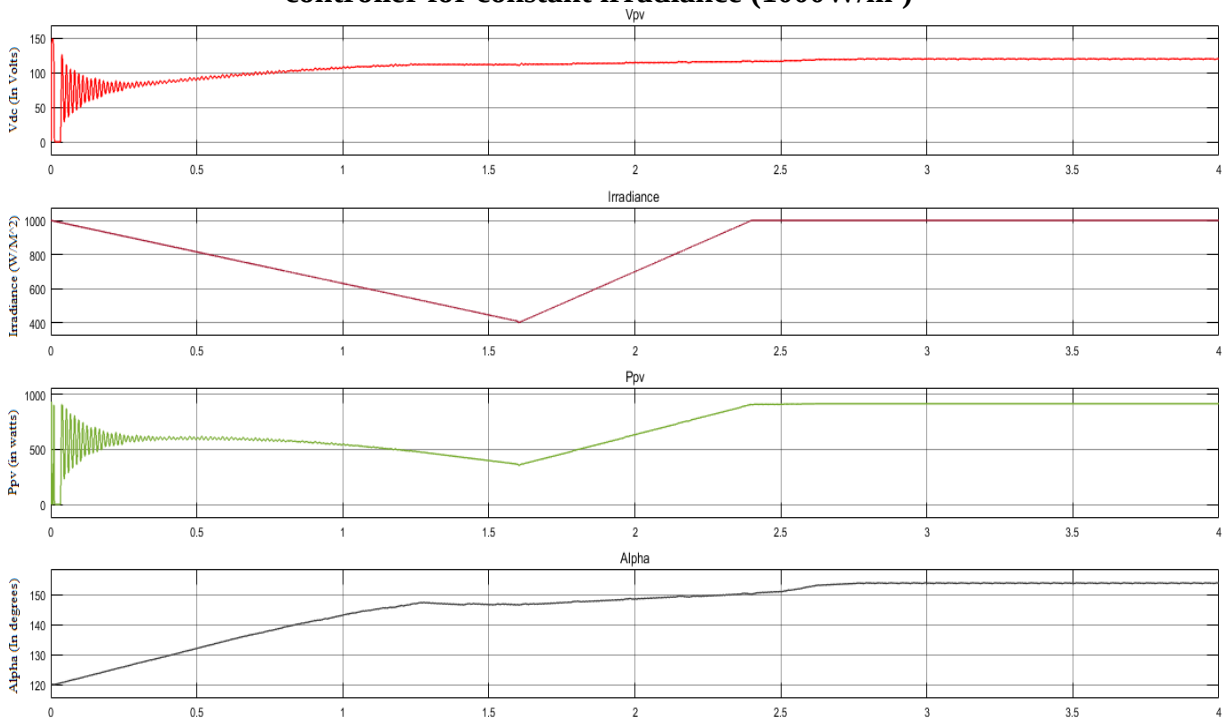

Figure 5. PV voltage (V_{PV}), VaryingIrradiance(W/m²),PV array power (P_{PV})and Firing angle Alpha (α) withMPPT controller for varying irradiance

MPPT controller sense the change in power output by PV array concerning change voltage of the array (ΔP/ΔV) and generates a pulse at zero instant holding the worth of firing alpha. Thus, it's observed in simulation that the α settles at the value reminiscent of the voltage which is able to lead to maximum power from PV array Fig. 4 shows PV array voltage (V_{PV}), the power delivered by it (P_{PV}), and firing angle (α) with the controller. The MPPT controller keeps the firing angle constant at MPP ensuring maximum power point operation.

To research the effectiveness of the MPPT controller the simulation is additionally performed for varying irradiance concerning time. for every change within the value of irradiance and, the power delivered varies accordingly and therefore the controller tries to take care of firing angle (α) at MPP effectively resulting to maximum point operation. Fig. 5 shows the PV array power (P_{PV}), PV array voltage (V_{PV}), and Firing angle Alpha (α) with MPPT controller for varying irradiance.

4. Conclusion

The study proposes an effective MPPT algorithm for a grid-connected PV system. System is simulated in MATLAB/Simulink. Results validate the assurance and feasibility of the developed architecture. There's no need for dedicated synchronizing to keep up synchronism while such PV array and AC grid interface. The simulated results showed that the MPPT mechanism developed is effective and straightforward to trace the MPP**.**

References

1. J. M. Kumbhare, M. M. Renge. (2014). Line commutated Converter for grid interfacing of solar photovoltaic array. International Conference on Power Electronics, Drives and Energy Systems(PEDES)978-1-4799-6373-7/14/$31.00.
2. Bimal K.Bose(2000).Energy, Environment, and Advances in Power ElectronicsIEEE Trans. On Power Electronics. IEEE Transactions On Power Electronics, VOL. 15, NO. 4, JULY 20000885–8993/00$10.00.
3. RamanujaPanigrahi,Santanu K. Mishra. (2020). Grid Integration of Small-Scale Photovoltaic Systems in Secondary Distribution Network. A Review. IEEE Transactions on Industrial Applications, VOL. 56, and NO. 3, 0093-9994.
4. Abhishek Kumar Gupta, Ravi Saxena. (ICICCS 2016). Review on widely-used MPPT Techniques for PV Applications. 1st International Conference on Innovation and Challenges in Cyber Security, 978-1-5090-20843/16/$/31.00.
5. S. Lenin Prakash, M. Arutchey, S. Stephy Sharon. (ISCO 2015). Simulation and Performance Analysis of MPPT for Single Stage PV Grid Connected System. IEEE Sponsored 9th International Conference on Intelligent Systems and Control,978-1-4799-6480-2/15/$31.00.
6. Saurabh Thakran, Jaspreet Singh, Prof. Rachan Garg, Dr.Priya Mahajan. (2018) .Implementation of P&O Algorithm for MPPT in SPV System. International Conference on Power Energy, Environment and Intelligent Control (PEEIC)G. L. Bajaj Inst. of Technology and Management Greater Noida, U. P., India, 978-1-5386-2341-1/18/$31.00.
7. Yasir Sheikh, Sudarshan Khond, Dr. M. M. Renge. (Dec 2019). Interfacing of PV Array with AC Grid using Twelve Pulse Converter. Helix Journal, Vol. 9, No. 6, 5884-5888.
8. O.Wasynczuk. (September1989). Modelling and dynamic performance of line-commutedphotovoltaic inverter system. IEEE Transactions on Energy Conversion, Vol. 4, No. 3, 0885-8/89/0900-0337$01.00.
9. T. Shanthi, N. Ammasai Gounden. (2007). Power Electronic Interface for Grid-Connected PV array using Boost Converter and Line-Commutated Inverter with MPPT. International Conference on Intelligent and Advanced Systems, 882–886. 1-4244-1355-9/07/$25.00.

INFLUENCE ON PROPERTIES OF CONCRETE DUE TO ADDITION OF NANO TITANIUM OXIDE PARTICLES: A REVIEW STUDY

G.Rawat[1], S.Gandhi[2] and Y. Iyer Murthy[3]
Department of Civil Engineering, Jaypee University ofEngineering & Technology, Guna, INDIA,
[1]garimaknp07@gmail.com

ABSTRACT

Nanomaterials has drawn tremendous scientific attention due to possible uses of molecules at nanometer range using which the cement properties such as durability, mechanical properties, pore structure and microstructure of cement based matrix can be improved. However its optimum content is also justified on the basis of water-binder ratio, condition of curing (age), pozzolonic content/type and chemical admixture. It enhances the concrete mix design by eradicating chloride penetration, chemical shrinkage resistance, abrasion resistance, fire and freeze resistance. Study also suggests investigation of different nanomaterials such as TiO_2, nano ZnO, nano ZrO_2, nano Al_2O_3 and nano Fe_3O_4 and their addition in cement based materials for the purpose of enhancement of properties.

Keywords: *Nanomaterials, Replacement, Durability, Mechanical Properties.*

1. Introduction

The characteristics of good quality concrete are its fabrication, low cost, better performance, and its applicability. However, the impediments of concrete, such as low strength, vulnerability to cracking, and sudden failure due to brittle nature, have led to its deterioration and high repairing costs. Most of the degradation occurs in the marine environment due to the high concentration of chloride ions and sulfate ions that affect the durability of concrete structures. Several components affect the corrosion rate of embedded reinforcement, such as chloride ion concentration, type of cement, alkalinity, and temperature. Salman et al. [1] stated that concrete behavior is influenced by its durability, porous nature, and resistance against penetration of harmful agents such as sulfate and chloride ions. The penetration of these agents lowers the performance by causing the local breakdown of the passive layer and corroding the embedded steel rebars.

As per Nazari et al.[2], the capillary pores form an interconnected network that facilitates impurities' penetration into the concrete. Pores can be categorized as air trapped, air-entrained, gel, and capillary pores, and they contribute to the transport of impurities through diffusion, permeation, and migration. There is a need for sustainable infrastructure with higher durability and low repairing costs. The development of new-age cement-based materials by incorporating auxiliary cementitious materials such as pozzolans and nanomaterials to subside the degradation of structures is extensively done. Recently, the use of nanomaterials has drawn tremendous scientific attention due to the possible benefits of molecules at the nanometer range (10^{-9} m). This is possibly due to nano sizes which can amend properties of molecules having foreseeable particle size and the same chemical composition. According to Nazari et al. [3], the incorporation of nanomaterials in concrete specimens has received global attention to improving the durability, mechanical properties, pore structure, and microstructure of cement-based materials. Wang et al.[4], used nano titanium dioxide to enhance the effect through various approaches, such as filler material, hydration of cement, and high-density C-S-H structure formation through parallel packing.

Work presented by Iyappan et al.[5] demonstrates nano titanium dioxide to facilitate the resistance of concrete against physical and chemical deteriorations and its favorable effects on the technical properties of concrete. Joshaghani et al. [6] state that nano-titanium dioxide has achieved so much attention due to its high catalytic activity, chemical stability, and low price. It contributes to the improvement of mechanical properties, rheological and durability properties of cement-based materials.

1. Theory and Discussion

Workability and Setting Time

Salemi et al. [7] observed that the addition of 2 % nano titanium dioxide leads to a reduction in the workability of concrete. In contrast, the

slump was 60 mm while it is 120 mm for the control mixture. Nazari et al. [8], investigated the workability of concrete with nano TiO_2 with 0 %, 0.5%, 1 %, 1.5 % and 2 % replacement of cement by weight. There was a reduction in the workability seen due to nano TiO_2, and it increases with increasing nano TiO_2 content. Li et al. [9] also reported a reduction in workability of concrete mixtures due to partial replacement with nano TiO_2 at 0 %, 1 %, and 3 % levels. Li et al. [10], and Li [11], observed the slump values of concrete modified with nano TiO_2 at proportions of 0 %, 1 %, 3 %, and 5 % by weight. The results indicated a reduction in the slump values with the addition of 1 % or 3 % nano TiO_2 was 54.54 %, while withthe addition of 5 % of nano TiO_2, the reduction was 72.75 %. Table 1 below shows the slump value obtained by various authors when TiO_2 is used.

	Slump (cm)		
ref	**0% TiO_2**	**1%TiO_2**	**2% TiO_2**
Nazari et al.[7]	8.52	6	2.98
Nazari et al.[25]	8	5.3	2.2
Sorathiya et al.[34]	7.2	4.25	2.6

Table-1: Slump of nano titanium dioxide blended concrete

Jalal et al. [13] investigated the slump flow of self-compacting concrete mixtures partially replacedwith nano TiO_2 at proportions of 0 %, 1 %, 2 %, 3 %, 4 %, and 5 % by weight and finds it reduces.

Jalal et al.[14] also tried to determine the properties of high-strength self compacting concrete mixed with nano TiO_2 at proportions of 0 %, 1 %, 2 %, 3 %, 4 %, and 5 % by weight. The result indicated a reduction in the workability due to an increment in nano TiO_2 in the mixture. Also, reduction in slump diameter reported was 1.25 %, 2.5 %, 5 %, 7.5 % and 8.75% respectively.

Senff et al. [15]analyzed the rheological and flow table of mortar mixtures incorporated with nano TiO_2 at levels 0 %, 1.3 %, 2.6 %, and 5.2 % by weight and found increment in torque values yield stress. As the nano content increases, these values increased accordingly.

	Initial Setting Time(min)				
ref	**0% TiO_2**	**0.5%TiO_2**	**1.0% TiO_2**	**1.5% TiO_2**	**2.0% TiO_2**
Nazari et al.[7]	225.36	171.53	145.98	119.52	104.92
Nazari et al.[8]	225.1	170.12	145.22	119.29	105.8
Khataee et al.[13]	160	152	141	134	120

Table-2: Initial setting time of nano titanium dioxide blended concrete

	Final Setting Time(min)				
ref	**0% TiO_2**	**0.5%TiO_2**	**1.0% TiO_2**	**1.5% TiO_2**	**2.0% TiO_2**
Nazari et al.[7]	335.74	261.85	252.77	221.66	207.4
Nazari et al.[8]	335.65	262.5	251.02	220.9	206.5
Khataee et al.[13]	270	268	257	249	240

Table-3: Final setting time of nano titanium dioxide blended concrete

Chen et al. [17] considered two kinds of nano TiO_2, P25 (75% anatase and 25% rutile) and anatase (99% anatase). They investigated the initial and final setting time of concrete with nano TiO_2 at levels 0 %, 5 %, and 10 % by weight. The results indicated that pastes with the higher nano TiO_2 content had a shorter setting time. Lee [18]observed the initial and final setting time of concrete mixtures partially replaced with nano TiO_2 with 0 %, 5 %, and 10 % by weight and found a significant reduction in the initial and final setting time. Nazari et al. [2] reported the same result for the replacement with nano TiO_2 at levels of 0 %, 0.5 %, 1 %, 1.5 % and 2 % by weight. Essawy and Abd Elhaleem [19] reported that in sulfate resisting cement blended with micro silica incorporated

with 5 %, 7 %, and 10 % nano TiO_2 reduces the setting time. Tables 2 and 3 show the initial and final setting times of concrete with nano mix.

From the above analysis of the literature, it is concluded that the workability decreases with nano TiO_2 in the mixture. This may be attributed to the requirement of more water for wetting the cement particles due to the higher surface area of nano TiO_2 particles [8]. One of the disadvantages of using this material that may limit its wide use by engineers is reducing workability. With the inclusion of nano TiO_2 particles, there was a decrease in the initial setting time of the mixture. This is because there is a rapid consumption of free water with the incorporation of nano titanium dioxide particles, leading to the speeding up of the bridging process of gaps. As a result, the viscosity increases, and solidification occurs earlier [17]. Also, the reduction in the setting time is due to the large surface area of nano TiO_2 that provided a greater availability of nucleation site that leads to a faster hydration rate [18]. The setting time shortening by nano TiO_2 depends on the application that the nano TiO_2 mixture is used for.

Water absorption

Salemi et al. [7] observed that the inclusion of 2 % nano titanium dioxide reduces approximately 22 % of water absorption at the age of 28 days. Nazari [20] investigated the modified concrete at ages of 7, 28 and 90 days with nano-titanium dioxide at proportions of 0 %, 0.5 %, 1 %, 1.5 % and 2 % by weight. The result indicates a decrease in water absorption, rate of water absorption, and coefficient of water absorption with the addition of nano titanium dioxide. For the samples cured in water, the decrease in the water absorption was 59.1 %, 54.1 %, 51.1 %, and 47.5 %, respectively. For the samples cured in saturated limewater, the decrease in the water absorption was 73.73 %, 71.45 %, 68.65 %, and 65.85 %, respectively. However, the optimum replacement proportion was found to be 0.5 %. The samples cured in limewater had much lower water absorption values and a lower water absorption rate than those cured in water.

Soleymani [21], [22] investigated the concretes incorporated with nano-titanium dioxide at proportions of 0 %, 0.5 %, 1 %, 1.5 % and 2 % by weight of cement for the percentage of water absorption. The results show an increment in the percentage of water absorption with the incorporation of nano titanium dioxide at the age of 7 days, while there was a decrease in the percentage of water absorption at ages of 28 and 90 days at all curing conditions. The specimens cured in saturated lime water indicated a lower percentage of water absorption than those cured in water. For specimens cured in water, the reduction was 59.11 %, 54.11 %, 51.1 %, and 47.5 %, respectively, at 28 days. For the specimens cured in saturated limewater, the reduction was 73.73%, 71.45 %, 68.65 %, and 65.85 %, respectively, at the age of 28 days. The lowest percentage of water absorption was at 0.5 % nano titanium dioxide. Table 4 shows the percentage of water absorption in blended concrete.

	Percentage of water absorption %		
ref	**0% TiO_2**	**1% TiO_2**	**2% TiO_2**
Nazari et al.[6]	9.14	6.59	6.14
Nazari et al.[7]	5.6	2.57	2.94
Nazari[14]	4.8	1.12	1.63
Jalal[16]	5.12	4.93	4.68

Table-4: Percentage of water absorption of nano titanium dioxide blended concrete

Jalal [13]studied the self-compacting concretes incorporated with nano-titanium dioxide at proportions of 0 %, 1 %, 2 %, 3 %, 4 %, and 5 % by weight of cement for the water absorption and capillary absorption at the age of 14 days. The results exhibited that there was a reduction in capillary absorption and water absorption with nano titanium dioxide. The optimum content of nano titanium dioxide displays the lowest water absorption or capillary absorption value, and it was 4 %. Jalal et al.[14] investigated the high strength self-compacting concretes modified with nano-titanium dioxide at levels of 0 %, 1 %, 2 %, 3 %, 4 %, and 5 %

by weight of cement for thepercentage of water absorption and capillary water absorption at the age of 90 days. Results indicated that there was a reduction in the rate of water absorption and capillary water absorption. The lowest percentage of water absorption and capillary water absorption was exhibited after 4 % nano titanium dioxide.

Nazari and Riahi [25], [26] studied the self-compacting concretes modified with nano-titanium dioxide at proportions of 0 %, 1 %, 2 %, 3 %, 4 %, and 5 % by weight of cement the percentage of water absorption at ages of 2, 7 and 28 days. There was a reduction in the percentage of water absorption at the ages of 7 and 28 days. The lowest percentage of water absorption was seen after the inclusion of 4 % of nano titanium dioxide. On the other hand, with nano titanium dioxide, there was an increment in the percentage of water absorption at the age of 3 days. Jalal [24] studied the concretes containing 45 percent of slag by weight for the percentage of water absorption at ages of 7, 28, and 90 days. The binder materials were incorporated with nano-titanium dioxide at proportions of 0 %, 1 %, 2 %, 3 %, and 4 % by weight. The results indicated that with nano TiO_2, the percentage of water absorption reduced at all ages. At the age of 28 days, the reduction in the percentage of water absorption was 38.42 %, 41.35 %, 45.75 %, and 43.4 %, respectively. The optimum content of nano TiO_2, which showed the lowest percentage of water absorption, was at the addition of 3 % nano TiO_2.

Shekari and Razzaghi [27] studied the concretes containing 15 % metakaolin modified with nano TiO_2 for the percentage of water absorption at the age of 28 days. The inclusion of nano TiO_2 was 1.5 % of cement weight, which results in a reduction of 75.74 % water absorption.

From the above overview of the literature, it is understood that nano-titanium dioxide reduces the percentage of water absorption in most cases. Still, sometimes it increases the rate of water absorption at early ages. The decrease in the percentage of water absorption might be due to the pozzolanic action and filler effect of nano TiO_2 particles [20]. According to some studies [20], [22] it is indicated that the lowest percentage of water absorption is shown at 0.5 % nano titanium dioxide, while others [28] [26] [14] [13] reported at 4 %. With the inclusion of 5 % silica fume, the optimum nano TiO_2 content is 2 % [29]. Hence, the optimum range of nano TiO_2 varies according to curing condition, hydration age, nano TiO_2 particle size, type, w/b ratio, and the content of pozzolan that replaced cement.

2.3 Porosity

Behfarnia et al. [30]observed that replacing cement with 1 %, 2 %, 3 %, 4 %, and 5 % nano titanium dioxide reduces the permeability of concrete. The lowest permeability was exhibited after the addition of 4 % nano TiO_2. Chen et al. [17] investigated the porosity of pastes modified with nano- titanium dioxide at levels 0 %, 5 %, and 10 % by weight of cement at ages of 3, 7, and 28 days. A decrease in porosity at all ages after the addition of nano titanium dioxide is clearly seen. The reduction in the porosity of the specimens containing 5 % and 10 % P25 was 11.68 % and 14.65%, respectively, in the 28 days, while for the samples containing 5 % and 10 % anatase, it was21.36 % and 21.65 %, respectively.

However, the nano-particles seemed to act as effective fillers. As hydration continued, the conglomerations containing the nano-particles expanded, and the void space around them filled up gradually. The hydration reaction rate accelerated significantly due to the presence of these “nuclei.” Therefore, decreased porosity due to accumulated hydration rapidly grew outwards into the water-filled pores. Essawy and Abd Elhaleem [19] observed that sulfate resisting cement blended with micro silica modified by the addition of 5 % nano titanium dioxide results in decreased porosity, while 7 % and 10 % did not lower the porosity. Mohammadi et al. [31] observed that calcium phosphate cement modified by adding 2.5 %, 5 %, and 10 % nano titanium dioxide by weight reduced total porosity. Table 5 shows the effect on porosity due to the replacement of cement suggested by various authors.

Porosity%		
ref	**0% TiO2**	**5%TiO2**
Chen et al.[4]	22.92	21.63
Lee[5]	47.41	41.12
Nazari et al.[6]	45.7	32.95
Teixeira et al.[11]	35.09	36.64
Nazari[14]	49.95	43.5
Li et al.[29]	15.6	13.3

Table 5: percentage porosity of nano titanium dioxide blended concrete

Nazari and Riahi [23], [26] investigated the porosity of concretes containing different amounts ofslag at the age of 90 days. The binder materials were partially replaced with nano-titanium dioxide at proportions of 0 %, 1 %, 2 %, 3 %, and 4 % by weight. The results indicated that the inclusion of nano titanium dioxide decreased the porosity of the specimens. The lowest porosity was exhibited at 3 % optimum content of nano titanium dioxide. With the inclusion of 1 %, 2 %, 3 % and 4 % nano titanium dioxide, decrease in the porosity was 1.64 %, 4.33 %, 5.67 % and 5.07 % respectively.

2.4 Mechanical Properties:

Li et al.[35] studied that adding 1% nano titanium dioxide of cement weight to the concrete mixture increased its compressive strength by approximately 36 %. Nazari [20] and Soleymani [36] investigated the concrete modified with nano-titanium dioxide based on flexural strength at ages of 7, 28, and 90 days. Cement was replaced with nano-titanium dioxide at 0 %, 0.5 %, 1 %, 1.5 %and 2 % by weight. Some specimens were cured in water and the others in limewater. The results indicated an increase in the flexural strength with the addition of nano titanium dioxide at all ages (i.e., Fig. 1). The increment in the 28-day flexural strength cured in water was 13.64 %, 20.45 %,
15.91 %, and 11.36 %, respectively. For the specimens' cured limewater, the increment in flexuralstrength was 36.58 %, 48.78 %, 56.1 %, and 65.85 %, respectively.

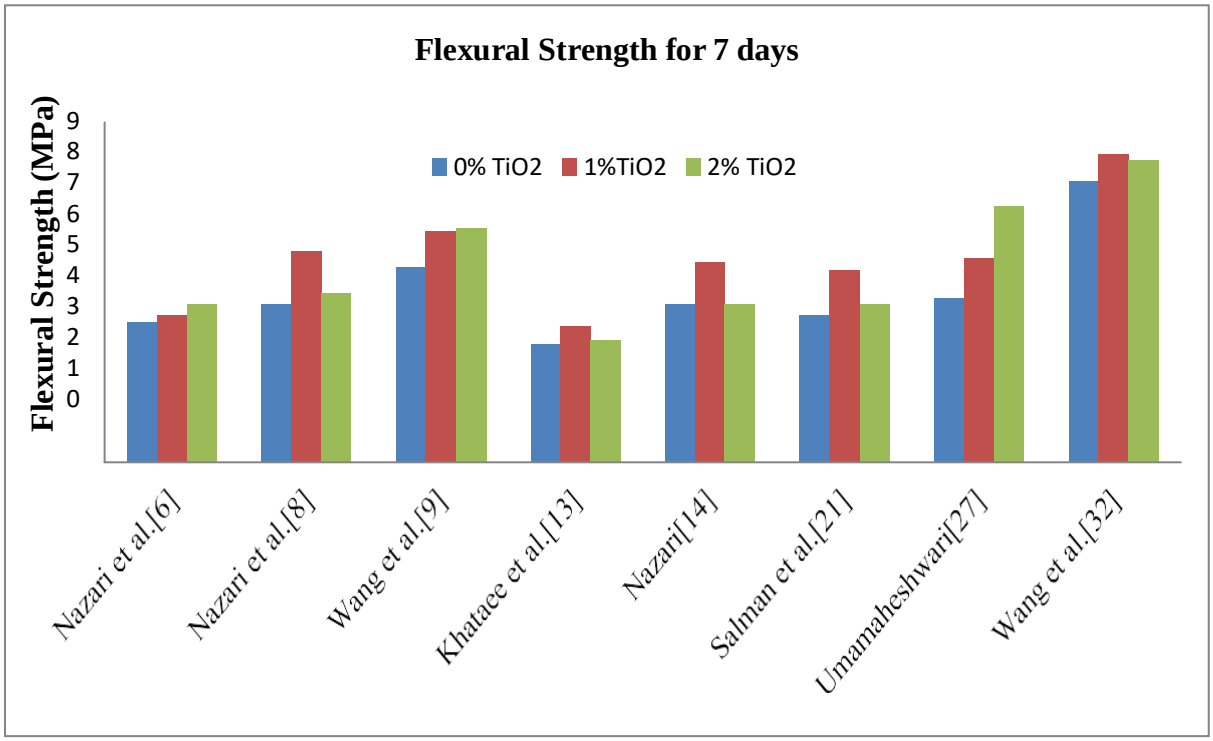

Fig.-1 The effect of nano titanium dioxide on the 7 day flexural strength of plain and blended concrete

The flexural strength for the samples cured in saturated limewater was higher than those that werecured in water. The addition of 1 % nano titanium dioxide indicated the highest flexural strength in water, and the highest flexural strength specimen cured in limewater was at 2 % addition of nano titanium dioxide. Soleymani [37] investigated the compressive strength of concrete at ages of 7, 28, and 90 days modified with nano-titanium dioxide at proportions of 0 %, 0.5 %, 1 %, 1.5% and 2 % by weight.

The result indicates an increase in compressive strength with nano-titanium dioxide for all curingconditions. The increment in the 28 days compressive strength cured in water was 13.86%, 17.93%, 15.49%, and 6.79%, respectively[38]. For the samples cured in limewater, the increment in strength was 21.47 %, 29.1 %, 35.88 %, and 40.96 %, respectively. The compressive strength of samples cured in limewater was higher cured in water. 1% addition of nano titanium dioxide exhibited the highest compressive strength for specimens that were cured in water, but 2 % indicated the highest compressive strength cured in limewater. Similar results of splitting tensile strength results were observed by Soleymani [39].

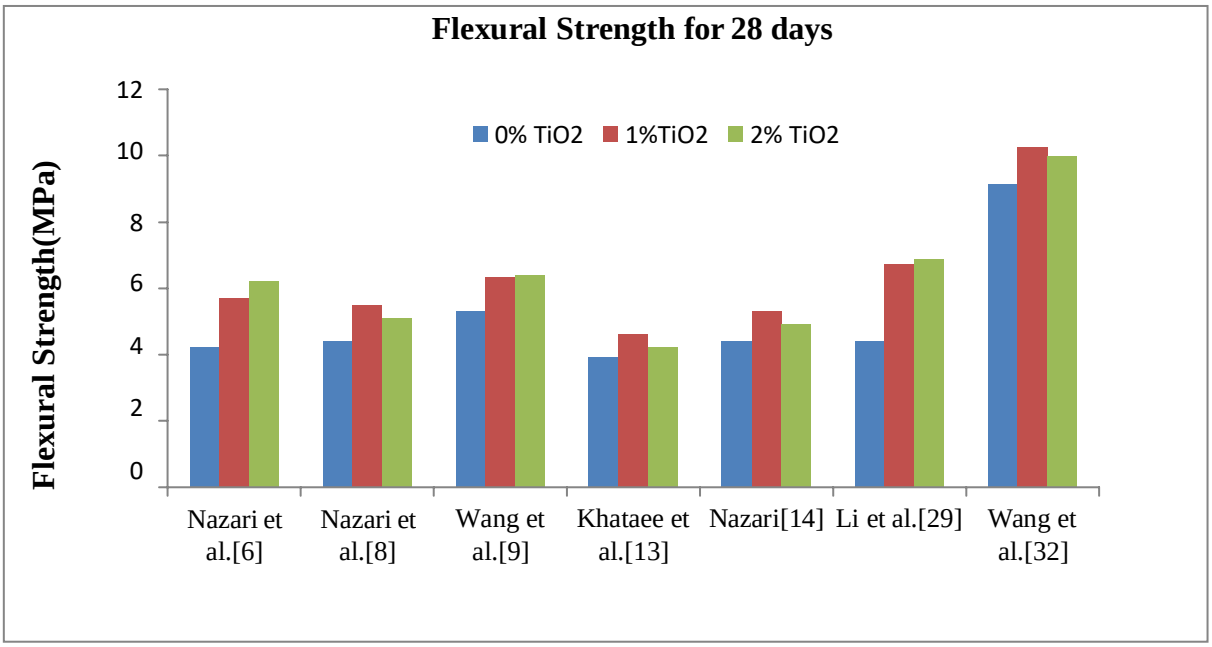

Fig.-2 The effect of nano titanium dioxide on the 28 day flexural strength of plain andblended concrete.

Nazari et al. [23] studied the splitting tensile and flexural strength between 7, 28, and 90 days. Concrete was modified with nano-titanium dioxide at 0 %, 0.5 %, 1 %, 1.5 % and 2 % by weight.The results exhibited that both splitting tensile strength and flexural strength increased with the modification of nano titanium dioxide at all ages. The increment in 28 days flexural strength was 5.91 %, 25 %, 22.73 % and 15.91 % respectively, while the increment in the 28 days splitting tensile strength was 44.44 %, 66.67 %, 50 % and 5.55 %. Nazari et al. [8] studied the compressive strength of the same previous mixtures with the addition of 0.5 %, 1 %, 1.5 %, and 2 % nano titanium dioxide. The increment in 28 days compressive strength was 13.86 %, 17.93 %, 15.49 %and 6.79 % respectively. Salemi et al. [7] observed gain in the compressive strength of concretes with 2 % nano titanium dioxide. The increment in the compressive strength was at proportions 12%, 22.71 %, and 27 % at ages of 7, 28, and 120 days respectively. Jayapalan et al. [40] investigated the flexural strength at the age of 28 days of concrete. Cement was replaced with nano-titanium dioxide at proportions of 0 %, 1 %, and 3 % by weight. Results show gain in the flexural strengthwith nano titanium dioxide, as shown in Fig. 2. The addition of 1 % nano titanium dioxide exhibited higher flexural strength than that of 3 %, and the increment in the flexural strength was 10.27 % and 2.93 %, respectively. The inclusion of 1 % nano

titanium dioxide indicated the best flexural fatigue performance.

Li et al. [10] and Zhang and Li [11] investigated the compressive and flexural strength at 28 days of concrete. Cement was replaced with nano-titanium dioxide at proportions of 0 %, 1 %, 3 % and 5 % by weight. The results indicated a gain in the compressive strength with the addition of nano titanium dioxide. The addition of 1 % nano titanium dioxide exhibit the highest compressive and flexural strength. The gain in the compressive strength was 18.03 %, 12.76 %, and 1.55 %, respectively. The addition of 1 % and 3 % nano TiO_2 enhanced the flexural strength by 10.28 % and 3.04 %, respectively, while 5 % nano TiO_2 decreased the flexural strength by 3.27%.

Nazari and Riahi [25] reported the compressive, splitting, flexural strength at ages of 2, 7, and 28 days of self-compacting concrete admixed with nano titanium dioxide. Cement was partially replaced with 0 %, 1 %, 2 %, 3 %, 4 % and 5 % by weight. The results indicated an increment in all strengths with the addition of nano titanium dioxide. The increment in the 28 days compressive strength was 11.39 %, 21.2 %, 40.82 %, 58.54 % and 54.1 % respectively

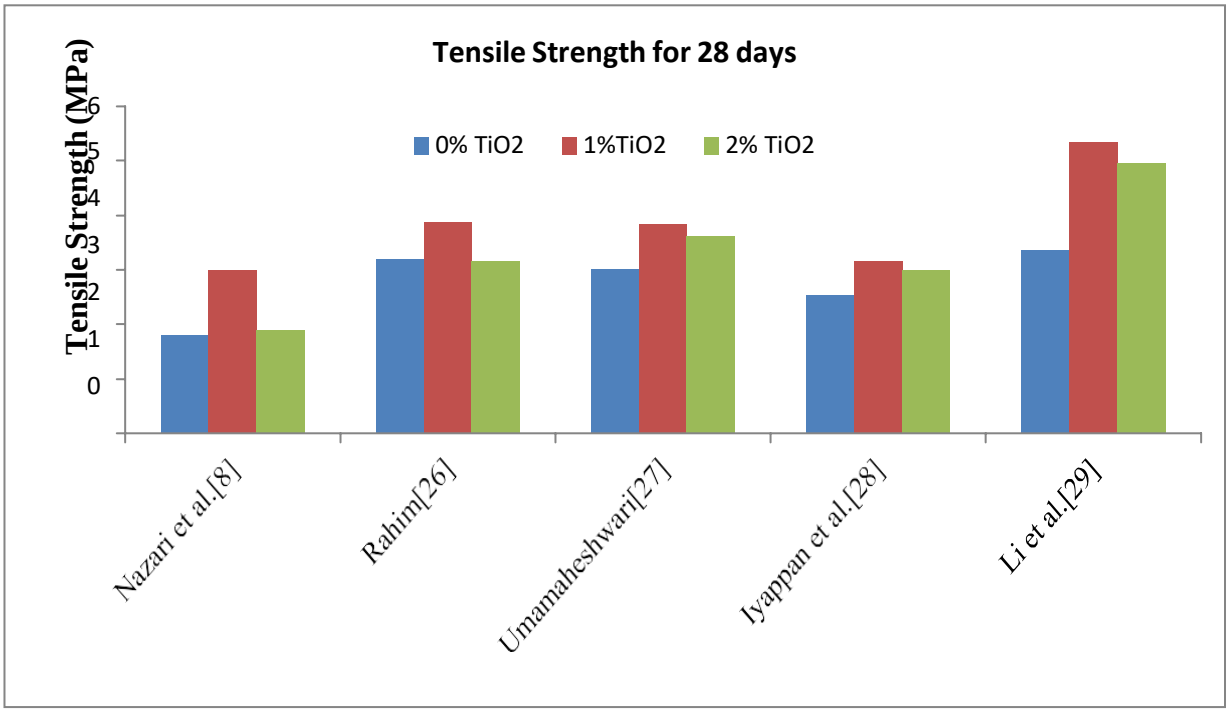

Fig.-3 The effect of nano titanium dioxide on the 28 day tensile strength of plain andblended concrete.

In a similar study, Jalal et al. [14] investigated the splitting tensile strength and flexural strength at ages of 7, 28, and 90 days of high strength self-compacting concrete altered with nano titanium dioxide. Cement was replaced with nano-titanium dioxide at levels of 0 %, 1 %, 2 %, 3 %, 4 % and 5 % by weight. The result indicates an increment in all strengths with nano titanium dioxide, as shown in Fig.3. The addition of 4 % nano TiO_2 showed the highest splitting tensile and flexural strength. Increment in 28 days splitting tensile strength was approximately 8.8 %, 18.61 %, 27.78 %, 36.67 % and 30 % respectively, while the increment in the 28 days flexural strength was 10.58 %, 21.75 %, 29.4 %, 44.67 % and 36.46 % respectively. Senff et al. [28] observed a slight gain in the compressive strength of mortar, with the inclusion of 5 % nano titanium dioxide by weight. Onthe other hand, Behfarnia et al. [30] observed that the compressive strength of concrete decreased with nano titanium dioxide. With the addition of 1 %, 2 %, 3 %, 4 %, and 5 % nano titanium dioxide, the decrease in the compressive strength was 20.73 %, 27.17 %, 14 %, 15.97 % and 26.33% respectively.

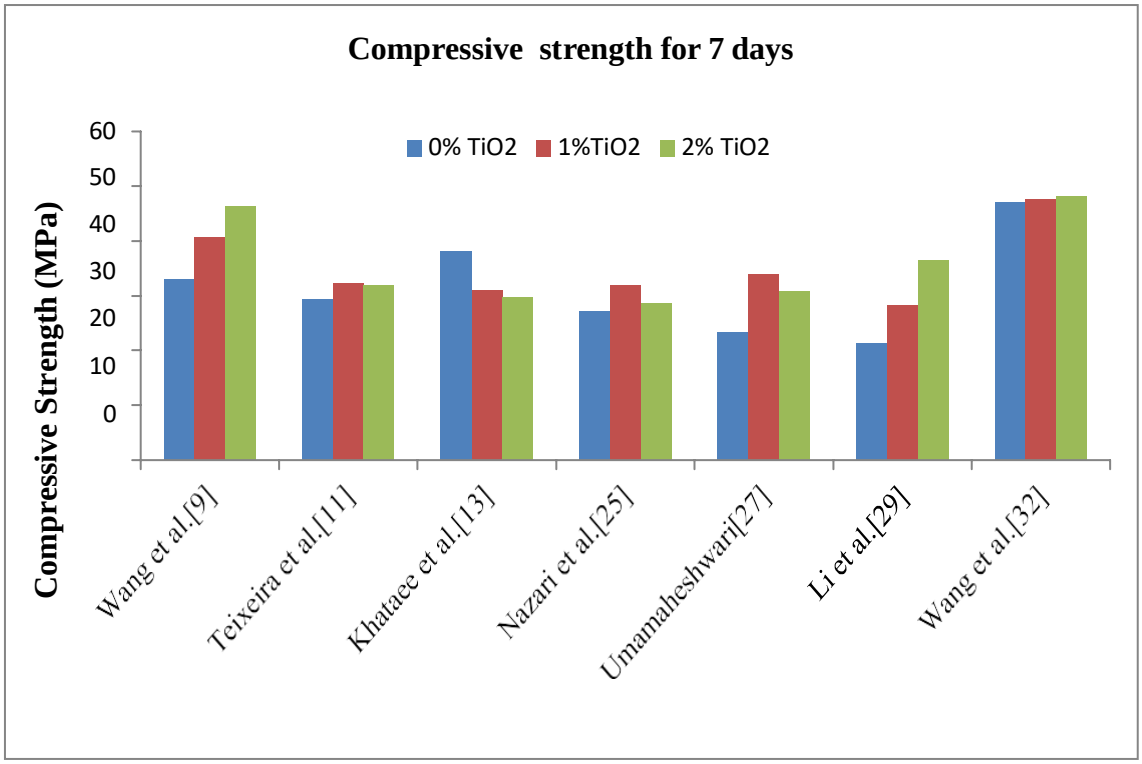

Fig.-4 The effect of nano titanium dioxide on the 7 day compressive strength of plain and blended concrete.

Chen et al. [17] reported the compressive strength at 3, 7, and 28 days of mortars modified two kinds of nano titanium dioxide, P25 (75% anatase and 25% rutile) and anatase (99 % anatase) were used. The nano titanium dioxide was added to the cement at proportions of 0 %, 5 %, and 10 % by weight. The results indicated a gain in the compressive strength at all ages with the addition of nano TiO2. Lee [18] investigated the compressive strength of pastes modified with nano-titanium dioxide at ages of 1, 3, 7, 14, and 28 days. Cement was admixed with nano-titanium dioxide at levels of 0 %, 5 %, and 10 % by weight. The results indicated an increment in the compressive strength of 1, 3, and 7 days with the addition of 5 % nano titanium dioxide, while a reduction in the compressive strength at 28 days was found. The increment was obtained in the 1 and 7 days compressive strength with the addition of 10 % nano titanium dioxide, while a loss in compressive strength was obtained at the remaining ages. Mohammadi et al.[31] observed an increase in the compressive strength by addition 5 % and 10 % nano titanium dioxide in calcium phosphate cement. Meng et al. [41] investigated the compressive strength of mortars admixed with nano-titanium dioxide at ages of 1, 3, 7, and 28 days. Cement was replaced with nano-titanium dioxideat proportions of 0 %, 5 %, and 10 % by weight. There is gain in the early strength and loss in evening strength with increasing content of nano titanium dioxide. With the addition of 5 % and 10 % nano titanium dioxide, the gain observed in 1-day compressive strength was 46 % and 47 %, respectively. At the same time, there is a reduction in 28 days compressive strength with 5 % and 10 % nano titanium dioxide. Nazari and Riahi [23] [26] investigated the flexural strength of concrete containing different amounts of slag and partially replaced with nano-titanium dioxide atlevels of 0 %, 1 %, 2 %, 3 %, and 4 % by weight at ages of 7, 28 and 90 days. The results indicatedthat there was an increase in the flexural strength at 7, 28, and 90 days with nano titanium dioxide. The highest flexural strength at all ages was indicated with the addition of 3 % nano titanium dioxide. The increment in the flexural strength with the addition of 1%, 2%, 3% and 4% nano titanium dioxide at age of 28 days was 5.56 %, 14.81 %, 27.78 % and 16.67% respectively. Nazari and Riahi [26] [42] investigated the compressive strength and the splitting tensile strength, including 1 %, 2 %, 3 %, and 4 % nano titanium dioxide of the same previous mixtures.

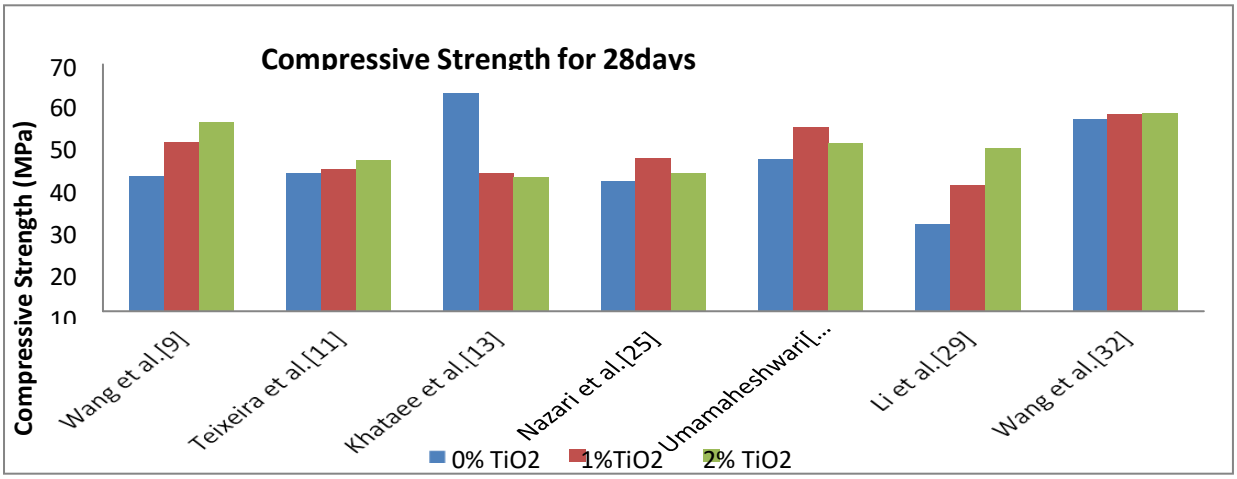

Fig.-5 The effect of nano titanium dioxide on the 28 day compressive strength of plain and blended concrete

Some observations [17] believed that nano-titanium dioxide enhanced mechanical strength. Still, the rate of strength gain was higher at early ages than that of the samples partially replaced with nano-titanium dioxide at late ages. This may be related to the fact that nano-particles have a slower reaction of C2S hydration, which contributed to longer-term properties. The nano TiO2 could only affect the early hydration (C_3A and C_3S), and much of the hydrated cement pastes might be less affected [43]. This means that curing condition, curing age, w/b ratio, type, and content of the cementitious material affect the matrix's optimum nano titanium dioxide content.

3. Concluding Remarks

The current review paper provides a comprehensive overview of the previous works that studied the effect of nano titanium dioxide on few properties (workability, setting time, mechanical strengths, water absorption, and porosity) of plain or blended cement systems. However, some key findings from the review are concluded as follows:

- Increasing nano titanium dioxide content, workability, flowability, initial setting time, and finalsetting time of cement system reduced.
- In general, the inclusion of nano titanium dioxide increases the mechanical strength up to the specified limit. The optimum content may depend on many factors such as w/b ratio, curing condition, curing age, pozzolana type, pozzolana content, chemical admixture, and nano-particle size[44]. However, 1-4% nano titanium dioxide in concrete seemed suitable content that indicated good strength [45].
- The percentage of water absorption and permeability decreases with the addition of nano titanium dioxide into the matrix, but sometimes at early ages, water absorption increases. Most of the studies reported the optimum content is 4 %, but few others observed 0.5 %, 1 %, 2 %, and 3 % as the suitable optimum content for decreased water absorption.
- Based on the above review, it can be concluded that the inclusion of nanomaterials in concrete enhances the properties such as mitigating chloride penetration, chemical shrinkage resistance, abrasion resistance, fire, and freeze resistance.

References

1. M. M. Salman, K. M. Eweed, and A. M. Hameed, “Influence of partial replacement TiO2nanoparticles on the compressive and flexural strength of ordinary cement mortar,” Al- Nahrain Univ. Coll. Eng. J., 19(2)265–270
2. A. Nazari, S. Riahi, S. Riahi, S. F. Shamekhi, and A. Khademno, “Improvement the mechanical properties of the cementitious composite by using TiO2

nanoparticles," J. Am.Sci., 6 (4):98–101,
3. A. Nazari and S. Riahi, "The effects of TiO2 nanoparticles on properties of binary blended concrete," J. Compos. Mater., 45(11)1181–1188,
4. L. Wang, H. Zhang, and Y. Gao, "Effect of TiO2 nanoparticles on physical and mechanical properties of cement at low temperatures," Adv. Mater. Sci. Eng.,
5. F. FranklinS, A. Professor, and B. Student, "Replacement of Cement by using Nano Titanium Dioxide in Concrete," IJSRD-International J. Sci. Res. Dev., 5(7):2321–0613.
6. A. Joshaghani, "Evaluating the effects titanium dioxide on resistance of cement mortar against combined chloride and sulfate attack," Struct. Concr., 19(5):1318–1327,
7. N. Salemi, "Effect Of Nanoparticles On Frost Durability Of c r v i h o ef c f," 15.(3)411–420.
8. A. Nazari, S. Riahi, S. F. Shamekhi, and A. Khademno, "Assessment of the effects of the cement paste composite in presence TiO2 nanoparticles," J. Am. Sci., 6(4)43–46,
9. H. Li, M. hua Zhang, and J. ping Ou, "Flexural fatigue performance of concrete containing nano-particles for pavement," Int. J. Fatigue, 29(7)1292–1301.
10. H. Li, M. hua Zhang, and J. ping Ou, "Abrasion resistance of concrete containing nano- particles for pavement," Wear, (260)1262–1266,
11. M. H. Zhang and H. Li, "Pore structure and chloride permeability of concrete containing nano-particles for pavement," Constr. Build. Mater., 25 (2)608–616
12. J. Sorathiya, S. Shah, and S. Kacha, "Effect on Addition of Nano "Titanium Dioxide" (TiO2)on Compressive Strength of Cementitious Concrete," (1)219–211,
13. J. Mostafa, A. A. Ramezanianpour, and M. K. Pool, "Effects of titanium dioxide nanopowder on rheological properties of self compacting concrete," J. Am. Sci.,8(4) 285– 288.
14. M. Jalal, M. Fathi, and M. Farzad, "Effects of fly ash and TiO2 nanoparticles on rheological,mechanical, microstructural and thermal properties of high strength self compacting concrete," Mech. Mater.,(61)11–27
15. L. Senff, D. Hotza, S. Lucas, V. M. Ferreira, and J. A. Labrincha, "Effect of nano-SiO2 and nano-TiO2 addition on the rheological behavior and the hardened properties of cement mortars," Mater. Sci. Eng. A, (532)354–361.
16. R. Khataee, V. Heydari, L. Moradkhannejhad, M. Safarpour, and S. W. Joo, "Self-cleaning and mechanical properties of modified white cement with nanostructured TiO2," J. Nanosci. Nanotechnol.,13 (7) 5109–5114
17. J. Chen, S. C. Kou, and C. S. Poon, "Hydration and properties of nano-TiO 2 blended cement composites," Cem. Concr. Compos., 34(5): 642–649.
18. L. B. Y, B. Y. Lee, and L. B. Y, "Effect of titanium dioxide nanoparticles on early age andlong term properties of cementitious materials,"
19. A. A. Essawy and S. Abd, "Physico-mechanical properties, potent adsorptive and photocatalytic efficacies of sulfate resisting cement blends containing micro silica and nano- TiO2," Constr. Build. Mater.,(52)1–8.
20. A. Nazari, "The effects of curing medium on flexural strength and water permeability of concrete incorporating TiO2 nanoparticles," Mater. Struct. Constr., 44(4):773–786
21. E. E. Boaden, "No 主観的健康感を中心とした在宅高齢者における 健康関連指標に関する共分散構造分析Title," (7): 1–7
22. Unda, "No Title طرق تدريس اللغة العربية," Экономика Региона, 8(5):32,
23. A. Nazari and S. Riahi, "The effects of TiO2 nanoparticles on physical, thermal and mechanical properties of concrete using ground granulated blast furnace slag as binder," Mater. Sci. Eng. A, 528, (4–5): 2085–2092.
24. M. Jalal, "Durability enhancement of concrete by incorporating titanium dioxide nanopowder into binder," J. Am. Sci., 8(4) 289–294.
25. A. Nazari and S. Riahi, "The effect of TiO2 nanoparticles on water permeability and thermal and mechanical properties of high

strength self-compacting concrete," Mater. Sci. Eng. A, 528(2):756–763.
26. A. Nazari and S. Riahi, "TiO2 nanoparticles effects on physical, thermal and mechanical properties of self compacting concrete with ground granulated blast furnace slag as binder,"Energy Build., 43(4) :995–1002.
27. A. H. Shekari and M. S. Razzaghi, "Influence of nano particles on durability and mechanical properties of high performance concrete," Procedia Eng.,(14)3036–3041
28. L. Senff, D. M. Tobaldi, S. S. Lucas, D. Hotza, V. M. Ferreira, and J. A. Labrincha, "Formulation of mortars with nano-SiO2 and nano-TiO2 for degradation of pollutants in buildings," Compos. Part B Eng., vol. 44(1): 40–47.
29. N. Farzadnia, A. A. Abang Ali, R. Demirboga, and M. P. Anwar, "Characterization of high strength mortars with nano Titania at elevated temperatures," Constr. Build. Mater., (43): 469–479.
30. K. Basalts and F. Ree, "ch i Ar ve of Ar ch i of," 16(4):617–630.
31. M. Mohammadi, S. Hesaraki, and M. Hafezi-Ardakani, "Investigation of biocompatible nanosized materials for development of strong calcium phosphate bone cement: Comparison of nano-titania, nano-silicon carbide and amorphous nano-silica," Ceram. Int.,40(6):8377–8387
32. B. Y. Lee and K. E. Kurtis, "Influence of TiO2 nanoparticles on early C3S hydration," J. Am. Ceram. Soc., 93(10):3399–3405
33. K. P. Teixeira, I. P. Rocha, L. D. S. Carneiro, J. Flores, E. A. Dauer, and A. Ghahremaninezhad, "The effect of curing temperature on the properties of cement pastes modified with TiO2 nanoparticles," Materials (Basel)., 9(11):1–15.
34. B. Ma, H. Li, J. Mei, X. Li, and F. Chen, "Effects of nano-TiO2 on the toughness and durability of cement-based material," Adv. Mater. Sci. Eng.,
35. H. Li, H. Xiao, X. Guan, Z. Wang, and L. Yu, "Chloride diffusion in concrete containing nano-TiO2 under coupled effect of scouring," Compos. Part B Eng., (56):698–704,
36. У. А. Лобач, "Полацкі Этнаграфічны Зборнік. Вып. 2. Ч. 1 : Народная Проза Беларусаў Падзвіння," 7(12):290
37. Unda, "No Title طرق تدريس اللغة العربية," Экономика Региона, vol. 8(3): 32
38. H. Wang, P. Zhao, S. Wang, L. Lu, and X. Cheng, "Effect of well-dispersed nano-TiO2 on sulphoaluminate cement hydration and its application in photo-degradation," Ceram. - Silikaty, 61(4): 301–308.
39. Unda, "No Title طرق تدريس اللغة العربية," Экономика Региона, vol. 8(6):32.
40. A. R. Jayapalan, B. Y. Lee, and K. E. Kurtis, "Effect of Nano-sized Titanium Dioxide on Early Age Hydration of Portland Cement," Nanotechnol. Constr. (3):267–273
41. T. Meng, Y. Yu, X. Qian, S. Zhan, and K. Qian, "Effect of nano-TiO 2 on the mechanical properties of cement mortar," Constr. Build. Mater.(29):241–245.
42. A. Nazari and S. Riahi, "TiO2 nanoparticles' effects on properties of concrete using ground granulated blast furnace slag as binder," Sci. China Technol. Sci.,54(11): 3109–3118.
43. A. R. Jayapalan, B. Y. Lee, S. M. Fredrich, and K. E. Kurtis, "Influence of additions of anatase TiO2 nanoparticles on early-age properties of cement-based materials," Transp. Res. Rec., (2): 41–46.
44. T. Nadu and T. Nadu, "Experimental Investigation of Concrete Using Titanium," no. May. 2326–2330.
45. A. Rahim and S. R. Nair, "Influence of Nano-Materials in High Strength Concrete," J. Chem. Pharm. Sci.,(3):15–22

PUBLIC SAFETY NETWORK DESIGN FOR SMART CITIES: A MULTI-SENSOR AND SOCIAL NETWORKS APPROACH

S.Upadhye[1], P.Bagde[2], R.Ghumde[3] and A.Bhave[4]

[1]Department of Computer Application, Shri Ramdeobaba College of Engineering and Management, Nagpur

[2, 3] Department of Mathematics, Shri Ramdeobaba College of Engineering and Management, Nagpur

[4]Inter Institutional Computer Centre Rashtrasant Tukadoji Maharaj Nagpur University, Nagpur

[1] upadhyesd@rknec.edu,[2]bagdepo@rknec.edu, [3]ghumderg@rknec.edu [4]arvind_mbhave@yahoo.com

ABSTRACT

Growth in urbanization and population density has led risks of natural and man-made (accidents, fire, burglary etc.) disasters on all-time high. In smart cities, these factors may lead to unparalleled emergencies, which must be handled to maintain safety in the city. Indeed, a smart system is required to handle such situations. In this paper, we consider a safety network architecture which will connect UAVs, smart sensors and social sensors i.e. citizens using social network for gathering information. The UAVs act as moving sensors, providing overall rough monitoring data. The sensor layer on ground will monitor environment and assist UAVs in their task. Social sensors i.e. citizens using social networks will also act as an eye for reporting incidents that above sensors may fail to report or assembled the things if require. A central agent will analyze this data various techniques to provide various alerts to public and adjust system as per the specific task requirements.

Keywords: *Crowd Sensing, Distributed Sensors, Multi-robot System, Public Safety, Smart City, Social Sensors, UAV.*

1. Introduction

Advances in the field of drones and sensors technology, machine learning, various data analysis and pattern recognition techniques have paved the way for smart cities of future. As the population grows natural and man-made disasters have a larger impact on society. Therefore, it is essential to have a safety network in smart cities that can accurately monitor such incidents and guide local authority to take appropriate actions. Such intelligent system improves the efficiency of urban management and enhances the security of residents. In this article, the smart surveillance system and event handling in smart cities is considered. An urban area that become a smart city in which different types of electronic methods and sensor are used to collect data, the collected data are used to manage assets, resources and city services effectively. Data collected form the UAV, smart sensor and crowd social sensors are processed, analysis, monitor and managed for any natural or human made disasters. Smart city concepts used the ICT (Internet and Communication Technology) and IoT (Internet of Things) to optimize the Operation / Services in the city and also connected the citizens in the city.

The concepts of smart city application is to manage the urban flows and allow to real time response. Along with the ICT, the smart city is also required the data analysis to assess the information provided by the smart city systems so that any problems can be addressed and necessary action will be taken. Smart city management includes the observation of threaten, handling the problem, distribution of resources, community services, etc. Smart cities consist of various kinds of electronic equipment applied by some applications, such as cameras in a monitoring system, sensors in a transportation system, and so on. The smart city management includes surveillance of threatens, event handing, distribution of resources, community services etc.

Crowd sensing is also play an important role for safety of smart city. In smart city context report generated by citizen or city visitor eye witnesses may provide valuable information to by other means. In this information the observation or experiences in the physical world. Public safety reports about crimes and hazards related to the smart city may be obtained from city's crowds (Louta, M., **2016**). It helping to detect potential disturbances before they deteriorate. It enable the timely reaction by control agent. Such "social sensor" readings may be further bonded with physical sensors spread across the city. It is also reducing the overall uncertainty and improving the data fusion accuracy. Two unique

challenges in crowd sensing or social sensing context, first one is detection method with high precision and recall properties is required. The main challenged is large volumes of irrelevant reports and much lower amounts of relevant ones. Second is many social sensors may provide reports related to the city, some of them may include reports by people who were not first sight observers of the actual event within the city's context. Therefore, location and time validation of social sensor readings is of extreme importance (Louta, M., **2016**; Raghu Ganti,**2011**).

Present security system (RätyT. D., **2010**) consists of surveillance cameras installed at critical locations such as banks, supermarket, railway station, airport etc. where the probability of crime is high. A security personnel constantly monitors the video footage from these cameras for suspicious activities. This mode too stressful since the security personnel has to monitor several places simultaneously with high concentration and inefficient because it may involve flaws due to human error. This method is more labour intensive. A smart alarming system is required where huge amount of data is gathered and analyzed automatically to enhance working efficiency. But such system is only effective if data sources can be changed dynamically otherwise it will be just a surveillance system assisting authorities to take decisions. A smart system should be able to monitor and handle events automatically which can reduce delays (HollandsR. G., **2008**).

(FilipponiL. &et. al.,**2010**), Smart system include the automation not only in data collection, but also make its own decision in emergency. It should be able to access the public request and solve their problems. The role of people in smart system is adjustable like when some uncontrolled/unpredictable problem occur the human intervention in the smart system able to fix the problem.

We propose a smart system for emergency that should not only collect data but also analyze this data and handle events automatically. It should also accept request from citizens and help them accordingly. The role of the human should be to adjust and maintain the system and providing a human response to threats where system requires human interference (PalmieriF.,**2016**; Upadhye S.,**2017**) However, it is difficult to develop such intelligent system for urban environment but with increasing development in technology it will be possible develop such system in near future. Our proposed public safety network system architecture is intelligent system that supervised the city area and maintained it regular activity. It ensure the safety of all resident by detecting and handling the upcoming emergency. Proposed smart city architecture manage the distribution of resource, supervising the threatens, event handling and community services.

To build such system, it is necessary to setup a reasonable structure. Here we propose a three-layer architecture consisting of UAV layer, sensor network layer and social sensor layer i.e. local residents reporting incidents through social network as in Figure 1. The UAV layer is the most flexible layer which has the largest data collection and changes their supervising areas based on events occurred. In this way, UAV layer can monitor threats in large area and report to central agents. Though UAV layer is flexible it cannot provide detailed information. UAV layer detect the looms in the large area around them and they can move fast to change their supervising areas. It is very flexible and fast. To provide detailed information and continuous monitoring of suspicious areas, we need static distributed sensors. In each area there is local control center which supervises the environment by analyzing data from sensors. Once it detects problem, it will inform nearby UAVs or provide alerts to citizens using social sensors network.

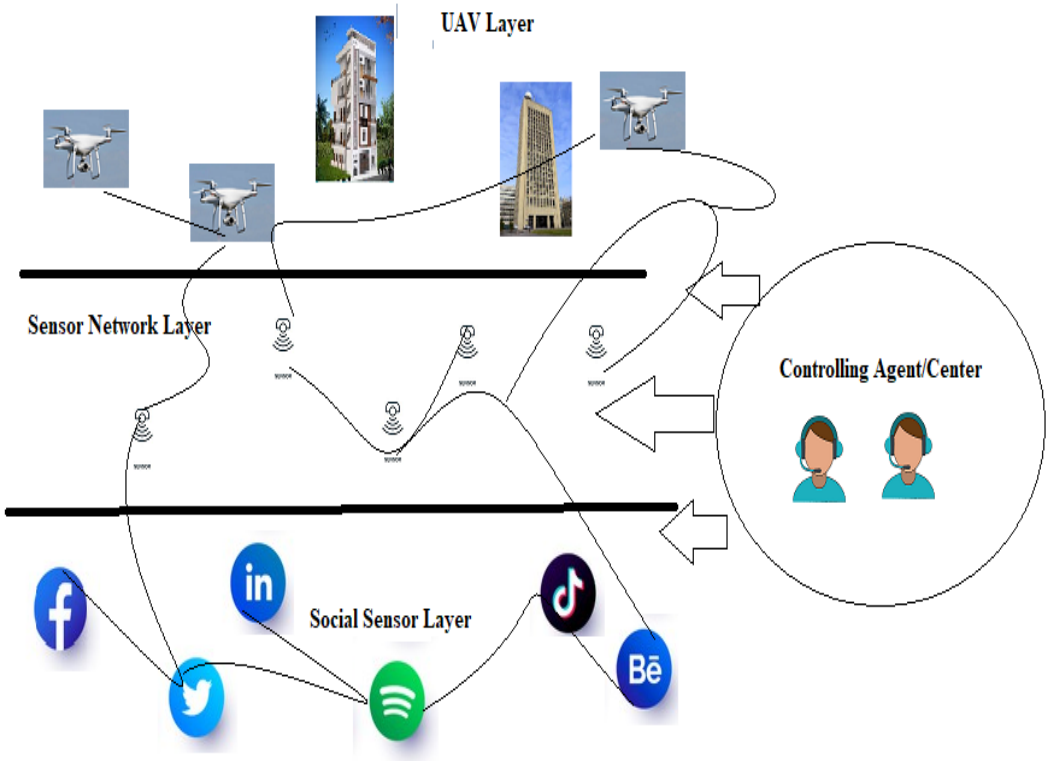

Figure 1: General Architecture of proposed model.

The social sensors layer consisting of local residents sharing information on social network every moment. Though above sensors are fully automated they may fail to monitor some very important details since devices may malfunction. They will also report incidents on social network or through some dedicated mobile application. Apart from these, there is a main control centre which synthesizes bulk of data reported by three layers. On the basis of analysed data, the centre will send commands to the UAVs and sensors or provide critical alerts to citizens regarding their safety.The article is organized as follows: We first introduced the complete structure of the system and analyses its function in the section 1. In section 2, UAV layer and its issues are considered. Then in section 3, the role of sensor is analysed. In section 4, we discuss the concept of social crowd sensors and its related work and issues. Afterward, the role of control centre/agent is discussed in section 5. Finally, in section 6 conclusion is given.

2. The UAV Layer

UAV layer monitors a large area from sky thus they react to a situation much faster given their high speed and flexibility. Suppose there is fast moving target with which local authorities cannot catch up, in that case the UAVs can continuously track that from sky and guide authorities on ground to co-operate with event handling. The UAV can launch other UAVs on base station to co-ordinate with them if there is need for assistance. It will also respond to reports of social sensors.

Figure 2 design for the UAV layer is given. In normal state, the UAVs will fly over city gathering data of the urban area with on-board sensor. The collected data will be reported to the control centre and an emergency detection algorithm will check for emergency. Though UAVs are flexible way for collecting data, the data collected is rough since they fly over city. Thus, for more detailed information, the static sensors will be contacted by control centre. The control centre will also check if there is any new report from the social sensors in that area.

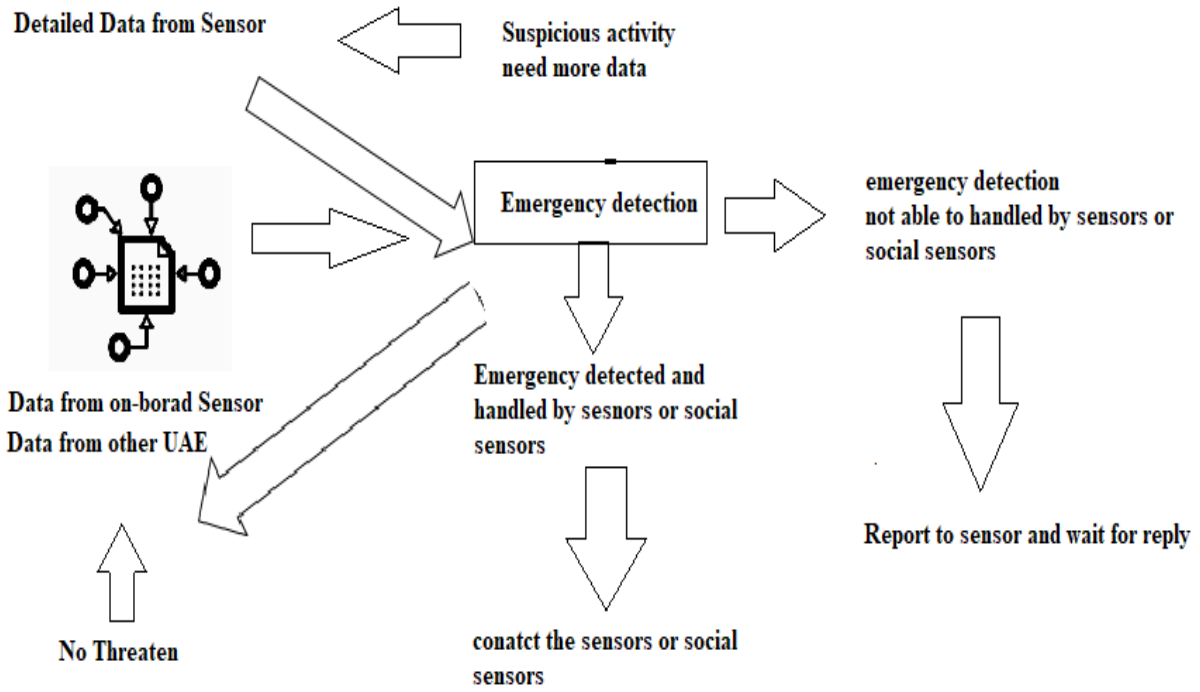

Figure -2: The general flow design of the UAV layer.

After analysis of data, if there is an emergency detected, the local authorities of that area are contacted. In the meantime, till authorities get there, the UAVs will keep track of the target. Afterwards it will wait above the scene to provide additional information to the authorities. Finally, when event is handled or no threat is detected, the UAVs will return to their normal state.

2. 1 Related Problems and Technologies

Localization is the fundamental problem in the system. Most of the layer's functions should be based on the knowledge and understanding in surrounding environment, which includes its position in the working space and the positions of its target.To accomplish this task, we require a robust localization algorithm which having larger scope for implantation. The combination of Inertial Navigation Systems (INS) and Global Positioning Systems (GPS) is the one of the method for UAV localization. INS provide the UAV positions, velocity and attitude. But it has bias errors which accumulate as time increasing. The GPS can estimate the bias errors and give improved UAV localization (Nemra A., & Aouf N.,**2010**). For improving, we should use the landmark areas such as towers, sculpture, etc. by referring this landmark we can reduce the localization errors. Localization of target with on-board sensor is another problem, this can be solved by image processing techniques, visual localization (Minaeian S., Liu J., & Son Y. J.,**2016**).

The next challenge for UAV is that, number of videos covered by UAV, it is very difficult to derive the meaning full information. The pattern recognition is the technology to understand meaning of videos which was covered by UAV. Most challenging situation in this case is the target detection algorithm. Detecting is not the solution of problem, as need to identify the progress of the event because system is not only detect the problem it also handle the event in emergencies case. There are many pattern recognition algorithm but for our system we require an algorithm that support vector mechanism and principal component analysis, for that we also require the neural network structure. The UAV need to recognise the road accident, fire disaster, abnormal human activity, etc. they inform this incident to the social sensor or the central agent so that necessary public alert is being their or some action will be taken by central agent (BeshahT., et al. **2011**; RasouliS., et al.,**2015**).

For UAVs, the obstacles (Frew E. & Sengupta R. **2004**; BudiyantoA., **2015**) mainly include high buildings and flying items such as birds or other UAVs. The UAVs fly depending on the rotors rather than the wings. In the system for emergency, UAVs have to fly in a low altitude

so as to observe the ground, which enhances their possibility to meet obstacles. These problems can be solved using optimization path planning and that path also aware about the possible obstacles. We should also provide the dynamic detection of coming up obstacle. For that we can use the computer vision, millimetre wave, GPS etc. Communication between the UAVs and control agent or social sensors is somehow important problem because UAVs collect data more rapidly and with same speed need to communicate. For that we require real time communication system. Power supply is a basic problem for nearly all systems. To ensure a quick supplement of power resources, power stations should be set around the city. In the future development, the combination of solar energy and rechargeable batteries may be a good solution.

3. The Sensor Layer

It is mainly used for controlling local areas and supporting nearby UAVs to complete their tasks by giving them with essential information. Based on such functions, there are distributed sensors for each critical area. Sensors include smart parking, noise management, fire safety, waste water management. Traffic congestion, etc.

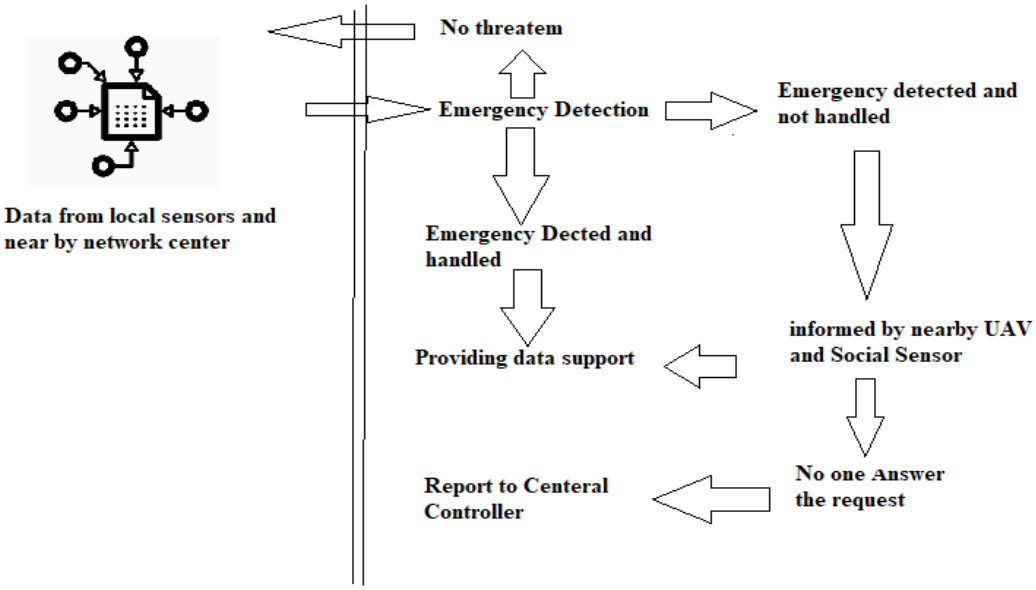

Figure. -3: The general design of the senor network layer.

Sensor network layer uses the visual algorithm to detect the potential or ongoing emergency. Data of specified area (sensors are placed) is collected by distributed sensors, sent to local center. The center can also contact to local center for nearby area data if needed. If an emergency case and central agent is not able to handle it in that case sensor contact with UAVs or social sensors (LinkedIn, Instagram, Twitter, Facebook). The sensor mainly used in area where UAVs is not able to identify.

3.1 Related Problems and Technologies

To confirm the resourceful overseeing of the local areas as well as lower the cost on sensors, strategies of distributing sensors need to be developed, which is an optimization problem. There are lots of different supervising tasks. Based on different supervising tasks in different environments, sensors are different and the distribution strategies are not the same. The data analyzing algorithm needed to investigate to detect the events with reasonable calculation for being inform to the central agent for event management. Pattern recognition is also use in this case. The data is collected from distributed sensors, the information should be fused and analysed synthetically (Zha Z. J., &et. al.,**2013**). In case of unsupervised areas, the algorithm to estimate tract and connect different supervised areas that is also a challenging problem for research (Mazzon R. & Cavallaro A., **2013**). Unreliability is the problem because the sensors are distributed around the area. Some sensors are broken or stolen in that case it

provide wrong data, so local center should be able to identify the problem. if suppose unreliable data is in the local or central agent in that case using fault tolerant data analysis mechanism , we should be able to identify the emergency situation (De PaolaA. &et. al.,**2015**).

4. The Social Sensor Layer

The social crowd sensors are the leverage on the power and wisdom of crowd. It is also exploit human intelligence and ubiquity and mobility features. To this respect, people are empowered to contribute data sensed or generated from their social web/mobile application. It enable efficient monitoring of large-scale phenomena that cannot easily be measured. Or otherwise it would need costly investments in terms of hardware and software. Social sensor layer harnesses the power crowd sensor to analyze any incident in the surrounding. Above two layers, being based on electronic equipment are prone to error and failure. Hence, social sensor (crowd sensing) (Roitman H., &et. al.,**2012**). layer act as backup layer for cross checking the data by above two layers and reporting events that above layer may miss out. For this we also require the data mining algorithms in order to analyze spatiotemporal patterns, generate models and make prediction on it (Raghu Ganti & Fan Ye, **2011**). Recently the social crowd sensor are attracted researcher for environmental monitoring application in the area of air quality, traffic planning, public safety, smart parking, etc. The social crowd sensor have unique characteristics, people are involved in data collection, processing, analysing and sharing. Data are collected both from the physical world i.e. sensed data from devices such as mobile as well as from online communities i.e. social network services related (Bin Guo,& et. al., **2014**).

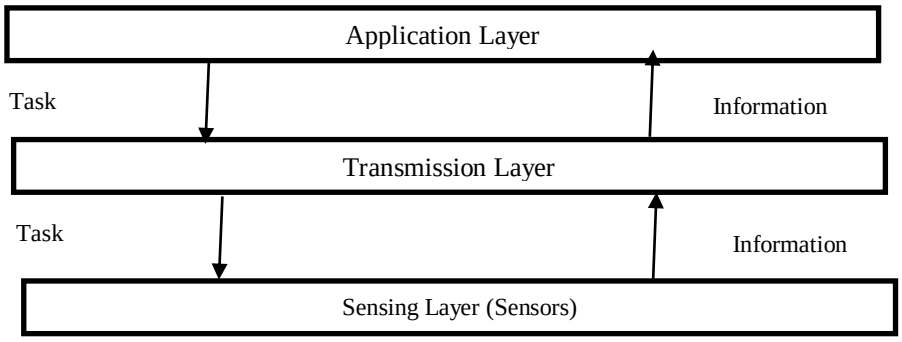

Figure -4: General architecture of social crowd sensors

Every moment, anywhere in the world, some people share reports about their observations or experiences in the physical world. Within a city's context, such reports by citizen or city visitor eye witnesses may provide important information to city officials, additionally to more traditional data gathered by other means (e.g., through the city's control centre, emergency services, sensors spread across the city, etc.). The general architecture of crowd sensing **Figure 4,** consist of sensor layer, transmission layer and application layer. The sensing layer basis and used for data acquisition. It usages many sensors, intergraded on devices to perceive material properties, environment status, behaviour patterns and human status. The best example is, recently in India use of Aarogya Setu mobile application to keep user information in case any person crossed paths with someone who has COVID tested positive patients. The transmission layer is mainly responsible for transferring the acuity data from the lower to the center server. Transmission layer consist of many core internet, next generation internet and various kind of networking.In the application layer, center servers store and process these acuity data to achieve various application tasks, because the acuity data are inaccurate, incomplete, inconsistent, and untimely (Abdul Razaque, **2019**). If data are not processed, these inaccurate, unreliable, and incomplete data are difficult to be used in various applications.

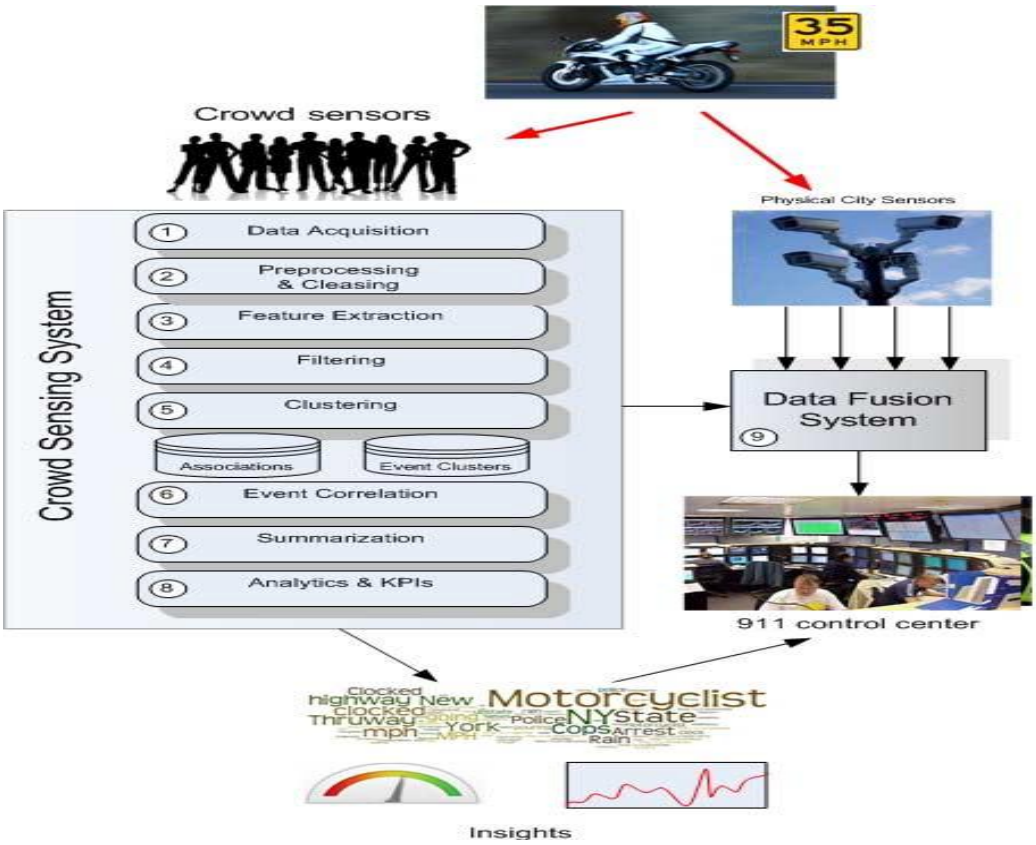

Figure -5: Crowd Sensing System Architecture (Zhao, Dong, &H. Ma., **2014**).

Figure 5 describes the high-level architecture for crowd sensing system. Crowd report data is delivered to the system from various sources such as social streams, mobile phones etc. Such data usually consists of short messages, expressed in (free) natural language, with reasonable amounts of noise such as spell-mistakes, ambiguity, and usage of special notations (e.g., # for hashtags and @ for mentions or location indicators in Twitter). Each report is first transformed into a uniform format, termed hereinafter data record. At the next stage, each data record is pre-processed. Such pre-processing includes several standard textprocessing steps such as tokenization, stemming, stopping, lemmatization, etc. Next, data records are filtered using several dedicated filters including language filter, topic-filters, and context filter.

Records that "pass" the filters are then clustered according to their semantic and contextual similarity. Topic detection and tracking (TDT) is used for finding and following event in the stream of broadcast news and stories. "Event" clusters and their data record associations are maintained within a persistent storage for the next stages. A correlation component is further used to detect related evolving events. Using various data analysis techniques, correlation between data and evolving events are established and accordingly alerts are generated.

4. 1 Related Work and Issues

(Weppner, Jens, & Lukowicz P., **2013**) presented concept that people can easily estimate population density in public places by using Bluetooth. The smartphones and their on-board sensing capabilities motivates crowd sensing. It has capability that power of crowd to collect sensor data from many mobile phone users.

(Ra, Moo Ryong, & et al., **2012**) presented the crowd sensing and runtime distributed system coordinates the execution of tasks between smartphones and a cluster on the cloud. It provides high level abstractions for specifying the steps required to complete a crowd sensing task.

(Simoens, Pieter, et al., **2013**).introduced that crowd sensing collect a large amount of data about videos and pictures captured by users to help to find lost people or help cop to catch criminals.

New sensing model of the internet, social crowd sensing provides a new way to realize deep social perception, but it also brings new

challenges to the research. The real challenge is several types' electronic devices, their sensing mechanism, computation,communi cation channel.

- **User privacy protection**

In crowd sensing networks, the collected sensing data contain many sensitive and private information of users. For example, location information, GPS, electronic compass, magnetic field sensor, etc after monitoring and analyzing the location information for a long time, the sensitive information of the user family and work place, daily activities, the common traffic route, can be found. These perceived data seriously threaten the user privacy.

- **Data and platform security**

Crowd sensing network converges user sensitive and private information. this can also excavate valuable information, which highly increases the risk of hacker attacks and confidential data leakage. For data's security, cryptographic encryption technology can be used to encrypt the acuity data. By using user authorization and identity authentication technology provides the platform security. By using key distribution and management mechanisms for complex encryption calculations that consume a large number of resources (Gallacher, Sarah, &et al.,**2014**).

- **Data authenticity and integrity**

Malicious users may submit false perceived data or, in the process of data transmission, may lose part of the data, which may lead to excavating wrong information and making wrong decisions, for that data authenticity and integrity is required

- **Common Platform and Efficient transmission**

Many academic and industrial community has designed and developed a wide range of intelligent sensing applications, which usually have overlapping the functions, so independent developing mode is inefficient, resulting waste of resource and time. Building a common platform of crowsensing network is a fundamental and basic problem (Zhao, Dong, &H. Ma., **2014**). The Crowd sensing application need to collect the data continuously and transmit to data center. This transformation is based on internet. This require more power and data traffic plan of the user equipment. Therefore, a design of an energy-efficient data transmission method is needed

In general, crowd sensing within a city's context is more challenging the crowd sensing in the general domain (e.g., event detection in online sources such as Twitter). We identify two main unique challenges in this context. First, as opposed to events formed and detected by traditional methods which may be reported by hundreds or even thousands of social sensors, events within a city may be observed by few eye witnesses. Even though, such reports may include crucial information that can assist in critical decision making (e.g., timely dispatch of emergency services in response to some reported incident). Therefore, a detection method with high precision and recall properties is required, challenged by possible large volumes of irrelevant reports (e.g., any Tweet that mentions the city's name) and much lower amounts of relevant ones.

Second, while many social sensors may provide reports related to the city, some of them may include reports by people who were not first sight observers of the actual event within the city's context (e.g., a tweet about an event that occurred in Nagpur made by some user in Twitter who is actually located in Pune and just retweeted someone else's tweet). Therefore, contextual (i.e., location and time) validation of social sensor readings is of extreme importance.

5. Central Agent

To execute the normal operation, there need a centre agent to adjust the whole system by human. When systematic problems occur, people can control the system through the centre. Data collected from the different layer is analyzed here, then the result guides people to adjust working mode of the system such as distribution of work, altering agency, taking appropriate action, etc. In our architecture, central agent controlled by human, human can assign tasks to the system from centre.

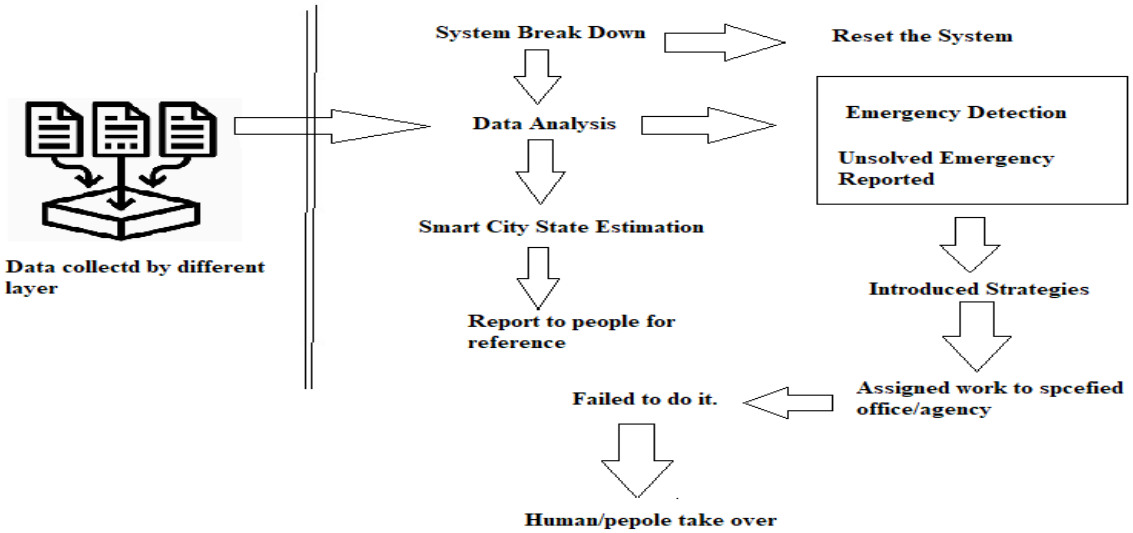

Figure -6: The design of the central agent structure.

Data of UAVs, sensors and social sensors is gathered by the central agent through network. Based on the data, the central agent can supervise the working condition of the whole system. If serious errors occur and the system is not working properly, the center can reset the system. In addition, based on big data analysis, the central agent can estimate the state of urban area. This can be provided for human as reference to adjust the system working mode. If emergencies are detected or some unsolved emergencies are reported, the center will start to make decisions to handle them. Central agent solve the problem in automatically mode, such as if riot is identified by social sensor and inform to central agent then central agent automatically inform the cop and cop will control the situation. If central agent not able to solved the task, human is also set in work directly.

5. 1 Related Issues

Data analyst is one who scrutinises information using **data analysis** tools. The meaningful results they pull from the raw **data** help of data analyst algorithm. It also identifying patterns and trends in **data** sets. In this architecture main job is to find information of interest and guide the system to work. Given information of interest, the huge data should be dealt with to find the relative results with acceptable cost on calculation, which includes several critical problems. There should be data mining theories to guide the process of finding result. In general big data algorithm should pick out the relevant data and find the relative results by data mining theories.

Security is the most important problem for this smart system. In our architecture the social sensor is nothing but social users, they may be hacker so our system should identify such users. In the practical, a hacker may attack the system to perform damage work. The UAVs and sensors are connected in a network. If the network is controlled by the hackers, the residents may be in a dangerous status. Therefore, there should be full proof encrypted systems using authentication, encryption/decryption so that hackers cannot break into system. Even if they succeed in capturing system, people should be able to shut it down for emergency.

6. Conclusion

Here we provided the public safety system architecture design and review the main required technology. We also highlighted some challenges and possible solutions. The structure is composed of three cooperative working layers and a controlling centre. We introduced different layers and discussed coordination between them for detecting and handling emergencies. The UAV layer covered the large area from the sky and react to situation faster with high speed and flexibility. But it is having some problems related with localization, pattern recognition, and physical safety about the UAVs. The INS and GPS are able to fix the problem of localization, by using vector mechanism and principal component analysis techniques we solve the problem data

analysis. Fault tolerant data analysis mechanism to identify the unreliable or damage sensor in the network. The social crowd sensing layer also have some real challenge, we can give solution using authentication, cryptography techniques. The smart public safety system can provide a reference for the future research to construct such a system.

References

1. Abdul Razaque, (2019).Survey of Crowd sensing: Architecture Classification and Security Challenges. SSRG International Journal of Electronics and Communication Engineering, ISSN: 2348–8549, 6(10), 1-15.doi:10.14445/23488549/IJECE-V6I10P101
2. BeshahT., EjiguD., Abraham A., Snasel V., & Kromer P. (2011). Pattern recognition and knowledge discovery from road traffic accident data. Proc. World Congr. Inf. Commun. Technol., 1241-1246.
3. Bin Guo, Zhiwen Yu, Daqing Zhang, Xingshe Zhou. (2014). From Participatory Sensing to Mobile Crowd Sensing. Proc. of the 12th IEEE International Conference on Pervasive Computing and Communications Workshops (PERCOM Workshop), 593 - 598,
4. Budiyanto A., Cahyadi A., Adji T. B., & Wahyunggoro O. (2015) UAV obstacle avoidance using potential field under dynamic environment. Proc. Int. Conf. Control, Electron, Renew. Energy Commun. (ICCEREC), 187-192.
5. De Paola A., Gaglio S., Milazzo G. L. Re, F.,&Ortolani M.(2015). Adaptive distributed outlier detection for WSNs. IEEE Trans. Cybern., 45(5),902-913.
6. FilipponiL., VitalettiA., LandiG., MemeoV., Laura, G. & Pucci P. (2010). Smart city: An event driven architecture for monitoring public spaces with heterogeneous sensors. Proc. 4th Int. Conf. Sensor Technol. Appl. 281-286
7. Frew E., Sengupta R. (2004). Obstacle avoidance with sensor uncertainty for small unmanned aircraft. Proc. 43rd IEEE Conf. Decision Control (CDC), 1, 614-619.
8. Gallacher, Sarah, et al. (2014). Investigating the Challenges of Crowd Sensing. Lessons from Zurich, Workshop structures of Knowledge Co-Creation between Organisations and the Public ACM.
9. HollandsR. G. (2008). Will the real smart city please stand up? Intelligent, progressive or entrepreneurial? City. 12(3), 303-320.
10. Louta, M., Mpanti, K., Karetsos, G. et al. (2016). Mobile crowd sensing architectural frameworks: A comprehensive survey. IISA 2016 - 7th International Conference on Information, Intelligence, Systems and Applications. ISBN 9781509034291. https://doi.org/10.1109/IISA.2016.7785385
11. Nemra A., Aouf N. (2010). Robust INS/GPS sensor fusion for UAV localization using SDRE nonlinear filtering. IEEE J. Sensors, 10(4),789-798.
12. Mazzon R., Cavallaro A. (2013). Multi-camera tracking using a multi goal social force model. Neuro computing, 100(2), 41-50.
13. Minaeian S., Liu J., & Son Y. J. (2016). Vision-based target detection and localization via a team of cooperative UAV and UGVs. IEEE Trans. Syst., Man, Cybern., Syst., 46(7), 1005-1016.
14. PalmieriF., Ficco M., Pardi S., & Castiglione A. (2016). A cloud-based architecture for emergency management and first responders localization in smart city environments. Comput. Elect. Eng., 56, 810-830.
15. Ra, Moo Ryong, et al. Medusa. (2012). A programming framework for crowd sensing applications. International Conference on Mobile Systems, Applications, and Services ACM, 337-350.
16. Raghu Ganti, Fan Ye, Hui Lei. (2011). Mobile crowd sensing: current state and future challenges. IEEE Communications Magazine, 49(11), 32-39.
17. RasouliS., Granmo O. C., & Radianti J. (2015). A methodology for fire data analysis based on pattern recognition towards the disaster management. Proc. 2nd Int. Conf. Inf. Commun. Technol.

Disaster Manage. (ICT-DM), Nov. 2015, pp. 130_137.
18. RätyT. D.(2010). Survey on contemporary remote surveillance systems for public safety. IEEE Trans. Syst., Man, Cybern. C, Appl. Rev., 40(5), 493-515.
19. Roitman H., Mamou J., Mehta S, Satt A., & Subramaniam L. V. (2012). Harnessing the Crowds for Smart City Sensing. IBM Research Haifa, Haifa 31905, Israel, IBM Research India, New Delhi, India
20. Simoens, Pieter, et al. (2013). Scalable crowdsourcing of video from mobile devices, Proceeding of the International Conference on Mobile Systems, Applications, and Services, 139-152.
21. Upadhye S.,Yadav P., Sayare A., & Mandal A. (2017). Design and Develop a Smart Digital Electrical Board for Home Automation Systems. International Journal of Innovations & Advancement in Computer Science IJIACS ISSN 2347 – 8616, 6(5).
22. Weppner, Jens, & Lukowicz P. (2013). Bluetooth based collaborative crowd density estimation with mobile phones. IEEE International Conference on Pervasive Computing and Communications IEEE, 193-200.
23. Zha Z. J., ZhangH., Wang M., Luan H., & Chua T.-S. (2013). Detecting group activities with multi-camera context. IEEE Trans. Circuits Syst. Video Technol., 23(5), 856-869.
24. Zhao, Dong, &H. Ma. (2014). Development and Challenges of Crowd Sensing Networks. Information & Communications Technologies.

EXPERIMENTAL INVESTIGATIONS AND COMPARISON OF MACHINABILITY OF TITANIUM ALLOY USING COOLANT AT AMBIENT TEMPERATURE AND WITH COOLANT AT ITS LATENT HEAT LOAD

P. Patil[1] and P. Karande[2]

[1]Department of Mechanical Engineering, K.J. Somaiya Polytechnic, Mumbai, India

[2]Department of Mechanical Engineering, Veermata Jijabai Technological Institute, Mumbai, India

[1]prpatil@somaiya.edu

ABSTRACT

In modern machining world a continuous effort is being made to find cost effective technique to machine hard materials, like Titanium alloys, super alloys etc. At the same time, it is also desired to improve the machining performances like tool life, surface roughness, cutting forces, retention of metallurgical properties of the material, etc. The primary objective of this research work is to analyze the effect of coolant at 0^0c on machining parameters on Titanium based alloy and determination of the optimum temperature of coolant for best machining performance. The performance on machining parameter like cutting force, surface finish, tool life, with castor oil based coolant at temperature of 0^0c was analyzed and was compared, with coolant at ambient temperature of 28^0c.It was found that at a coolant with temperature of 0^0c has a substantial improvement in various machining parameters, dimensional, and quality aspects of the job. The cryogenic cooling technique is used for machining of hard materials, but its economics and safety makes its use limited. An alternative to cryogenic cooling was thus proposed to manufacturing industries whose result is forty percent to that of cryogenic cooling. A unique experimental setupswere designed and fabricated for this research work.

Keywords: *Cutting velocity, Flank, Hardness, Refrigeration, Surface finish, Chips Morphology*

1. Introduction

Titanium alloys has been widely used in industrial as well as aerospace applications because of its unique material properties such as stability, material strength, biocompatibility and hardness. However, providing equivalence amongst thermal conductivity and mechanical properties has led to difficulties in machining. During cutting process, the heat generated at cutting zone builds up at extreme values, which tends to decrease the properties of the cutting material and base metal. Because of these actions, consequences such as rapid tool wear, reduction in cutting tool life and deterioration at end in machined surface integrity. In this research, we are concentrating on the issues arising in super alloy machining and the effect of varying temperature of coolant on the machinability and to find solution which will act a boon to industries.

The machining properties of Titanium alloy are poor in nature due to the inherent mechanical property of work hardening and poor thermal conductivity(Junaidh et al., 2018). Machinability is a quality characterized by the degree of difficulty in machining a work material under specified conditions. In case of high speed machining tool life is considerably reduced as the increase in metal temperature results in a reduction of tool life (Arun Kumar et al., 2018). The work hardening and low thermal conductivity are recognized to be responsible for the poor machinability of Titanium alloy and tool wear at a faster rate (Bruschi et al., 2019). Additionally, during machining, the chips fine particles adhere very firmly to the tool edge while cutting and when the chip is disintegrated from the workpiece, the particle cling to the tool face (Rahim & Dorairaju, 2018).

The temperature parameter affecting the surface material as well as cutting zone has been considered as a critical parameter in cryogenic machining(Celik et al., 2018).Coolant plays an important role in the machining of materials, as it provides ease in machining. It also reduces the cutting temperature and lubricates the cutting process(Liu et al., 2005). The temperature of coolant plays a important role as it improves the machinability of materials, enhance the tool life and also improve the surface finish of workpiece (Kümmel et al., 2014). Environmental aspects had played a vital role in the machining process, as research is more inclined to find an alternate system to replace coolant used in machining processes or at least to reduce the amount of coolant used in the

machining process(Eltaggaz et al., 2018). Various experiments with cryogenic fluids such as liquid carbon-di-oxide or liquid nitrogen as coolant have been used as coolant and improvements were noted in machining characteristics of workpiece (Yildiz & Nalbant, 2008). A researcher has demonstrated that machining with cryogenic coolant either with liquid carbon-di-oxide or liquid nitrogen minimizes the temperature developed at the tool-work interface and also reduces the friction that brings positive changes in machinability parameters (Sadik & Isakson, 2017). The results obtained from cryogenic machining has shown that there are considerable improvements in dimensional accuracy, tool life and surface finish of workpiece compared to other lubrication processes. To machine the work, harden materials or metal's which oxidized at room temperature, cryogenic machining is a viable alternative solution as it reduces the tool flank wear, cutting forces and improves the tool life(Tamil Alagan et al., 2019). The only limitation of cryogenic cooling is an extremely low temperature that makes it difficult to handle safely. Practical applications of cryogenic fluid as being coolant so far been minimal in various industries as economical and safety viability is at large impacting its actual use in practice (Suhaimi et al., 2018).

Another method widely used for machining lubrication is mist lubrication, where high pressurized air is mixed with coolant and sprayed on the workpiece, whose heat dissipation results is same as that of flood coolant(Chen et al., 2017). The advantage of the mist coolant system is that coolant usage is reduced which is detriment to the health of human beings and environment (Mia & Dhar, 2015).

To obtain the improvements in machining parameters like tool life, surface finish, dimensional accuracy in work hardening material like Titanium alloy, an experiment was conducted by using emulsion based coolant castor oil (8-9%) at 0^0c temperature. At 0^0c, coolant is still in the liquid state and it possess the inherent heat only in form of latent heat and this latent heat content is very negligible compare to heat generated in tool during cutting, and quickly dissipates the heat from tool surface. The low temperature of coolant was obtained by a simple vapor compression refrigeration system which was designed and fabricated at a low cost. The results obtained by refrigerated coolant for machining parameters were close to 60 percent as that obtained by cryogenic machining and cost involvement is only 17 percent. It provides a viable alternate solution to the industry.

2. Design and Fabrication of Experimental Set-Up

An innovative, simplified cost effective technique was adopted to design and fabricate the two different set up to perform the research based experiment, as stated below. The specifications of the tools, workpiece and various measuring technique is discussed at large in the appropriate section of this research work.

2.1. Vapour Compression Cycle Based Refrigeration with Coolant Pressure Generation System

A specialized refrigeration system was design, which was capable of reducing coolant temperature and also deliver at required pressure at machining work-tool zone contact area. To reduce the coolant temperature a vapor compression cycle (R134a) based cooling system was designed and fabricated. The pump sucks the coolant from the main coolant tank of turning center and stores it in an additional supplementary tank. An evaporative coil measuring 2m is placed in supplementary tank which reduces the temperature of the coolant and this coolant is again re-circulated to the main tank employing another centrifugal pump. A filter with 50-micron mesh has been installed in an inlet pipe of the supplementary tank which removes the chip fine particles coming from the main tank with coolant. The pressurized coolant is pumped to the work- tool zone interface area, where excessive heat is generated through a set of nozzle.

The CNC turning center was having inbuilt coolant tank with capacity of 50 litres and plunger pump was installed on tank, which discharge the coolant at 8bar with a discharge of 12 LPM. A separate supplementary tank was fabricated with a capacity of 20litreand made up of stainless steel. In this tank evaporative

coil made up of copper of length 2m was wound inside tank in cylindrical fashion. A hermetically sealed reciprocating compressor, having power rating of 0.246kW was used to pump the refrigeration R134a through heat exchanger and expansion device into evaporating coil, where refrigerating effect was produced. The condenser was having forced draft cooling system to liquefy the vapour coming from compressor and before entering into expansion device. The minimum temperature drop obtained at full load was found to be of -18^{0}c. A twin centrifugal pump having capacity of discharge pressure of 4 bar and 08LPM were installed in the system, to suck and deliver the coolant into main tank. The time taken by coolant to reach temperature from 28^{0}c to 0^{0}c is 73 min. As the temperature reaches 0^{0}c, heat contain in liquid is very less as it contains only latent heat and this latent heat load is utilized for experiment purpose. The power consumed by entire system was measured by means of watt meter and sensible heat removal from coolant was calculated, to determine the co-efficient performance of the system

Figure 1.Refrigeration Coolant System along with Pressure Generation System

Calculations for Co-efficient of performance (COP)

Sensible cooling (Q) = m*c_p*ΔT.

Substituting the values in above equation we get,

Q = 5861.8 kJ.

As 73 min were taken to reduce the temp, Q in terms of kW,

Q =1.33kW

The power rating of compressor = 0.246 kW.

$$COP = \frac{\text{Refrigerating effect}}{\text{Work done by compressor}}$$

COP = 5.40.

Thermostat was installed to maintain the temperature of coolant at 0^{0}c, in close proximity of 2^{0}c variation cut off limit. A number of experiments at varying temperatures was repeatedly performed and average reading was recorded. As from stopwatch readings 73 minutes were required to bring the temperature of coolant from 28^{0}c to 0^{0}c. In case if one desire to reduce temperature in less time high rated compressor will be required. During actual machining only latent heat load of coolant was used to remove the heat generated during actual cutting operations. A latent heat load can be also increased by adding coagulant to coolant which can further dip temperature without freezing.

2.2. Measurement of Temperature Generated Along the Cutting Edge

To measure the temperature generated on tool rake face of insert a contactless laser technology based temperature measurement gun was installed to measure the temperature generated during each millisecond. Temperature of chip close to the point of tool contact depends on two heat sources, a first heat source is in the chip forming area due to material deformation and the second heat source lies at the rake face of the tool, where chip makes the contact before leaving the workpiece (Li et al., 2021).The temperature recorded by laser gun is having a high accuracy of +/- 1.5%. An another simple method was

also proposed to measure the temperature generated at the tool face, by inserting a slot of 1.5mm is cut along the Centre of insert with the grinding tool on WIDIA CNC machine. A 'K' type thermocouple with a 0.5mm diameter is fixed in the slot and filled by brazing, so that thermocouple will remain at that position. The thermocouple tip was placed at a distance of approximately 2 mm from the cutting edge so that it will not interrupt the cutting phenomenon(Liu et al., 2005). The temperature recorded by laser gun was taken as benchmark reading due to accuracy of the system and ability to measure temperature in every millisecond. On comparison of both system, it was found that laser system was having higher accuracy and sensitivity was also too high, hence K type thermocouple temperature measurement system was discarded and laser gun system was adopted for the proposed work(Saez-de-Buruaga et al., 2018)

2.3Selection of Tool and Work Material as per ASTM Conventions

a) **Workpiece** -A Titanium alloy bar of diameter 40mm and length 100mm is chosen as a sample piece, as per ASTM Grade5 standard. The chemical composition of workpiece tested under lab condition were recorded as- C-0.08%, Fe -0.25%, N-0.05%, O_2-0.2%, Fe -0.2%, Al - 6.25%, V- 4.0%, H_2- 0.015%, Y-0.05% and remaining is Ti.

b) **Insert** - TiAlNi coated Sandvik make carbide tool insert CNMGS205 was selected as a cutting tool. The tool holder along with carbide insert was mounted on a Kistler make dynamometer for measuring forces generated during cutting. For every new experiment a fresh edge of insert was selected.

c) **Machine-** -Experiments are performed on Turning CNC turning center- Ace Micrometric LT-16 500 Lm. The machine was calibrated three months before performance of experiment

2.4Procedure Adopted for Experimental Work

A series of experiments were performed at a three set of temperatures i.e 0^0c, 10^0c, and 28^0c. For a particular set of temperatures, the input machining parameters like cutting velocity was done at 03 set of speed 80m/min, 150m/min and 200m/min depth of cut and feed was fixed at 0.5 mm 0.25mm/rev for per set of experimentations. Output parameters such as temperature generated at flank surface, cutting forces generated at tool face during machining, pre and post hardness and surface roughness of workpiece were measured after machining process. The cutting forces were measured for above mentioned input parameters to find whether a decrease in temperature results in the reduction of cutting forces, radial force and feed force (Seah et al., 2003). The surface roughness of the machined component was measured by device-surface roughness Mitutoyo tester-178-923-2.

The temperature of coolant in main tank was measured by means of thermometer. A specialized refrigeration system with an integral centrifugal pump is designed and fabricated especially for this experimental work. The coolant is supplied through a set of nozzles on tool-work zone area. The machining of workpiece was done at different cutting velocity of 80 m/min, 100 m/min and 150 m/min with a specified depth of cut of 0.5 mm, at a feed rate of 0.25 mm/rev. A number of experiments were performed with several permutation and combinations of input parameters to have concrete results. The temperature at tool face, tangential cutting force, surface hardness, and tool life were measured for all such sets of reading. The experiments were performed under control conditions to nullify the external factors effects.

In the first stage of the experiment at ambient conditions of coolant i.e. at 28^0c experiment was performed, with set of cutting velocity of 80m/min, 150m/min and 200m/min with fixed depth of cut as 0.5mm with a federate of 0.25mm/rev and output parameters like surface finish, cutting temperature, surface hardness were noted and recorded. In the second stage, the refrigeration and pumping system was turned on and the temperature of the coolant was reduced to 10^0c and temperature is maintained constant at 10^0c by means of a thermostat. The thermostat is operational in a range of 2^0c (10-12^0c coolant temperature). The output parameters are again noted and recorded in a tabular format. In third stage, coolant temperatures are further reduced to 0^0c

by changing thermostat setting (0-2^{0}c), and at a given set of experiments were performed and output were measured and recorded. At 0^{0}c, the coolant possess very less heat and contains only latent heat of liquid state known as latent heat load which is less and is effectively use to remove the heat from tool face during machining operations. A comparison of output parameters was made to obtained output data with respect to different coolant temperature used for the machining process and detail analysis were carried out to derive conclusions.(P.Patil, 2019).

3. Results and Discussions

3.1 Temperature Rise and Heat Concentration Along the Tool Face

Seventy percent of the heat developed during the machining process is carried away by the fragmented chips generated during the machining, around 20% of the heat generated in process is absorbed by the tool material resulting in the post machining hardness of the material. The heat generated at workpiece-tool contact area governs various output machining parameters such as post machining hardness, surface roughness, tool life, etc.A K-type thermocouple was affixed in the slot provided on the tool face of the insert to measure the temperature generated on the rake face of tool during actual cutting. In combination with the setup of experiment a contactless laser technology based temperature measurement gun was installed to measure the temperature generated during each millisecond. Fig.2 shown below indicates that, when the refrigerated coolant at 0^{0}c is flooded on the workpiece, the temperature generated at the tool rake face is substantially less, as compared to coolant used for machining at a temperature of 10^{0}c and 28^{0}c. The less temperature may be due to effective heat disposal to coolant from the shearing zone area of workpiece. The effective heat disposal also affects various other machining parameters like surface roughness, hardness in a positive manner as discussed below.

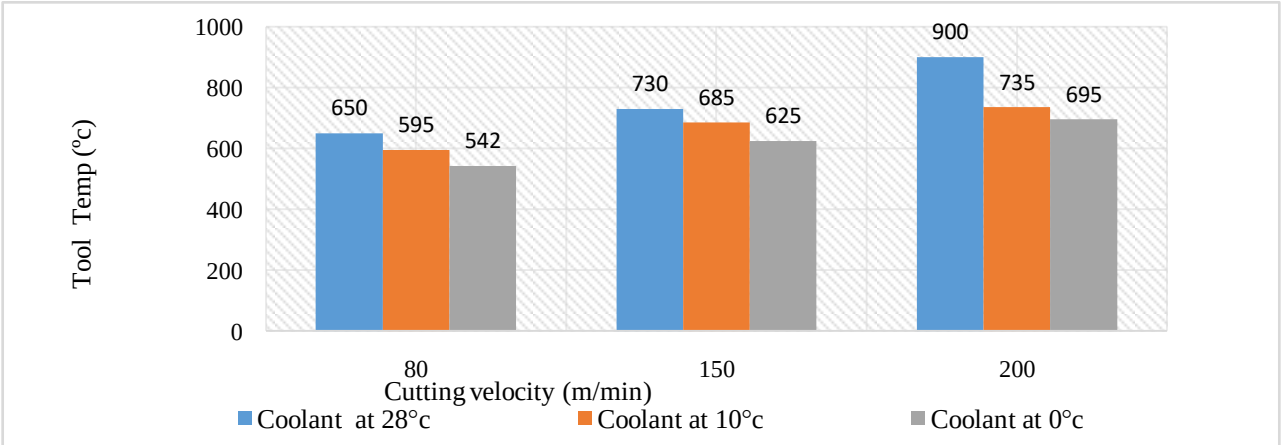

Figure 2. Temperature Generation During Machining

3.2 Post Machining Surface Roughness and Surface Integrity

The surface roughness was investigated for the titanium alloy under set of input conditions and reason for variance was analyzed with literature available in public domain. A comparative result of surface texture roughness, when the machining of Titanium alloy was done with castor based coolant at a temperature of 0^{0}c, 10^{0}c and 28^{0}c (ambient temperature) with different cutting speeds of 80, 150 and 200 m/min at a constant feed of 0.25mm/rev and depth of cut as 0.5 mm is shown in Fig.3. The surface roughness of the machined surface was measured on Mitutoyo make 178-923 surface roughness tester. The surface integrity and texture obtained post machining with coolant temperature at 0^{0}cshows better performance than machining done with a coolant at 28^{0}c.The result indicates that roughness values are reduced when the coolant temperature is maintained at 0^{0}c. It confirms that there is less wear and tear of the tool when machining is done with coolant at a temperature of 0^{0}c. The abrogation for improvement in a surface roughness is due to the retention of tool tip hardness and sharpness

at high temperature, which leads in less thermal distortion of workpiece and improves the cutting process, ultimately resulting in improvement in dimensional accuracy and surface finish(Junaidh et al., 2018).

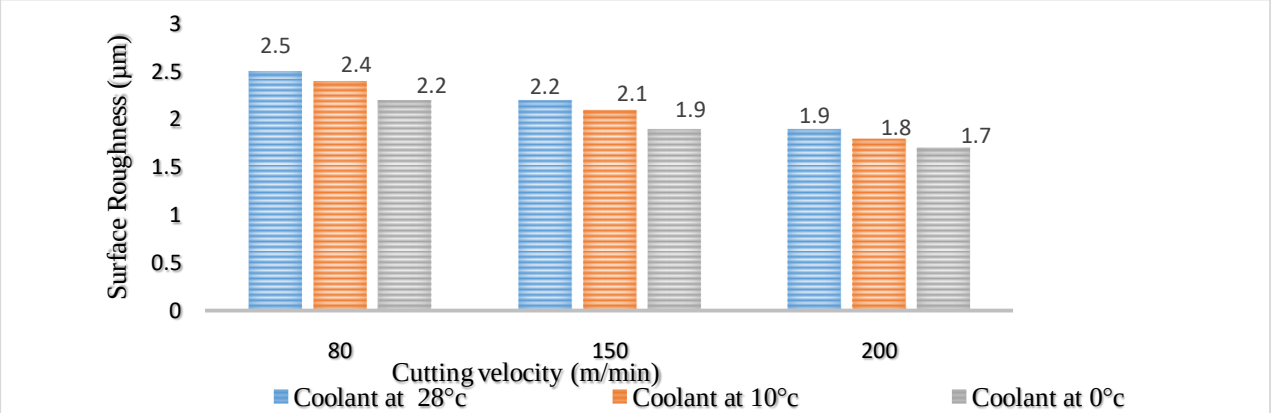

Figure 3. Surface Roughness Comparison

3.3 Measurement of Cutting Forces Generated During Turning Process

The effect of temperature of coolant on the tangential cutting forces at a different cutting velocity of 80, 150 and 200 m/min with 0.2mm/rev of feed at 0.5 mm depth of cut is shown in Table1. It indicates that when the temperature of the coolant is maintained at 0^0c, there is reduction in cutting forces approximately 17% compared to machining done at 28^0c. The reduction in forces is attributed to the presence of plasticity in the material due to uniform cooling of material and retention of cutting edges of insert(Nomani et al., 2017). The readings were recorded after 240 seconds of machining time

CuttingVelocity(m/min)	**Cutting force** (N)		
	Coolant at 28^0c	Coolant at 10^0c	Coolant at 0^0c
80	207	180	150
150	162	138	124
200	139	110	100

Table1. Comparison of Cutting Forces at Different Cutting Speed

A graphical representationin form of line chart is presented for cutting forces in fig4. The reduction in cutting force when machining was done at 0^0c also contributes to less tool wear rate. The other two components of cutting forces like feed and radial force were also less when machining was done at 0^0c compare to machining at 28^0c.

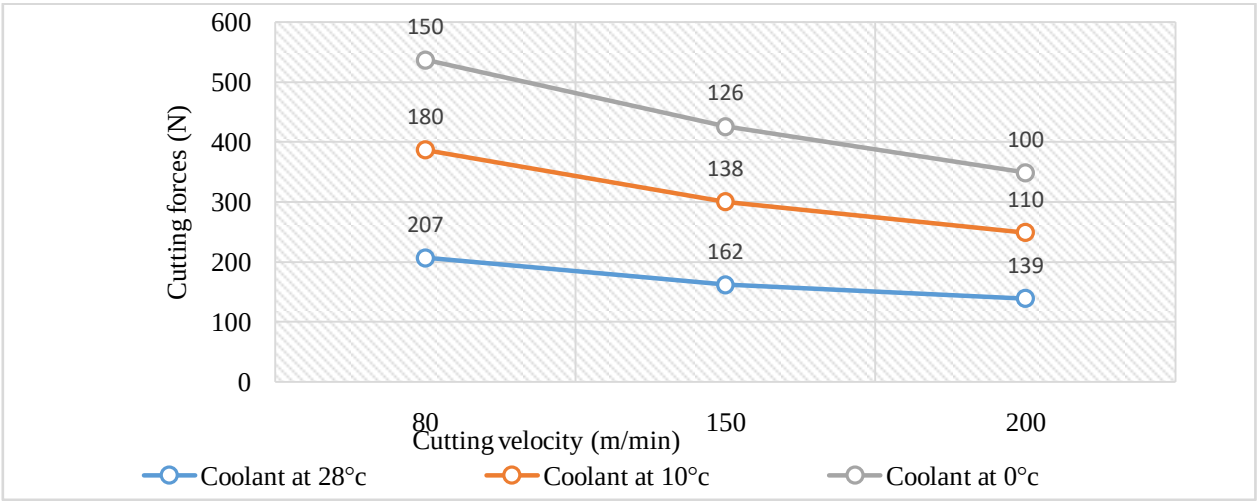

Figure 4. Cutting Forces Variation with Coolant at Varying Temperature

3.4 Heat Affected Zone and Post Machining Surface Hardness

Titanium alloys have a good corrosion resistance, relatively high strength to weight ratio and is characterized by high surface hardness and good layer adhesion(binding) properties(Chetan et al., 2016). The post machining hardness of workpiece done for set of experimental conditions were inspected by portable digital hardness tester as per ASTM A956-02 standards. In cryogenic machining, the post hardness of material was found to enhance by 4-6 HRC.The machining of Titanium alloy with cryogenic coolant like liquid nitrogen has shown an increase in hardness from 42 HRC to 46HRC. On performance of experimentation, it was found that the hardness of the material nearly same, when machining was done with emulsion coolant at 28^0c, while machining with castor coolant 0^0c is enhance hardly by 2.5HRCas shown in fig.5. The retention in hardness also helps in reduction of heat treatment process if any further operations are to be performed on work material. The increase in post hardness of workpiece may be attributed to a reduction in ductility and fracture toughness at low temperatures(Chen et al., 2017).

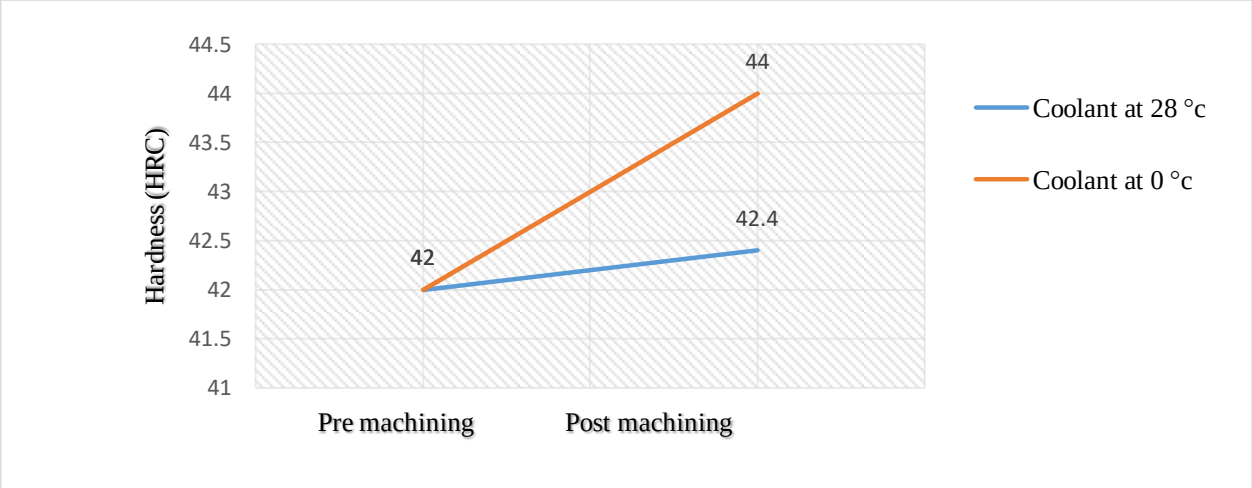

Figure 5.Effect of Coolant Temperature on Hardness

3.5Comparison of Tool Life at Variable Cutting Speed

The tool is continuously used for machining as long as it retains the cutting edge or surface roughness of workpiece is maintained with its surface integrity. The, life of tool decreases as one increases the cutting velocity and if other machining parameters are kept constant as per Taylors equation. The image processing technique was adopted in measuring wear of tool, in this technique number of images are continuously recorded and by mathematical linear regression technique one can calculate the wear of tool during machining. The tool life was significantly enhanced, when machining was done with coolant at 0^0c as compared to machining done at 28^0c. The wear in tool was reduced from 99 µm to 82 µm when machining was done at cutting velocity 200m/min and temperature of coolant was maintained at 0^0c from 28^0c and is shown in fig-6. Tool life increases as there is a significant reduction of tool wear due to low heat generation in tool and improved cutting edge. The thermal softening phenomenon also leads to improvement in tool life edge as Titanium alloy is work hardening material where strength and hardness are reduced at high temperature(Pradhan et al., 2019). The tool life was increased approximately by 25-30% when machining of Titanium alloy was done with a cutting speed in a broad range of 80 m/min to200 m/min.

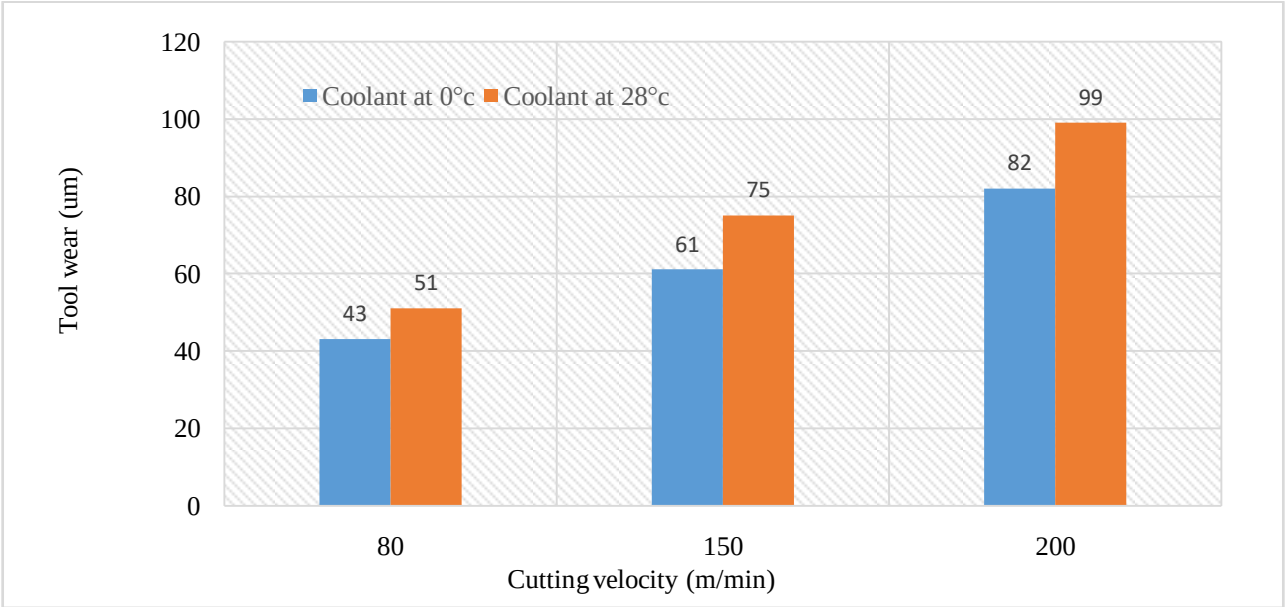

Figure 6. Effect of Coolant Temperature on Tool life

3.6 Comparison of Tool Morphology

In order to have physical verification of effect of coolant at different temperature on tool wear, the wear of tool was observed under SEM (Scanning Electron Microscope) and it was found that wear of tool is less when machining was done with coolant at 0^0c than compared to machining done at ambient conditions. Figure 7 shows that there is chipping of tool and more severe wear take place, when machining is done at ambient temperature and resulting in reduced life of tool. Titanium alloy being hard material as always issue with effective heat disposal and when coolant was used at 0^0c, it was found that there is less wear of tool and less chipping effect on rake face of tool and the physical abrogation may be less heat containment in tool face due to less temperature of coolant as shown in figure 8.

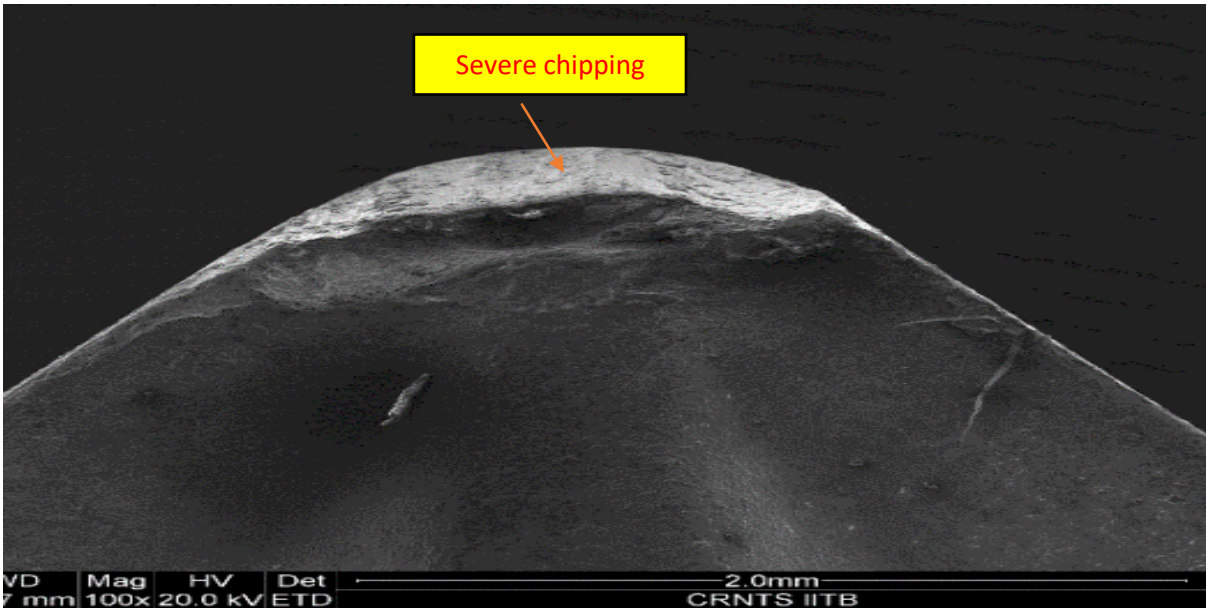

Figure 7.Morphology of Tool Wear with Coolant at Ambient Temperature

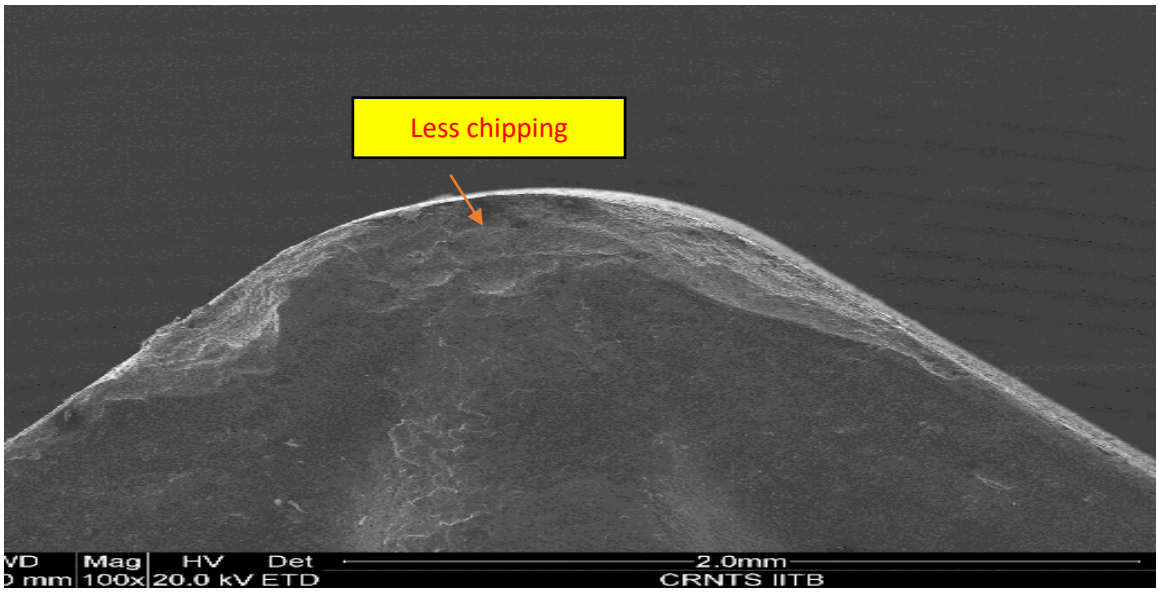

Figure 8. Morphology of Tool Wear with Coolant at Zero Degree (Latent Load) Temperature

4. Conclusions

The proposed research was conducted with the ultimate aim of providing the alternative solution to cryogenic machining can be summarized under following points –

1. The results obtained by using coolant at a temperature of 0^0c were very positive and shows improvements in increase in tool life by 1.25 times and surface finish was also improved by 20% when compared with machining done with coolant at room temperature.
2. The change in hardness of the workpiece post machining was also negligible compared to cryogenic machining, where hardness varies more than 12 percent.
3. The refrigeration system designed for this purpose was very effective and affordable. The COP of the system was about 5.46, which is considered to be thermodynamically efficient.
4. The results obtained with coolant at 0^0c, was approximate to 40% of that can be obtained by Cryogenic machining. The cost involvement was just 10% of the cryogenic system per gram of material removed from the workpiece.
5. The machining of materials using cryogenic coolant has limitations of safety risk and technical feasibility and this has been overcome in the current system. The coolant with latent heat load provides a viable alternative solution to the machine tool industry.

References

1. Arun Kumar, S., Yoganath, V. G., & Krishna, P. (2018). Machinability of Hardened Alloy Steel using Cryogenic Machining. Materials Today: Proceedings, 5(2).
2. Bruschi, S., Pezzato, L., Ghiotti, A., Dabalà, M., & Bertolini, R. (2019). Effectiveness of using low-temperature coolants in machining to enhance durability of AISI 316L stainless steel for reusable biomedical devices. Journal of Manufacturing Processes, 39.
3. Celik, O. N., Sert, A., Gasan, H., & Ulutan, M. (2018). Effect of cryogenic treatment on the microstructure and the wear behavior of WC-Co end mills for machining of Ti6Al4V titanium alloy. The International Journal of Advanced Manufacturing Technology, 95(5–8).
4. Chen, L., Tai, B. L., Chaudhari, R. G., Song, X., & Shih, A. J. (2017). Machined surface temperature in hard turning. International Journal of Machine Tools and Manufacture, 121.
5. Chetan, Behera, B. C., Ghosh, S., & Rao, P. V. (2016). Wear behavior of PVD TiN coated carbide inserts during machining of Nimonic 90 and Ti6Al4V superalloys under dry and MQL conditions. Ceramics International, 42(13).

6. Eltaggaz, A., Zawada, P., Hegab, H. A., Deiab, I., & Kishawy, H. A. (2018). Coolant strategy influence on tool life and surface roughness when machining ADI. The International Journal of Advanced Manufacturing Technology, 94(9–12).
7. Junaidh, A. P., Yuvaraj, G., Peter, J., Bhuvaneshwari, V., Kanagasabapathi, & Karthik, K. (2018). Influence of Process Parameters on the Machining Characteristics of Austensite Stainless Steel (AISI 304). Materials Today: Proceedings, 5(5).
8. Kümmel, J., Gibmeier, J., Müller, E., Schneider, R., Schulze, V., & Wanner, A. (2014). Detailed analysis of microstructure of intentionally formed built-up edges for improving wear behaviour in dry metal cutting process of steel. Wear, 311(1–2).
9. Li, S., Zhang, D., Liu, C., Shao, Z., & Ren, L. (2021). Influence of dynamic angles and cutting strain on chip morphology and cutting forces during titanium alloy Ti-6Al-4 V vibration-assisted drilling. Journal of Materials Processing Technology, 288.
10. Liu, J., Han, R., & Sun, Y. (2005). Research on experiments and action mechanism with water vapor as coolant and lubricant in Green cutting. International Journal of Machine Tools and Manufacture, 45(6).
11. Mia, M., & Dhar, N. R. (2015). Effect Of High Pressure Coolant Jet On Cutting Temperature, Tool Wear And Surface Finish In Turning Hardened (Hrc 48) Steel. Journal of Mechanical Engineering, 45(1).
12. Nomani, J., Pramanik, A., Hilditch, T., & Littlefair, G. (2017). Stagnation zone during the turning of Duplex SAF 2205 stainless steels alloy. Materials and Manufacturing Processes, 32(13).
13. P.Patil, P. Karande. (2019). Machining of SS304 using coolant with zero sensible heat. MAchining of SS304 Using Coolant with Zero Sensible Heat, Copen proceddings, 11(18-22).
14. Pradhan, S., Singh, S., Prakash, C., Królczyk, G., Pramanik, A., & Pruncu, C. I. (2019). Investigation of machining characteristics of hard-to-machine Ti-6Al-4V-ELI alloy for biomedical applications. Journal of Materials Research and Technology, 8(5).
15. Rahim, E. A., & Dorairaju, H. (2018). Evaluation of mist flow characteristic and performance in Minimum Quantity Lubrication (MQL) machining. Measurement, 123.
16. Sadik, M. I., & Isakson, S. (2017). The role of PVD coating and coolant nature in wear development and tool performance in cryogenic and wet milling of Ti-6Al-4V. Wear, 386–387.
17. Saez-de-Buruaga, M., Soler, D., Aristimuño, P. X., Esnaola, J. A., & Arrazola, P. J. (2018). Determining tool/chip temperatures from thermography measurements in metal cutting. Applied Thermal Engineering, 145.
18. Seah, K. H. W., Rahman, M., & Yong, K. H. (2003). Performance evaluation of cryogenically treated tungsten carbide cutting tool inserts. Proceedings of the Institution of Mechanical Engineers, Part B: Journal of Engineering Manufacture, 217(1).
19. Suhaimi, M. A., Yang, G.-D., Park, K.-H., Hisam, M. J., Sharif, S., & Kim, D.-W. (2018). Effect of Cryogenic Machining for Titanium Alloy Based on Indirect, Internal and External Spray System. Procedia Manufacturing, 17.
20. Tamil Alagan, N., Hoier, P., Zeman, P., Klement, U., Beno, T., & Wretland, A. (2019). Effects of high-pressure cooling in the flank and rake faces of WC tool on the tool wear mechanism and process conditions in turning of alloy 718. Wear, 434–435.
21. Yildiz, Y., & Nalbant, M. (2008). A review of cryogenic cooling in machining processes. International Journal of Machine Tools and Manufacture, 48(9).
22. Zhu, Z., Sui, S., Sun, J., Li, J., & Li, Y. (2017). Investigation on performance characteristics in drilling of Ti6Al4V alloy. The International Journal of Advanced Manufacturing Technology, 93(1–4).

DESIGN AND ANALYSIS OF VEGETABLES AND FRUIT PROCESSING UNIT.

A.A.Uplap[1], A.Sane[2], A.Pande[3], N.Mali[4] and M.Barbate[5]
Mechanical Engg. Govt. College of Engg., Nagpur

ABSTRACT

Size reduction of vegetables and fruits is an essential operation in food industries. Manual size reduction operation is a slow process, unhygienic and it needs attention. The objective of the project was to design processing unit which has simple construction, less cost and is multi- functional. So design of food processing unit was developed considering other operations assistingthe size reduction. Today in Indian market, small scale eateries and community kitchens are developing trend. The food processing unit was conceptually designed and developed for micro, medium and small scale industries. The machine consists of washing unit, conveyor unit, cutting and juicing unit. Structural analysis was conducted on the frame and force was evaluated on gearbox operating for cutting and juicing operation.

Keywords:-*Conveyor, Cutter, Gearbox, Juicer, Washer*

1. Introduction

Vegetables and fruits are an important part of a healthy diet. Average intake of fruits and vegetables in India is 3.5 servings per day, which comprises 1.5 servings of fruit and 2 servings ofvegetables. The WHO panel on diet, nutrition and prevention of chronic disease recommended a daily intake of at least 400gm (5servings, 1serving=80gm) of fruits and vegetables. Lifestyle is the topmost reason provided by the survey respondents for their inability to meet WHO recommendation.(As per the report of ICRIER)Fast lifestyle make people depend on eateries andoffice canteens to fulfil their daily meal requirement. The underprivileged depends upon subsidiary canteens by government such as Amma Canteen, Shiv Bhojanthali, etc.Some foundations and NGO's such as AkshayPatra, Annamitra, ISKON are providing nutritious mid day meal to students in school. It is found that manual cutting and slicing of vegetables is still used in some of the eateries or kitchen's, which has proved to be very time consuming and prone to risk the contamination of food leading to high rates. Various methods have been implemented previously in the process of size reduction of vegetables but their high pricing and less efficiency these machines are not preferred. Hence, a vegetable and fruit process unit was designed taking into consideration the techno-economic status of micro, small and medium scale food industries and canteens. The project is to design a unit which can facilitate the size reduction of vegetables and fruits. In addition to size reduction, cleanliness of vegetables and fruit is of utmost importance for healthy and nutritious diet. Also for this purpose feed system with less or no human intervention is necessary. The community kitchens have low funding and eateries have to maximize the profit. Hence, industries need machine which costs less, have less maintenance and also can be used in small and medium scale industries. According to the survey, small eateries or canteens need alternate source of income which can be provided by incorporating juicer in existing machines.The project deals with cutting, juicing and washing of the vegetables and fruits. The vegetables or fruits are first washed in a cylindrical washer unit inclined at a small angle then conveyed to the cutting unit with the help of conveyor and feed in systematic way due to the baffle plate. The vegetables and fruits are sliced in the unit. Alternative inputs are provided for different types of cut and also for juicing purpose. The cutting and juicing unit works on different angular velocity and Torque. A gearbox is used to provide different power requirements which uses gear arrangement for significant reduction in rotations per minute of the shaft.

2. Literature Review

Manual cutting and slicing of vegetables has proved to be very time consuming and is prone

to the risk of contamination of the food leading to high rates of food borne diseases. Various methods have been implemented in the process of size reduction of vegetables ranging from manual, electric and automated. The desire to make a design that simplifies, that saves time, that is relatively cheaper and efficient during the process of size reduction of vegetables was the main scope of the whole project. The contaminant free products will be produced through the use of U.V light and this machine will incorporate U.V light as its integral component. The principle of operation of the machine is attached to the theory of rotating hollow discs. Experiments were conducted at the Department Laboratory and a force of 19.5N was obtained for the hardest vegetable. The machines available in Zimbabwe have posed to be very expensive while they are only availed abroad. The machine must always be used with caution since it has rotating elements. In conclusion, the objectives were met and the most importantly the cost was in the desired range hence acceptable to the market. From the cost analysis, the total price required for the vegetable cutter and slicer is $890.73. [1] In Small-scale Food processing units, material handling is taken by manually due to high capital required for an advanced material handling

system. These small units are looking a conveyor system which will reduce manpower, space, money, and time for production. In many materials handling equipment's, belt conveyors are popular. This paper describes a new design and development of adjustable height belt conveyor system which works satisfactorily to meet design point of view. It is reliable, compact, adjustable, saves working man-hours and increasing profitability of small units engaged in material handling. These transports are versatile and it tends to be adjusted by the activity and its need. A legitimate structuring of the adjustable height belt conveyor will influence its productivity, working, and life expectancy. Our current attempt is towards fabricating an economical adjustable belt conveyor material unloaded by adopting the existing simple design procedure. [2] Several varieties of juicy fruits are available in abundant quantities in many parts of Nigeria, most especially during the harvesting seasons. Incidentally, there is an increasing demand for fruits juices among people of all age groups due to the vitamins, mineral and fibre contents. These products are essential for human and animal growth, aid metabolic activities and improve health standards. I designed, constructed and evaluated the performance of the extractor in the laboratory using orange fruits. The fruits were washed and weights (1kg, 1.5kg and 2kg respectively) of fruit slice (8 and 16 slices) were then processed using the extractor to extract the juice. The juice yield, extraction loss and extraction efficiency were determined by standard formulae and methods. Maximum juice yield of 64.6 % extraction efficiency of 68.2 % and corresponding extraction loss of 7.05 % respectively were obtained from the 16 slice lengths orange fruit. [3].Internal transport (means of continuous transport) is an inseparable element of technological processes in the food industry. The selection of appropriate parameters of the transport equipment depends on the product being manufactured, its design features, packaging and transport conditions. The paper presents the characteristics of a plate conveyor, selection of operating parameters in the juice transport process in a glass bottle. The paper presents selected test results depending on the linear speed of the plate conveyor, the angle of inclination of the load mass transport module and the position of the gravity centre. The work defined the linear speed ranges of the conveyor and the angle of inclination of the conveyor transporting module for transported glass bottles filled with juice. [4] Now days in industries it is very necessary to use material handling system for to move material from one place to another place continuously to minimize operation time. Various conventional conveyor systems like belt conveyors, bucket elevators, screw conveyors, pneumatic and vibratory conveyors, and roller conveyor system are used in industry, like food, chemical, plastic, material processing industry. In our case, selected industry being run on small scale

certainly have limitations to adopt these conventional material handling systems to convey the powders economically and precisely.In this paper the suitability of flexible spring conveyor system is studied critically and compared with other conventional systems the manual material handling.[5]

3. Methodology

Design and Components

3D Cad Model of the Machine:

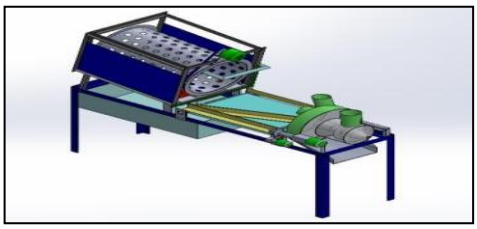

Fig. 1. Isometric View

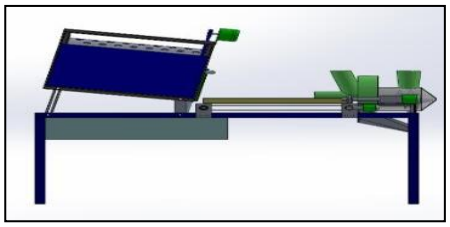

Fig. 2. Side View

1) WasherUnit

It generally does the function of washing the Vegetables and fruit which is feed into it.There are various types of washer available such as cylindrical vertical, square vertical, square horizontal, etc.But we use cylindrical in shape and horizontal about its axis. It consists of roller stand and roller which is made up of Mild Steel and SS sheet of 1.3mm respectively. It also consists of smallholes on the circumference for removal of water after cleaning. To run that washing unit we are using 400-500 watt motor.In that unit, pump has been provided to lift water from tank given below.In that pump, we use filter so that we can reuse water for cleaning.To protect Vegetables from falling while the cylindrical washer is inclined we have provided a fibre made plate which will be supported by slot provided there.

2) Conveyor:

Flat belt conveyors are some of the most prevalent and versatile belt conveyor systems in commonuse. Flat belt conveyors use a series of powered pulleys to move a continuous flat belt of natural or synthetic fabrics such as polyester, nylon, or other materials. We are using roller belt conveyor, for belt driven roller conveyor systems, a series of rollers supported by a structure, suitable for unit handling loads which are driven by a belt. The belt driven roller conveyor systems are suitable for handling a great variety of heavy and light loads of regular or irregular shape. Main function of conveyor is to feed vegetables to cutter from washer, preventing inefficient loading. We are using a single phase AC motor to drive the roller belt of power output 300 to 500 watts.The rollers for bearing used are ball bearing due to their smooth functioning. Total 4 numbers of bearings are used. Material of belt is food grade nylon belt. Which prevents further contamination of vegetables by chemically reacting with material. Overall length of belt: 30 inch (0.762 meters).

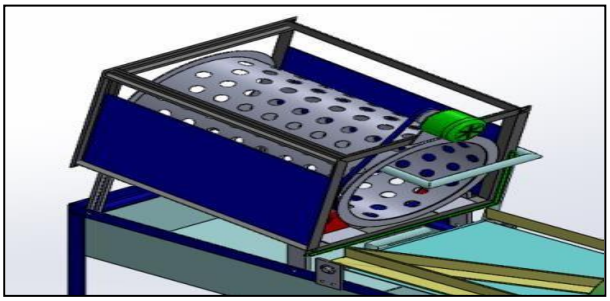

Fig. 3. Washing Unit

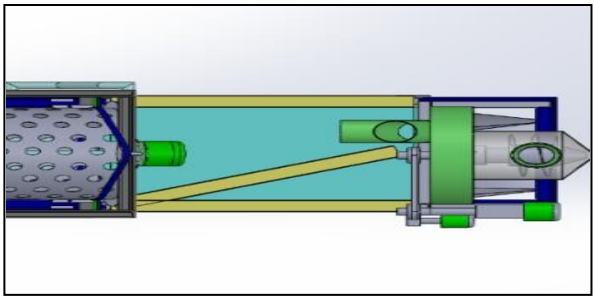

Fig. 4. Conveyor Unit

3) Guide ways

They play vital role in guiding vegetables to

cutter. They prevent the washed vegetables from skidding or falling down from the conveyor which also secures the smooth flow of feeding of vegetables to the cutting section. Material used: Mild steel angle bar Total numbers used are 2; Length: 0.381 meters.

4) Baffle plates

They play an important role in guiding the vegetables to the cutter blade input opening. This guides called as Baffle plates help to narrow down the path of vegetables on the conveyor and helps in making the vegetables move in a single line into the cutter compartment. Material used for this purpose is generally stainless steel plates. Their length can be varied with respect to the size of thevegetables

5) Transmission unit(gearbox)

Gearbox is used for transmitting power to the shafts. The gearbox is used for significant reduction in power. The gearbox is arrangement of 8 gears made of cast iron. The splined shaft provides continuous transmission to pulley.

6) Cutting Unit

Cutting unit consist of stainless steel blades, which cut the vegetable and fruits in different shapes. Blades are made up of SS food grade 304, which is used to cut the Vegetables and fruit. Blades are kept in the blade housing, which is made up of material SS or Plastic fibre. In that unit; Juicer has been given to extract juice from fruits by screw type juice extractor. A lever has been provided due to which a single motor can operate both cutting and juicing operation one at a time.

Fig. 5. Cutting Unit

: Assembly Drafting of Machine:

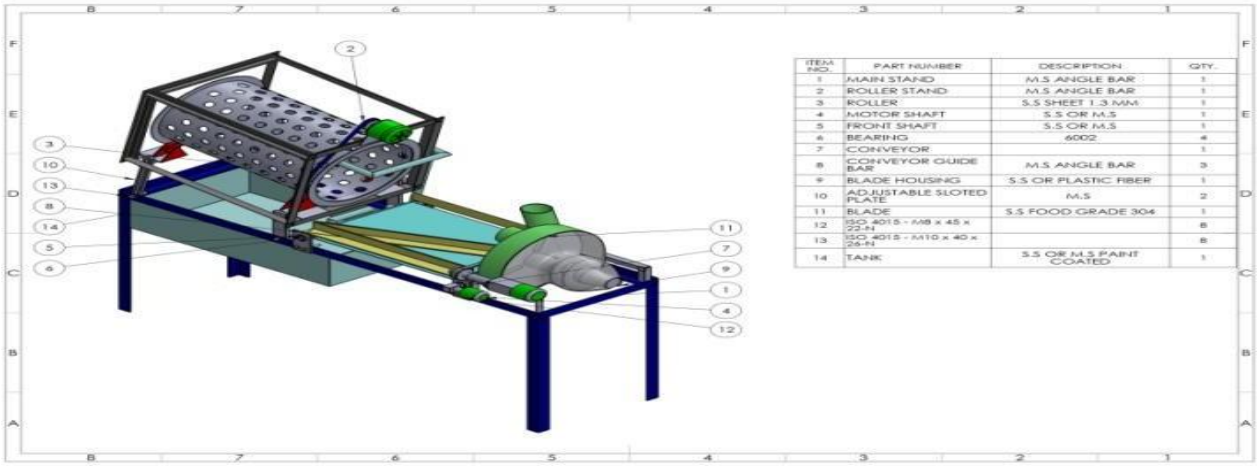

ITEM NO.	PART NUMBER	DESCRIPTION	QTY.
1	MAIN STAND	M.S ANGLE BAR	1
2	ROLLER STAND	M.S ANGLE BAR	1
3	ROLLER	S.S SHEET 1.3 MM	1
4	MOTOR SHAFT	S.S OR M.S	1
5	FRONT SHAFT	S.S OR M.S	1
6	BEARING	6002	4
7	CONVEYOR		1
8	CONVEYOR GUIDE BAR	M.S ANGLE BAR	3
9	BLADE HOUSING	S.S OR PLASTIC FIBER	1
10	ADJUSTABLE SLOTED PLATE	M.S	2
11	BLADE	S.S FOOD GRADE 304	1
12	ISO 4015 - M8 x 45 x 22-N		8
13	ISO 4015 - M10 x 40 x 26-N		8
14	TANK	S.S OR M.S PAINT COATED	1

Fig. 6. Assembly Drafting

Calculations

1. For Washer Power =
300 watts Speed, N =
300 rpm
Angular velocity, ω = 2*pi*N
= 2*pi*(300/60) =31.41 rad/sec
W=pi*D/t
T = (pi*0.355)/31.41 =0.035/sec
Power = (2*pi*N*T)/60 300 = 2*pi*300*T/60
Torque = 9.55 Nm
2. For ConveyorWeight = 10 kg μ =0.3
Tension on belt, T1=10*9.81*0.3 = 29.43 N
Power = 300 watts
300 = 2*pi*300*T/60
T= 9.55 Nm
3. For cutter
Speed of motor =900
Torque = (power* 60)/(2*pi*N)
=542*60/(2*pi*900)
=5.76 Nm
4. For juicer
Speed of motor= 57
Torque= (power*60)/ (2*pi*57)
= (542*60)/ (2*pi*57)
=90.84 Nm
5. Design of driver shaft:
T=Π/16Ƭd3 (Ƭ=200mpa for mild steel)
2.47=3.14/16×200×106×d3
d=4mm (minimum diameter)
Design of driven shaft:
P=2ΠNT/60 where N=156rpm and P=0.5hp
Substituting the values we get,T=23 Nm
T= (Π/16)Ƭ×d3
23×16/3.14×200×106 =d3
6. For Gearbox
NG1=NG_2
& NG1=NG3
N3* D3 = N4* D4 900 x
25 = 100x N4
N4= 225 RPM NG4 =
NG5 225x25 = N6 x 100
N 6= 56.25 57 = 57 RPM
NG8= NG7
If we engage G7 to G8, G8 = D = 50mm
NG8= 57x25 50 =28.5
= 29 RPM

Details- 1Hp motor is used
Motor RPM = 900 RPM
G_1 = 100 mmG_2 =
100 mmG3=25
mm G4=100 mm
G5= 25 mm
G6=100mm
G7=25 mm G8 =
50 mm
If we connect shifter to the dock arrangement then it gives 900 RPM for chopper axle. If we connect gear G7 & G8it gives 29 RPM for juicer.

Working

The model is divided into 3 sections i.e.

1) Washer machine
2) Conveyor mechanisms
3) Cutter and juicer machine

Washer machine consist of mainly four to five main components, which are the cylindrical washing vessel, inclined washer holding frame consisting of the motor mounted on the frame which will help in running the washer as per requirement. Then there is the tub like structure which provides water supply to the washing unit. There is a pump provided to pump the water through the nozzles provided in the inner rod of the cylinder washer. After this the rotating cylinder drops the Vegetables on the conveyor. The conveyor mechanisms consist of two rollers shafts of which one attached to the motor which rotates the conveyor belt warped around these rollers. To keep the vegetables on the belt there are to metal guards mounted on both the sides of the belt. And to guide the vegetables in to the cutting input opening there is a baffle plate placed on the belt whose inclination can be changes as per the size of the vegetables to be processed. Now the main part thecutting machine or compartment which is the main component of this machine. It consists of two main parts First one is the input component which helps to feed the Vegetables to the cutting blades and Second one is the cutting blades itself.

The input component has two opening horizontal surface opening and the other is the

inclined vertical one, both have different uses. After this comes the cutting blades which have 3 slits wherethe blades are mounted on the circular plate which is then mounted on a shaft. This shaft is connect to a motor and gearbox which help to alter the speed and torque of the motor as per requirement. Atthe end of the cutting blade shaft there is one more tool attached which is the juicer tool used to produce juice of various fruits and Vegetables as required. The input part of this juicer is a bit different. There is a top feeder mounted just above the juicer blades which help to give input and apply little nit pressure if required. At the end there will be a curved plate to guide the sliced Vegetables into the container kept below the exit or end point of the tools.

4. Analysis

Analysis Of Frame

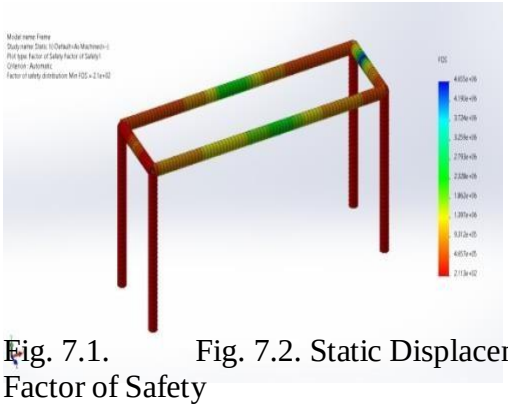

Fig. 7.1. Fig. 7.2. Static Displacement Factor of Safety

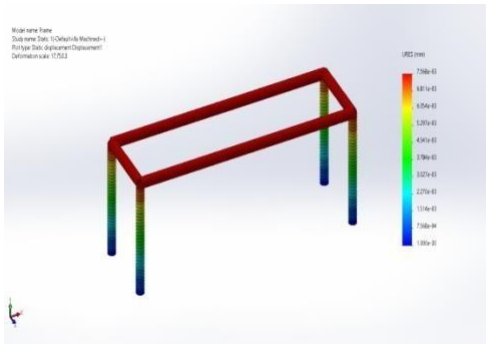

Fig. 7.2

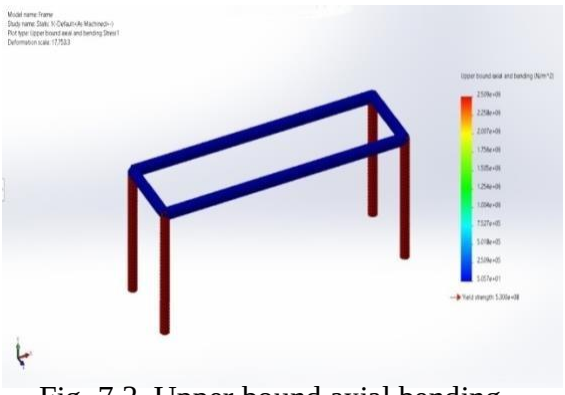

Fig. 7.3. Upper bound axial bending stress

4. Conclusion:

Thus, we have come up with a optimal design of food processing unit. We have been able to design and develop a machine which can process vegetables and fruits according to the requirement. In this paper, attempt made to design a machine with simple construction and suitable for small and medium scale industries were successful.

5. Acknowledgement:

We express our gratitude to Prof. A.A.Uplap, Associate Professor, Department of Mechanical Engineering, faculty member and staff of Department of Mechanical Engineeringfor extending all possible help in carrying out this research work directly or indirectly.

References

1. Guide S Ganyani, Tawanda Mushiri, "Design of an Automated Vegetable Cutter and Slicer", University of Zimbabwe, Department of Mechanical Engineering, Post Office Box MP167, Mount Pleasant Harare, Proceedings of the International Conference on Industrial Engineering and Operations Management Pilsen, Czech Republic, July 23-26, 2019.
2. Rahul. K. Bhoyar, Sandeep.M. Pimpalgaonkar, Swapnil. J. Bhadang, "Adjustable Height Belt Conveyor for Small-Scale Food Processing Unit",International Journal of Engineering and Advanced Technology (IJEAT) ISSN: 2249 – 8958, Volume-8 Issue-2, December 2018.
3. Bamidele, Christopher S., "Design, Fabrication And Evaluaton Of A Motorized Fruit Juice Extractor", January, 2011
4. J Caban, A Nieoczym, W Misztal and D Barta, "Study of operating parameters of a plate conveyor used inthe food industry", 2019 IOP Conf. Ser.: Mater. Sci. Eng. 710 012020
5. Mr. Pranay S. Chaudhari, Prof. V.A. Kolhe, Prof. S.B. Ambekar, "A Review Paper on Flexible Spring Conveyor System for Material Handling System.", International Research Journal of Engineering and Technology (IRJET), Volume: 03 Issue: 04, Apr-2016

SPEED SENSORLESS CONTROL OF INDUCTION MOTOR

I.D. Bageshwar[1] and S.B. Bodkhe[2]
Shri Ramdeobaba College of Engineering and Management, Nagpur, India
[1]bageshwarid@rknec.edu,[2]bodkhesb@rknec.edu

ABSTRACT

This paper presents a simulation study of different methods used for estimating the rotor speed of a three-phase induction motor. Comparison is made between the open loop speed estimator and close loop observer based on model reference adaptive system (MRAS). The voltage model and current model of the machine are used to form the reference model and adjustable model of MRAS. These models calculate the rotor flux linkages by different approaches. The former one makes use of stator voltage equations whereas the equations of the adjustable model require the rotor speed for the calculation of flux linkages. The difference between the outputs of both models is processed with the help of PI controller to find the estimated speed. Both methods of speed estimation are modelled, simulated and tested at different operating conditions. A qualitative analysis is presented based on the observed results. The MATLAB Simulink software is used for the simulation study.

Keywords: *Induction motor, Model Reference Adaptive System, estimated speed, flux linkage, open loop estimator*

Nomenclature

V_{ds^s}, V_{qs^s}	direct and quadrature components of stator voltage in stationary frame
i_{ds^s}, i_{qs^s}	direct and quadrature components of stator currentsin stationary frame
Ψ_{ds^s}, Ψ_{qs^s}	direct and quadrature axis stator flux linkages in stationary reference frame
Ψ_{dr^s}, Ψ_{qr^s}	direct and quadrature axis rotor flux linkages in stationary reference frame
Ψ_{dr^r}, Ψ_{qr^r}	direct and quadrature axis rotor flux linkages in rotor reference frame
V_{qs^e}	quadrature axis stator voltage in synchronous frame
i_{qs^e}	direct axis stator current in synchronous frame
$\overrightarrow{i_{s^s}}$	space phasor of stator current in stationary frame
$\overrightarrow{\Psi_r}, \overrightarrow{\Psi_s}$	space phasor of rotor and stator flux linkage in stationary frame
R_s, R_r	stator and rotor resistance
L_s, L_r, L_m	stator, rotor and mutual inductance
L_{ls}, L_{lr}	leakage inductance of stator and rotor
T_e, T_L	electromagnetic and load torque
ω_r, ω_m	actual, mechanical speed
$\widehat{\omega_r}$	estimated speed
T_r	rotor time constant
P	number of poles
J	inertia
X_d, X_q	State variables that are obtained from the measured values of stator quantities
$\widehat{X_d}, \widehat{X_q}$	State variables calculated by adaptive model

1. Introduction

In various industrial drive applications, the most popularly used machine is an induction motor and quantifies to 70-80% of all types of motors. This is due to its high reliability, low initial cost, low running cost, rugged construction and possibility to control the torque and speed very precisely, because of the availability of modern power electronics systems and modern control methodologies [1]-[7].

The motivation behind speed-sensorless control is the current trend which has practically recognized it as a de-facto industrial standard. The modern trend is to go for the estimation of rotor speed in place of actually measuring it with the help of physical sensor. In conventional speed drive, the measuring the rotor speed of induction motor using sensors such as tachometer, optical encoder etc. results in hardware complexity, performance delay, increased space requirement, increased cost, and low reliability [3]. Also, in the hostile and high-speed environments, the used of actual speed transducer is not preferred [8]. Because of these limitation in conventional system, the mechanical speed sensor is eliminated and replaced by an algorithmic speed estimator.

These estimators require the stator currents, stator voltages and machines parameters in their calculations. The use of speed sensorless control overcomes the above limitations of the systems with speed sensor along with high noise immunity and reduced drift factor [2].

The speed sensorless techniques are classified in two broad categories [9]. (1) Machine model-based estimators and (2) those based on magnetic saliencies of the motor. The machine model-based estimators are further classified as (1) Open loop estimators and (2) close loop observers. The open loop estimators can be formulated in different ways. The difference between them are based on the number of integrators, differentiators and machine parameters involved in the algorithm. In open loop estimator the estimated speed is obtained from machine equations by measuring phase voltages and currents [2]. They are relatively simple and less costly but have a limited speed range. Because of this, researchers have shown interest in open loop estimators and are popularly used in low-cost system. Many different types of close loop observer are suggested in literature. The most popular amongst them are (1) Deterministic observer (2) Stochastic observer. In Deterministic observer, uncertainties are less. e.g., Extended Luenberger Observer (ELO) also called as full order adaptive state observer. In this rotor speed is considered as a parameter. In stochastic observer, uncertainties in input can be allowed. e.g., Extended Kalman Filter (EKF) [10]-[11]. In this rotor speed is considered as state variable. This observer can use any quantities not only the rotor speed. The ELO and EKF use internal feedback loop together with the machine model to improve the estimation accuracy and robustness against parameter variations. However, they are difficult because of heavy mathematical approach and their tuning difficulties [1]. 2 One more close loop speed estimator is proposed in literature and available commercially named as the model reference adaptive system. It is one of the most established techniques due to its simplicity and accuracy [9]. MRAS consists of two models; reference model and adaptive model [10]. The reference model contains state variables which do not include the parameters to be estimated. On the other hand, the adaptive model contains same state variables but different equations which does include the parameters to be estimated. To find out the minimizing error between the outputs of these two models, an adaptive mechanism is used which normally consist of PI controller and the Popov's hyper stability criteria is used for its design [1]-[2]. Different types of MRAS are available in literature such as rotor flux linkage based MRAS, back emf MRAS, reactive power MRAS, stator current MRAS, high frequency injection based MRAS, X-MRAS, Z-MRAS, ANN based MRAS, fuzzy logic based MRAS etc. [3]-[10], [12]- [15]. Out of these types the rotor flux based MRAS is studied and modelled in this paper.

It presents a comparative study of open loop estimator scheme and rotor flux based MRAS for speed sensorless control of induction motor drive. The performance of these two schemes is tested, under different operating condition like step change in speed, load application and speed reversal. The paper is organized as follows. Section 2 and 3 gives a detailed discussion on speed sensorless control and different types of open loop estimators in general. A review of various MRAS schemes is provided in Section 4. Section 5 presents a simulation study with comparative analysis between open loop estimator and flux linkage based MRAS followed by conclusion in section 6.

2. Speed sensorless control

By the last few years, speed sensorless control of induction motor has been extensively explored. The rotor speed is estimated without use of a physical sensor. In conventional system, we need a physical speed sensor i.e., an additional object is required as shown in Fig.1. It adds its own drawbacks like it contributes time delay in overall system response, makes the system slightly sluggish, increases the sensitivity of system, makes it less robust and hikes the overall cost. For some applications, typically at high speed, it is difficult to mount a speed sensor and that is not possible. In hostile environments, it may be impossible to mount a speed sensor on motor shaft. So, today speed sensorless control has become an effective industrial standard.

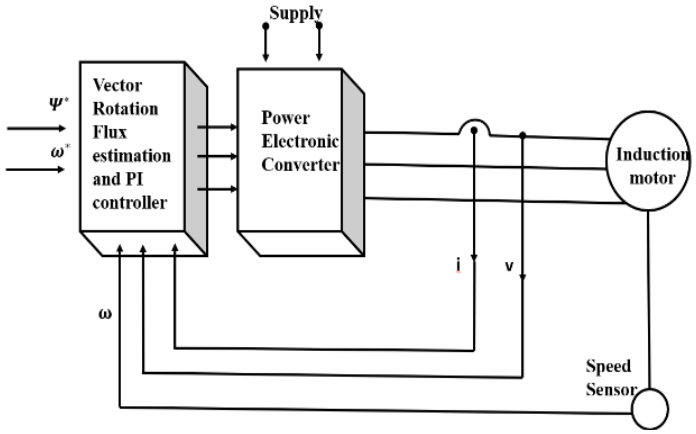

Figure 1. Conventional close loop speed control

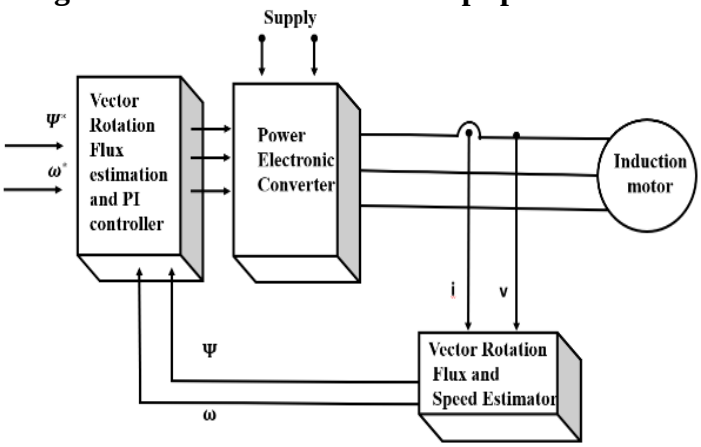

Figure 2. Speed Sensorless control

Fig. 2 shows a schematic diagram of speed sensorless control. It adds another block that shows vector rotation, flux and speed estimator. It also includes transformation from a- b-c to d-q and vice versa. This block receives the stator currents and stator voltages as input and it gives estimated flux linkages and estimated speed. These two values are then compared with the command flux linkage and command speed to generate appropriate gate signals for the power electronic converter. The scheme has flux control loop and speed control loop for effective close loop control of the drive. The speed of the rotor varies continuously with the load condition with the input frequency or the input voltage etc. So, this speed estimator should be able to calculate the exact value of speed at different operating conditions.

The advantages of sensorless motor drives are low cost, increased reliability, reduced hardware complexity, better noise immunity and less maintenance requirements.

3. Open loop estimators

In general, the accuracy of open loop estimators depends on the accuracy of machine parameters used and therefore is reduced at low rotor speed [2]. Especially at low speed, the stator resistance has important effect on the stator flux linkages. And if the rotor flux linkage is obtained from the stator flux linkage, then the rotor flux linkage accuracy is also deflected by stator resistance and the integration involved in computation. In some schemes, the rotor time constant can also vary which is required for the estimation of rotor flux linkage. Rotor resistance can vary due to temperature effect and skin effect while the rotor self-inductance can vary due to saturation effect and skin effect. The open loop estimators are classified follows [2]:

A. Scheme 1

$$\omega_r = \left[-\frac{d}{dt}\Psi_{dr}{}^r - \frac{\Psi_{dr}{}^r}{T_r} + \frac{L_m}{L_r} i_{ds}{}^s\right] / \Psi_{qr}{}^r \quad (1)$$

where, the flux linkages are

$$\Psi_{dr^r} = \frac{L_r}{L_m}(\Psi_{ds^s} - L_s i_{ds^s})$$

$$\Psi_{qr^r} = \frac{L_r}{L_m}(\Psi_{qs^s} - L_s i_{qs^s})$$

It involves two integrators, two differentiators and five machine parameters. Its accuracy is limited at low speed.

B. Scheme 2

$$\omega_r = -\frac{\left[V_{ds^s} - \left(R_s + \frac{L_s}{T_r}\right) i_{ds^s} - L_s \frac{d}{dt} i_{ds^s} + \frac{\Psi_{ds^s}}{T_r}\right]}{\left(\Psi_{qs^s} - L_s i_{qs^s}\right)} \quad (2)$$

where, the flux linkages are

$$\Psi_{ds^s} = L_s i_{ds^s} + L_m i_{dr^r}$$

It involves two integrators, one differentiator and four machine parameters. The complexity is similar to first scheme. It gives satisfactory results down at 2 Hz.

C. Scheme 3

$$\omega_r = V_{qs^e} / \left(|\overline{\Psi_s}| - L_s i_{qs^e}\right) \quad (3)$$

where,

$$\overline{\Psi_s} = \left(\Psi_{ds^s} + j\Psi_{qs^s}\right) = L_s \overline{i_s^s} + \frac{L_m}{L_r}\overline{\Psi_r}$$

It involves two differentiators, one integrator and four machine parameters. It gives satisfactory results at very low speeds but parameter variation reduces the accuracy.

D. Scheme 4

$$\omega_r = \frac{1}{|\overline{\Psi_r}|^2}\left[\left(\Psi_{dr^s}\frac{d}{dt}\Psi_{qr^s} - \Psi_{qr^s}\frac{d}{dt}\Psi_{dr^s}\right) - \text{LmLr}\Psi\text{drsiqss} - \Psi\text{qrsidss}\right] \quad (4)$$

where, the flux linkages are

$$\Psi_{dr^s} = \frac{L_r}{L_m}\left[\int (V_{ds^s} - R_S i_{ds^s})dt - \sigma L_s i_{ds^s}\right]$$

$$\Psi_{qr^s} = \frac{L_r}{L_m}\left[\int (V_{qs^s} - R_S i_{qs^s})dt - \sigma L_s i_{qs^s}\right]$$

It involves two integrators, two differentiators and three machine parameters. The stator voltages can be reconstructed from dc link voltage and the switching states of the inverter. By using speed of the rotor flux-linkage space vector or stator flux-linkage space vector, the rotor speed estimator is estimated as shown in Fig. 3. It requires the computation of the appropriateslip frequency [2].

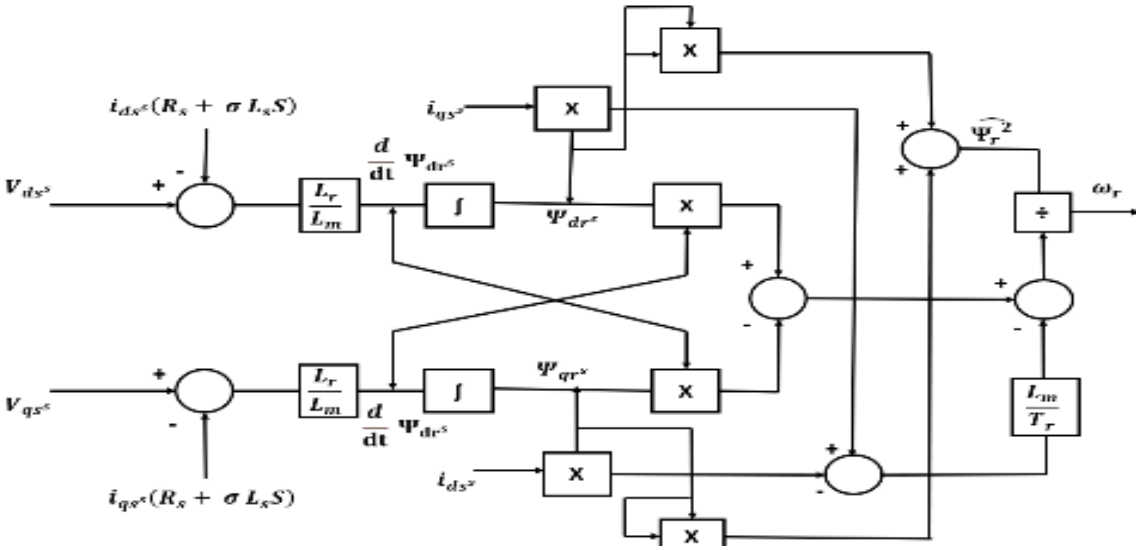

Figure 3. Speed estimation by open loop estimator scheme-4

4. Model reference adaptive system

MRAS is a close loop estimator in which correction term involving the estimation error is used to adjust the response of the estimator. In model reference adaptive system, two different models of the induction machine are estimated state variables like back-emf components or rotor flux-linkage components etc. [5]. These two models consist of reference model and adaptive model. The reference model estimates state variables from measured quantities like stator voltages and currents. The adaptive model requires the above measured quantities as well as estimated rotor speed $\widehat{\omega_r}$ as inputs. The state variable vectors estimated by reference model and the adaptive model are denoted by x and $\hat{x}$ respectively. These two variables are compared and difference between two is called an error and is given to the adaptive mechanism which makes incremental change as required in the value of speed guess.

This estimated value again given to the adaptive model and the process repeats till the error becomes zero. This is as shown Fig.4.

Various types of MRAS are reported in literature. They are; rotor flux based, back emf based, reactive power(Q) based, stator current based, high frequency injection based, XMRAS, ANN based and fuzzy logic based MRAS [3]- [10],[12]-[15]. Some of them are as discuss below.

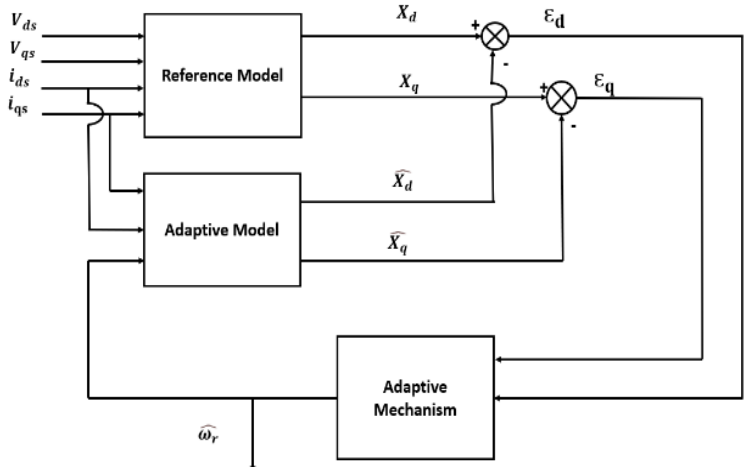

Figure 4. Block diagram of MRAS

The stator voltage equations in synchronously rotating frame are expressed as [9]

$$V_{ds} = R_s\, i_{ds} + \sigma L_s \frac{d}{dt} i_{ds} + \frac{L_m}{L_r}\frac{d}{dt}\Psi_{dr} - \sigma L_s\, \omega_e\, i_{qs} - \omega_e \frac{L_m}{L_r}\Psi_{qr} \quad (5)$$

$$V_{qs} = R_s\, i_{qs} + \sigma L_s \frac{d}{dt} i_{qs} + \frac{L_m}{L_r}\frac{d}{dt}\Psi_{qr} + \sigma L_s\, \omega_e\, i_{ds} - \omega_e \frac{L_m}{L_r}\Psi_{dr} \quad (6)$$

where,

leakage factor $\sigma = \left(1 - \frac{{L_m}^2}{L_s L_r}\right)$

and synchronous speed $\omega_e = \omega_r + \omega_{sl}$

A. Reactive power (Q) based MRAS

This MRAS eliminates the need of rotor flux estimation in its estimation process [10]. The expression for instantaneous reactive power is obtained as in (7) and it is independent of rotor speed and therefore it is used as reference model.

$$Q_{MRAS} = V_{qs}\, i_{ds} - V_{ds}\, i_{qs} \quad (7)$$

By substituting the values of voltages from (5) and (6) into (7) and replacing $\Psi_{dr} = L_m i_{ds}$ and $\Psi_{qr} = 0$, the expression of Q which is independent of flux term will be as shown in (8). It is dependent on rotor speed and therefore is used as adaptive model.

$$\widehat{Q}_{MRAS} = \sigma L_s\, \omega_e \left({i_{ds}}^2 + {i_{qs}}^2 \right) + \omega_e \frac{{L_m}^2}{L_r} {i_{ds}}^2 \quad (8)$$

The error signal $\varepsilon = Q_{MRAS} - \widehat{Q}_{MRAS}$

B. X – MRAS

X is a fictitious quantity which is neither reactive nor active power. The instantaneous value of X is given as in (9) and it is independent of rotor speed. Thus, is used as reference model.

$$X_{MRAS} = V_{qs}\, i_{ds} + V_{ds}\, i_{qs} \quad (9)$$

Substituting values of voltages from (5) and (6) into (9) and replacing $\Psi_{dr} = L_m i_{ds}$ and $\Psi_{qr} = 0$. The expression of X which is independent of both flux term and derivative operations is shown in (10). It contains synchronous speed and hence is used as adaptive model.

$$\widehat{X}_{MRAS} = \omega_e \left[L_s {i_{ds}}^2 - \sigma L_s {i_{qs}}^2 \right] + 2 R_s\, i_{ds}\, i_{qs} \quad (10)$$

The error signal $\varepsilon = X_{MRAS} - \widehat{X}_{MRAS}$

C. Z- MRAS

The difference of impedances Z_d and Z_q is considered for this MRAS and it represents the ohmic values. This does not carry any physical significance in terms of electrical machines [7].

As (11) is independent of speed, it is used as reference model.

$$Z_{MRAS} = \frac{V_{ds}}{i_{ds}} - \frac{V_{qs}}{i_{qs}} \quad (11)$$

where,

$$Z_d = \frac{V_{ds}}{i_{ds}} \; and \; Z_q = \frac{V_{qs}}{i_{qs}}$$

By substituting values of voltages from (5) and (6) into (11) and under field orientation; replacing $\Psi_{dr} = L_m i_{ds}$ and $\Psi_{qr} = 0$. Since the resulting equation is dependent on synchronous speed, it is used as adaptive model.

$$\hat{Z}_{MRAS} = -\hat{\omega}_e L_s \left(\frac{i_{ds}}{i_{qs}} + \sigma \frac{i_{qs}}{i_{ds}} \right) \quad (12)$$

D. Rotor flux-linkage based MRAS

In rotor flux based MRAS (RF-MRAS), the rotor flux linkages are obtained from stator and rotor voltage equations of induction machine in stationary reference frame. They are given by (13)-(16). The reference model represented by (13) and (14) is independent of rotor speed while the adaptive model represented by (15)-(16) involves rotor speed [6]. This is also shown in Fig.5

$$\Psi_{dr^s} = \frac{L_r}{L_m}[\int (V_{ds^s} - R_S i_{ds^s})dt - \sigma L_s i_{ds^s}] \quad (13)$$

$$\Psi_{qr^s} = \frac{L_r}{L_m}\left[\iint (V_{qs^s} - R_S i_{qs^s})dt - \sigma L_s i_{qs^s}\right] \quad (14)$$

$$\frac{d}{dt}\Psi_{dr^s} = -\frac{1}{T_r}\Psi_{dr^s} - \omega_r \Psi_{qr^s} + \frac{L_m}{T_r} i_{ds^s} \quad (15)$$

$$\frac{d}{dt}\Psi_{qr^s} = -\frac{1}{T_r}\Psi_{qr^s} + \omega_r \Psi_{dr^s} + \frac{L_m}{T_r} i_{qs^s} \quad (16)$$

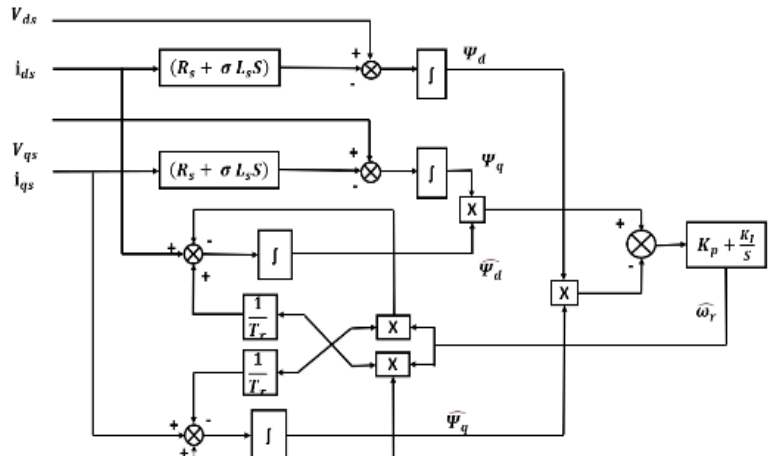

Figure 5. Structure of RF-MRAS scheme

The estimation of rotor flux linkages by above two models is followed by an adaptation mechanism which is responsible to state whether the system is stable or not. For stable response, the adaptation mechanism is normally design using Popov's hyper stability criteria [2]. It can also consist of a PI controller with tuned constants. The adaptation mechanism converts the error signal (x - $\hat{x}$) into speed tuning signal which is given as an input to the PI controller. The PI controller output is the estimated rotor speed $\widehat{\omega_r}$. The reason behind integrator in PI controller is that the error tends to become zero asymptotically.

5. Simulation results

Simulation of V/f strategy in inverter fed induction motor drive with (1) open loop estimator of scheme-4 (Fig.3) and (2) RF-MRAS Fig. (5) is implemented in MATLAB environment. In this model, both frequency and voltage are adjusted to enforce the given operating conditions. The simulation models of three phase induction motor and three phase inverter are developed from their dynamic equations [1]. For this purpose, the a-b-c quantities are transformed into d-q stationary reference frame [16]. Both speed sensorless schemes are tested at different operating conditions as presented below in Fig. 6- Fig. 8.

They show command speed, actual speed and estimated speed.

The schemes were simulated using variable step, ode 23t (mod. Stiff/Trapezoidal) solver with minimum and maximum step size of 0.00001 and 0.0001. The machine parameters are given in the appendix.

A. Step Change in command speed at no load

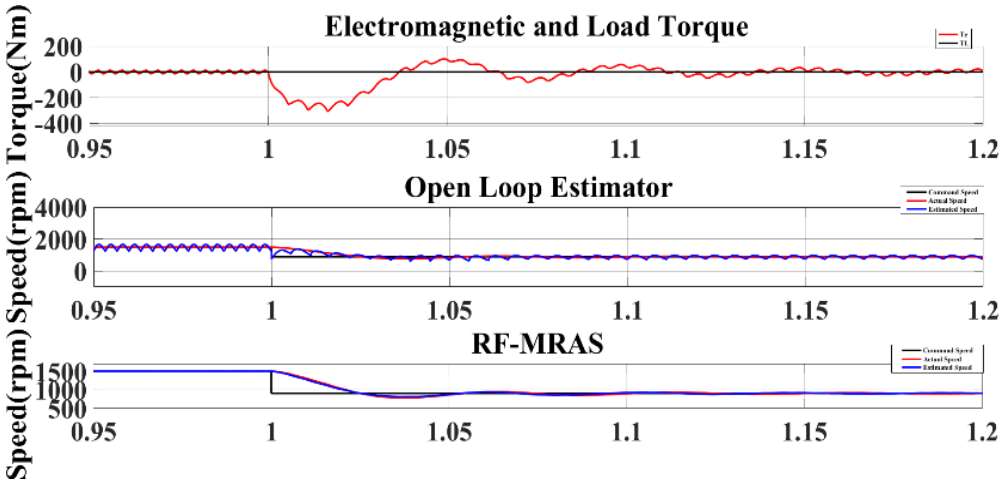

Figure 6. Simulations result for step change in command speed

Initially the motor is made to run at rated speed of 1480 rpm and at t=1sec, a step change in speed command from 1480 rpm to 900 rpm is applied. This is shown in Figure 6. The speed estimated by both open loop estimator and RF-MRAS follow the command speed and within a settling time of 0.2 sec approximately, they reach the steady state value. However, the speed estimated by open speed estimator has more ripples and the ripple frequency varies proportionally with the magnitude of rotor speed.

B. Step Change in Load torque

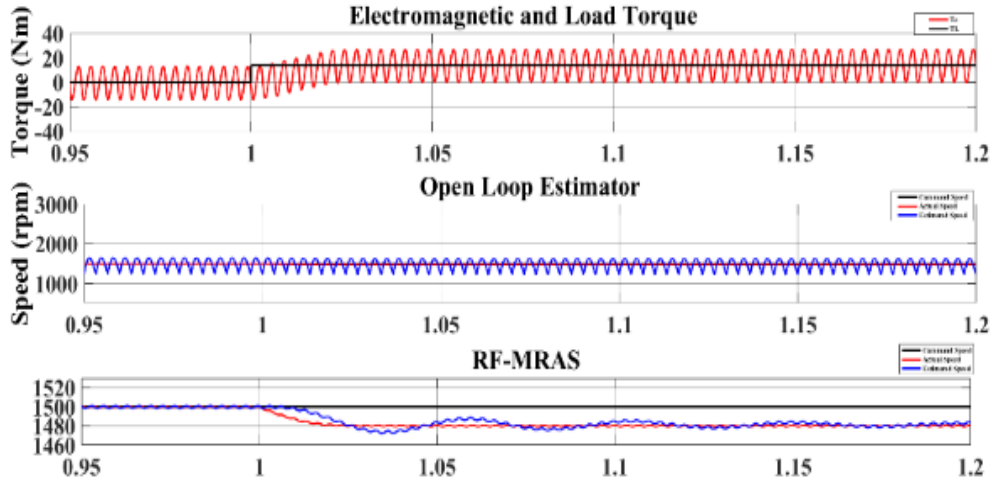

Figure 7. Simulations result for step change in load

As shown in Figure 7, the motor is made to run at rated speed and a step load of rated value (14 Nm) is applied at t=1sec. Due to unbalance in equilibrium condition there is a drop in rotor speed and the same is observed with both types of estimators. However, due to high ripple magnitude in estimated speed by open loop estimator, it cannot be used in high performance applications. On the contrary the speed estimated by RF-MRAS follows the command speed with better accuracy.

C. Speed reversal at no load

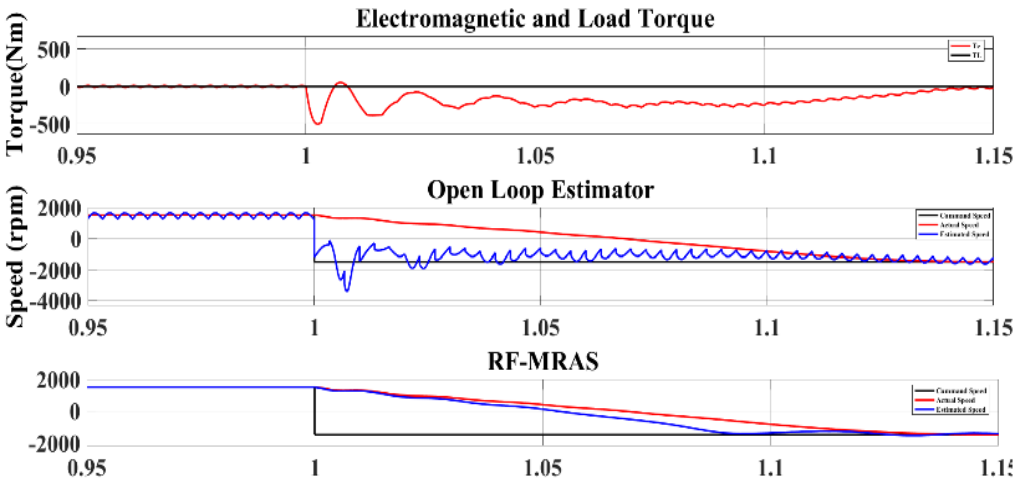

Figure 8. Simulations result forspeed reversal

Above results in Figure 8 shows speed reversal at no load. Change in speed command from 1500 rpm to -1500 rpm at t = 1sec. The actual speed goes to steady state at time 0.15 sec and estimated speed follows it. The electromagnetic torque at time 1 sec goes negative and then settle to final steady state value at 0.15 sec.

6. Conclusion

The comparison of the performance of open loop estimator and RF-MRAS speed estimator in MATLAB Simulink is analyzed for different operating condition like step change in speed, load application, speed reversal. It is found that estimated speed of both open loop estimator and RF-MRAS follows actual speed. However, the ripple content in given open loop estimator is large. As, the rotor speed increases, the ripple frequency in speed estimated by open loop estimator gets increased and vice-versa. Whereas it is observed that the MRAS estimator gives more accurate results at different operating conditions and therefore can be preferred in high performance drive applications. Thus, the MRAS scheme is superior over open loop estimators.

7. Appendix

Table 1. Induction Motor Parameters

Electrical parameters	Specification
Motor rating	3 HP
Frequency	50 Hz
Voltage	440 V
Stator Resistance (R_s)	0.435 Ohm
Leakage Inductance of stator (L_{ls})	0.002 H
Rotor resistance (R_r)	0.816 Ohm
Leakage Inductance of rotor (L_{lr})	0.002 H
Mutual Inductance (L_m)	0.69347 H
No. of poles	4
Inertia (J)	0.089 kg/m^2

References

1. B. K. Bose (2002). Modern Power Electronics and AC drives. Prentice Hall.
2. P. Vas (1990). Sensorless Vector and Direct Torque Control. Oxford University Press.
3. P. Karlovsky, R. Linhart, J. Lettl (2006). Sensorless Determination of Induction Motor Drive Speed Using MRAS Method. IEEE Int. Conf. Electronics, computer and artificial Intelligence, Romania.
4. Tiwari, B. Kumar, Y. K. Chauhan (2017). ANN based RF-MRAS Speed Estimation of Induction Motor Drive at Low Speed. IEEE Int. Conf. Electronics,

communication and aerospace technology, India.
5. Iqbal, M. A. Husain (2018). MRAS based Sensorless Control of Induction Motor based on Rotor Flux. IEEE Int. Conf. Computational and characterization techniques in engineering and science, India.
6. M. Ankarao, M. V. Kumar, P. Dmesh (2018). Dynamic Performance Analysis of Reactive Power and Improved Rotor Flux Based MRAS for Induction Motor Drives Employing PI and Fuzzy Controller. IEEE Int. Conf. Power electronics, intelligent control and energy systems, India.
7. S. Das, R. Kumar, A. Pal (2019). MRAS based Speed Estimation of Induction Motor Drive Utilizing Machine's d- and q- Circuit Impedances. IEEE Trans. ind. Electronics, vol. 66, no. 6, pp. 4286 – 4295.
8. R. Kumar, S. Das, A. K. Chattopadhyay (2016). Comparative assessment of two different model reference adaptive system schemes for speed-sensorless control of induction motor drives. IET Electr. Power Appl., vol. 10, no. 2, pp. 141-154.
9. V.R. Jevremovic, V. Vasic, D.P. Marcetic, B. Jeftenic (2010). Speed-sensorless control of induction motor based on reactive power with rotor time constant identification. IET Electr. Power Appl., vol. 4 no. 6, pp. 462-473.
10. R. Kumar, S. Das, P. Syam, A. K. Chattopadhyay (2015). Review on model reference adaptive system for sensorless vector control of induction motor drives. IET Electr. Power Appl., vol. 9, no. 7, pp. 496-511.
11. Xu, B. Wang, G. Zhang, G. Wang, Y. Yu (2018). A Review of Sensorless Control Methods for AC Motor Drives. CES trans. Electrical machines and systems, vol. 2, no. 1, pp. 104-115.
12. R. Kumar, S. Das, A. K. Chattopadhyay (2015). Comparison of Q- and X-MRAS for speed sensor less induction motor drive on. Michael Faraday IET Int. summit, pp. 319-324.
13. M. Ta-Cao, Y. Hori and T. Uchida (2001). MRAS-based speed sensorless control for induction motor drives using instantaneous reactive power. IEEE Conf. Ind. Electronics society, pp. 1717-1422.
14. A. Pal, S. Das, A.K. Chattopadhyay (2018). An Improved Rotor Flux Space Vector Based MRAS for Field Oriented Control of Induction Motor Drives. IEEE Trans. Power electronics, vol. 33, no. 6, pp. 5131-5141.
15. M. Munshi, S. G. Choudhuri (2016). Model Reference Adaptive System using Rotor Flux and Back Emf Techniques for Speed Estimation of an Induction Motor operated in Vector Control Mode: A Comparative Study. IEEE Int. Conf. Electrical, computer and electronics engineering, India.
16. R. Krishnan (2010). Electric Motor Drive Modeling, Analysis and control. PHI.

TO STUDY THE EARTHQUAKE RESISTANT RCC MULTISTOR STUCTURE WITH DIFFERENT TYPES OF BRACING

S.P. Kawale[1] and V.N. Mendhe[2]
Civil Engineering Dept., YCCE Nagpur, Maharashtra, India
[1]shubhamkawale88.ak@gmail.com, [2]vashalimendhe@gmail.com

ABSTRACT

The most of the RCC buildings were failed in the past due to lateral load. Bracings systems are one ofthe lateral load resisting system which has got structural importance specially in reinforced concrete buildings. Different bracing systems are efficient enough for seismic responses. Steel bracing systems have both practical and economical advantages. The application of steel bracings is faster to execute. The steel bracings are usually installed between existing vertical members. Braced frames are known tobe efficient structural systems for buildings under high lateral loads such as seismic or wind loadings. The fact that the lateral resistance of frame can be significantly improved by the addition of a bracing system has led to the idea of retrofitting seismically inadequate reinforced concrete frames with steel bracing system. Its intention is to obtain the functioning characteristics like Storey displacements, Storeydrift, Natural time period, and Base shear to evaluated and compare with unbraced frame structure. A structure situated in high seismic area will have to withstand lateral load along with the gravity load. This may result in the development of high stress which leads to the severe damage of the structure. Shear wall, bracings are the most common type of lateral load resisting systems. The types of bracing, location of bracing have significant effects to the lateral capacity of the structure.

Key Words: *Bracing, Earthquake Force, Storey displacements, Storey drift, and Base shear.*

1. Introduction

In earthquake design the building has to go through regular motion at its base, which leads to inertia force in the building that consecutively causes stresses. India has experienced number of earthquakes that caused large damage to residential and industrial structure. For earthquake resistant design the normal building should be able to resist minor, moderate, sever shaking. The behavior of the buildings during earthquake depends not only on the size of the members and amount of reinforcement, but to a great extent on the placing and detailing of the reinforcement. Therefore, it is necessary to provide special mechanism that to improve lateral stability of the structure. There are various types of bracing systems like X bracing, V bracing, inverted V bracing, K bracing, diagonal bracing and so on. There are various ways of providing bracings to improve seismic performance of buildings. The different bracing configurations typically used are: Diagonal bracing, Cross bracing(X), Chevron bracing, and V-bracing. Each bracing configurations has its own merits and demerits as compared to other.

2. Objective

a. Base shear – To calculate the total design lateral force at the structure and to analyze the effect of different configuration of bracing on structure.
b. Storey displacement – To evaluate the lateral displacement that occurs in each storey of high risebuildings.
c. Storey Drift- To calculate the storey drift at each floors.

3. Modelling & Analysis Of Building

Building Descriptions

No of stories	G+12
No of bay in X-dir	4
No of bay in Y-dir	4
Type of Building	Residential
Plan dimension	16m*16m
Typical height stories	4m
Bottom storey height	4m
Total height	52m

Table 1 Geometrical Data

Thickness of Slab	150mm
Column Size	450mm*400mm
Beam Size	400mm*350mm
Bracing	ISA100*100*12

Table 2 Member Properties

Zone	III
Zone Factor	0.16
Response Reduction Factor	5
Importance Factor	1.2
Structure Type	SMRF
Soil Condition	Medium
Building	RCC

Table 3 Seismic Load

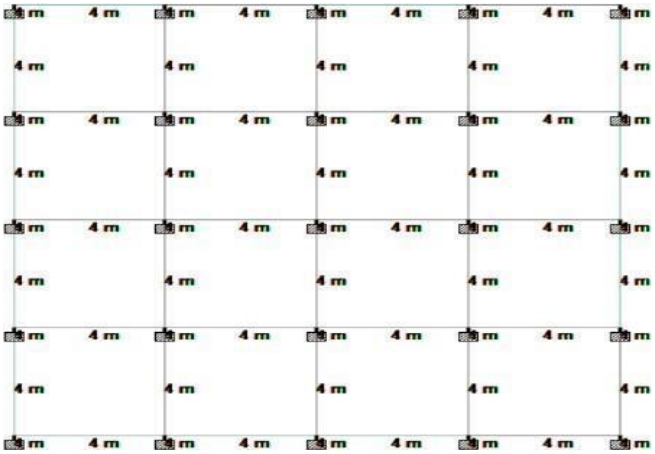

Fig1 Plan of models

Fig2 Elevation of Bare Frame

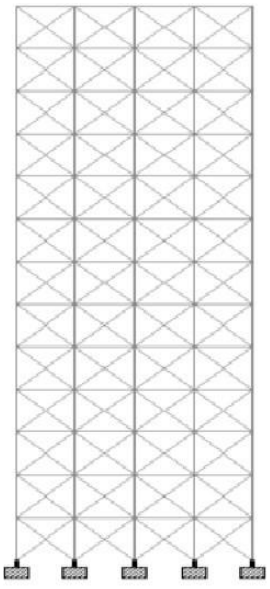

Fig3 Elevation of frame with X-Bracing

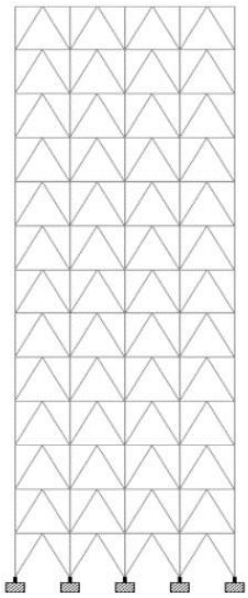

Fig4 Elevation of frame with Inverted V-Bracing

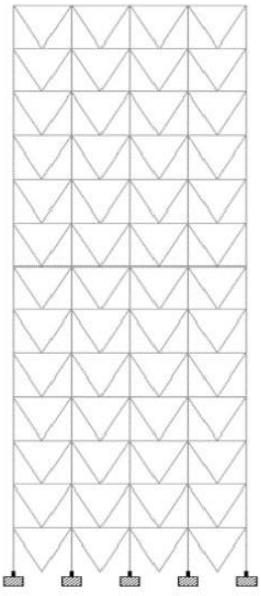

Fig5 Elevation of frame with V-Bracing

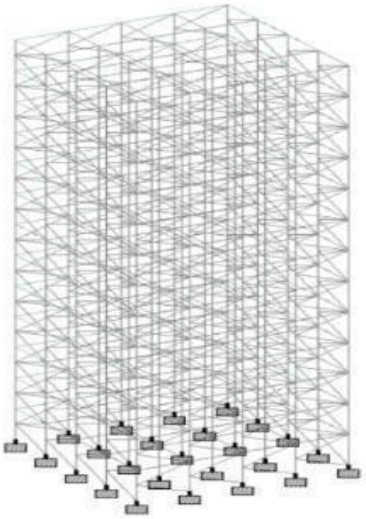

Fig6 Rendered View of Bare Frame with X-Bracing

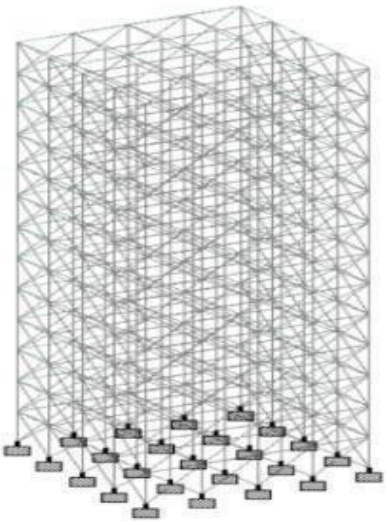

Fig7 Rendered View of Frame with Bracing

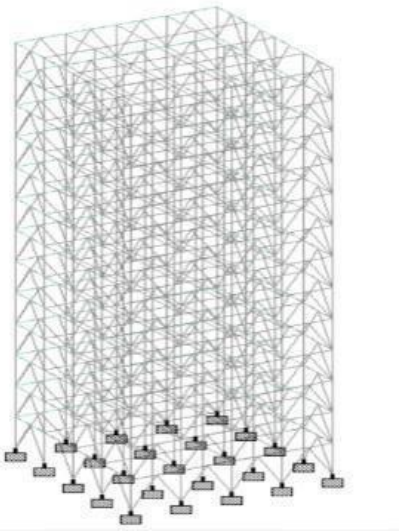

Fig8 Rendered View of frame with Inverted V-Bracing

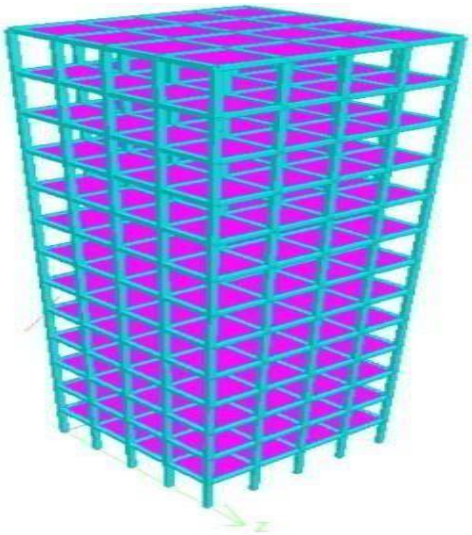

Fig9 3D View of Bare Frame

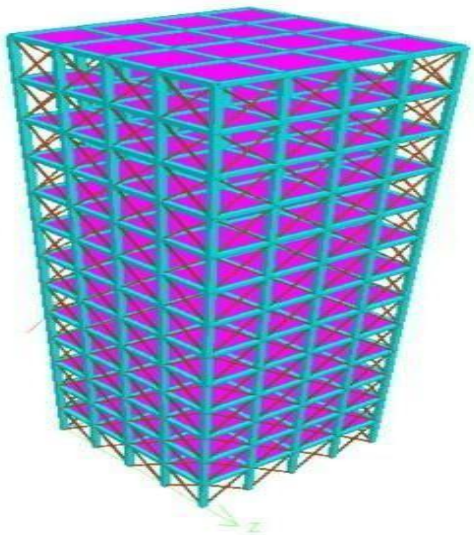

Fig10 3D View with X-Bracing

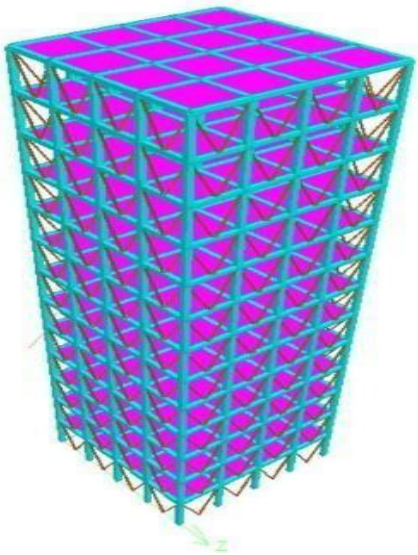

Fig11 3D view with V-Bracing

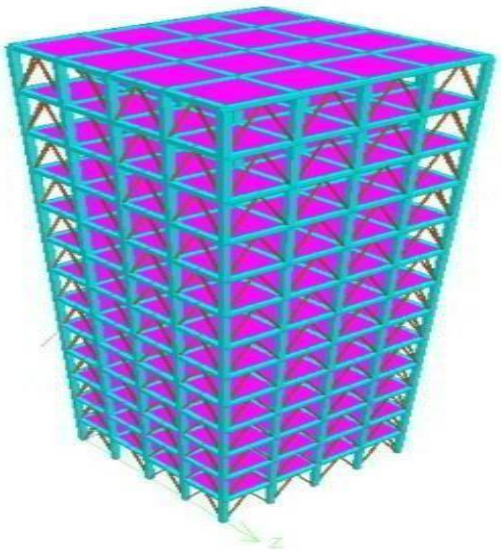

Fig12 3D View with Inverted V-Bracing

4. RESULT

3.1 Result of Weight of Structure

4. Type of model	Weight of structure (KN)
Bare Frame Without Bracing (Manuallly)	36225.875
Bare Frame Without Bracing (STADD PRO)	36062.613
Bare Frame With X-Bracing	45296.847
Bare Frame With V-Bracing	44119.369
Bare Frame With Inverted V-Bracing	44123.873

Table 4.1.1 Weight of structure

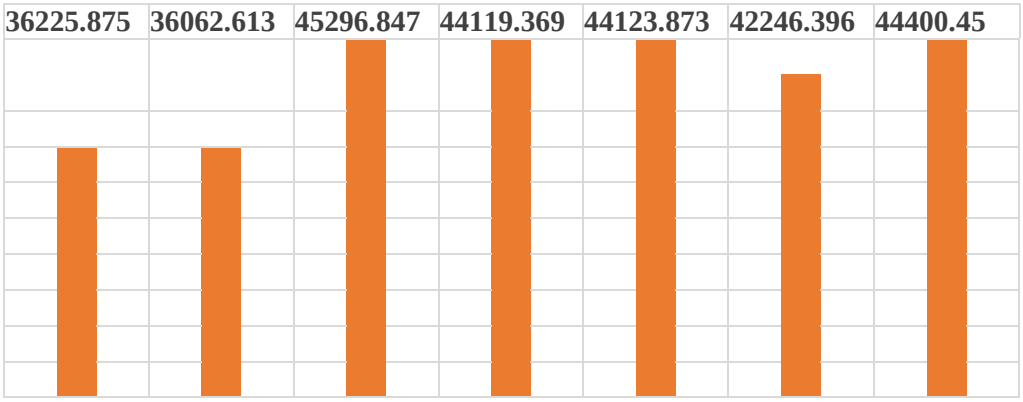

Graph 4.1.1 Weight of Structure for various models with and without bracings

Form the Graph we can see that, the value of Weight is increase for the structure with bracings. And the maximum increase in Weight is for frame with X-Bracing. The weight for frame with V-Bracing and Inverted V-Bracing is nearly same. Form this we can conclude that the weight of structure is increase as the Bracings are applied.

Result of Base Shear

Type of Frame	Base Shear in X-direction	Base Shear in Y-direction
Bare Frame	804.21KN/M2	804.21KN/M2
Bare Frame (Stadd Pro)	800.59KN/M2	800.59KN/M2
X-bracing	1005.59KN/M2	1005.59KN/M2
V-bracing	979.45KN/M2	979.45KN/M2
Inverted V- bracing	979.55KN/M2	979.55KN/M2

Table 4.2.1 Base Shear for model with and without Bracings

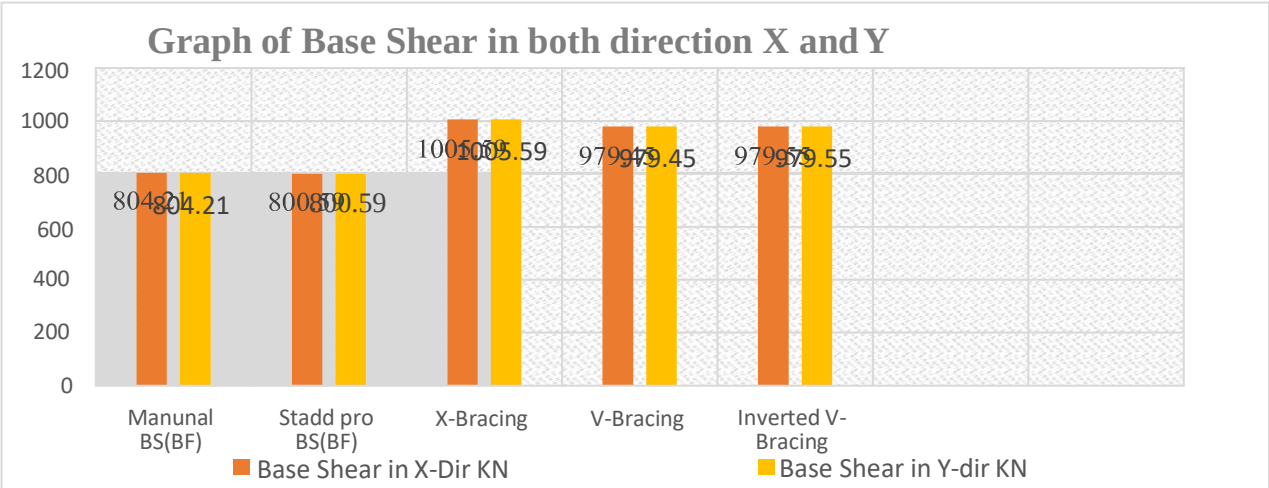

Graph 4.2.2.1 Comparison of Base Shear for unbraced and braced structure

Base Shear of structure with bracings is more than base shear of unbraced structure. In this base shear of X-bracing is more than that of other bracings system. The value of base shear for X-Bracing in X and Y direction are 1005.59KN and 1005.59KN respectively. That is 25.60% increase in base shear with X-Bracing as compared to unbraced structure.

Results For Story Displacement

Floor No	Displacement in X direction (mm)	Displacement in Y direction (mm)
Ground Level	0.00	0.00
1st Floor	5.458	7.519
2nd Floor	13.722	17.906
3rd Floor	22.484	28.702
4th Floor	31.334	39.547
5th Floor	40.133	50.301
6th Floor	48.753	60.811
7th Floor	57.047	70.905
8th Floor	64.851	80.378
9th Floor	71.977	89.006
10th Floor	78.219	96.533
11th Floor	83.354	102.686
12th Floor	87.154	107.171
Roof Level	89.543	109.841

Table 4.3.1 Storey displacement without Bracing (Bare Frame) in X and Y direction

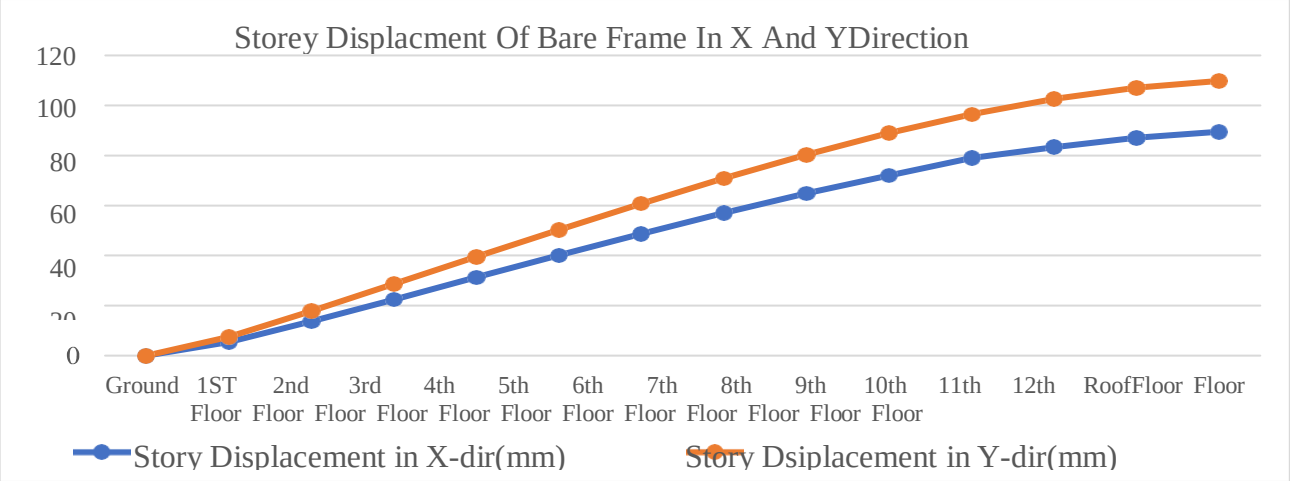

On X-axis No of Floor On Y-axis Storey Displacement(mm)

Graph Show Story Displacement Of Bare Frame In X And Y Direction.

From the analysis result it is observed that, storey displacement goes on increasing from ground floor toupper floors in both X and Y direction.

Floor No	Displacement in Xdirection (mm)	Displacement in Ydirection (mm)
Ground Level	0.00	0.00
1st Floor	1.021	1.101
2nd Floor	2.458	2.565
3rd Floor	4.047	4.178
4th Floor	5.756	5.917
5th Floor	7.559	7.754
6th Floor	9.428	9.659
7th Floor	11.326	11.595
8th Floor	13.216	13.521
9th Floor	15.054	15.396
10th Floor	16.790	17.169
11th Floor	18.364	18.776
12th Floor	19.693	20.124
Roof Level	20.734	20.141

Table 4.3.2 Storey Displacement with X-bracing in both X and Y direction

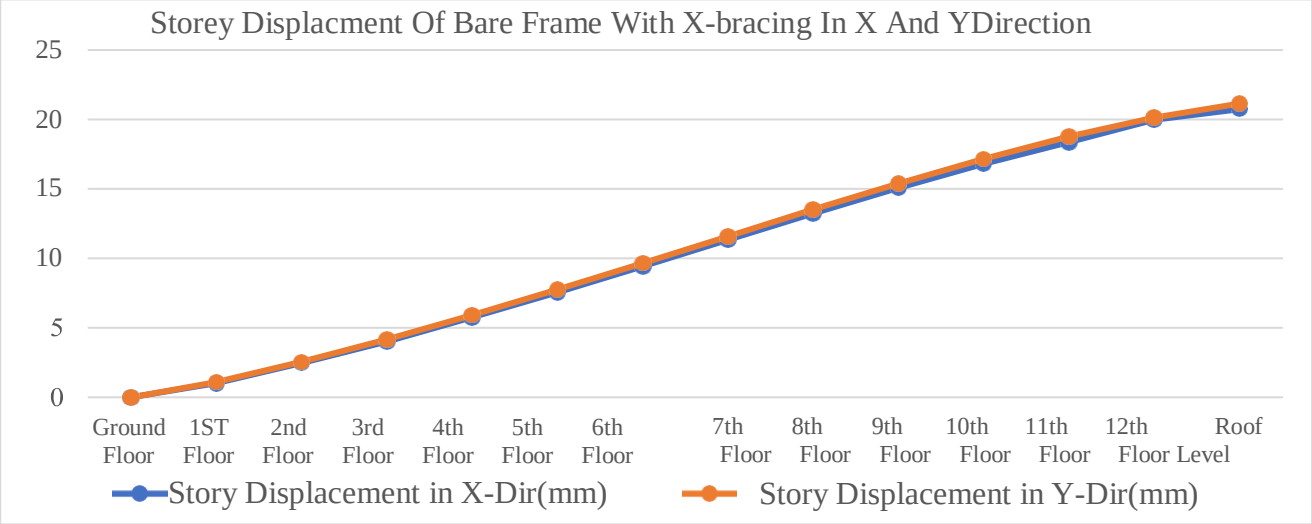

On X-axis- No of Floor On Y-axis- Storey Displacement(mm)

Graph Show Story Displacement Of Bare Frame With X-Bracing In X And Y Direction

Floor No	Displacement in Xdirection (mm)	Displacement in Ydirection (mm)
Ground Level	0.000	0.000
1st Floor	4.716	6.804
2nd Floor	7.749	10.238
3rd Floor	10.514	13.199
4th Floor	13.241	16.055
5th Floor	15.971	18.896
6th Floor	18.705	21.734
7th Floor	21.414	24.542
8th Floor	24.052	27.276
9th Floor	26.564	29.878
10th Floor	28.887	32.283
11th Floor	30.944	34.411
12th Floor	32.645	36.158
Roof Level	34.007	37.528

Table 4.3.3 Storey Displacement with V-bracing in both X and Y direction

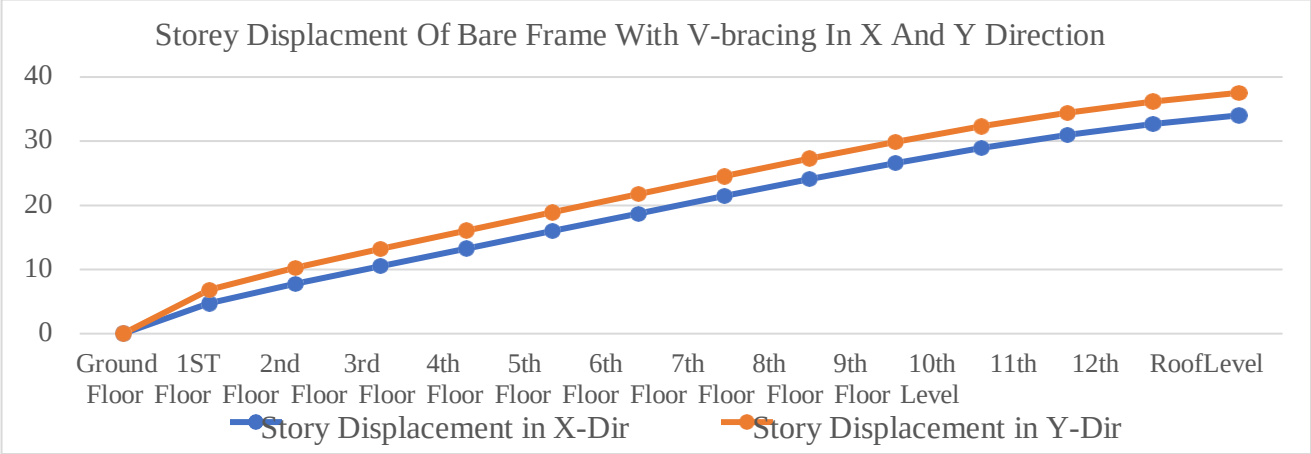

On X-axis- No of Floor On Y-axis- Storey Displacement(mm)

Graph Show Story Displacement Of Bare Frame With V-Bracing In X And Y Direction.

From the analysis result it is observed that the Storey Displacement get reduced as compared to the unbraced structure in both X and Y direction. After providing V-Bracing Storey Displacement is by 38% as compare to X-Bracing. The reduction in storey displacement is 60% as compared to unbraced structure.

Floor No	Displacement in Xdirection (mm)	Displacement in Ydirection (mm)
Ground Level	0.00	0.00
1st Floor	1.590	2.092
2nd Floor	3.756	4.848
3rd Floor	6.085	7.839
4th Floor	8.532	11.007
5th Floor	10.061	14.293
6th Floor	13.633	17.632
7th Floor	16.611	20.954
8th Floor	18.690	24.184
9th Floor	21.068	27.246
10th Floor	23.259	30.057
11th Floor	25.185	32.524
12th Floor	26.754	34.529
Roof Level	27.913	35.985

Table 4.3.4 Storey Displacement with inverted V-bracing in both X and Y direction

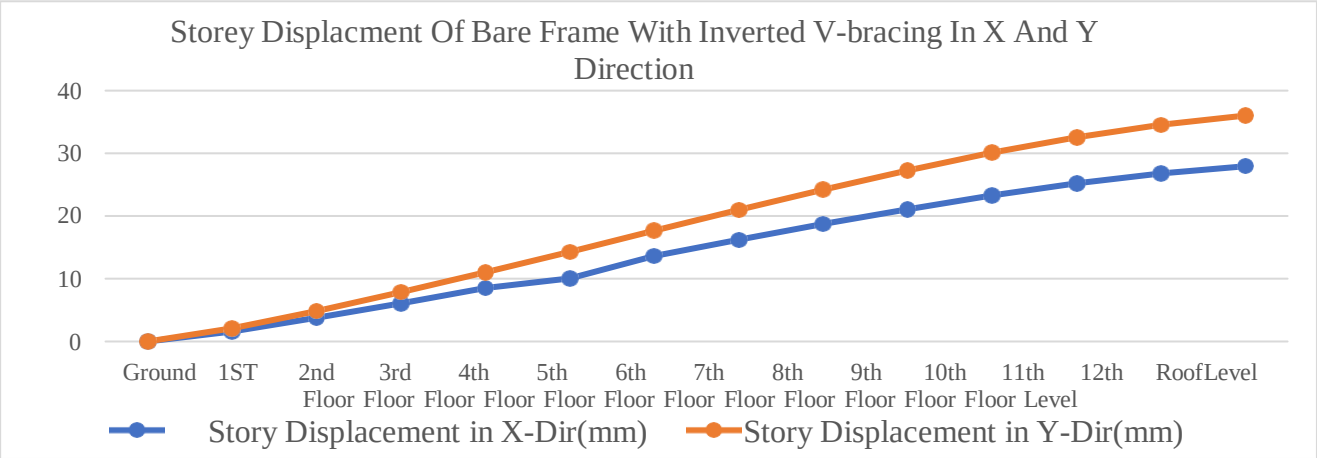

On X-axis No of Floor On Y-axis Storey Displacement(mm)

Graph Show Story Displacement Of Bare Frame With Inverted V-Bracing In X And Y Direction

From the analysis result it is observed that the Storey Displacement get reduced as compared to the unbraced structure in both X and Y direction. The reduction in storey displacement is 68% as compared to unbraced structure

Result of Storey Drift

Floor No	Storey Drift in X direction (mm)	Storey Drift in Y direction (mm)
Ground Level	0.00	0.00
1st Floor	5.458	7.519
2nd Floor	8.226	10.388
3rd Floor	8.762	10.796
4th Floor	8.850	10.845
5th Floor	8.799	10.753
6th Floor	8.620	10.511
7th Floor	8.295	10.093
8th Floor	7.804	9.474
9th Floor	7.126	8.627
10th Floor	6.242	7.528
11th Floor	5.135	6.152
12th Floor	3.801	4.485
Roof Level	2.389	2.670

Table 4.4.1 Storey Drift for unbraced structure in both X and Y direction

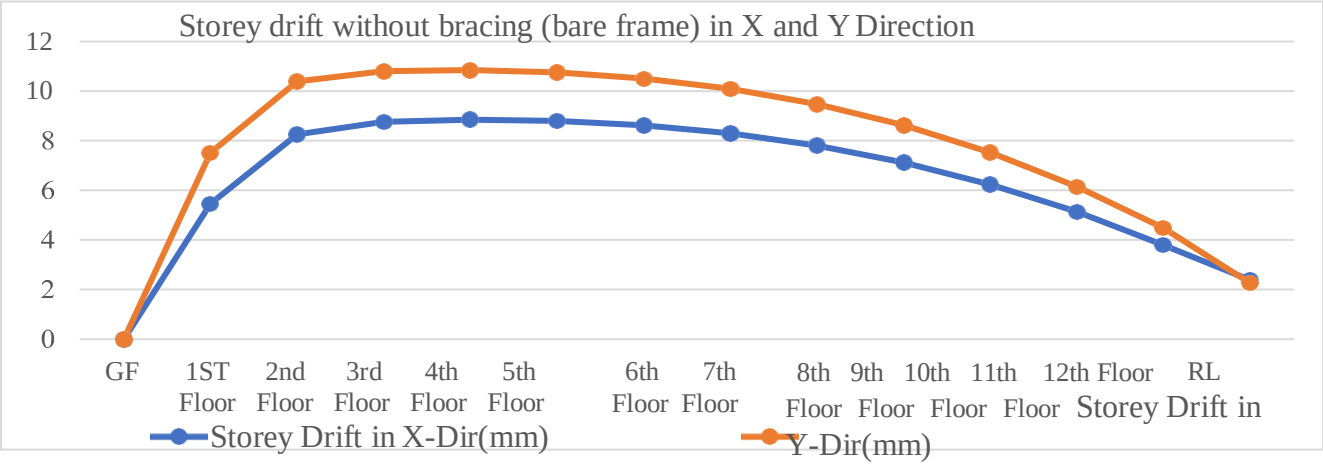

On X-axis- No of Floor On Y-axis- Storey Drift(mm)

Graph Show Story Drift Of Bare Frame In X And Y Direction.

Floor No	Storey Drift in X direction (mm)	Storey Drift in Y direction (mm)
Ground Level	0.00	0.00
1st Floor	1.021	1.101
2nd Floor	1.437	1.464
3rd Floor	1.589	1.613
4th Floor	1.709	1.739
5th Floor	1.804	1.838
6th Floor	1.869	1.905
7th Floor	1.898	1.935
8th Floor	1.890	1.927
9th Floor	1.837	1.875
10th Floor	1.737	1.775
11th Floor	1.529	1.608
12th Floor	1.329	1.348
Roof Level	1.041	1.018

Table 4.4.2 Storey Drift for structure with X-Bracing in both X and Y direction

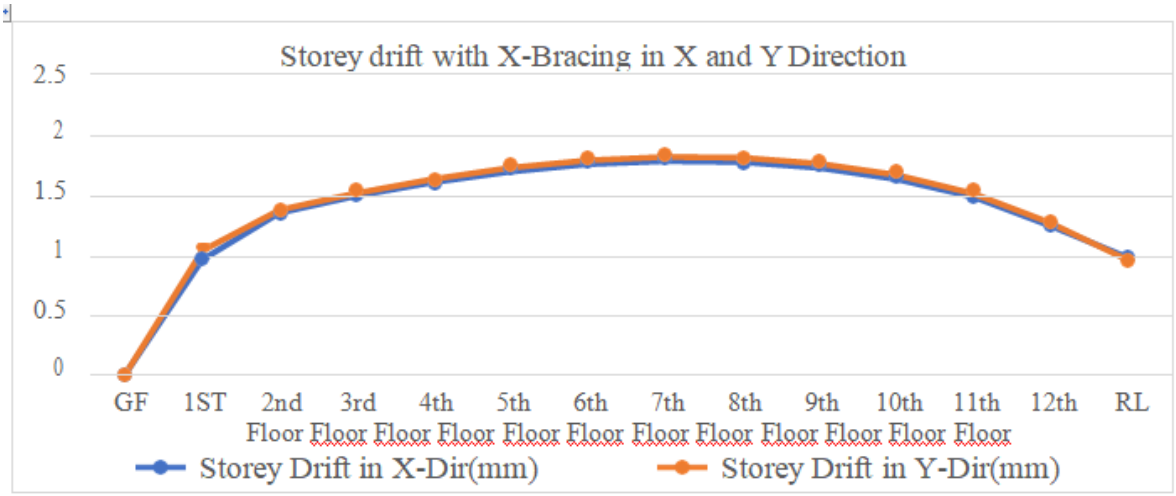

On X-axis- No of Floor On Y-axis- Storey Drift(mm)

Graph Show Story Drift Of Bare Frame with X-bracing In X And Y Direction.

From the analysis result it is observed that the Storey Drift is get reduced as compared to the unbracedstructure in both X and Y direction.

Floor No	Storey Drift in Xdirection (mm)	Storey Drift in Ydirection (mm)
Ground Level	0.00	0.00
1st Floor	3.401	4.709
2nd Floor	3.033	3.434
3rd Floor	2.765	2.962
4th Floor	2.747	2.856
5th Floor	2.730	2.840
6th Floor	2.724	2.838
7th Floor	2.708	2.809
8th Floor	2.638	2.734
9th Floor	2.512	2.602
10th Floor	2.323	2.405
11th Floor	2.057	2.128
12th Floor	1.701	1.747
Roof Level	1.362	1.365

Table 4.4.3 Storey Drift for structure with V-Bracing in both X and Y direction

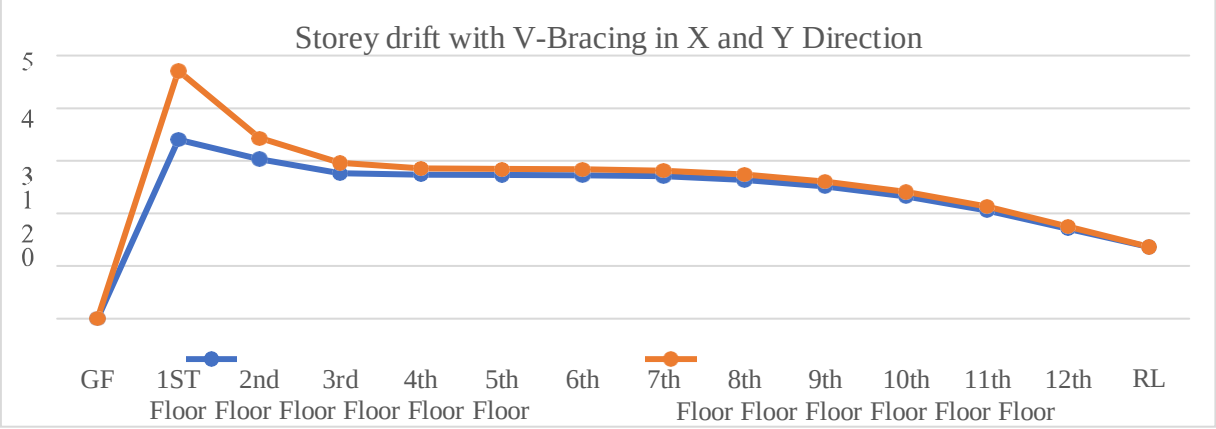

On X-axis- No of Floor On Y-axis- Storey Drift(mm)

Graph Show Story Drift Of Bare Frame with V-bracing In X And Y Direction

From the analysis result it is observed that the Storey Drift is get reduced as compared to the unbracedstructure in both X and Y direction. But it is observed that storey drift is slightly more than the storey drift with X-Bracing.

Floor No	Storey Drift in Xdirection (mm)	Storey Drift in Ydirection (mm)
Ground Level	0.00	0.00
1st Floor	1.590	2.092
2nd Floor	2.166	2.756
3rd Floor	2.329	2.991
4th Floor	2.447	3.168
5th Floor	2.529	3.286
6th Floor	2.569	3.339
7th Floor	2.561	3.321
8th Floor	2.499	3.230
9th Floor	2.378	3.062
10th Floor	2.190	2.811
11th Floor	1.926	2.466
12th Floor	1.569	2.006
Roof Level	1.159	1.456

Table 4.4.4 Storey Drift for structure with Inverted V-Bracing in both X and Y direction

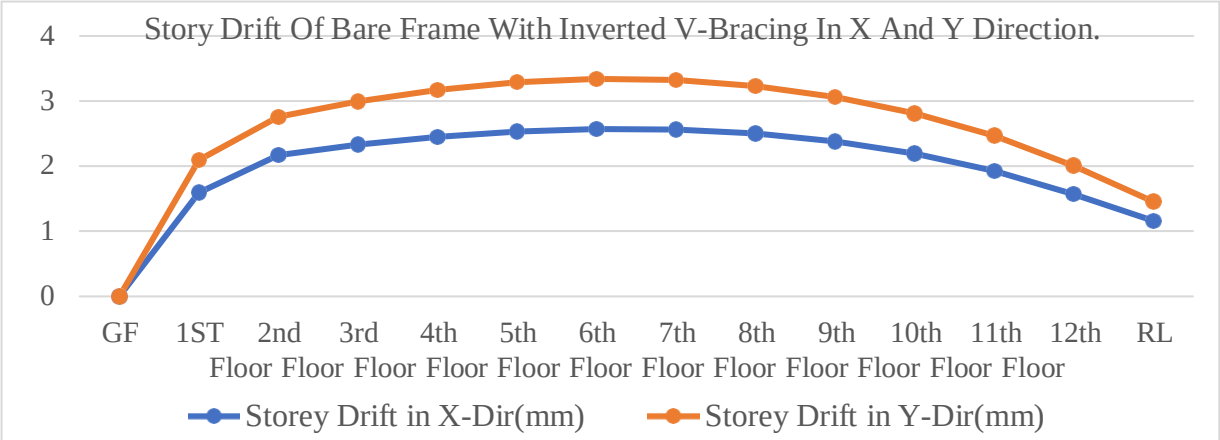

On X-axis- No of Floor On Y-axis- Storey Drift(mm)

Graph shows Story Drift Of Bare Frame With Inverted V-Bracing In X And Y Direction.

From the analysis result it is observed that the Storey Drift is get reduced as compared to the unbracedstructure in both X and Y direction. But it is observed that storey drift is slightly more than the storey drift with X-Bracing and with V-Bracing.

5. Conclusion

a. The base shear is increase after the application of bracing. The base shear maximum in X-Bracing as compare to the other bracings.
b. The weight is increase as the bracing are provided. The maximum weight is in X-Bracing ascompare to bracings.
c. The increase in weight and base shear of structure by using V and inverted V bracings does not show any significant difference.
d. The storey displacement reduce in frame with bracing are provided, maximum reduction occur in frame with X-bracing.

References

1. Manish S. Takey and S. S. Vidhale, "Seismic response of steel building with linear bracing system (A software approach)", International Journal of Electronics, Communication and Soft Computing Science and Engineering, 2(1), pp 17-25, 2012.
2. Desai J. P., Jain A. K. and Arya A. S., "Seismic response of R. C. braced frames", Computers and Structures Volume 29 No.4, pp 557-568, 1988.
3. IS 1893(part 1) – 2002, "Criteria for earthquake resistant design of structures, part 1-general provisions and buildings", fifth revision, Bureau of Indian Standards, New Delhi, India.
4. Nauman Mohammed, Islam Nazrul, "Behaviour of Multistorey RCC Structure with Different Type of Bracing System", Vol. 2, Issue 12, December 2013.
5. Umesh R. Biradar1, Shivaraj Mangalgi, "Seismic response of reinforced concrete structure by using different bracing SYSTEMS", Volume: 03 Issue: 09 Sep-2014.
6. Dhanaraj M. Patil and Keshav K. Sangle, Seismic Behavior of Different Bracing Systems in High Rise 2D Steel Buildings, Science Direct, Structures vol 3, 2015, pp 282 –305.
7. M.D. Kevadkar and P.B. Kodag, Lateral Load Analysis of R.C.C. Building, IJMER, Vol.3, Issue.3,2013, pp- 1428-1434.
8. Kulkarni J. G and Kore P. N, Seismic response of reinforced concrete braced frames, IJERA, Vol.3, Issue 4, 2013, pp-1047-1053.
9. Using is code, IS1893-2016, IS13920-2016 and many more.

DISCHARGE EQUATION IN SUPERCRITICAL FLOW REGIME BY CUTTHROAT FLUME FOR DIFFERENT SLOPE CONDITION

Shrikant Tekade[1], Tejas Bhatkar[2], Ashay Shende[3], Kiran Tajne[4] and Ashwin Gawai[5]
[1,4,5]Department of Civil engineering, Government College of Engineering, Nagpur, Maharashtra, India
[3]Department of Civil Engineering, KDKCE, Nagpur, Maharashtra, India
[2]Technical manager, SD Geotesting solutions and consultant, Amravati, Maharashtra, India

ABSTRACT

The design of energy dissipaters involves understanding of supercritical flow regimes. The measurement accuracy of supercritical flow regime parameters governs the efficiency and effectiveness of the design of these dissipaters. Conventionally there are many devices and methods which can measure required parameters, but with special and costly modifications. A cutthroat flume is one option which has a flat bed and does not requires any special change to be made in the system. The present paper finds the feasibility of cutthroat flume as a measurement device in supercritical flow regimes under free flowconditions for different slope condition of tilting flume. A good correlation is found to exist between the Q and h_a* which is well within standard allowable error limits.*

Keywords: *Cutthroat flume, Flow measurement, Supercritical flow, Open channel flow*

1 Introduction

Determination of flow rate in open channels has been and still is the most important aspect of water resources management. Mostly open channel flow is subcritical in nature having low approach velocity but for water treatment plants and industries, condition of supercritical flow can be applied for transporting sediment load at higher velocity through any measuring devices. Also measurement of flow in supercritical regime is important for the design of energy dissipaters and to study erosion pattern of channel. There are various types of flow measurements devices and technologies currently used in India. For measurement of flow rates in irrigation channels and water treatment plants generally critical flumes are used (Bos 1989).

Cutthroat flume is a type of critical flume which is used for measurement of open channel flow due to less expensive, fairly accurate, easy calibration, simple geometry and horizontal bed. The bed of cutthroat flume is kept horizontal and consists of converging inlet section having length L/3 with angle 1:3 and 2L/3 for diverging outlet section with angle 1:6, where L= total length of flume. The flume has no throat length and hence called as cutthroat flume (V. Skogerboe, Wynn R. 1972). The entire bed of the flume is kept horizontal and the walls are vertical. Therefore all cross section across the flume length are rectangular in shape (Skogerboe and Hyatt 1967). The details of Cutthroat flume is shown in fig. 1.

Cutthroat flumes are commonly used for measurement of subcritical flow. Under free flow condition(A.S. Ramamurthy 1985) tested three geometrically similar throat-less flumes. A pressure correction factor for non hydrostatic pressure distribution was determined experimentally by (A.S. Ramamurthy 1985) and it incorporates a free flow discharge equation developed for energy principles. For validating the expression the present data and previously published data were compared by the author, which helped him to conclude that equation are valid for geometrically similar flumes in which the depth of flow in the approach channel is less than twice the channel width. Therefore

For a particular type of cutthroat flume there must exist a relationship between discharge and head at 2/3rd position from inlet converging section. The discharge for cutthroat flume having different throat width for subcritical flow is given by (Skogerboe et al. 1967, 1972)

$$Q = C \times (h_a)^{n_1} \quad (1)$$

Where Q = discharge in m^3/sec, C= free flow coefficient, h_a = Head at inlet section n_1 = exponent for h_a. To determine the discharge for supercritical flow the Skogerboe formula has been used with shifting of control section. In this analysis head (h_a) at inlet section has been shifted to $2/3^{rd}$ position from inlet converging section, as at this position the flow gets converted from supercritical to subcritical. (Keller R.J. 1984) attempted to find out the significance of scale effect on discharge characteristics of geometrically similar cutthroat flumes. Authors carried out experimental work on three different sizes of flumes in scale range 1:4 and establish a relation between discharge and head. By taking same flume dimensionless ratios of L/W, Ha/W and $[Q/\sqrt{g}\times W\ (Ha)^{1.5}]$. Then finding out variation of two dimensionless variables it is concluded that no correlation is observed between these dimensionless variables.

For the measurement of subcritical flow under submerged flow condition experimental work carriedout by (A.S. Ramamurthy 1988) to find out the average pressure coefficient 'k' at the throat section, which acts as control section. No single relation for discharge is suggested for free flow condition under sub critical flow.

A single relation for measurement of discharge for different sizes of cutthroat flume were developed by (V.L. Manekar 2007) and validate with the discharge relation proposed by (Skogerboe et al. 1972) for the factors such as standard deviation, % error, mean discrepancy ratio, standard deviation of discrepancy ratio. It was observed that predicted discharge by investigator was more accurate than Skogerboe et al. method. For measurement of supercritical flow (Christopher I. Thorton 2009) used small parshall flume and tested it by varying channel slopes, approach channel roughness and flume convergence. He determined that a single parshall flume can be used to measure both subcritical and supercritical flow within ± 5%. By modifying original parshall flume equation unique expressions were developed by (Thorton 2009), for estimating
discharge in subcritical and supercritical flow regimes.

For measurement of supercritical flow using cutthroat flume (S. A. Tekade 2016) carried out experimental work on three different sizes of cutthroat flumes having different length and throat widths. Investigator proposed relationship between dimensionless discharge and dimensionless head for measurement of supercritical flow using cutthroat flume also, proposed relationship between dimensionless discharge Vs. coefficient of discharge.

Available standard literature mainly focuses on the measurement of subcritical and supercritical flowby using cutthroat flume and parshall flume, but no attempt has been made to measure the supercritical flow by using cutthroat flume for different slope. The aim of this research is to test the accuracy of the cutthroat flume in supercritical flow regime for various slope and establish a standard validated procedure so that, thisflume can also be widely used in the said regime. For this experimentation was carried out in the flume with following specifications, W= 0.34 m, L= 1.10 m and S = 0.00900, 0.0105

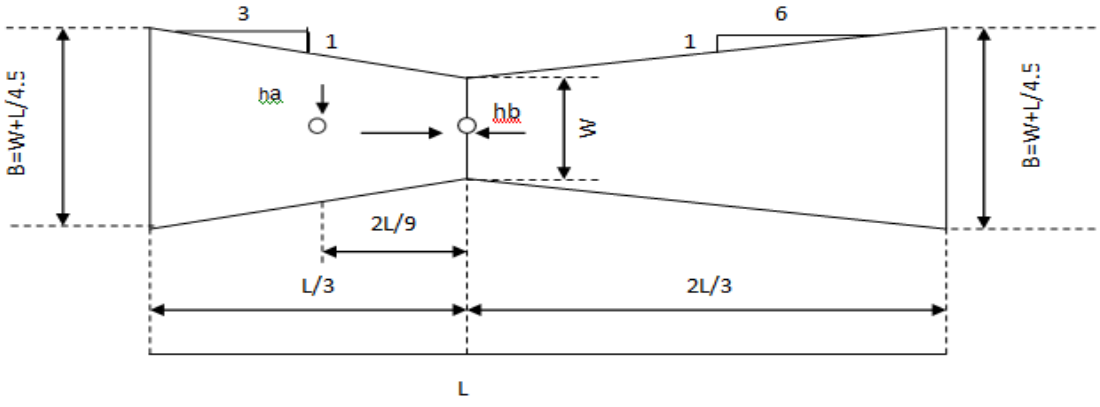

Figure 1. Schematic diagram of cutthroat flume (source:- S. A. Tekade 2016)

2. Experimental setup

The complete work was carried out in Hydraulics and Fluid Mechanics Laboratory of the Department of Civil Engineering Visvesvaraya National Institute of Technology Nagpur. The rectangular tilting flume having 0.6 m bed width and 21 m length with U/S and D/S gates. To analyze the effect of flow a cutthroat flume of throat width 0.3937 m and length 0.914 m were fabricated in laboratory. The experimental setup is a self contained 30 HP pump having circulating mechanism work efficiently in the flume. The flume is installed with perplex glass sheet as side walls which make the viewing of the experimental run easy. For measuring bed elevation and water surface elevation a vernier type gauge with accuracy ± 0.1mm was used. A Krohne Marshall Make electromagnetic flow meter calibrated of 150 mm diameter was fitted to the same diameter pipe line. Proper care was taken to avoid any electric or magnetic field being formed in the vicinity of this flow meter.

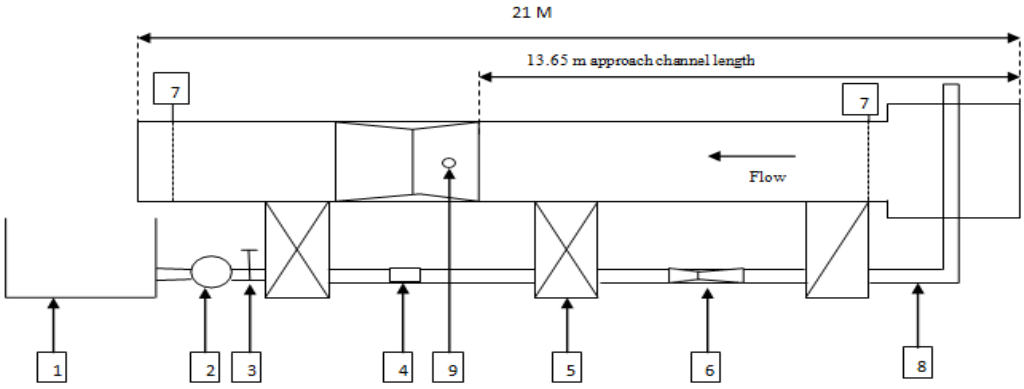

Figure 2. Side view of experimental set up (source:- S. A. Tekade 2016)

1- Sump tank, 2- Pump, 3- Valve, 4- Electromagnetic flow meter, 5- G.I. stand ,6- Venturimeter ,7- Inletand Outlet gate ,8- 0.15 m dia. Pipe, 9- h_a measurement point at 2/3 rd position from inlet section.

3. Experimental procedure

To check the accurate position of cutthroat flume in the direction of flow, bed slope and bed level was maintained. For the generation of supercritical flow long approach channel having length 13.65 m was provided as shown in Fig. 2. The sump tank having size 3×2×1 m provided at the delivery end of the flume. Prior to measuring of flow in supercritical regime the cutthroat flume having size throat width 0.3937 m and length 0.914 m was fitted in tilting flume. To check the accurate position of cutthroat flume in the direction of flow bed slope and bed level was maintained. To measure the flow depth, vernier type gauge with accuracy ± 0.1mm was used at head measurement point to measure the flow depth. Calibrated electromagnetic flow meter was used to measure the discharge. The discharge was varied from 0.0125 to 0.0526 m^3/s. The observations of head and discharge are given in "Appendix1". Froude numbers for the specific range of discharge 0.0125 to 0.0526 m^3/s and bed slope of the channel (S) = 0.00900, 0.0105 are calculated for measured discharges and flow depths at the section on upstream side of cutthroat flume. It can be noticed that for all the observations the Froude numbers are greater than 1, means the flow is in supercritical regime on upstream side of cutthroat flume. For downstream side of cutthroat flume the Froude number lies in between 0.94-1.0 establishing that the flow is in a subcritical regime.

4. Theoretical Expression for Discharge

By assuming critical condition of flow at throat section Ven Te[1988] and Streeter[1988] the total energy at the measuring section of cutthroat flume with the total energy at the throat section is expressed as,

$$Q = C_d \times 0.544 \times \sqrt{g} \times W \times E_1^{3/2} \qquad (2)$$

Where Q= Discharge (m^3/s) W= Width of throat section (m) E_1= Total energy Cd= Coefficient of discharge

To obtain universal equation between dimensionless discharge and dimensionless energy, discharge and energy is required to convert in dimensionless form, therefore eq. (2) can be written as

$$Q^* = 0.544 \times C_d \times E^{*3/2} \qquad (3)$$

$$Q^* = \frac{Q_1}{\sqrt{g \times W^{2.5}}} = \text{dimensionless discharge}$$

$$\text{And } E^* = \left(\frac{E1}{W}\right) = \text{Dimensionless Energy}$$

for all values of discharge the critical condition of flow will not occur at the throat section, but may occur on D/S side of throat section therefore, eq. (3) should be modified to more general exponential form as

$$Q^* = K \times E^{*n} \qquad (4)$$

The values of coefficient K and exponent n are to be determined from experimental observations.

5. Observations & Results

The results and observations for flow measurement and measurement of head are taken under two Categories of flow conditions. In first category the data of flume having throat width 0.3937 m considered for different slope of tilting flume separately. In second category combined data of different slope is considered. These observations are taken to establish the use of cutthroat flume for measurement of supercritical flow for different slope condition. This is achieved b comparing the relation between measured flow and measured head with the relation derived from basic theoretical consideration.

Observations for flow measurement and head which are given in Appendix 2. The observed values of Q*, h_a* and E* are shown Appendix II respectively.

Category-I

Variation of Q* with E*for slope (S) 0.00900 and 0.0105 are shown in fig. 3 & 4. Based on the regression analysis following relationship is obtained as,

$$Q^* = 0.499 \times E^{*1.438} \qquad (5)$$

With coefficient of regression (R^2) = 0.995For Slope (S)= 0.0105

$$Q^* = 0.454 \times E^{*1.675} \qquad (6)$$

With coefficient of regression (R^2) = 0.977

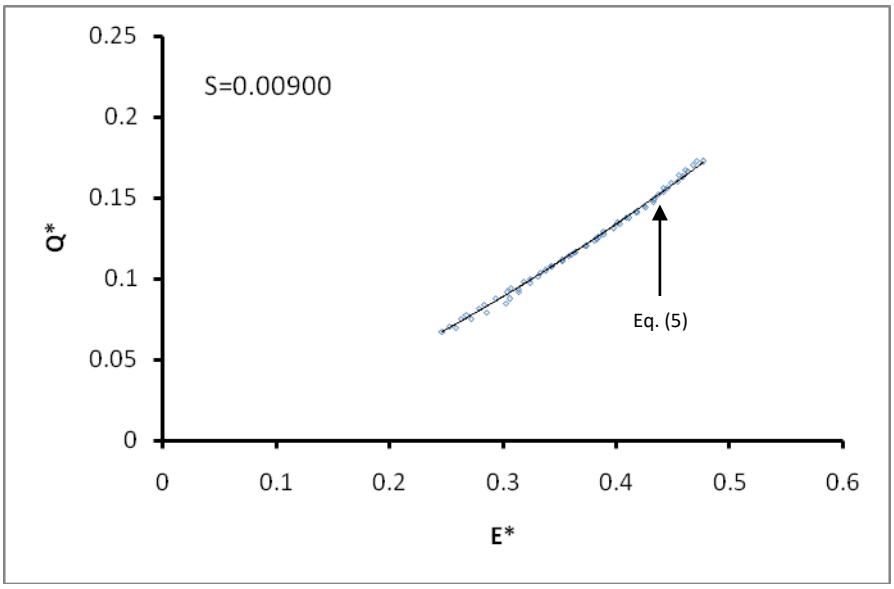

Fig. 3 Relation between Q* vs. E* from experimental data.

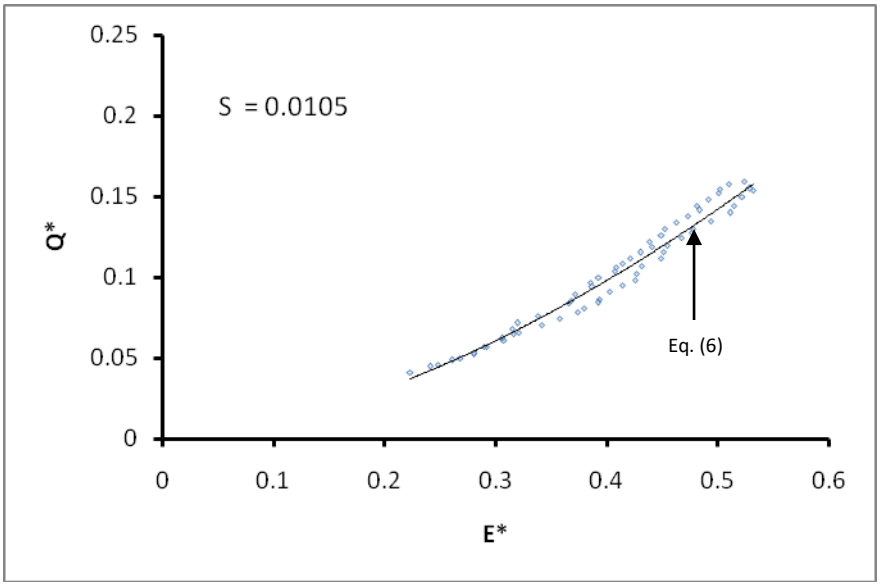

Fig. 4 Relation between Q* vs. E* from experimental data.

By comparing Theoretical Eq. (3) with Eq. (5) & (6) the value of coefficient of discharge (C_d) is obtainedas,

$$C_d = \frac{0.9172}{E^{*0.062}} \qquad (7)$$

$$C = 0.8345 \times E^{*0.175} \qquad (8)$$

The variation of C_d^d with respect to E* are shown in fig. 5 & 6

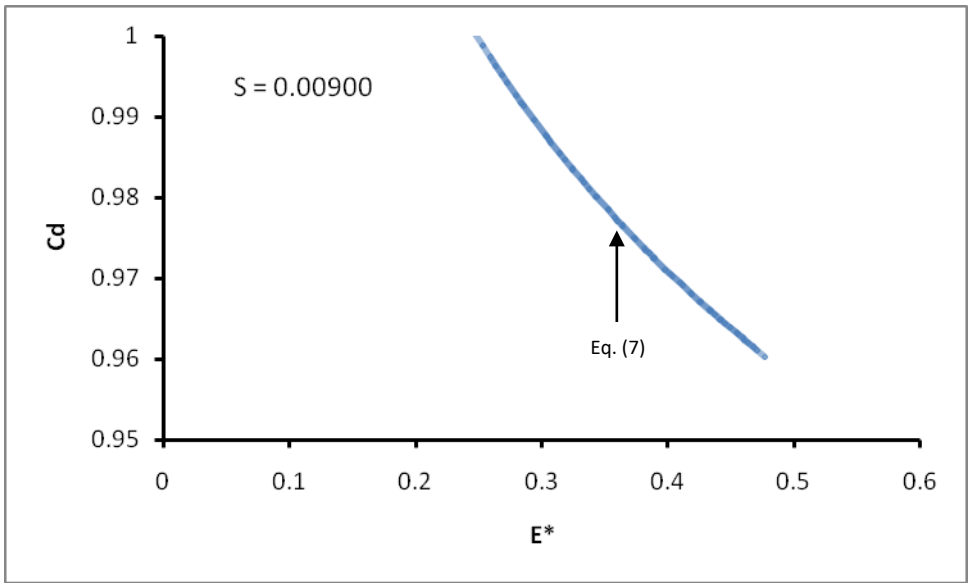

Fig. 5 Relation between C_d vs. E^* from experimental data.

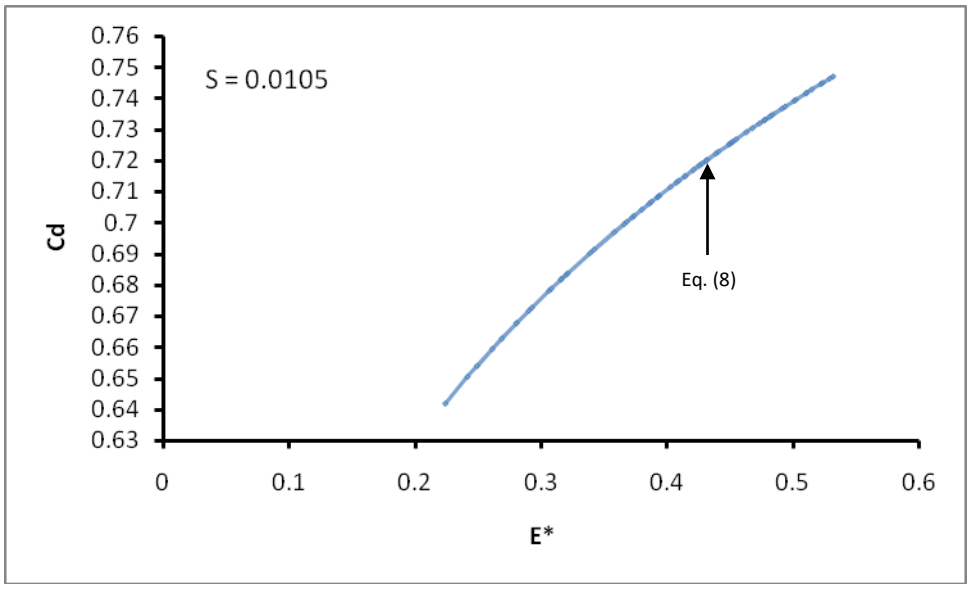

Fig. 6 Relation between C_d vs. E^* from experimental data.

Due to implicit in character of Eq. 5 to Eq. 8 , Eq. 5 & 6 is to be solved by iterative procedure. Therefore thedirect calculation of Q is not possible. Hence, it is considered that an approximate relation between Q* and ha* will be useful in calculation of the first trial value of Q*. Regression analysis was carried out between Q* and ha* which establish relation between Q* and ha* as Eq. (9) & (10) with R^2= 0.984 and 0.988. This relationship shown in fig. 7 & 8

$$Q^* = 2.054 \times h^{*1.607} \qquad (9)$$

$$Q^* = 1.729 \times h_a^{*1.339} \qquad (10)$$

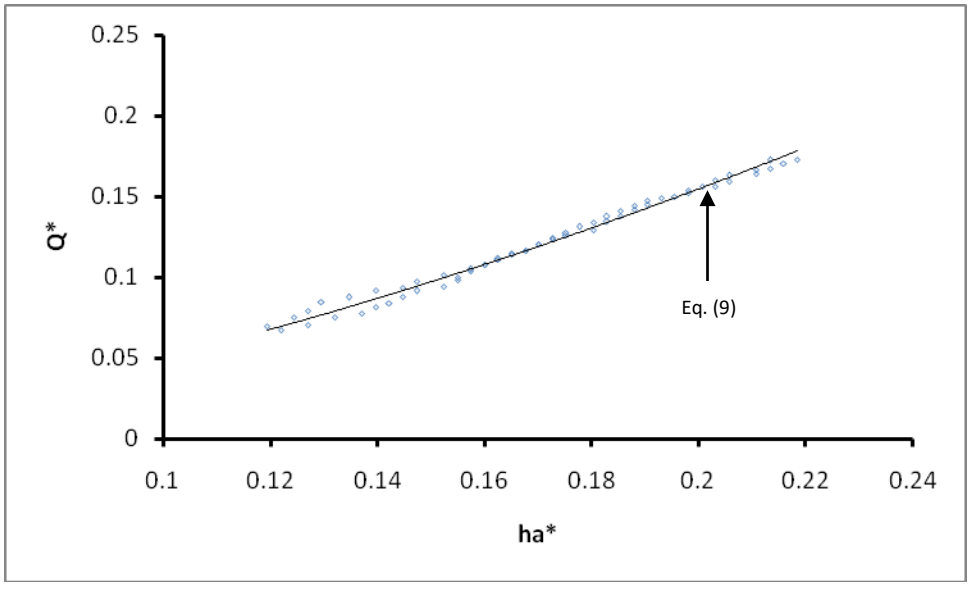

Fig. 7 Relation between Q* vs. ha^* from experimental data.

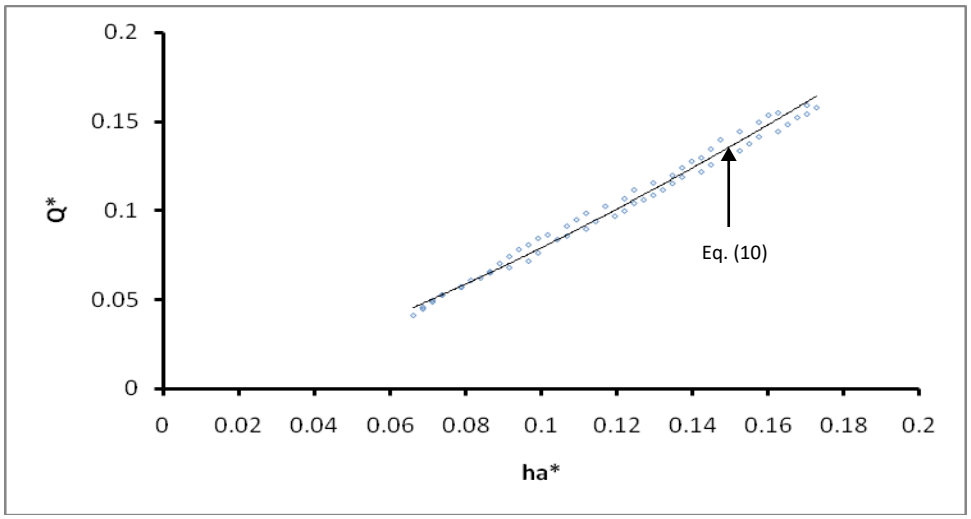

Fig. 8 Relation between Q* vs. ha* from experimental data.

Category –II

From category I it is clear that the cutthroat flume can be used for measurement of discharge in supercritical flow regime as critical flow occurs at throat section which is checked by observations of roller formation just downstream of throat section. So for finding out the general discharge relation, 130 observations are carried out for different slope condition. In all observations the Froude number at throat section and downstream of throat section is lies in range 0.93-1.00 and at measurement location the Froude number isalways greater than 1.

To determine the values of coefficient K of Eq. (4) observations are taken shown in Appendix II. for eachvalue of Q and ha values of Q* , E* ha* and Cd are calculated and plotted as shown in fig. 9,10 and 11

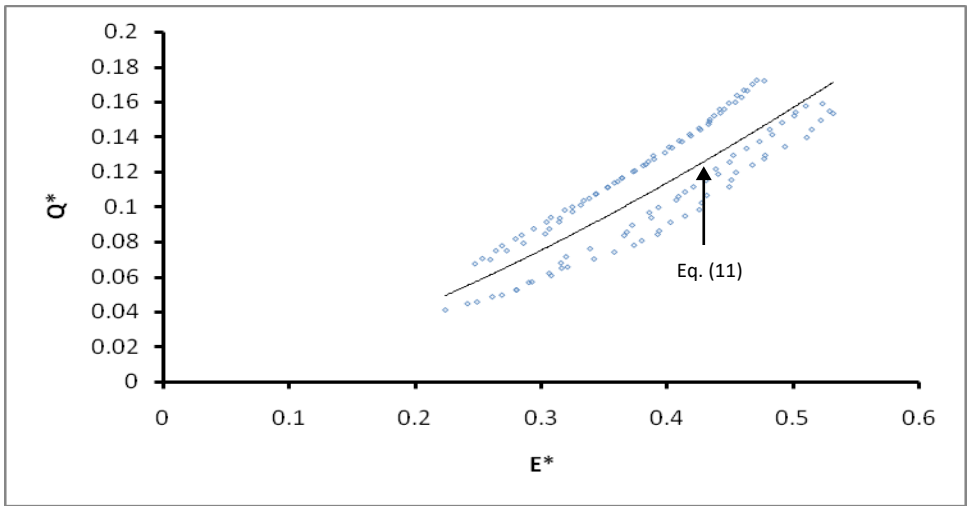

Fig. 9 Relation between Q* vs. E* from experimental data.

Regression analysis between Q* and E* was carried out which established relation as Eq. (11) with R^2 =0.758 shown in fig. 9

$$Q^* = 0.423 \times E^{*1.431} \quad (11)$$

By comparing Theorotical Eq. (3) with Eq. (11) the value of coefficient of discharge (C_d) is obtained as,

$$C_d = \frac{0.7775}{E^{*0.069}} \quad (12)$$

Conclusions

Based on the observations carried on

discharge measurement in cutthroat flume in supercriticalregime the following points are concluded:

1. The Cutthroat flume is economical to fabricate, easy to install and does not require any specialchanges to be made in the research flume.
2. The flat bed of the cutthroat flume is an added advantage while measuring head.
3. The dimensionless discharge relation in supercritical flow regime for cutthroat flume having throatwidth 0.3937m for different tilting flume slope condition can be predicted by

$$Q^* = 0.423 \times E^{*1.431} \quad (11)$$

4. The first approximation of dimensionless discharge in supercritical flow regime can be expressed as

$$Q^* = 0.840 \times ha^{*1.051} \quad (13)$$

5. For supercritical flow regime the coefficient of discharge for cutthroat flume is given by,

$$C_d = \frac{0.7775}{E^{*0.069}} \quad (12)$$

Discussion

The above Eq (13) is helpful in calculating first approximate value of Q*, which is required initerative procedure for calculating correct value of Q* by Eq (11) or Eq (12)

Appendix I:

S= 0.009090		**S= 0.0105**	
Q(m^3/sec)	**ha**	**Q(m^3/sec)**	**ha**
0.02056	0.503	0.0139	0.027
0.02148	0.505	0.0151	0.028
0.02285	0.507	0.016	0.029
0.02371	0.509	0.0173	0.031
0.02491	0.51	0.0185	0.032
0.02557	0.511	0.0198	0.034
0.02668	0.512	0.0207	0.036
0.02785	0.513	0.0218	0.038
0.02865	0.515	0.0232	0.039
0.02993	0.516	0.0255	0.041
0.03049	0.516	0.0261	0.042
0.03158	0.517	0.0273	0.044
0.03277	0.518	0.0286	0.045
0.03391	0.519	0.0295	0.047
0.03468	0.52	0.0304	0.048
0.03555	0.521	0.0317	0.049
0.03678	0.522	0.0323	0.05
0.03789	0.523	0.0331	0.051
0.03841	0.524	0.034	0.052
0.03995	0.525	0.0351	0.053
0.04081	0.526	0.0362	0.054
0.04188	0.527	0.0371	0.056
0.04289	0.528	0.0383	0.057
0.04395	0.529	0.0395	0.059
0.04491	0.53	0.0407	0.06
0.04572	0.532	0.0419	0.061
0.04689	0.533	0.0431	0.062
0.04753	0.534	0.044	0.064
0.04876	0.535	0.0452	0.065
0.04961	0.536	0.0464	0.066
0.05077	0.538	0.047	0.067
0.0525	0.539	0.0481	0.068

0.0213	0.502	0.0125	0.026
0.02285	0.504	0.0136	0.027
0.02416	0.505	0.0148	0.028
0.02578	0.506	0.016	0.029
0.02665	0.508	0.0174	0.031
0.02788	0.51	0.0189	0.033
0.02851	0.512	0.02	0.034
0.02965	0.513	0.0214	0.035
0.03081	0.515	0.0226	0.036
0.03198	0.517	0.0238	0.037
0.03272	0.518	0.0246	0.038
0.03388	0.519	0.0257	0.039
0.03491	0.52	0.0263	0.04
0.03552	0.521	0.0278	0.042
0.03666	0.522	0.0289	0.043
0.03771	0.523	0.03	0.044
0.03882	0.524	0.0312	0.046
0.03941	0.526	0.0325	0.048
0.04092	0.527	0.034	0.049
0.04202	0.528	0.0352	0.051
0.04315	0.529	0.0365	0.053
0.04421	0.53	0.0378	0.054
0.04533	0.531	0.0389	0.055
0.0464	0.533	0.0395	0.056
0.04752	0.535	0.041	0.057
0.0486	0.536	0.0426	0.058
0.04994	0.538	0.044	0.06
0.05085	0.539	0.0456	0.062
0.0519	0.54	0.0468	0.063
0.0526	0.541	0.0472	0.064
		0.0485	0.067

Appendix II

S= 0.009090			**S= 0.0105**		
Q*	**ha***	**E***	**Q***	**ha***	**E***
0.0674955	0.1219202	0.2469039	0.0456317	0.0685801	0.2484675
0.0705158	0.1270003	0.2527106	0.0495711	0.0711201	0.2682564
0.0750133	0.1320803	0.2634989	0.0525257	0.0736601	0.279871
0.0778365	0.1371603	0.2683739	0.0567934	0.0787402	0.2896563
0.081776	0.1397003	0.2791661	0.0607329	0.0812802	0.3074376
0.0839427	0.1422403	0.2839552	0.0650006	0.0863602	0.3157985
0.0875866	0.1447803	0.2935831	0.0679551	0.0914402	0.3151879
0.0914276	0.1473203	0.303797	0.0715663	0.0965202	0.3192573
0.0940539	0.1524003	0.3071656	0.0761623	0.0990602	0.3383535
0.0982559	0.1549403	0.3182227	0.0837129	0.1041402	0.3654677
0.1000943	0.1549403	0.3243032	0.0856826	0.1066802	0.3675731
0.1036726	0.1574803	0.3332669	0.089622	0.1117602	0.3718443
0.1075792	0.1600203	0.3432447	0.0938897	0.1143002	0.3870675
0.1113217	0.1625603	0.3525849	0.0968443	0.1193802	0.3854777
0.1138495	0.1651003	0.3577521	0.0997989	0.1219202	0.392802
0.1167056	0.1676403	0.3639471	0.1040666	0.1244602	0.4069898
0.1207435	0.1701803	0.3739917	0.1060363	0.1270003	0.4087181
0.1243874	0.1727203	0.3826347	0.1086626	0.1295403	0.4138731
0.1260945	0.1752604	0.384773	0.1116171	0.1320803	0.4206181
0.1311501	0.1778004	0.3979032	0.1152283	0.1346203	0.4305666
0.1339734	0.1803404	0.4035642	0.1188394	0.1371603	0.4403303
0.137486	0.1828804	0.4114231	0.121794	0.1422403	0.4383955
0.1408017	0.1854204	0.4185506	0.1257334	0.1447803	0.4493501
0.1442816	0.1879604	0.4261347	0.1296728	0.1498603	0.4522429
0.1474331	0.1905004	0.4325678	0.1336123	0.1524003	0.4627519

0.1500922	0.1955804	0.4336335	0.1375517	0.1549403	0.4730991
0.1539332	0.1981204	0.4420765	0.1414911	0.1574803	0.4832876
0.1560342	0.2006604	0.445012	0.1444457	0.1625603	0.4812841
0.1600721	0.2032004	0.4539133	0.1483851	0.1651003	0.4911153
0.1628625	0.2057404	0.4588794	0.1523246	0.1676403	0.5008049
0.1666706	0.2108204	0.463319	0.1542943	0.1701803	0.5019007
0.17235	0.2133604	0.4768686	0.1579054	0.1727203	0.5099617
0.0699249	0.1193802	0.2590171	0.0410357	0.0660401	0.2232618
0.0750133	0.1244602	0.2721736	0.0446469	0.0685801	0.2408999
0.0793138	0.1270003	0.2854274	0.0485863	0.0711201	0.2606056
0.0846321	0.1295403	0.3027042	0.0525257	0.0736601	0.279871
0.0874881	0.1346203	0.3059907	0.0571217	0.0787402	0.2920708
0.0915261	0.1397003	0.3138248	0.062046	0.0838202	0.3058237
0.0935943	0.1447803	0.3143701	0.0656571	0.0863602	0.3204031
0.0973367	0.1473203	0.3243708	0.0702531	0.0889002	0.341549
0.1011448	0.1524003	0.3310221	0.0741926	0.0914402	0.3576369
0.1049858	0.1574803	0.3376897	0.078132	0.0939802	0.3733214
0.1074151	0.1600203	0.342693	0.0807583	0.0965202	0.3794216
0.1112232	0.1625603	0.3522529	0.0843694	0.0990602	0.3921
0.1146045	0.1651003	0.3602854	0.0863391	0.1016002	0.393342
0.1166071	0.1676403	0.3636198	0.0912634	0.1066802	0.4023083
0.1203495	0.1701803	0.372679	0.0948746	0.1092202	0.4139367
0.1237965	0.1727203	0.3806668	0.0984857	0.1117602	0.4252814
0.1274405	0.1752604	0.3892204	0.1024251	0.1168402	0.4271261
0.1293774	0.1803404	0.3886664	0.1066929	0.1219202	0.4311389
0.1343345	0.1828804	0.4011697	0.1116171	0.1244602	0.4490752
0.1379456	0.1854204	0.409281	0.1155566	0.1295403	0.4507479
0.1416553	0.1879604	0.4176258	0.1198243	0.1346203	0.4544293
0.1451351	0.1905004	0.4251516	0.124092	0.1371603	0.4674818
0.1488119	0.1930404	0.4332274	0.1277031	0.1397003	0.4768658
0.1523246	0.1981204	0.4370523	0.1296728	0.1422403	0.4775963
0.1560014	0.2032004	0.4414392	0.1345971	0.1447803	0.4934175
0.1595468	0.2057404	0.4487697	0.1398497	0.1473203	0.510719
0.1639459	0.2108204	0.4552052	0.1444457	0.1524003	0.5146708
0.1669333	0.2133604	0.4607077	0.1496983	0.1574803	0.521863
0.1703803	0.2159004	0.4675011	0.1536377	0.1600203	0.531692
0.1726783	0.2184404	0.4708909	0.1549508	0.1625603	0.5289289
			0.1592186	0.1701803	0.5232397

List of Symbols

L= Length of Cutthroat Flume g= Acceleration due to gravity h_a*=H_a/W= Dimensionless Head K= Constant of equation in free flow condition n=Exponent of equation in free flow condition Q= discharge through flume in (m^3/sec) R^2= Coefficient of Determination W= throat width of Cutthroat Flume L/3= Length of converging section from throat section2L/3= length of diverging section from throat section H_a= upstream head at 2/3 rd position from converging inlet sectionS=Bed slope of rectangular flume C_d= coefficient of dischargeHP= horse power C= free flow coefficient E*= Dimensionless Energy Q*= Dimensionless Discharge

References

1. Bos M G (1989) Discharge measurement structures. International Institute for Land Reclamation and Improvement, ILRI, Wageningen
2. Christopher I. Thornton et. all. (2009). Supercritical flow measurement using a small parshall flume. J. Irrig. Drain. Eng. Vol. 135(5), 683-692.
3. Keller, R. J. (1984). Cutthroat flume characteristics. J. Hydraul. Eng. 110(9), 1248–1263.
4. Ramamurthy, A. S., Rao, M. V. J., and Dev Auckle, (1985). Free flow discharge characteristics of throatless flumes. J. Irrig. Drain. Eng. 111(1), 65–75.
5. Ramamurthy A. S. Ngoc Diep VO, R. Balachandar (1988). Submerged flow characteristics of throatless flume. J. Irrig.

Drain. Eng, 114(1) 186-194
6. S. A. Tekade, A. D. Vasudeo, A. D. Ghare, R. N. Ingle (2016). Dimensionless Discharge in Supercritical Flow Regime for Different Sizes of Cutthroat Flumes. Arabian Journal for Science & Engineering, 41(10) 4235-4245
7. Skogerboe, G. V., Bennett, R. S., and Walker, W. R. (1972). Generalized discharge relations for cutthroat flumes. J. Irrig. Drain. Eng. Div 98(4), 569–583.
8. Skogerboe G.V. Wyann R. Bennett R.S. Tsu-Yang Wu(1973). Slope discharge ratings for cutthroat flumes
9. ASCE vol.16, 78-81
10. Streeter V. L.: Benjamin E : Wylie Fluid Mechanics (7^{th} edition) Mcgraw Hill Publication. ISBN 0-07-548015-8
11. V.L. Manekar (2007) Discharge relation for cutthroat flume under free flow condition J. Irrig. Drain Eng.
12. 133(5), 495-499
13. Ven Te. C.: Open Channel Hydraulics. Mcgraw Hill Publication. ISBN 07-010776-9 (1988)

ELECTRONIC COMPONENT IDENTIFIER & VALUE CALCULATOR

P.R. Deshmukh[1], H. N. Verma[2], S. R. Tiwari[3], A. G. Nagpure[4] and U. Ahmed[5]
Department of Electronics and Telecommunication, Government College of Engineering Nagpur, MS, India
[1]pr_deshmukh@yahoo.com [2]hardikverma98@gmail.com [3] sagark13599@gmail.com
[4]artinagpure1999@gmail.com [5]umaisaahmed01@gmail.com

ABSTRACT

Electronic Component Identifier and Value Calculator is an algorithm which can be used to identify basic electronic components in places where human hands cannot practically reach. It can be used in complex electronic machinery with the help of a micro-camera attached to a device like laptop or a smartphone. This system runs on the prime ideology of Object Detection making use of Convolutional Neural Network (CNN) technology. This system uses a camera to intake images of the subject and then sends it in to the YOLO v3 CNN. It then processes the data and compares it with trained models and gives out the output as the name of the component detected. It then searches for color line codes to calculate the magnitude/value of the component's characteristic phenomenon. ECI-VC showcased satisfactory results and was proved to be faster than few other CNNs and more accurate than YOLO v5.

Keywords: *Object Detection, Electronic Components, CNN, YOLO v3.*

1. Introduction

With the advent of the latest technologies, it has become harder and harder every day to keep up with the advancements. Technology is getting better and compact day by day. Machine vision is an important development because image information can be obtained, which accurately judges the state information of industrial products, so as to reduce human effort and increase automation operation. With the development of computer technology and information processing technology, object recognition based on deep learning and computer vision is one of the most popular directions in machine vision field.

The Electronic Component Identifier and Value Calculator fills this industrial gap and acts as a need for those who have little-to-no knowledge about electronic components and is an advancement in technology for the effortless calculation of values of various electronic components.

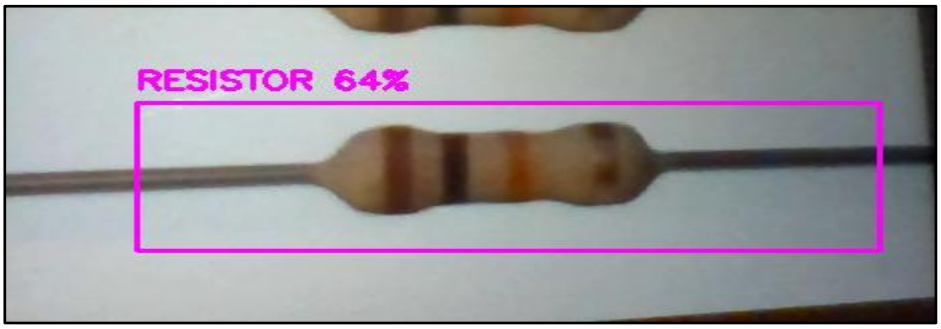

Fig.1 : A Resistor as working example for Electronic

The above image depicts a resistor. This project will work in the following way: The algorithm for Electronic Component Identification with the help of YOLO v3 CNN will identify the object. The individual has to keep the resistor in front of the camera and with help the of object detection algorithm it will be identified hence being helpful for the person who doesn't know what it is. Secondarily, it will track the color-coded lines on the resistor and using the generalized calculation chart, calculate and give out the value in ohm of resistance.

2. Architecture & Tools

2.1 Convolutional Neural Networks (CNN/ConvNet)

A Convolutional Neural Network (ConvNet/CNN) is a Deep Learning algorithm also known as space invariant algorithm, because of their shared-weights architecture, which can take in an input image, assign probability values to various parts of the image and be able to differentiate one from the other.

In a ConvNet architecture each neuron is only connected to the neighboring neurons, which decreases the load on every neuron and indirectly increases the processing speed.

The advantage that the ConvNet has over other Neural Network is that there is no need for Feature Extraction. The system extracts feature by itself and the features in next layer are convoluted with different filters to generate more invariant and specific features and the process continues till one gets final output. The activation functions which CNN uses known as ReLU (Rectified Linear Unit) activation function, identifies the neurons with higher confidence value and uses them to train the model in a more efficient manner.

Convolutional Neural Networks benefit from the actual fact that the input consists of pictures and that they constrain the architecture during a lot of wise approach. The layers of a ConvNet have neurons organized in three dimensions: width, height, depth. For instance, the input pictures in CIFAR-10 are an input volume of activations, and also the volume has dimensions 32x32x3. The neurons in a layer can solely be connected to the neighboring neurons, rather than all of the neurons during a fully-connected manner. The ultimate output layer for CIFAR-10 would have dimensions 1x1x10, as a result the top of the ConvNet design we'll cut back the total image into one vector of class scores, organized on the depth dimension (Refer [1]) Here may be a visualization:

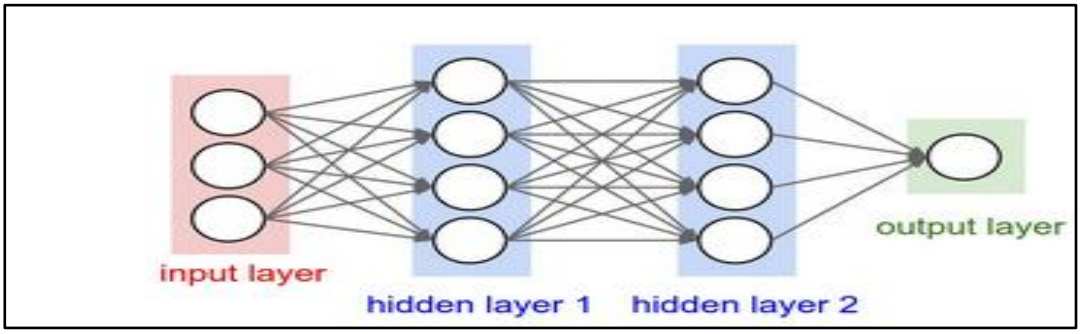

Fig.2 : A regular 3-layer Neural Network

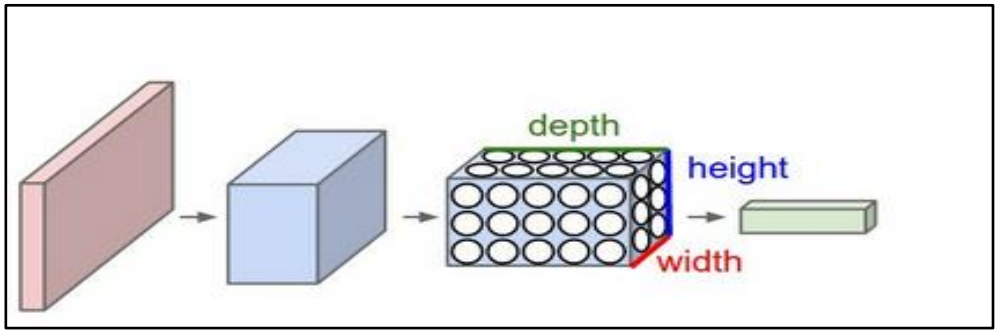

Fig.3 : A ConvNet arranges its neurons in three dimensions (width, height, depth), as visualized in one of the layers.

Each layer of a ConvNet converts the 3D input volume to a 3D output volume of neuron activations. During this example, the red input layer holds the picture, thus its dimensions would be the size of the image, and also the depth would be 3 (Red, Green, Blue channels)

2.2 YOLO v3

YOLOv3 is a variant of a preferred object detection algorithmic program YOLO – You Only Look Once. YOLOv3 which is a Convolutional Neural Network algorithm (CNN) based on the DarkNet53 Framework. The YOLO algorithm applies a neural network to the full image at once and then the algorithm compares the trained module with the input image and gives out the probability of match.

DarkNet53's pre trained model which we are using is used to assist our model in training at the final layers so that it can yield faster and accurate results. The Darknet53 Framework consists of 106 layers out of which the 82nd, 94th and the 106th layers act as output layers but the final output is achieved via the 106th layer.

Testing the model gives rise to the activation function which is ReLU (Rectified Linear Unit Function) it helps to identify those neurons which has maximum probability or accuracy values and then shifts them to the end of the neural network so as to fasten the training and it also increases the accuracy. In the Figure 4 one of the layers has been skipped to the end. This was done because the ReLU activation function identified that this layer had accuracy or probability values that were so relevant that it had to be shifted towards the end, so as to make way for their contribution in the output layer. (Refer [1]) Below is that the theoretical rationalization of how YOLO works:

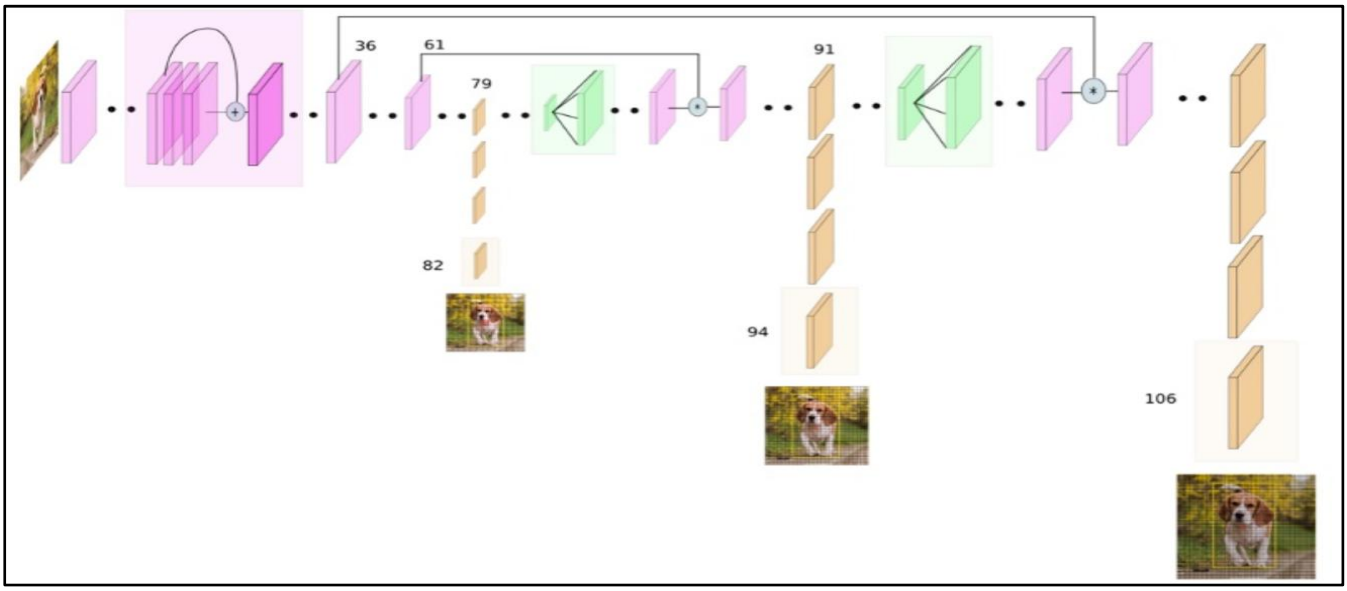

Fig.4 : Working of YOLO CNN

Open CV is an open-source library that has many computer vision algorithms. OpenCV features a standard structure, which suggests that the package includes many shared or static libraries (Refer 3) . This project uses Open CV extensively in the testing program.

2.4 Google Colab

Google Colaboratory, or "Colab" for short, allows us to write and execute Python and Linux command line programs in our browser, with the advantage of zero-configuration, easy sharing and access to world-class GPUs. This project uses Nvidia Tesla T4 GPU of 16GB memory which is a high-performance GPU and is available to use through Google Colab.

2.5 Camera

The first light of this project is through a webcam of laptop or PC, or a smartphone's camera. Both of them take in the images (or continuous frames in case of a video) and sends them to the YOLO v3 to further process the image and perform object recognition on them.

3. Methodology

The Electronic Component Identifier follows the below procedural methodology.

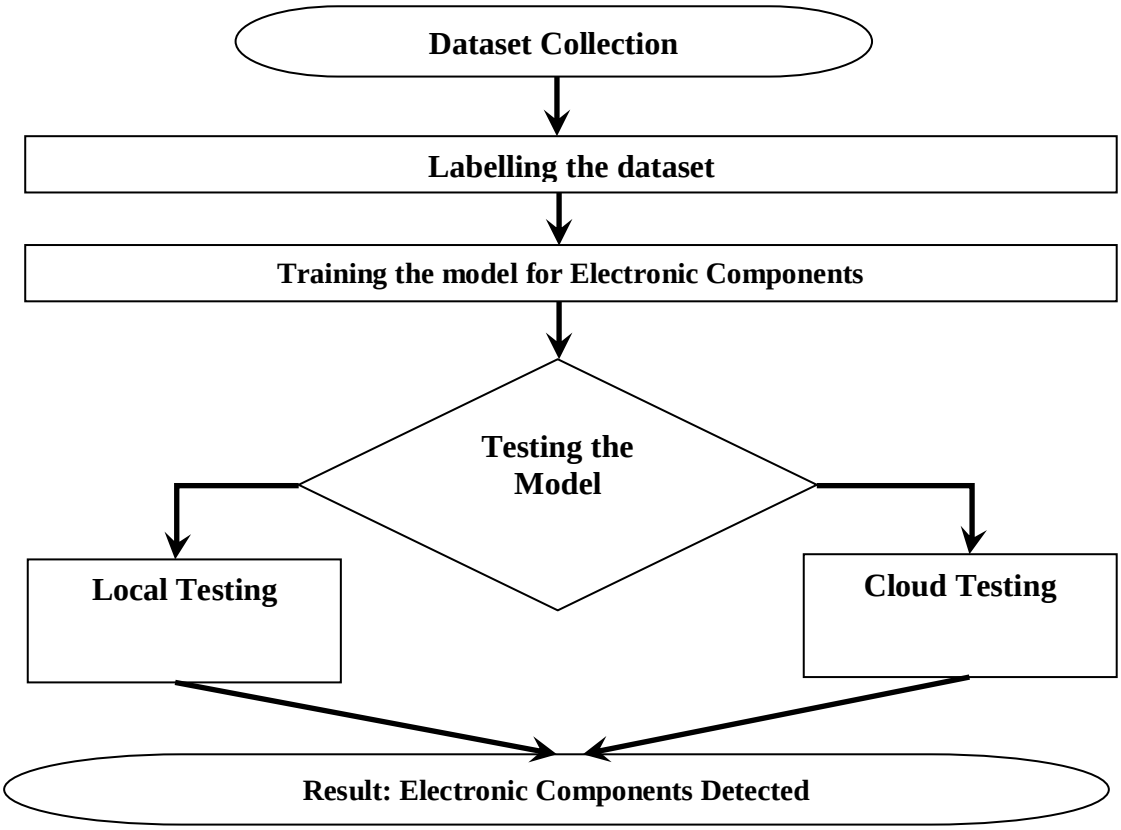

A set of images of electronic component were downloaded and arranged accordingly based on the names of the electronic components like Resistor, Capacitor, LED, Transistor. These images were sorted and finalized based on the quality, visibility of distinct features and pixel resolution of the picture. Labelling is a process of defining the specific area of the objects to be detected inside an image from the data set. Labelling is done by marking a bounding box around the desired objects in the image and the labeled file of every corresponding image is a text file containing the details about the object and the coordinates of the vertices of the corresponding bounding boxes.

3.2 Training the Model

DarkNet53 is the backbone of YOLO v3, and to make use of this backbone we used the complete repository of DarkNet53 in our work environment i.e., Google Colab Notebook. The model was trained on the basis of Transfer Learning methodology which used DarkNet53.conv.74 pre-trained model to assist our custom model in learning. Training process took 2-10 hours and used resources from Google Colab like Nvidia Tesla T4 GPU of 16GB memory which is a high-performance GPU. Trained model's Precision and Recall graphs can be found in the Result section.

3.3 Testing the Model

The testing process can be done by two methods depending on the number of images in the trained model and the constraints of time and processing power. The local testing provides reliability in terms of the actual process but takes a heavy toll in terms of processing power. The cloud computing route is faster and more accurate because of the freely available high-performance GPUs but cannot be fully reliable due to Internet connectivity. As this project uses a large number of images, we opted for cloud testing using Google Colab Notebook. The inputs can be in image (.jpg / .jpeg / .png) or video (.mp4) format. When the electronic component object is placed in front of the camera module or smartphone camera, its image is taken in by the system. This image is converted into low resolution black and white version of itself and then is converted into a matrix of ones and zeros This set of data is then finally fed into the YOLO v3 CNN where in the data is compared to the data of the trained models of different

electronic components. The result is the probabilities of matching the shown object to that of the pre-trained objects and this result is showcased or displayed on the screen of the device in which the system is placed. The complete explanation and demonstration of the python programs used can be found here.

4. Results

4.1 Training Results

Our trained model gave out the following patterns for Precision and Recall after training for Resistor, Capacitor, Transistor, Multimeter and LED after completion of the training process:

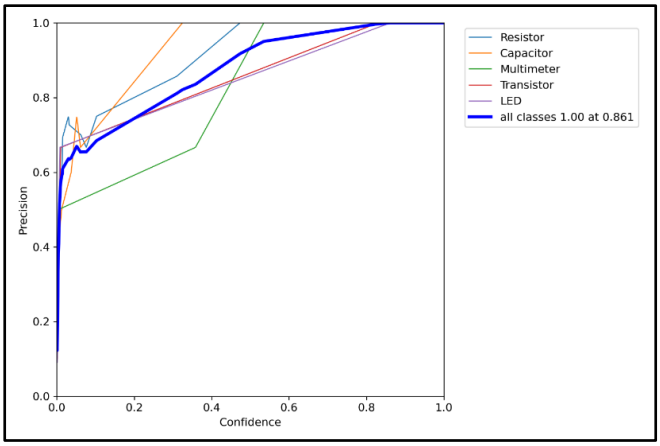

Fig.5 : Precision graph of trained model

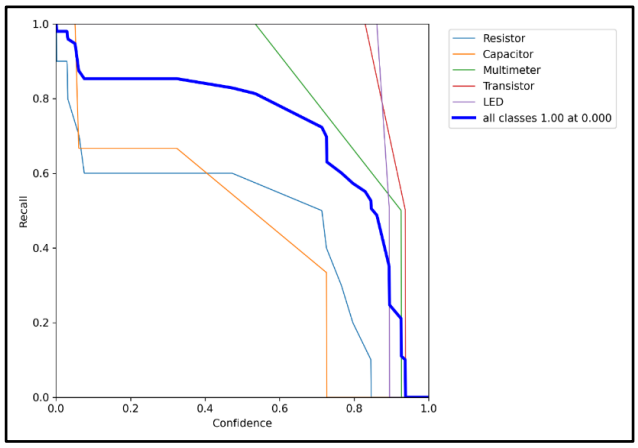

Fig.6 : Recall graph of trained model

4.2 Testing Results

The following are the results for various electronic components where we can see the bounding boxes with the probability values of different electronic components detected by our trained model:

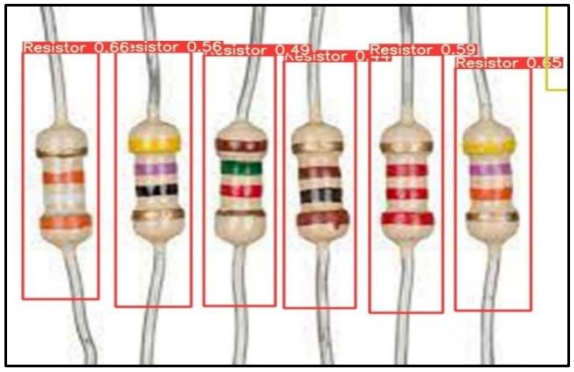

Fig.7 : Resistor detected with max 66% accuracy

Fig.8 : Transistor detected with max 88% accuracy

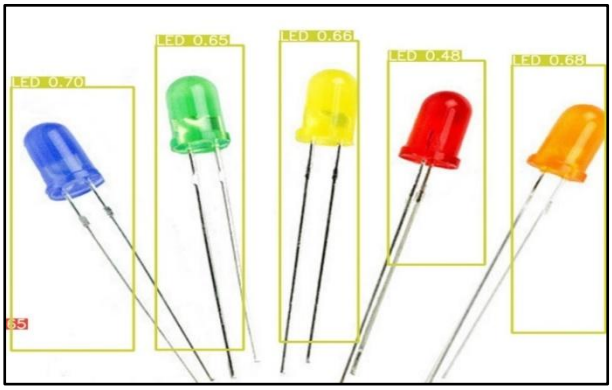

Fig.9 : LED detected with max 70% accuracy

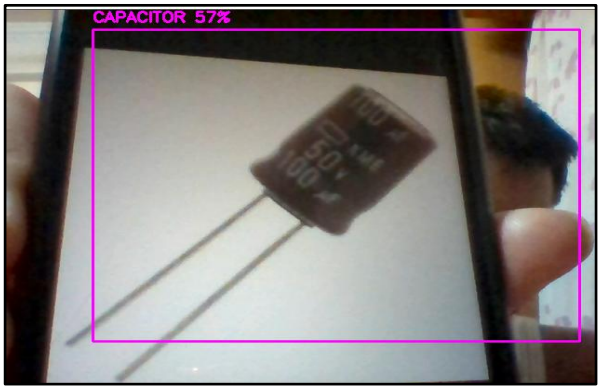

Fig.10 : Capacitor detected with max 57% accuracy

5. Discussion

Electronic Component Identifier & Value Calculator showcases satisfactory results in terms of object recognition accuracy and speed. The product stands out in terms of accessibility and affordability and turned out to be quite easy to understand for the matter of understanding and explaining it to the industry workers. The following are the comparison of this project's algorithm with other available object detection algorithms. It can also be considered as

Related Work and Findings.

5.1 YOLO v3 vs. YOLO v5

The Yolov3 uses Darknet53 as its backbone whereas the Yolov5 uses PyTorch as its backbone. While PyTorch is indirectly based on, or rather a rip-off version of Darknet53 model, it has overcome many problems faced by YOLOv3 and is able to achieve tremendous amounts of speed. This speed does come with a cost of accuracy.

While testing YOLOv3 and YOLOv5 for our dataset of Electronic Components, it was observed that YOLOv3 gives probability accuracy of up to 99% at 15-25FPS whereas YOLOv5 gives probability accuracy of up to 80% at 45-55FPS. This indicates that YOLOv5 is much faster but YOLOv3 is far more accurate. Following is the statistical comparison between the two.

Table.1 : Statistical comparison between testing performance of YOLOv3 and YOLOv5

Model	Backbone	Dataset	Objects	% Accuracy	FPS
YOLOv3 320 × 320	DarkNet-53	Electronic	Resistor	66 %	19
YOLOv3 320 × 320	DarkNet-53	Components	Capacitor	57%	24
YOLOv3 320 × 320	DarkNet-53	-----“”-------	Transistor	90%	20
YOLOv3 320 × 320	DarkNet-53	-----“”-------	LEDs	70%	18
YOLOv5 S	PyTorch	Electronic	Resistor	45 %	46
YOLOv5 S	PyTorch	Components	Capacitor	38%	51
YOLOv5 S	PyTorch	-----“”-------	Transistor	54%	55
		-----“”-------	LEDs	51%	49

While YOLOv5 may seem the choice for prototype projects but we in our project Electronic Components Identifier aimed for higher accuracy. Hence YOLOv3 was chosen for the training and testing of the models used in this project.

5.2 YOLO v3 vs. SSD

SSD (Single Shot Detector) is another object detection algorithmic program that forwards the image once although a deep learning network, however YOLOv3 is way quicker than SSD whereas achieving quite comparable accuracy. YOLOv3 provides quicker (Refer 4) than real-time results on a M40, TitanX or 1080 Ti GPUs. The time taken by YOLOv3 is 0.84 sec/frame, which is more as compared to SSD (Single Shot Detector) which is 0.17 sec/frame, but the accuracy of YOLOv3 which is upwards of 80.3% is far better than SSD accuracy of around 72.1%. As you can see that a precise compromise was made to achieve this accuracy. Below is a statistical comparison between the testing performances of YOLO v3 and SSD.

Table.2 : Statistical comparison between testing performance of YOLOv3 and SSD

Sl.no.	Parameters	YOLO v3	SSD
1	Speed	Low	High
2	Accuracy	80.3% High	72.1% Low
3	Time	0.84~0.9 sec/frame	0.17~0.23 sec/frame
4	Frame per second	45	59
5	Mean Average precision	0.358	0.251

5.3 Faster R-CNN

There are many literatures available on Faster R-CNN. A detailed study on the working of Faster R-CNN can be found in (Refer 5) . R-CNN have increased the rate of the detection networks. Region Proposal Networks (RPN) have been introduced that do full-image detection work, thus enabling to greatly reduce cost for region proposals. The RPN is end-to-end trained to generate high-quality region proposals, which is then used for Faster R-CNN.

5.4 Optimized SqueezeNet

A large number of literatures showcase the usage of SqueezeNet for deep learning in order to use for object recognition. But to address the problem of low recognition recall and low accuracy of traditional image recognition technologies and support vector machine (SVM)), there are research papers that selects multiple deep learning networks for testing and optimizes the SqueezeNet network. (Refer 6).

6. Conclusion

The operating experience and practice indicated that the Electronic Component Identifier & Value Calculator has the benefits, such as, testing speed is quick, the reliability of the system is high, the real time analysis of the component is accurate and the operating cost is low. From the experimental results we have observed that the Electronic Component Identifier overshadows the traditional methods of object recognition which use other Neural Network algorithms such as Artificial Neural Networks (ANN), Recurrent Neural Networks (RNN). The proposed system work is to automatically detect the type of electronic component with higher accuracy. These confidences of each component are then displayed to the user just above the bounding box. This helps the user to understand the type of electronic component so that they'd be aware of where to assemble the particular electronic component. Since everything is automatic, human labor is reduced. An external condition which decreases the accuracy of the system is eliminated. Hence accuracy has been preserved. The future work is to modify the proposed system to detect the values of electronic components and to add other complementary sensors to perform various other processes. The complete explanation and demonstration of the python programs used can be found here.

References

1. "Convolutional Neural Networks for Visual Recognition". https://cs231n.github.io/convolutional-networks/#architectures
2. Vidushi Meel, "YOLOv3: Real-Time Object Detection Algorithm" 2021. https://viso.ai/deep-learning/yolov3-overview/
3. "Introduction to Open CV", https://docs.opencv.org/master/d1/dfb/intro.html
4. Dr. S. V. Viraktamath, Pratiksha Navalgi, Ambika Neelopant, "Comparison of YOLOv3 and SSD algorithms" in International Journal of Engineering Research & Technology (IJERT), pp. 194-195, February 2021.
5. Shaoqing Ren, Kaiming He, Ross Girshick, and Jian Sun, "Faster R-CNN: Towards Real-Time Object Detection with Region Proposal Networks" in IEEE Transactions on Pattern Analysis and Machine Intelligence, pp. 1-1, June.2016.

6. Yuanyuan Xu, Genke Yang**,** Jiliang Luo, and Jianan He, "An Electronic Component Recognition Algorithm Based on Deep Learning with a Faster SqueezeNet" in Mathematical Problems in Engineering, pp. 1-1, Oct.2020.
7. Joseph Redmon, Ali Farhadi, "YOLOv3: An Incremental Improvement" in Computer Vision and Pattern Recognition on April 2018.
8. Sunita Nayak, "Training YOLOv3: Deep Learning based Custom Object Detector". https://learnopencv.com/training-yolov3-deep-learning-based-custom-object-detector/

NOVEL METHOD FOR FORECASTINGSOLAR ENERGY FOR GRID MANAGEMENT

J.Ambulkar[1], P. Bhoyar[2], H. Ramapure[3], C. Gharate[4] and N.D. Ghawghawe[5]
[1,2,3,4,5]Department of Electrical Engineering, Government College of Engineering, Nagpur
[`1]jayeshambulkar19@gmail.com, [2]bhoyarpranay07@gmail.com

ABSTRACT

Dependency on renewable sources has increased a lot in the past few years and integration of these sources with the electric grid becomes crucial for better energy management. Also, with the upcoming problems in the grid, the need of better management is important. Forecasting of solar energy and integrating this with the grid can solve the problem of managing the grids. The generation of solar energy depends upon various factors which are very dynamic in nature so by predicting these factors we can easily forecast the solar energy generated. In this paper, we will be studying about the Grid management of India, factors that affect the solar energy, how we can predict the energy and by integrating of these how we can have a better grid system.

Keywords: *Solar energy, grid management, forecasting, linear regression, planning.*

Introduction

Global warming, exhaustion of energy sources over time have stipulated to utilize and integration of renewable sources of energy. Inexhaustibility have made solar energy the most powerful and efficient energy source. According to the survey of 30th November 2020 renewable energy sources contributes 24% out of all energy sources for electricity generation and in this solar energy contributes around 38GW. The weather fluctuations affects the solar power, prediction of power generation utilizing forecasting of weather can improve the quality of service. Upgradation of solar energy into electric grids is increasing due to high energy demand. The interconnected circuit which is used for distribution of electricity from producers to user is called as electric grid.Basically, main factors used for forecasting are humidity, wind speed, etc. Plant owners and operators get the most out of their facilities by giving accurate weather conditions. System operators need to know in what percentage of energy a renewable plant can deliver and traders endeavor to get the better price for every megawatt-hour.

In the future transmission and circulation will be better and ready to control bidirectional energy streams (from grid to consumer and vice versa), for example, from sun-oriented boards on building, little wind turbines on rooftops, siphoned hydroelectric force, utilization of power devices, and different sources.Old grids were designed for one-way flow (from grid to consumer only), but if a local network creates more power than it consumes, the reverse flow might increase marketing opportunities while also lowering demand, therefore our grid delivers IT-based solutions that the traditional power grid lacks.Microgrids' more centralize power generation requires traditional grids to distribute complicated distribution systems.Households can save money on electricity by using microgrids instead of buying it from utilities.

Grid Management

The Indian Power system is demarked into five regions namely Northern region, Northeast region, Western region, South region, Eastern region, and are monitored by a National Load dispatch center at New Delhi. With a Generation Capacity of 374.2GW, the girds are interconnected to each other with a vision of one nation one frequency. The Regional grids are again divided into state load dispatch centres which are further divided according to the area load dispatch center. The western region where Maharashtra comes into have a generation capacity of around 133.8GW of which Maharashtra constitutes of 43GW of capacity. The national grid was built to manage the surplus/deficit energy for varying load, so that our national resources are used optimally. If one power station needs maintenance, consumers can still be supplied from others around the country.

The function of the state load dispatch center is to provide optimal scheduling and dispatch within the state, monitor grid operation, exercise supervision and control over an intrastate transmission system, load

forecasting, generation scheduling, planning to control to meet shortages etc. The demand is forecasted according to the previous data, seasonal variations and considering any special day. The generation schedule is done by collecting the data that the stations are going to generate the next day. Both distribution companies and generation companies send their estimated data around 10 am and then the load dispatch center schedules the plan for the next day. Forecasting and scheduling is very important for stable and efficient grid management. Estimating the non-renewable energies like coal, gas, etc is easy to predict but the renewable resources are not.

The government of India has considered the solar power sector as an integral part for the solution regarding the energy needs of the nation and an important player for the nation's energy security. They have targeted 100GW installation of grid-connected power by FY2022, for achieving this government has encouraged solar power generation by launching various schemes. By various such schemes launched or to be launched by the Government, the solar sector is tending to grow, and therefore the integration of grid becomes critically important.

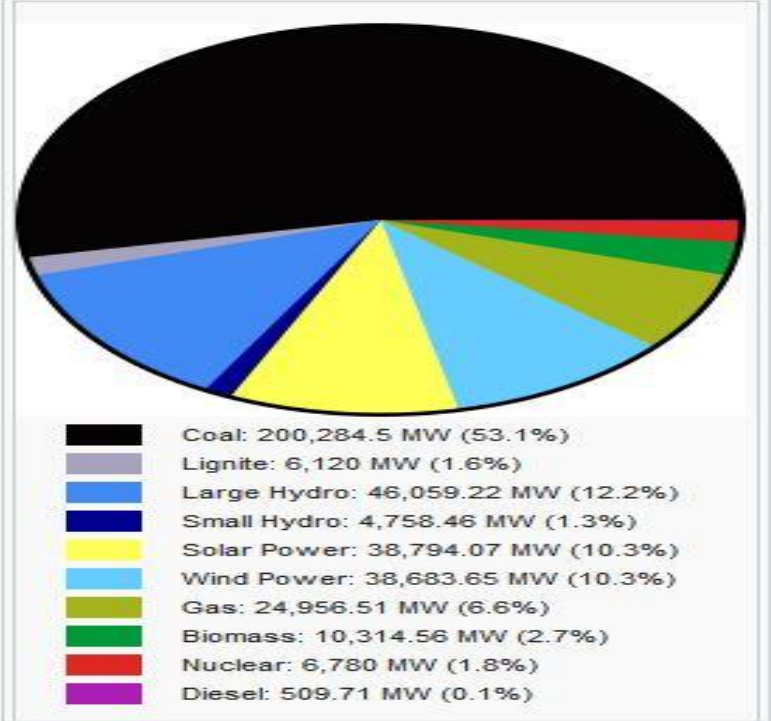

Figure-1: Energy Chart

Scheduling day ahead becomes the backbone of the operation for grid management, both at intrastate and interstate levels. Scheduling day ahead gives us optimal scheduling process and further helps us in the dispatch of the electricity based on the data given by the generator company. Most of the renewable energy sources depends on the weather and especially the solar energy dependence is quite significant. Therefore, good prediction systems are required for accurate data which can be send by the generator companies. Generators need to predict their demand and generation based on various factors like historical data, weather forecast, machine learning and modeling them.

Solar Forecasting

Solar generation forecasting depends upon number of weathering variable such as Temperature, Pressure, Humidity, and many more. Currently in our model we are using parameters for solar forecasting are as follows: 1) Temperature 2) Pressure 3) Humidity 4) Wind speed. It has been observed that four parameters vary with changing weather and does affect solar radiation directly. A process of releasing tremendous amount of energy

from a star due to dominance of electromagnetic force over nuclear force is nuclear fission which results in solar energy we receive on earth.Due to irregularity of the solar source, parameter such as irradiance, temperature level and other atmospheric conditions assist us in predicting solar energy.The air temperature originated by absorption of radiant energy directly from the sun which also affects the humidity and air pressure.In order to predict incoming solar radiation multiple machine learning algorithms should be used in parallel. In this paper we use standard Linear Regression model to predict solar radiation using artificial neural networks.

In Novel Method for Forecasting Solar Energy for Grid Management, we are using linear regression model to predict the value of solar radiation by finding relationship between our output and input parameters and find out intercept.

By using regression-based model we aim to predict output radiation such that the difference between the output and actual radiation should be minimum.By creating a dataset of numerous x1 and x2 values and setting best fit regression model the error between input and output can be minimized. First step in performing linear regression is finding a correlation between different parameters and radiation in data set. Heat map help us with finding the correlation between two variables and up to what length they affect each other.

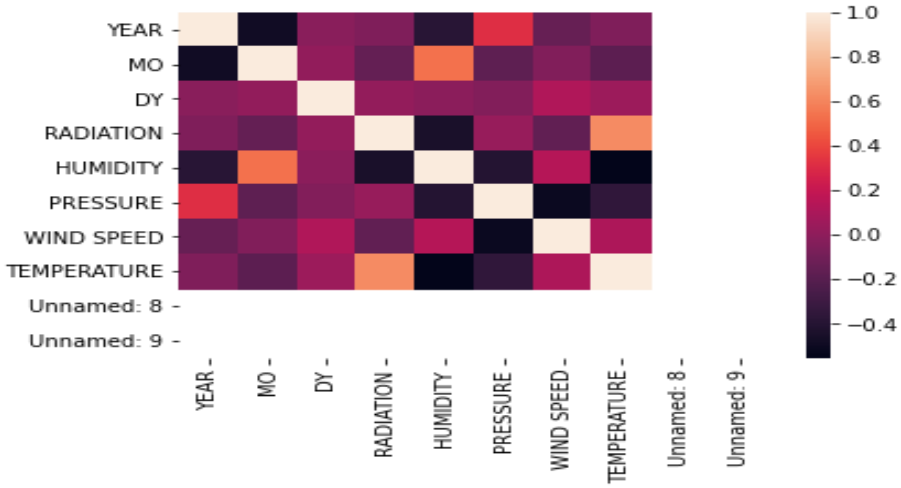

Figure-2: Heat Map

Fig-2 shows how each parameter is affecting the solar radiation whiter the color is more dependent parameters are on each other. (For performing this prediction, we have taken data of Nagpur city)

Train/Test is a method to measure the accuracy of the MLP model. This is the process of splitting our data into two sets training set and testing set. We split data into an 80/20 ratio for training and testing purposes.The split data is divided into training data and testing sample data, once the model is trained, we verify the evaluation of a final model fit on the training dataset. Verification is performed only after model is trained using training set. After that we use testing set to validate our model in a real-life scenario. Last step is fitting the given data set and calculating different intercepts to fit your data. The following equation is used to describe the fitting curve of

$$y=\beta_0X_0 + \beta_1X_1 + \beta_2X_2 + ... + \beta_nX_n + \mu$$

Final step of Multiple Linear Regression is visualizing predicted vs. actual value and how fitted curve is and also calculating R square value. Following image shows the graph for solar radiation prediction value for actual vs. predicted after training and testing the data.

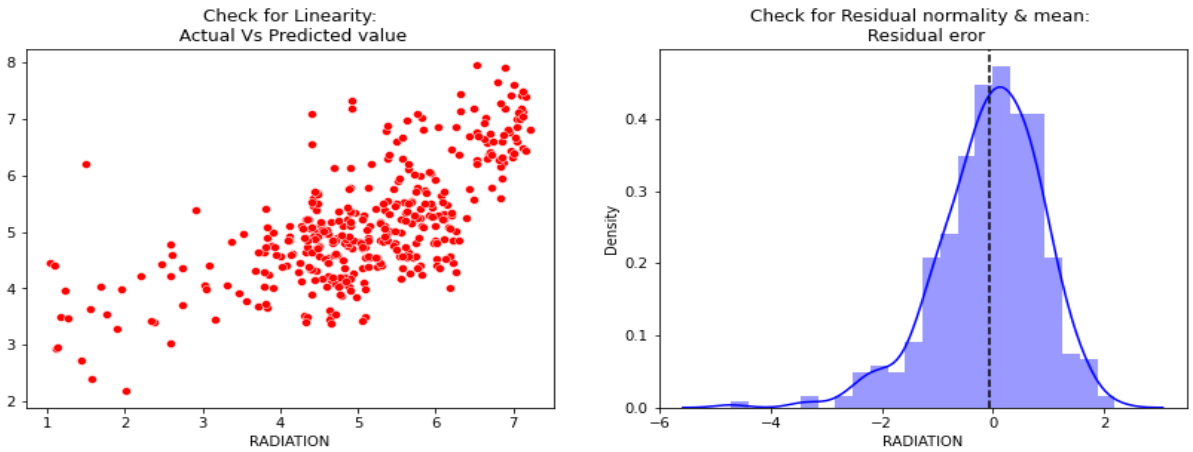

Figure - 3: Output Prediction

Integration

With extensive penetration of photovoltaic power, there areadverse effects on distribution part, particularly the management of energy in a grid is starring prime attention, plus there are problems related to voltage variations, power fluctuations,losses in grid, etc. Load prediction or Solar energy prediction could be a significant tool for operators, consumers moreover governing bodies of energy management and planning.

Forecasts have raised ample consequences rolling out across further businesses like energy exchange, resource management companies, financial planning in resources, etc. Forecasts being the principal for the system to obtain minimum finances for electricity. Companies are showing interest in smart grid implementations due to immense profit. Forecasting of energy unexpectedly has a greater significance inthe implementation of drafting demand-side requirements, maintenance, integrating renewable sources, scheduling of generation, etc. The consumer also gets to know more about demand and variations of electricity prices per unit.

The usage for household consumption of solar panels has remarkably risen due to its cost-effectiveness and also the subsidies provided by the governments. At present solar power is directly given to grid without inspecting the grid. It is only possible if the power produced by every solar panel is either known or doesn't surpass the limit. Although in the future, nearly everyone from industries to individuals will be having solar panels on their roofs,and the solar power into the grid will be rising. As the grid is constructed to bear a lesser amount of power within it. Hence to remove this concern and to maintain excess energy, we must have an estimated amount of solar power generating and given to the grid. If the predicted output of every household having solar power generated at a particular time is provided, and out of which if we can say it is excess or deficit power in terms of demand, then we can inform the grid management, the management will schedule the generation accordingly. This will aid the management to use assets to their minimum and maintainstability. Anticipating the output power also helps in planning demand as per load,electricity trade, etc but solar power can rapidly vary due to variations in various weather conditions.

For grids to maintain stability and operate economically as well as reliably, forecasting should be necessary, because it provides the amount of power produced at the consumer's end. The produced solar energy at the consumer's end is dependent upon numerous factors like weather (wind speed, humidity, temp.), day, events, etc. Some considerations in forecasts when advancing these prototypes are classifying load patterns of customers formed on the consumption, escalated perceptive of consumers to provide real-time rates as compared to conventional grids.

The huge inference of solar power in thegrid acquires new demand for the management, which is to maintain production-consumption balance. Eventually, the perspective is to reform the reserves and make thebest use of resources.

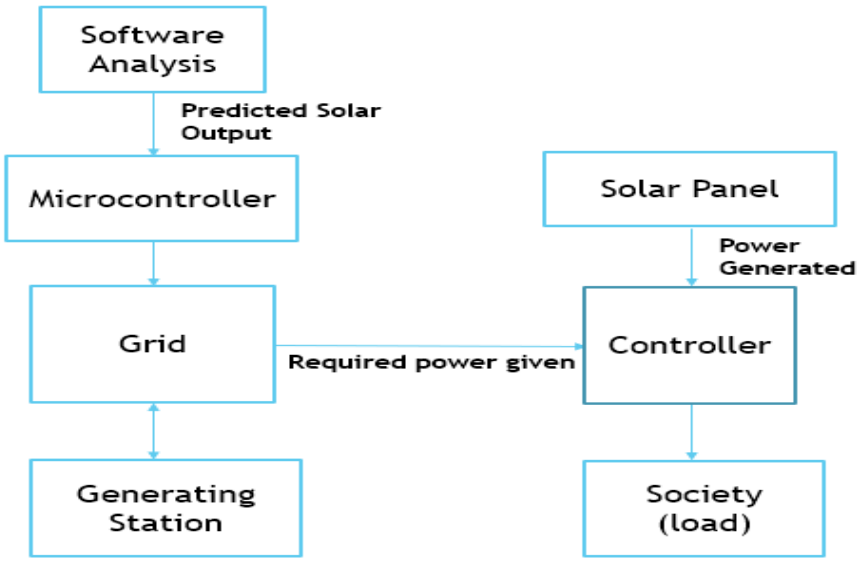

Figure 4: Flowchart

Fig-4 shows that solar energy would be predicted for the next day and given to the grid and accordingly grid will manage the generating stations energy properly so that no over generation or under generation takes place.

Result

Table 1& 2 shows the actual radiation and the predicted radiation of some previous know data of January 2015& Jan 16. The parameters taken into consideration here are Humidity, Pressure, Wind speed, Temperature.

Table1: Radiation for 2018

Date	Humidity	Pressure	Windspeed	Temperature	Actual Radiation	Predicted Radiation
28/1/2018	20.41	97.41	5.63	30.59	5.22	4.23
25/3/2018	14.62	97.38	9.39	38.46	6.74	6.68
10/5/2018	19.78	96.81	6.68	43.7	7.07	6.85
19/7/2018	89.01	96.85	10.35	27.39	1.87	1.84
29/9/2018	71.95	97.16	4.25	31.62	5.99	5.83
19/11/2018	45.83	97.55	4.77	33.42	4.66	4.72

Table 2: Radiation for 2019

Date	Humidity	Pressure	Windspeed	Temperature	Actual Radiation	Predicted Radiation
28/1/2019	37.85	97.98	9.4	24.39	5.15	5.20
25/3/2019	19.52	97.2	8.18	39.6	6.63	6.58
10/5/2019	19.31	96.68	11.02	43.88	7.11	6.12
19/7/2019	65.87	96.3	6.63	35.74	4.23	4.14
29/9/2019	94.02	97.3	5.1	27.15	2.63	3.95
19/11/2019	76.81	97.56	5.45	26.06	4.81	4.78

Conclusion

This paper shows the importance of grid planning and how solar energy forecasting can help us to achieve the same.

Following are some other conclusions derive from solar forecasting and grid management:

- Allows the management to propose well considering they have the future demand as well as consumptions.
- Forecasting aids in planning and maintaining the future power systems in terms of the capacity and type. By governing areas or regions with high demand or excess power, the utilities will most likely generate the power near the load or wherever there is a deficit. This reduces the transmission and distribution infrastructures as well as the correlated losses.
- It also provides assistance for planning stability and maintenance of the power systems. By considering the forecast, the utility can know when to carry out the troubleshoot and make sure that it has the minimum consequence on the consumers. For example, they may plan to do maintenance on residential areas during the day when most of the people are at work and demand is extremely low.
- The forecasting reduces the risk for utility for prevention of under generation or over generation.

References

1. P.A. Kulkarni, R.M. Holmukhe, “Infrastructural analysis of load dispatch centre” International Journal of Computer Applications 1(7):100-105, February 2010.
2. M. Ropp, J. Newmiller, C. Whitaker, and B. Norris, “Review of potential problems and utility concerns arising from high penetration levels of photovoltaics in distribution systems,” in Photovoltaic Specialists Conference, 2008. PVSC ’08. 33rd IEEE ed, 2008, pp. 1–6.
3. J. Zhao, Z. Liu, P. Li, K. Yuan, H. Huang, H. Huang, et al., “Analysis on the impacts of distribution systems with large-scale grid-connected photovoltaic based on DigSILENT,” in 2014 China International Conference Electricity Distribution (CICED) on, 2014, pp. 1215–1219.
4. X. Wang, J. Gao, W. Hu, Z. Shi, and B. Tang,“Research of effect on distribution network with penetration of photovoltaic system,” in 2010 (UPEC), 2010, pp. 1–4.
5. J. R. Aguro and S. J. Steffel, “Integration challenges of photovoltaic distributed generation on power distribution systems,” in Power and Energy Society General Meeting, 2011 IEEE, pp. 1–6.
6. H.-T. Yang, C.-M. Huang, Y.-C. Huang, and Y.-S. Pai, “A weather-based hybrid method for 1-day ahead hourly forecasting of PV power output,” IEEE Transactions on Sustainable Energy vol. 5, no. 3, pp. 917–926, Jul 2014.
7. Can Wan, Jian Zhao, Yonghua Song, Zhao Xu, Jin Lin, and Zechun Hu; "Photovoltaic and Solar Power Forecasting for Smart Grid Energy Management ", CSEE 2015, Vol. 1, no. 4, pp.1-7 December 2015.
8. H. Saima; J. Jaafar; S. Belabour; T. A. Jillan; “Intelligent methods for weather forecasting”, National Postgraduate Conference (NPC), Vol. 5, Issue 12, December 2016.
9. Ruby Nageema; Jayabarathi Rb” Predicting the Power Output of a Grid-Connected Solar Panel Using Multi-Input Support Vector Regression”, Procedia Computer Science, 2017
10. K.U. Jaseena, Binsu C. Kovoor. "Deterministic weather forecasting models based on intelligent predictors: A survey", Journal of King Saud University - Computer and Information Sciences, 2020
11. Smart, Edward, David Brown, and John Denman. "A Two-Phase Method of Detecting Abnormalities in Aircraft Flight Data and Ranking Their Impact on Individual Flights", IEEE Transactions on Intelligent Transportation Systems, 2012.
12. I S Jha, Subir Sen, ‘Smart Grid Development in India- A case study’ IIT Kharagpur National Power System Conference (NPSC) 2014

REMOVAL OF COPPER FROMWASTE WATER USINGTIDAL FLOW CONSTRUCTED WETLAND

R.P. Borkar[1], and P.S. Mahatme[2]
[1]Govt.College of Engineering, Amravati, India
[2]Department of Civil Engineering, PRMCEAM, Badnera, India
[2]parag.mahatme@rediffmail.com

ABSTRACT

Industrial waste water contains number of impurities but the heavy metal present in it is harmful for surface water, ground water and soil. Constructed Wetland considered as natural system with greater efficiency to treat industrial waste water. Tidal flow constructed wet lands as a type of 4th generation wet land systems for biological waste water treatment. This study reports the removal of copper from synthetic waste water using tidal flow constructed wet land. This study was carried out on laboratory scale tidal flow constructed wetlandsystem of dimension 35cm x 35cm x 120cm. A constructed wet land system, consisting of pair of cellsoperated in tidal flow for detention period of 7 days. The bed of cell arranged in layers with different media size, typhaspecies was used for vegetation. Copper removal was observed to be 89% in soillayer, 80% in course aggregate layer respectively for detention period of 7days.

Keywords: *Tidal Flow, Constructed Wetland, Waste water Treatment, Heavy Metal*

1. Introduction

Industrialization has become an important factor to the development of a country's economy, through the establishment of plants and factories. The waste or by-products discharged from them are severely disastrous to the environment consists of various kind of contaminants which contaminate the surface water, ground water and soil. The contaminant from the discharge is directly related to the nature of the industry. For example, in textile industry, the discharge is usually high chemical oxygen demand (COD), biochemical oxygen demand (BOD) and color. Paint, tannery industry is on the other hand, produces discharges which have high concentration of metal. There is a technology, which has been recognized and accepted as a creative, cost-effective and environmentally friendly system when compared to the expensive conventional treatment systems (Xi n xi Fu, *et al*.,2008). Wetlands are considered today as natural systems with great ecological significance which provide habitat for numerous species and support their life. It was gradually realized that natural wetlands had always been capable of providing water purification and improving water quality, at least up until the point where industrial contamination had become so intensive (Alexandros I. Stefanakis,2015).

2. Constructed Wetlands:

Constructed wetlands are engineered systems that have been designed and constructed toutilizethenaturalprocessesinvolvingwetlandvegetation,soils,and the associated microbial assemblages to assist in treating wastewaters. They are designed to take advantage of many of the same processes that occur in natural wetlands, but do so within a more controlled environment (Jan V ymazal *et al*., 2006).Constructed wetlands are artificial wastewater treatment systems consisting of shallow (usually less than 1 m deep) ponds or channels which have been planted with aquatic plants, and which rely upon natural microbial, biological, physical and chemical processes to treat waste water. They typically have impervious clay or synthetic liners, and engineered structures to control the flow direction, liquid detention time and water level. Depending on the type of system, they may or may not contain an inert porous media such as rock, gravel or sand (EPA, 2000). The constructed wetlands have evolved into a reliable wastewater treatment technology fo rvarious types of wastewater. The classification of constructed wetlands is based on: the vegetation type (emergent ,submerged, floating leaved, free-floating); hydrology (free water surface and subsurface flow); and subsurface flow wetlands can be further classified according to the flow direction (vertical or horizontal). In order to achieve better treatment performance, namely for nitrogen, various types of constructed wetlands could be combined into hybrid system as shown in fig.1.

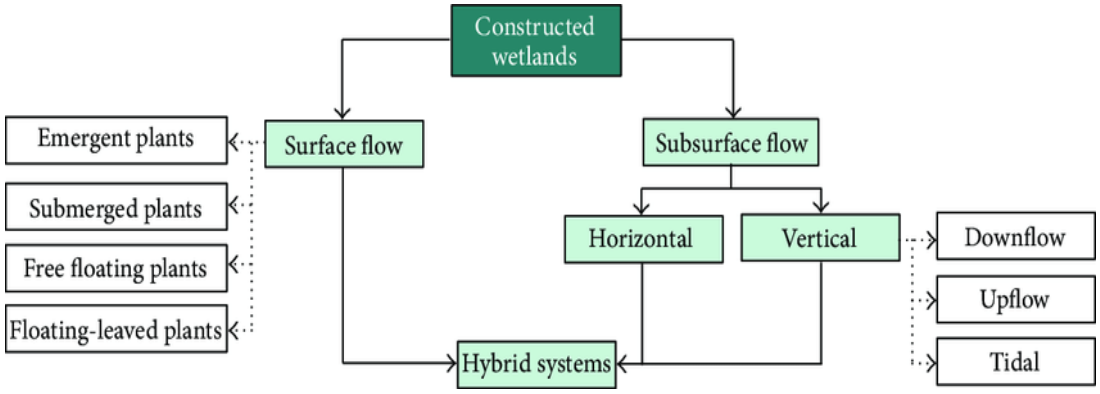

Fig.1Various Types of Constructed Wetlands (Qaisar Mahmood et.al;2013)

2.1 Tidal Flow Wetland

Ina Weinheimer (2015) explained tidal flow artificial wetlands (TFAW) as a type of 4th generation (or intensified) wetland systems as shown in fig. 2 for biological wastewater treatment that are designed to copy the processes of natural tidal wetlands. The Tidal Flow Wetland Living Machine in corporates as eries of wetland cells, or basins, filled with special gravel that promotes the development of micro-ecosystems. Tidal flow systems employ two or more flood and drain cycles per day within the wetland bed. These highly flexible cells may be integrated into exterior land scaping or built into a building or greenhouse. As water moves through the system, the cells are alternately flooded and drained to create multiple tidal cycles each day, much like natural wetlands, resulting in high quality reusable water. The micro-ecosystems within the cells efficiently remove nutrients and solids from the wastewater, resulting in high quality effluent. The final polishing stage, which involves filtration and disinfection, leaves water crystal clear and ready for reuse.

A TFAW operates by continually filling and draining the wetland cell with wastewater. This cycle of filling and draining introduces additional oxygen to the wetland cell. With this engineered CWvastly improved aeration and hence outstanding total nitrogen removal compared to traditional wetland systems is possible. Early research of tidal flow wetlands was done in the late 1990s and TFAWs were defined by having a fill and drain cycle of less than a day. A tidal flow wetland was created with different stages of wetland cells which were operated in series. The water that filled the first stage was drained to the next stage and so on.

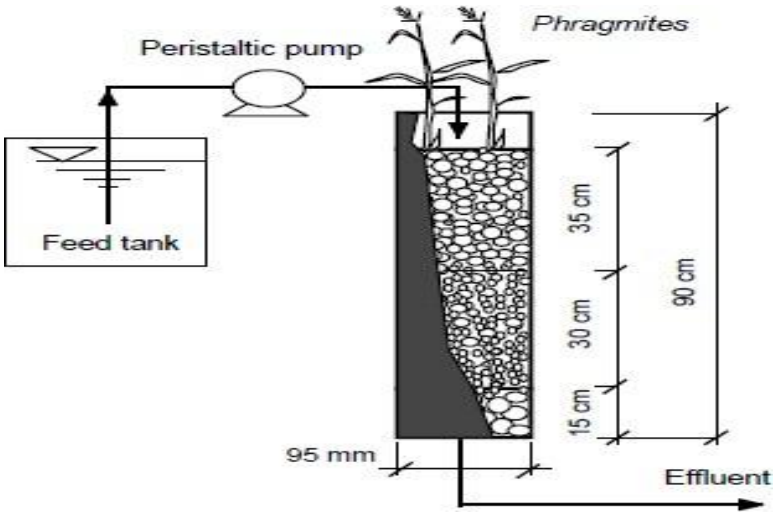

Fig.2 TidalFlowWetland

3. Methedology

3.1 Experimental Set-up

Tidal flow wetland system was fabricated; the constructed wetland units made up of acrylic having dimensions 35cm x 35cm x 120cm. The model was set up with overall capacity of 200 L. The system comprises of two wetland units having different layer of aggregates, coarse sand, fine sand and soil with *typha*. The inlet and outlet arrangements were provided at bottom of units at both ends, detail of the setup is shown in fig 3. The fill and drain cycle in bed for various detention periods were achieved by programming, electrically operated solenoid valve and moisture sensors. Each wetland cell is 1.2mindepth, different layer of filter media are provided within cell. Bottom layer consists of coarse gravel having depth of 7.5cm; above this layer fine aggregate is placed having depth 7.5 cm. After placing the fine aggregate the depth of 10cm of fine sand is provided. The top layer consists of soil up-to a depth of 70cm, *typha* is placed in unit which is collected from local stream.

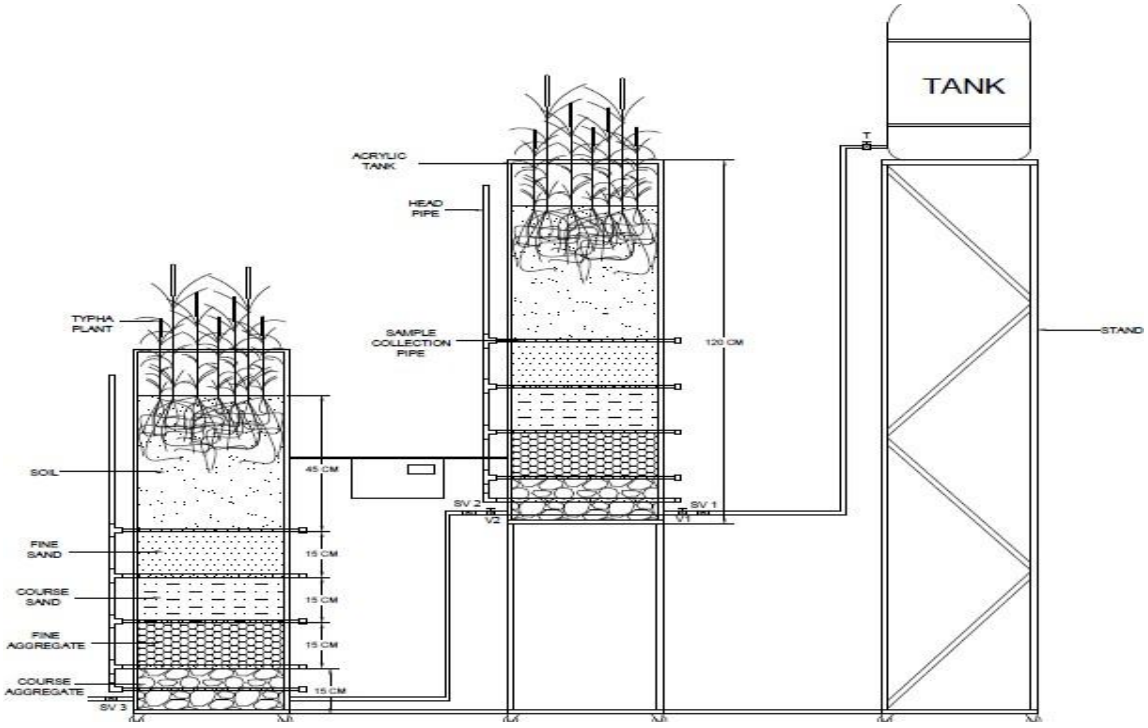

Fig. 3Laboratory Setup for Tidal Flow Wetland

3.2 Working of Model

Industrial wastewater sample was collected from the Nagpur (Butibori) MIDC based on the results of waste water characteristic, thesyn the tic waste water was prepared with known concentration of copper, to find the concentration of copper in treated wastewater calibration curve was prepared for the range of 1 mg/l to 10 mg/l as shown in fig 4. The prepared wastewater filled in storage tank. The flow is regulated by gravity and electrically operated solenoid valve. In step first the influent from storage tank is allow to pass through the wetland cell 1 with constant rate maintain by using regulating valve. As the level of waste water reaches to the root zone the moisture sensor detect the level. Then the inflow in cell 1 stop and the wastewater is detained for detention time required. After that the solenoid valve between the cells is open and the waste water from cell 1 is drain out to cell 2. Similarly water level is detected by moisture sensor, then the inflow in cell2 is stop and the waste water is detained for detention time required. After that the last solenoid valve is open and treated effluent is collected at the end of cell 2. Waste water was detained for the period of 7days in the wetland.

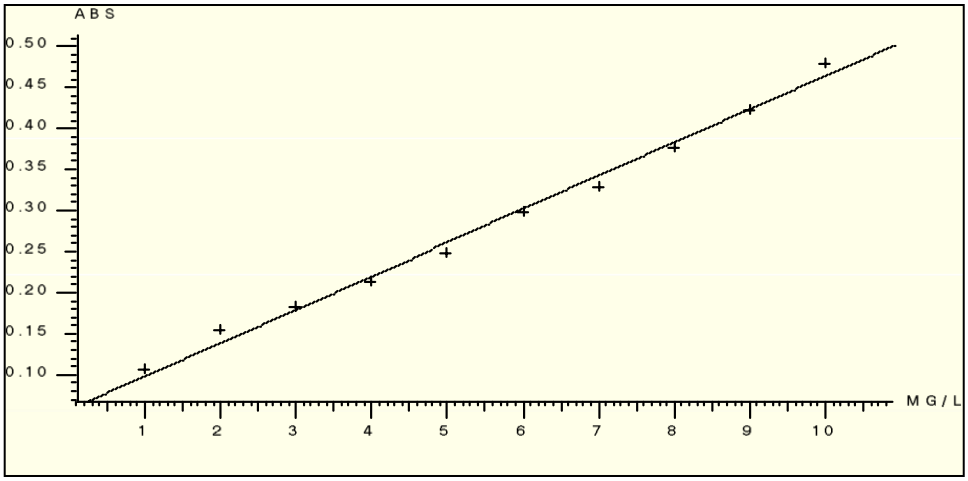

Fig. 4 Calibration Curve of Copper For1To10mg/l

4. Result and Discussion

The initial concentration of copper in synthetic wastewater was maintained to 10 mg/l which was detained for the period of 7 days in the wetland cells. Concentration of Copper was studied in each layer of the bed in each cell. Result of percentage removal for Copper for three different samples is expressed in table 1, 2, and 3.

Table1 Percentage removal of Copper inSample1for detention period of 7days

1st CELL			2nd CELL		
Layers	Conc. (mg/l)	%Removal	Layers	Conc. (mg/l)	%Removal
Soil	1.581	84.19%	Soil	1.072	89.28%
FineSand	1.611	83.89%	FineSand	1.611	86.39%
CourseSand	2.044	79.56%	CourseSand	1.638	83.63%
FineAggregate	2.086	79.14%	FineAggregate	1.762	82.38%
CourseAggregate	2.408	75.92%	CourseAggregate	2.156	78.44%

Table2 Percentage removal of Copper in Sample 2 for detention period of 7 days

1st CELL			2nd CELL		
Layers	Conc. (mg/l)	%Removal	Layers	Conc. (mg/l)	%Removal
Soil	1.298	87.02	Soil	1.113	88.87
FineSand	1.315	86.85	FineSand	1.195	88.05
CourseSand	1.608	83.92	CourseSand	1.443	85.57
FineAggregate	1.711	82.89	FineAggregate	1.505	84.95
CourseAggregate	2.001	79.99	CourseAggregate	1.876	81.24

Table3 Percentage removal of Copper in Sample 3 for detention period of 7days

1st CELL			2nd CELL		
Layers	Conc. (mg/l)	%Removal	Layers	Conc. (mg/l)	%Removal
Soil	1.381	86.19	Soil	1.092	89.08
FineSand	1.463	85.37	FineSand	1.195	88.05
CourseSand	1.773	82.27	CourseSand	1.422	85.78
FineAggregate	1.855	81.45	FineAggregate	1.463	85.37
CourseAggregate	2.003	79.97	CourseAggregate	1.835	81.56

The characteristic of the wastewater in the inlet and the characteristic of treated wastewater at The outlet were studied for the detention period 7 day for cell 1 during study, it was found that thepercentage removal of copper in soil layer was in the range of 87%, percentage removal of copper in fine sand layer was in the range of 86%. Fine Aggregate layer was in the range of 82% and shows the percentage removal of copper in coarse Aggregate layer was in the range of 79%. Figure5showsthe% removal of copper in different layers for cell 1.

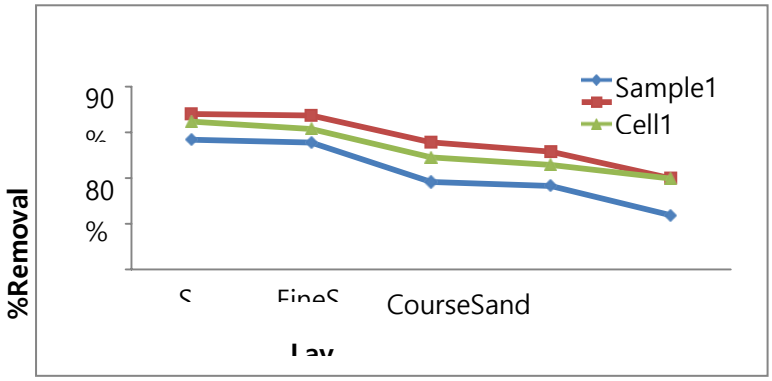

Fig.5 % Removal of Copper in different layers for cell 1

For cell 2 during study, it was found that the percentage removal of copper in soil layer was in the range of 89%, percentage removal of copper in fine sand layer was in the range of 88%. Fine Aggregate layer was in the range of 85% and shows the percentage removal of copper in coarse Aggregate layer was in the range of 81%. Figure 6 shows the % removal of copper in different layers for cell 2. Removal of Copper in waste water wetlands occur by *typha* up take, soil ads orption, and precipitation. The copper that pass by the root structure tend to accumulate on the structure of the root rather than being absorbed by the *typha*. Generally, the reduction of metal levels in wastewater can be attributed to the chemical, physical and biological processes occurring in the wetland that include, sedimentation, precipitation, adsorption, assimilation by plants and microbial activity (A. M. Khanetal 2015). The ability of plants to uptake metals depends on the type of plant and type of metal.

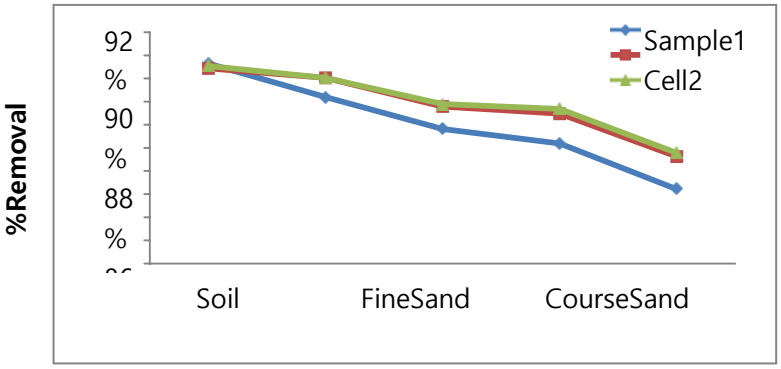

Fig.6 % Removal of Copper indifferent layers for cell 2

5. Conclusions

The results of this study have shown that the tidal flow constructed wetlands are suitable alternatives for removal of copper in wastewater. The maximum percentage removal efficiency for copper was found to be in the range of 89% in soil layer and minimum percentage removal efficiency was found to be in the range of 80% in course aggregate layer. Metals like copper that are required for plant and animal growth but these are in small amounts. John Mellem in his study found that removal of copper is mainly take place in root of plant. Removal of metals in waste water wetlands occur by plant uptake, soil adsorption, and precipitation. There are some types of plants which are capable of storing large amounts of metals in plant biomass and in its roots.

References

1. Alexandros I. Stefanakis (2015), "Constructed Wetlands: description and benefits of an eco-techwatertreatmentsystem", Researchgate,281-303,DOI:10.4018/978-1-4666-9559-7.ch012.
2. Ashutosh Kumar Choudhary, Satish Kumar and Chhaya Sharma, "Constructed wetlands: an approach for waste water treatment" ElixirPollution,**37**,2011,3666-3672.
3. Aysha Masood Khan, Chaudhary Sajjad Ahmad, Umer Farooq, Karamat Mahmood, MalihaSarfraz,KhaledS.Balkhair&MuhammadAqeelAshraf(2015)Removalofmetallicelementsfromindustrial waste water through biomass and clay, Frontiers in Life Science,8:3, 223-230, DOI:10.1080/21553769.2015.1041187
4. EPA(2000),"ConstructedWetlandsTreatmentofMunicipalWastewaters"
5. GSung,Y.Q. Zhao,S.J.Allen(2007),"AnAlternative ArrangementofGravelMediainTidalFlowReed BedsTreatingPig FarmWastewater",WaterAir and SoilPollution,**182**,13-19
6. Jan Vymazal, Margaret Greenway, Karin Tonderski, Hans Brix, ÜloMander (2006), "ConstructedWetlandsfor WastewaterTreatment",EcologicalStudies,**190**, 69-96.
7. John Mellem, "Phytoremediation Of Heavy Metals Using Amaranthusdubius" the Department of Biotechnology and Food Technology, Durban University of Technology, Durban, SouthAfrica
8. MsInaWeinheimer(2015),"WastewaterTreatmentusingTidalFlowWetlands",B.E.CivilDissertation, UniversityofSouthernQueensland.
9. Norton,StephenJohn."RemovalMechanisms inConstructedWastewaterWetlands."(2007).
10. QaisarMahmood,ArshidPervez,BibiSaimaZeb,HabibaZaffar,HajraYaqoob,Muhammad Waseem,Zahidullah,SumeraAfsheen,(2013),"NaturalTreatmentSystemsasSustainable Eco technologies for the Developing Countries", BioMed Research International, **2013**,1-19.
11. XinxiFu,XiaofuWu,SangyangZhou,YonghuaChen,MingliChenandRunhuaChen(2018)," AConstructed Wetland System for Rural Household Sewage Treatment in Subtropical Regions", Central South University of Forestry and Technology,10(716),1-12 doi:10.3390/w10060716

TRANSMISSION LINE FAULT DETECTION USING SYNCHROPHASOR

N.V. Khadse[1] and R.R. Shaha[2]
Tulsiramji Gaikwad College of Engg and Technology, Nagpur, India
[1]nehakhadse7@gmail.com, [2]radharaman2004@gmail.com

ABSTRACT

This papers gives the details about the synchrophasor technology which uses the GPS based time synchronization having the accuracy of the order of 1µs. Here we have explored the flexibility of the synchrophasor technology based current differential protection in Matlab simulink and presented the results for all types of faults with different fault resistance, inception angle, and fault location, and it is observed the current differential protection using synchrophasor technology has almost the 100% reliability.

Keywords: *Syncrophasors, WAP, GPS, Phase Measurement unit, Current Compensation*

1. Introduction

The power demand and generation has increased drastically in our country.Presently in India almost all regional grids are interconnected with the national grid, which makes the system more complex as far as the protection is concern. For getting good quality of supply from such a complex grid the major factor is that the reliability of the system should be very high, which is very challenging job for the engineers. So, there is a need of protection system which will have all the essential qualities such as high reliability, selectivity, sensitivity, stability etc. Following are the basic protection schemes which are generally used in electrical power system, each one has its advantages and disadvantages.

1.1 Differential Protection Scheme
1.2 Distance Protection Scheme

1.1 Differential Protection Scheme

Differential protection is generally a unit protection. Its main application is to give protection to generator, generator-transformer unit, large induction motor etc. Sometimes Differential protection is used for feeder.

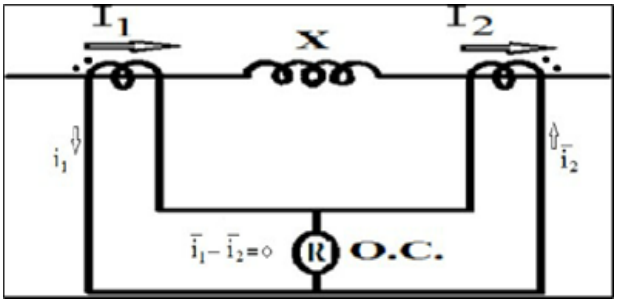

Figure 1. Basic principle of Current Differential Protection (Merz Price Protection)

1.1.1 Principle of Basic Current Differential Protection

Fig. 1.1 illustrates the basic principle of current differential protection. X is the winding of the protected machine. When there is no internal fault, current entering into X is equal in phase and magnitude to current leaving [8].

CT's are of such ratio that during the normal condition or external (through) faults the secondary currents of CT's are equal. These currents ($\bar{\imath}$ 1 & $\bar{\imath}$ 2) circulate in pilot wires. The polarity connections of CT's are such that both secondary current are in same direction in pilot wires during normal and through faults. Relay operating coil is connected between the middle of pilot wires. Relay used here is of over current type. During normal and through fault condition current through over current relay operating coil is zero ($\bar{\imath}$ 1-$\bar{\imath}$ 2=0).

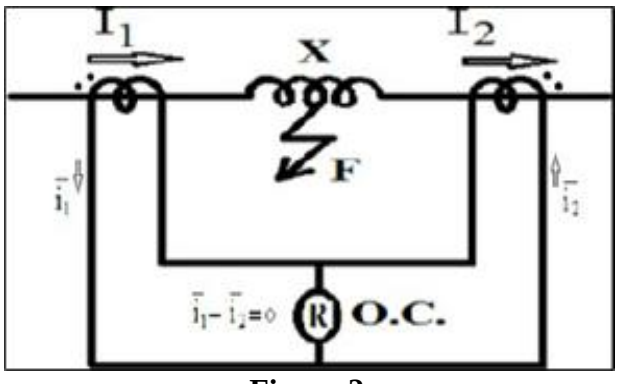

Figure 2

This balance gets disturbed for internal faults, when fault occurs in the protected zone. The current entering in the protected winding is no more equal to the current leaving the winding because some current flows to the fault. The

difference of currents ($\bar{I}_1 - \bar{I}_2$) flows through the operating coil of the relay and the relay operates when the operating torque is more than the restraining torque.

1.1.2 Advantages

- High selectivity for all types of fault.
- Operation at high speed with high sensitivity.

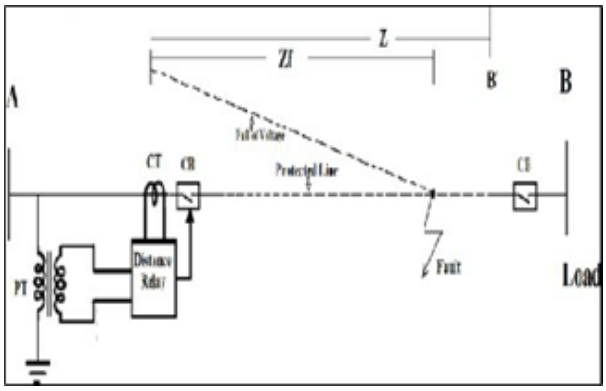

Figure 3

Mal-Operations

- In case of ground faults the arc resistance is measured along with the line impedance. This leads to mal- operation known as "under-reach". Due to under-reach the faults at the far end of zones of protection remain undetected.
- Due to dc offset during fault, the current value can jump to a larger value and hence the impedance seen will be such that the relaying scheme will give trip command leading to "over-reach" mal- operation. Due to this mal- operation even if fault occurs outside zone of protection, for instance in the adjoining transmission line then also this relaying scheme acts as if fault is in its zone of protection and trips.
- During power swings in case of double end feed transmission lines the impedance seen by the relay enters in tripping region of relay. Thus leading to mis-operation.
- Also, the present schemes provide relatively low accuracy in fault location. For example if there is an error of 5% in the estimate of fault location, in a 400 km line means a potential error of 20 km. This 20km region will have to be visually inspected to find the location of fault for repair or maintenance purposes.
- Distance protection is the most commonly used protection scheme for transmission line, but as we have seen above that it is being always affected with under-reach, over-reach, power swings etc.

2. Synchrophasor Technology

1.1 Synchrophasors

The advents of satellite-based time-keeping systems and advances in computer technology have made possible protective relay sampling synchronization within1µs. These relays can now provide synchronized phasor measurements that eliminate the need to have different devices for protection, control, and electric power system analysis for system-wide applications and traditional protection applications.

In this technology, we have suggested a protection scheme which uses the concept of current differential protection using synchrophasors. Current phasors at both ends of a transmission line are measured by Phasor Measurement Units (PMU) and are sent to a central location using communication link and are synchronously compared to determine the state of the system at that particular instal.

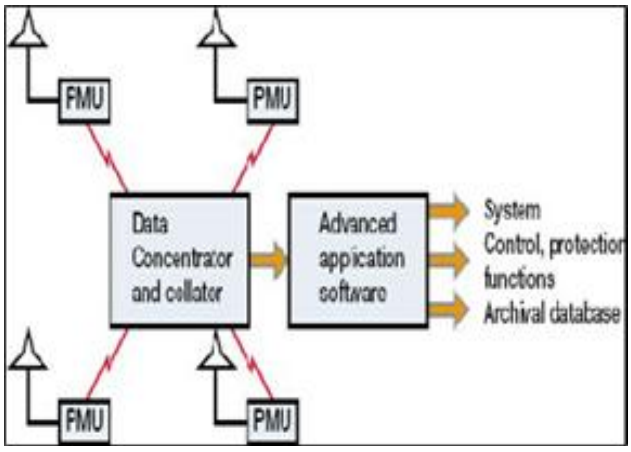

Figure 4

Benefits Of Pmus

- It provides precise measurement of the power system state. It can be obtained at frequent intervals, enabling dynamic phenomena to be observed from a central location, and appropriate control actions can be taken.
- Post-disturbance analysis is much improved because precise snapshots of the

system states are obtained through GPS synchronization.

- Advanced protection based upon synchronized phasor measurements is possible.

2. Synchrophasors Applications

2.1 Synchrophasors Applications

2.1.1 Applications Overview

Phasor data applications can be grouped into three categories:

- Applications to support real-time grid operations by providing wide-area visualization and increased state awareness,
- Applications to improve system planning and analysis, including power system

Performance base lining, event analysis and model validation, and Response-based control applications that use real-time wide area information to take automated control actions on the power system.

2.1.2 Phasor data use for real-time operator use for real-time operations

All real-time operations, uses of phasor data exploit the insight these data offer due to high sampling speed, new granularity into phase angles and other grid conditions, and time synchronization. These measurement characteristics also enable exceptional visualization, analytics and alarming all of which improve operators ability to see and understand what is happening on the bulk power system, anticipate or identify potential problems, and identify, evaluate, implement and assess remedial measures.

2.1.3 Wide-area situational awareness

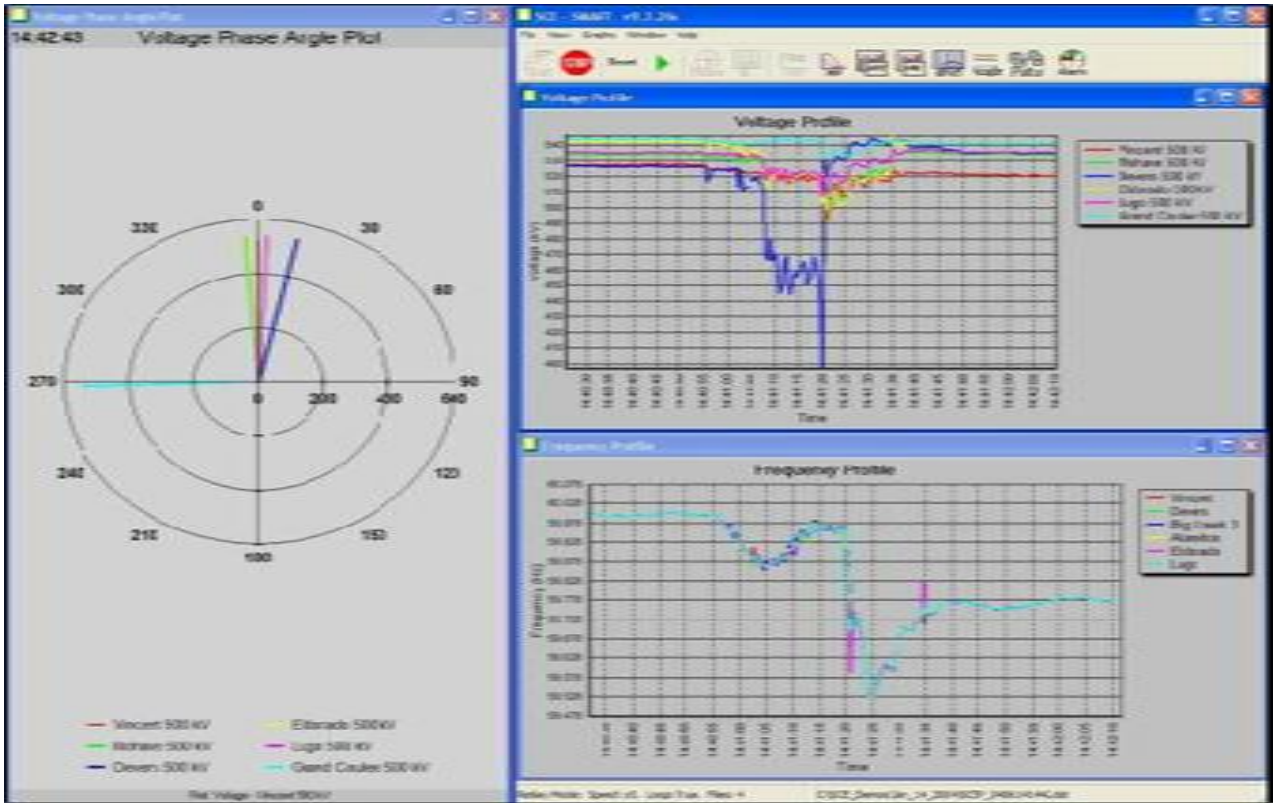

Figure 5

RTDMS software, developed initially with funding from the U.S. Department of Energy, is a phasor data-based software platform used by grid operators, reliability coordinators, and planning and operations engineers for real-time wide-area visualization, monitoring and analysis of the power system. RTDMS offers a real-time dashboard generation loss. System frequency is also a good indicator of integrity of an interconnection during system events involving separation or islanding if a bus frequency in one part of the system stays at 60.5 Hz while frequency in another part of the

system holds at 59.5 Hz for several minutes, it is a sure indication of the system separation.

2.1.4 Frequency stability monitoring and trending

System frequency is the key indicator of the load-resource balance. The size of the frequency deviation is well generation loss. System frequency is also a good indicator of integrity of an interconnection during system events involving separation or islanding if a bus frequency in one part of the system stays at 60.5Hz while frequency in another part of the system holds at 59.5 Hz for several minutes, it is a sure indication of the system separation.

2.1.5 Power oscillations

Detection of power system oscillations and ambient grid damping are among the premier applications that require the high-speed data that PMUs provide and conventional SCADA does not. Low-frequency oscillations occur when an individual or group of generators swing against other generators operating synchronously on the same system, caused by power transfers and high-speed, automatic turbine controls attempting to maintain an exact frequency.

3. Differential Protection Scheme Using Synchrophasor Technology

3.1 Introduction

Differential protection for transmission line is given. There were some limitations like, difference in pilot wire length, CT saturation, inrush current etc. How to overcome these limitations also discussed. The main problem in differential protection is the transmission line length which forced it to be almost impossible for long transmission line protection. But this major drawback can be overcome by using the synchrophasors.

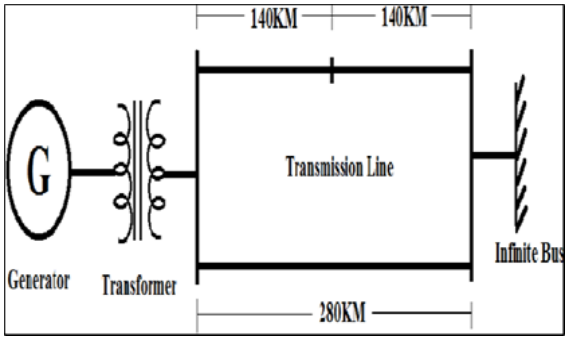

Figure 6: Simulated System Single Line

t	Pmax	sinδ	Pe= Pmaxsinδ	Pa= Pm-pe	Δt*Ta/ (M)= 5.11Pa	Δσ	δ
0-	1.55	0.52	0.602	0.0	--------	--------	31.44
0+	0.46	0.52	0.2392	0.3608	--------	--------	31.44
0avg		0.52		0.1809	0.92	0.92	31.44
0.05	0.46	0.535	0.246	0.35	1.78	2.7	32.36
0.1	0.46	0.57	0.264	0.33	1.71	4.415	35.06
0.15	0.46	0.63	0.2924	0.307	1.57	5.98	39.47
0.2	0.46	0.712	0.327	0.27	1.39	7.35	45.45
0.25	0.46	0.79	0.366	0.23	1.19	8.54	52.8
0.3	0.46	0.877	0.403	0.196	1	9.51	61.34
			Tcr<.3s				70.88

Diagram Specifications

Generator- 600 MVA, 22 KV, 60 Hz, H= 4.4 MW-S/MVA, Xd= 1.81pu, Xd'= 0.3pu, Xd"= 0.23pu, Tdo'=8s, Tdo"=0.03s, Xq= 1.76pu, Xq"= 0.25pu, Tqo"=0.03pu

- Vbc: 22000 Vrms [1 pu] -86.23°
- Vca: 22000 Vrms [1 pu] 153.77°
- Ia: 14260 Arms [0.9056 pu] -2.61°
- Ib: 14260 Arms [0.9056 pu] -122.61°
- Ic: 14260 Arms [0.9056 pu] 117.39°
- P: 5.4e+008 W [0.9 pu]
- Q: 6.0389e+007 Vars [0.1006 pu]
- Pmec: 5.4148e+008 W [0.9025 pu]
- Torque: 1.4363e+006 N.m [0.9025pu]
- Vf: 2.014 pu

The hand calculations for calculating the critical clearing time using step by step method are as follows

- Pm= 0.6 pu , (presumed)
- Pmax1= 1.155 pu ,
- Pmax2= 0.46 pu ,
- Pmax3= 0.77 pu ,
- H= 4.4MW-S/MVA (given),
- Δt Critical clearing time (Tcr) ≤ 0.3sec= 0.05 sec, δo=31.44, δmax=128.82, δcr=62.21

4. Differential Protection With Charging Current Compensation

Now to check whether the simulation we have done is correct or not we have created a fault of line to ground type on phase 'a' at 0.2second and cleared at 0.3second on lower line as shown above, the power swings observed on upper parallel line at sending end. The voltage and current waveforms are observed on scope 'VaIa', as shown in fig.

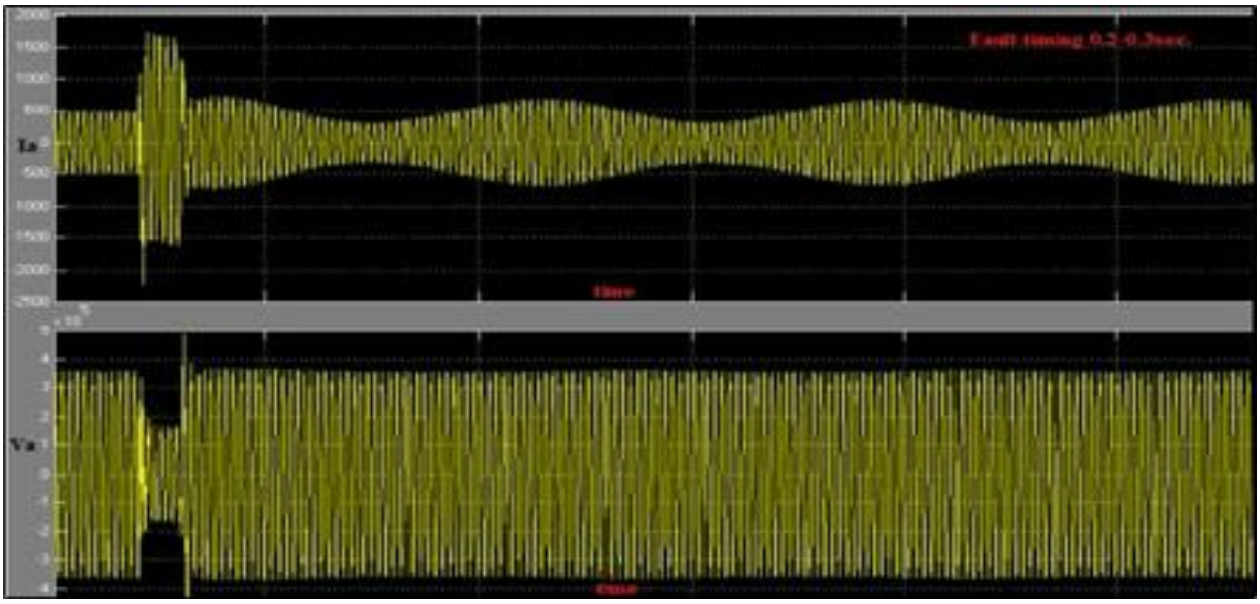

Figure 7: Power swings observed

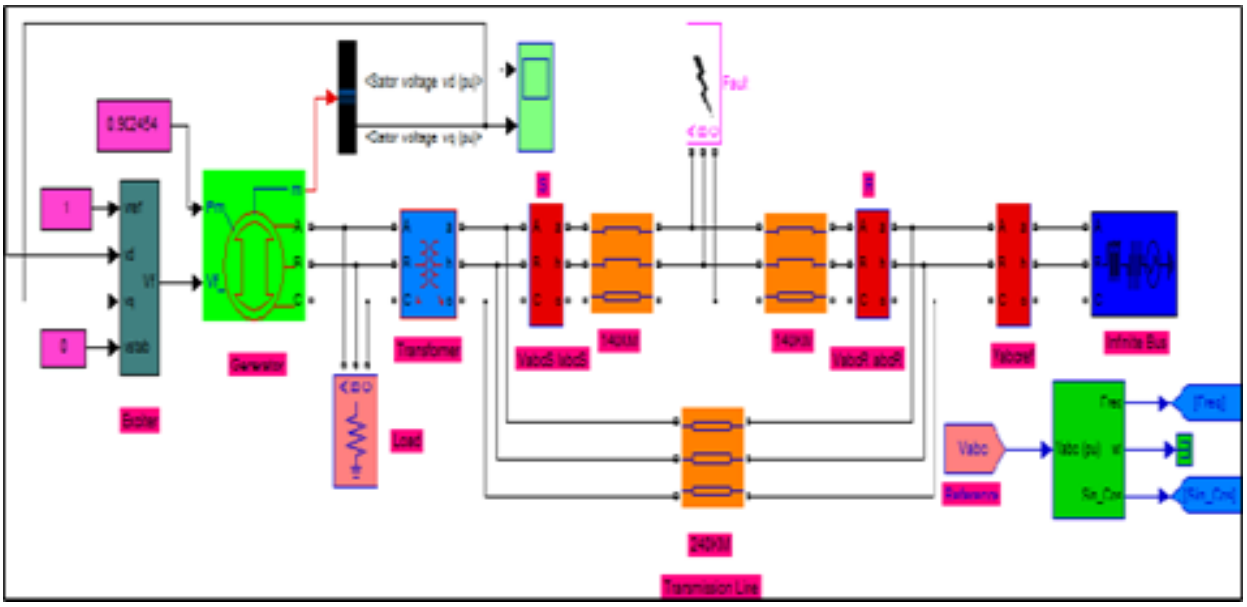

Figure 8: Current differential protection scheme to upper parallel line

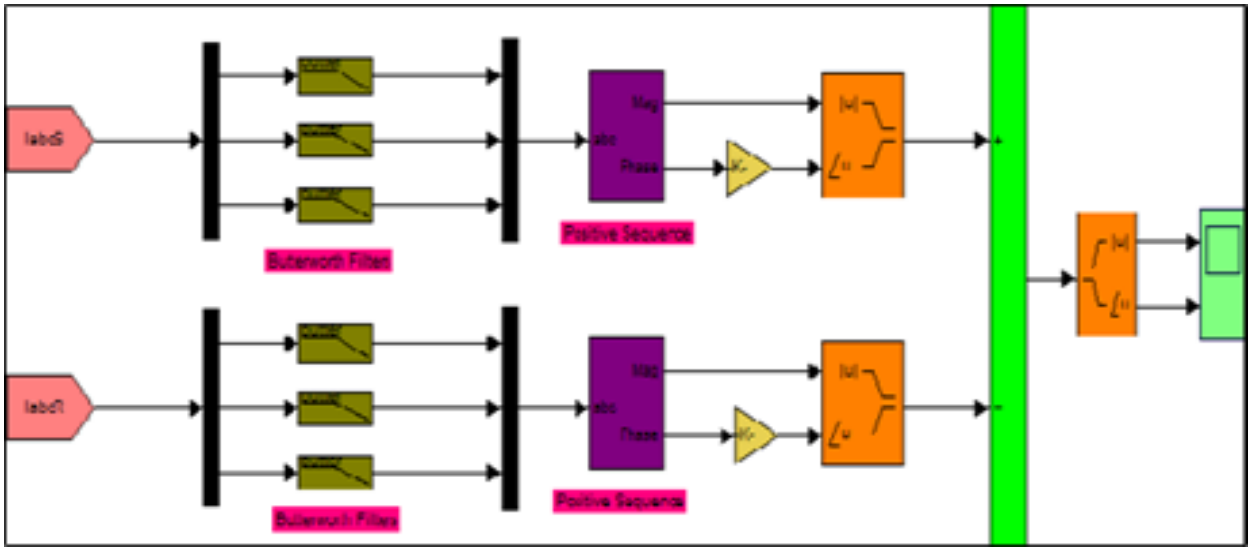

Figure 9: Simulation for difference of sending end and receiving end current phasors

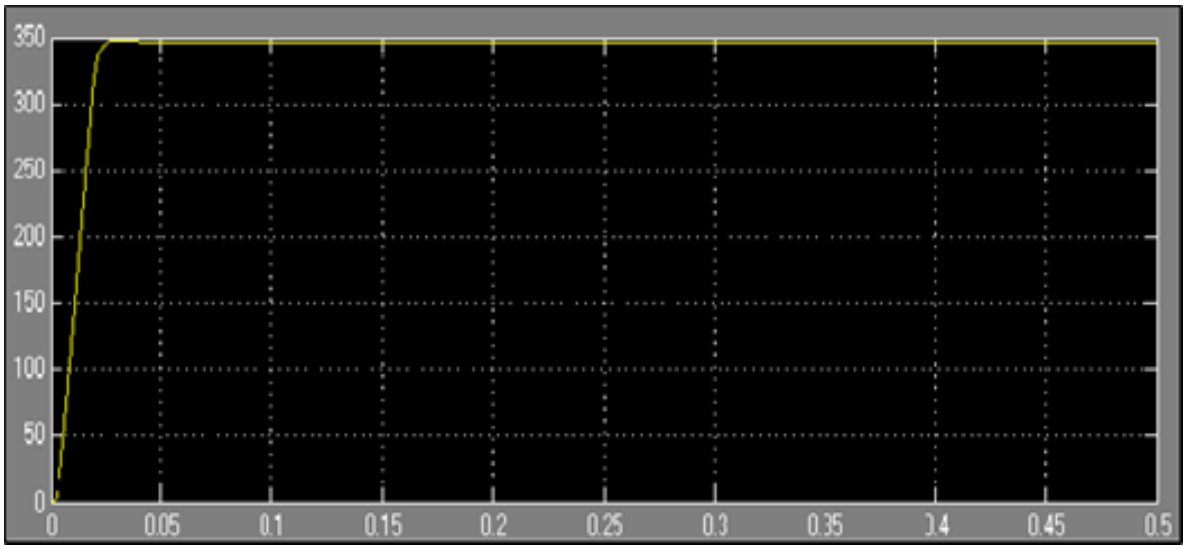

Figure 10: Difference of sending and receiving end current phasors without any fault

The above result shows that there is a difference of about 350A current even though there is no fault condition; this is the major challenge for relay setting. This happens because of charging current which flows because of capacitance between transmission line and earth. It increases as transmission line length increases. With the presence of this charging current we can set the relay at higher values but it affects the sensitivity and selectivity of the protection system. So, to overcome this problem we need to compensate this charging current. One of the charging current compensation methods is explained.

5. Conclusion

The results of the synchrophasors based current differential protection scheme shows that, whatever may be the type of fault, inception angle, fault resistance and fault location, the fault is being detected. Means this synchrophasors based current differential protection scheme gives almost 100% reliability, which would have not got in case of Distance protection scheme. Also, because of Global Positioning System (GPS) there is no limit on transmission line length which is to be protected. This feature of this technique makes it the better replacement for present Distance Protection system.

References

1. Sukumar M. Brahma, Member, IEEE,"Distance Relay with Out- of-Step Blocking Function Using Wavelet Transform" IEEE Transactions on Power Delivery, Vol. 22, No. 3, July 2007
2. Z. Yining S. Jiale, "Phaselet-based current differential protection scheme based on transient Capacitive current compensation" IET Generation, Transmission, Distribution, 2008, Vol. 2, No. 4, pp. 469–477/469 doi: 10.1049/iet-gtd: 2007.0494.
3. G. Preston Z.M. Radojevic C.H. Kim V. Terzija, "New settings- free fault location algorithm based on synchronized sampling" IET Generation, Transmission, Distribution, 2011, Vol. 5, Iss. 3, pp. 376–383 377 doi: 10.1049/iet-gtd.2010.0053
4. A. Mechraoui and D. W. P. Thomas, "A new blocking principle with phase and earth fault detection during fast power swings for distance protection," IEEE Trans. Power Del., vol. 10, no. 3, pp. 1242–1248, Jul. 1995.
5. Yuan R., Chen D., Yin X., Zhang Z., Ma T., Chen W.: 'Principle and property investigation of the transient current differential protection based on correlation analysis'. Presented at the IEEE Int. Conf. Power Engineering Society Winter Meeting, 2000, pp. 1945– 1949
6. Ito H., Shuto I., Ayakawa H., Beaumont P., Okuno K.: 'Development of an improved multifunction high speed operating current differential relay for transmission line

protection'. Presented at the 7th IEE Int. Conf. Developments in Power System Protection, April 2001, pp. 511–514

7. Jiale S., Xiaoning K., Guobing S., Zaibin J., Baoji Y.: 'Survey on relay protection using parameter identification', Proc. CSUEPSA, 2007, 19, (1), pp. 14–20
8. Takagi, K., Yomakoshi, Y., Yamaura, M., Kondow, R., Matsushima, T.: "Development of a new type fault locator using the one terminal voltage and current data", IEEE Trans. Power Appar. Syst., 1982, PAS-101, pp. 2892–2898
9. Djuric´, M., Terzija, V.: "A new approach to the arcing faults detection for fast autoreclosure in transmission systems", IEEE Trans. Power Deliv., 1995, 10, (4), pp. 1793–1798
10. IEEE Std C37.114-2004: "IEEE Guide for Determining Fault Location on AC Transmission and Distribution Lines". 2005, pp. 0– 36, doi: 10.1109/IEEESTD.2005.96207
11. Tawfik, M., Morcos, M.: "ANN-based techniques for estimating fault location on transmission lines using Prony method", IEEE Trans. Power Deliv., 2001, 16, pp. 219–224

MARATHI SPEECH RECOGNITION SYSTEM

G. Dhopavkar[1], N. Ingole[2], N. Chaware[3] and P. Damodhare[4]
[1,2,3,4]Department of Computer Technology YCCE, Nagpur, India;
[1]gauri.ycce@gmail.com, [2]nilkhant99@gmail.com,[3]niharchaware@gmail.com,
[4]priyanshu.s.damodhare@gmail.com

ABSTRACT

This paper reflects on the work underway on speech-to-text transcription in the Marathi language using ASR. ASR (known as Automatic speech recognition) is a method to convert any verbal utterances into their equivalent textual representation. It can be achieved with the help of statistical models and the most commonly used is Hidden Markov Models (HMMs). Hidden Markov Model is a statistically operating Markov model which will have a different output distribution for each distinct word or phoneme in a given language. HMM provides a simple and effective framework for ASR. Marathi vowels and consonants and their combinations are used as training data. Mel Frequency Cepstral Coefficients (MFCCs) are generated for each vowel and consonant utterances which are then fed to HMM as feature vectors. Thus the trained model will be a phoneme-based system. The feature vectors obtained from the training dataset will act as a reference for testing feature vectors for unknown speech.

Keywords: *Hidden Markov Model (HMM), Mel Frequency Cepstral Coefficients (MFCC), Fast Fourier Transform (FFT)*

1. Introduction

We humans primarily communicate by speaking and it is an effective way of communicating with and conveying information to others. Human speech has many distinct features, which can be used to extract information from speech, such as recognition of speakers, languages, and etc.

Human speech ranges to a certain frequency which is in between 0 - 5 KHz. To extract certain features from speech we use Automatic Speech Recognizer(ASR).

The spoken words contained in speech have certain components such as phonemes which act as a marker for identification of the words. In ASR, mathematical models are used for this task , most commonly used is the Hidden Markov Model(HMM). When ASR evaluates words with a mathematical model, the word is evaluated and most likely match is determined.

Marathi is the most commonly uttered language in Maharashtra state. There are five different regional varieties of Marathi Language. Marathi language generally consists of 13 vowels (अ आ…) and 36 consonants (क ख...). These vowels and consonants are used in isolation or as a set of combinations (का कि...).

The section 3 covers the general overview of the model's architecture and its workflow. In section 4, the training dataset is explained along with the feature extraction in form MFCCs and the testing part. Section 5 concludes about the proposed system and its future scope.

2. Literature Survey

In the paper by Manish K., Sharma, Avaaz Gajurel, Anup Pokhrel, Basanta Joshi [2], described HMM-based isolated Nepali word recognition system in their paper. The system does not depend on the person speaking, that is this system is independent of the speaker. Continuous speech recognition of language can also be done with the extension of HMM structures. Using Delta coefficients and Double Delta coefficients for extraction of features the system can provide more accurate results.

In the paper by Narendra D. Londhe, Ghanahshyam B. Kshirsagar,[3] used an ASR (Automated Speech Recognition) for Chhattisgarhi. The implementation is done by using ANN, SVM, and certain MFCC features. The recognition and mapping of every utterance uttered by people to the corresponding character is done by extracting speech characteristics by using Mel frequency cepstral coefficient (MFCC) method.

In the paper by Geetha K, Chandra,[4] presented in their paper the development of Tamil words or isolated Tamil words. It uses MFCCs from the frequencies of the input sample as speech vectors for training. The

system was based on a monosyllable concept using continuous density HMM for the Tamil words. It uses MFCC feature sets, states and Gaussian mixtures for testing of HMMs.

In the paper by Sarfaraz Masood, Danish Raza Rizvi, Madhav Mehta, Namrata[5], it used features like MFCCs, length of the word, etc. to implement isolated word recognizers. Various experiments were performed on the existing as well as their proposed system on MFCC based isolated word recognition. Also by adding some additional acoustic feature functionality and the performance of the system is greatly enhanced.

In the paper by Hemakumar G., Punitha P.,[6], presented a system that is speaker-dependent for Kannada speech recognition. HMMs are used for the implementation of the system. The preprocessing of the original Kannada speech signal is done which is followed by framing the signal. Then the audio frames are detected through calculating the dynamic threshold with the methods of short time energy and magnitude of signal.

3. System Overview

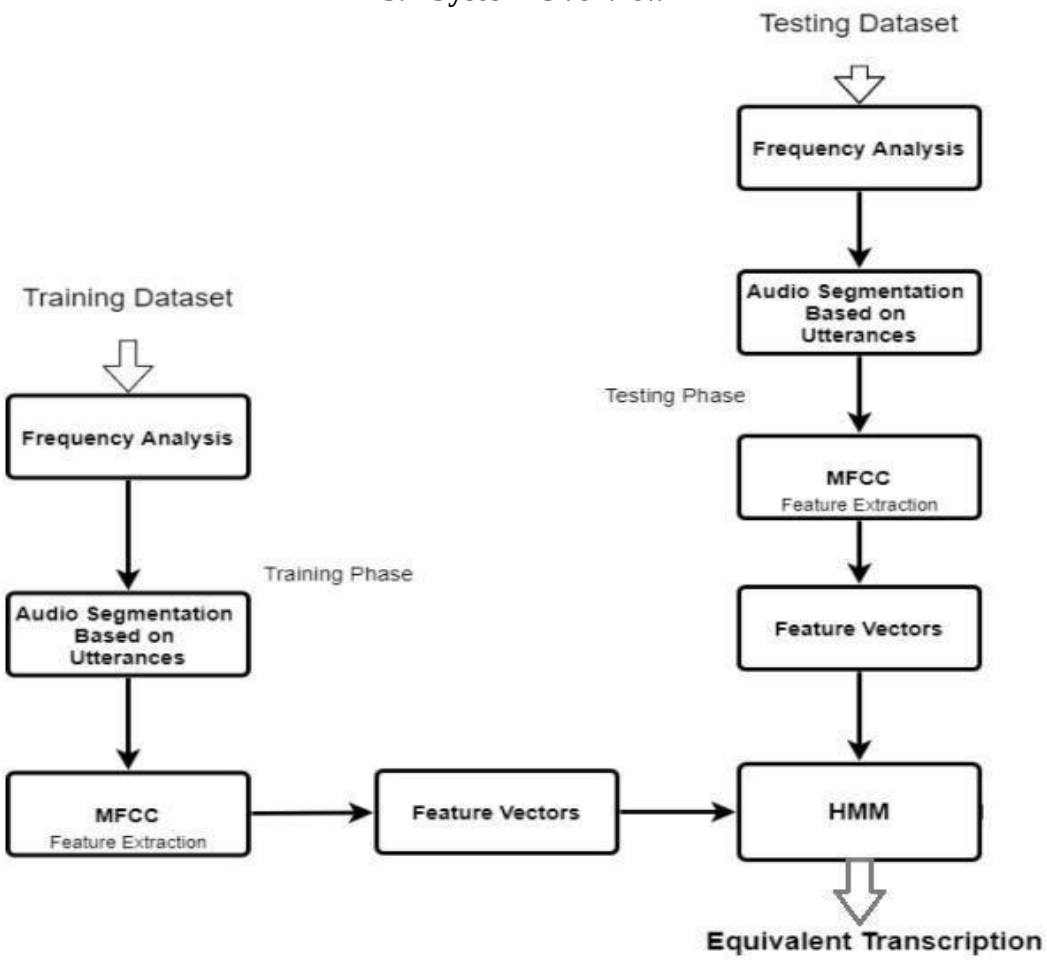

Fig. -1: Block Diagram of Transcription System

The system comprises two phases, training and testing phase. The training phase consists of audio segmentation, followed by feature extraction and selection using MFCC, generating feature vectors for each vowel and consonant and then these feature vectors are used to train the model. In the testing phase, the input sample speech data to be tested is segmented, feature vectors are generated using MFCC and fed to the trained HMM model for recognition.

In recognition, the feature vectors generated for testing are compared with the feature vectors generated in the training phase. The most probable phonemes are then given as a recognized phoneme. The identified phonemes are then remapped with the equivalent language characters.

4. MFCC Feature Extraction Method

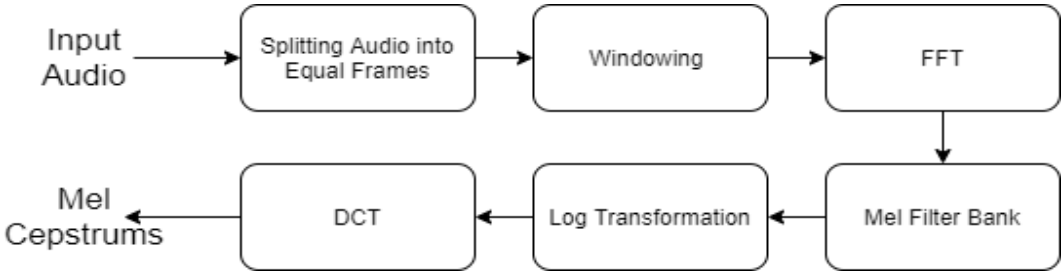

Fig. -2 : Architecture of MFCC Feature Extraction

MFCC Feature Extraction Process:

4.1 Framing

Framing Technique refers to dividing the speech signal into equal frames of short time intervals. Frame overlapping is done with the previous frame by a defined size which smoothens the frame to frame transition.

4.2 Windowing

The frames are windowed so as to eliminate the discontinuities at the ends of the frames. Hamming window is mostly used during speech recognition.

4.3 Fast Fourier Transform

Fast Fourier Transform is performed on each frame obtained. It transforms the speech signal of the time domain to the frequency domain.

4.5 Mel Filter Bank

Generally the frequency is measured in linear scale but human ears perceive the sound non linearly. The mel scale transforms the frequency so that it can be perceived by the human ear. The frequency above 1kHz is logarithmic spaced while frequency below 1kHz is spaced linearly by the mel frequency scale.

$$Mel(f) = 2595*\log_{10}(1 + f/700)$$

4.6 Discrete Cosine Transform

Discrete Cosine Transform is used to revert back the frequency domain mel coefficients to its equivalent time domain. The resulting will be Mel Frequency Cepstral Coefficients. Normally 26-40 Cepstral Coefficients are used.

5. Hidden Markov Model

Hidden Markov model is defined by-

$Y = \{y_1, y_2 \quad ,..., y_M\}$ – This symbol represents output observation. MFCC will be considered as this in speech recognition.

$X = \{1, 2, 3,...., N\}$ – This symbol represents the state space.

s_t is denoted as the state at time t. Phoneme labels will be considered as this, the set of characters will be the text.

$T = \{t_{ij}\}$ – This symbol represents the transition probability matrix, where

t_{ij} is the Probability of taking a transition from state i to state j.

$E = \{e_i\ (k)\}$ –This symbol represents output probability distribution, where $e_i\ (k)$ is the probability of emitting symbol y_k when in state i.

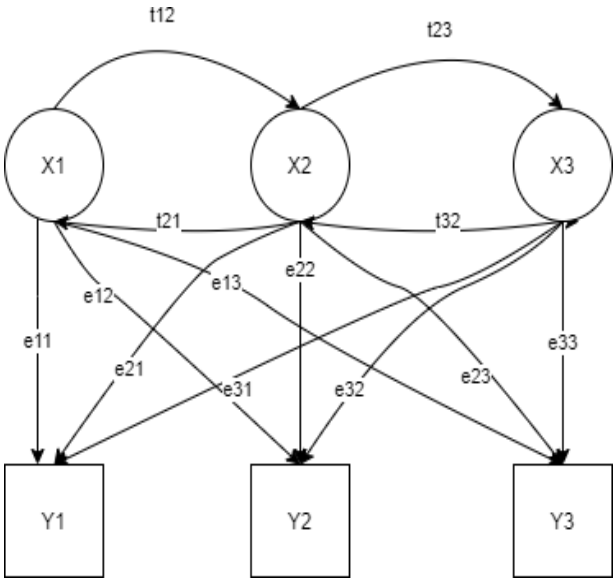

Fig. 3 : Basic Structure of Hidden Markov Model

6. Methodology

6.1 Training Dataset

Marathi language vowels (13), consonants (36), and their combinations along with their utterance are taken as training data. The training dataset is a list of tuples consisting of character/phonemes and recorded speech utterances.

The following tables (Table.1, Table.2) are sample training dataset representation:

Marathi Vowels/Consonants	Transliteration	IPA
अ	a	/ə/
आ	ā	/a:/
इ	i	/i/
ई	ī	/i:/
उ	u	/u/
ऊ	ū	/u:/
ऋ	ṛ	/ru/
क	ka	/kə/
ख	kha	/k^hə/
च	ca	/tɕə/ or /tsə/
छ	cha	/$tɕ^h$ə/

Table -1: Sample Marathi Vowels and Consonants[7]

Script	Pronunciation (IPA)
ग	/gə/
गा	/ga:/
गि	/gi/
गी	/gi:/
गु	/gu/
गू	/gu:/

Table - 2 : Sample Marathi Consonant-Vowel Combination (with ग)[7]

6.2 Feature Extraction using MFCC

Feature vectors represent every distinct phoneme. They are obtained by transforming the training and testing samples through the mel feature vectors which are then required to train the HMM model. The MFCC method applies FFT(Fast Fourier Transform) on speech signals to generate corresponding feature vectors. For each pair of phonemes and its utterance, a feature vector is generated. The MFCC features represent phonemes as a shape of the sound generated by vocal tracts. The feature vectors obtained using the MFCC method are labeled with corresponding phonemes in the HMM model. These labeled feature vectors will be used as reference for testing purposes.

6.3 Testing

In testing, the unknown speech is processed in such a way that every frame bracket contains a phoneme which is then passed to MFCC feature extraction to obtain its equivalent feature vectors and fed to a trained HMM model. The score is calculated based on the maximum matching sequence and thus matched sequence is identified as equivalent transcription.

7. Conclusion

In this paper, Marathi speech transcription is done with the help of Marathi vowels and

consonants. The transcription performance can be enhanced by using Marathi vocabulary, where the generated word can be validated with the existing words. To overcome the accent problem, the model can be trained with a speech from different speakers from different regions.

References

1. Anand H. Unnibhavi, D S Jangamshetti. LPC Based Speech Recognition for Kannada Vowels. International Conference on Electrical, Electronics, Communication, Computer and Optimization Techniques. (ICEECCOT) 2017, IEEE.
2. Manish K., Sarma, Avaas Gajurel, Anup Pokhrel, Basanta Joshi. HMM-based Isolated Word Nepali Speech Recognition. International Conference on Machine Learning and Cybernetics (ICMLC) 2017, IEEE.
3. Narendra D. Londhe, Ghanahshyam B. Kshirsagar. Speaker Independent Isolated Words Recognition System for Chhattisgarhi Dialect. International Conference on Innovations in Information, Embedded and Communication Systems (ICIIECS) 2017, IEEE.
4. Geetha K, ChandraE. Monosyllable Isolated Word Recognition for Tamil Language using Continuous Density Hidden Markov Model. IEEE International Conference on Electrical, Computer and Communication Technologies (ICECCT), 2015.
5. Sarfaraz Masood, Madhav Mehta, Namrata, Danish Raza Rizvi. Isolated Word Recognition Using Neural Network. Annual IEEE India Conference (INDICON), 2015.
6. Hemakumar G., Punitha P. Speaker Dependent Continuous Kannada Speech Recognition Using HMM, International Conference on Intelligent Computing Applications (ICICA) 2014, IEEE